GENCORP
AEROJET

Transpiration Cooled Throat for Hydrocarbon Rocket Engines

Contract NAS 8-36952
Final Report, KEE6-FR
December 1991

Prepared For:
National Aeronautics and Space Administration
George C. Marshall Space Flight Center
Marshall Space Flight Center, AL 35812

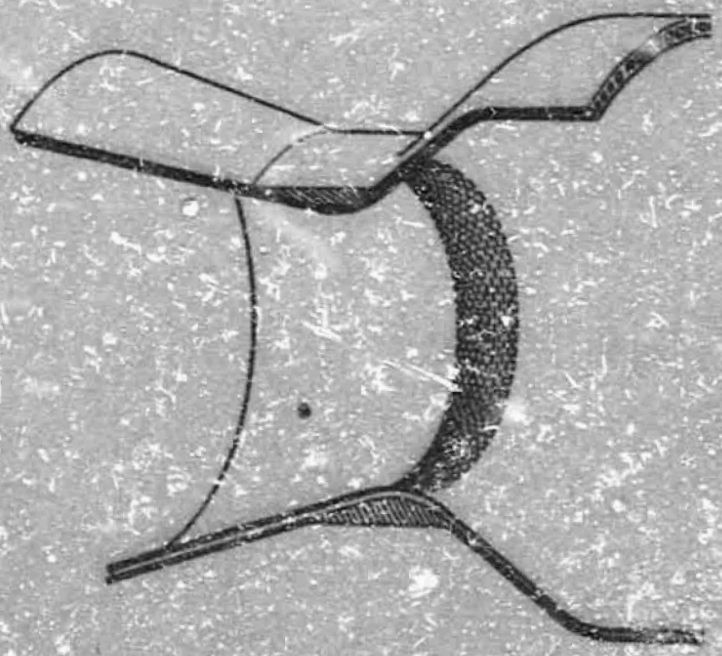

(NASA-CR-184272) TRANSPIRATION COOLED THROAT FOR HYDROCARBON ROCKET ENGINES Final Report (Aerojet-General Corp.) 251 p
CSCL 21H
N92-17495
Unclas
G3/20 0069275

Propulsion Division

Report No. KEE6-FR

December 1991

TRANSPIRATION COOLED THROAT FOR HYDROCARBON ROCKET ENGINES

Contract NAS 8-36952

Final Report

Prepared For

NASA / George C. Marshall Space Flight Center
Huntsville, Alabama 35812

Prepared by:

Lee May
Project Engineer

Approved by:

W.M. Burkhardt
Program Manager

Aerojet Propulsion Division
P.O. Box 13222
Sacramento, California 95813-6000

Foreword

The Transpiration Cooled Throat For Hydrocarbon Rocket Engines Program (Contract NAS 8-36952) was conducted by Aerojet Propulsion Division (APD) for NASA George C. Marshall Space Flight Center. Fred Braam was the NASAprogram manager. At APD, the program manager was Marvin F. Young from January 1988 to January 1989, and Wendel M. Burkhardt has been the program manager from February 1989 to the present. The project engineer was Scott N. Sieger from January 1988 to December 1988, E.L. Van Winkle from January 1989 to October 1989 and Lee R. May from November 1989 to the present. The program analysts were Dongmoon Kim and Scott N. Sieger; the program designer was Judy A. Schneider; and the test engineers were Arnold R. Keller and William A. Thompson. Significant contributions to this program were also made by the following APD personnel:

Chris T. Goodrich
Kin Y. Wong
Shirley J. Reed
Donald C. Rouser
H. H. Mueggenberg
W. A. Hayes
Eugene M. Vanderwall

ii INTENTIONALLY BLANK

PRECEDING PAGE BLANK NOT FILMED

TABLE OF CONTENTS

	Page
Foreword	iii
1.0 Introduction	1
1.1 Background	1
1.2 Objectives	2
2.0 Summary	2
3.0 Conclusions and Recommendations	3
3.1 Conclusions	3
3.2 Recommendations	3
4.0 Technical Discussion	4
4.1 Hardware Descriptions	4
4.1.1 Component Descriptions	4
4.2 Component Fabrication	20
4.2.1 Platelets (Metering, Diffusion and Separator	20
4.2.2 Platelets (Thermocouple Assembly)	20
4.2.3 Liner Fabrication	25
4.2.4 Nozzle Assembly Fabrication	27
4.3 Test Facility	29
4.3.1 Propellants	29
4.3.2 Injector Oxidizer	29
4.3.3 Injector Fuel	29
4.3.4 Igniter Fuel	29
4.3.5 Transpire Nozzle Coolant (Methane)	29
4.3.6 Transpire Nozzle Coolant (RP-1)	31
4.3.7 Propellant Feed System	31
4.3.8 Instrumentation	33
4.4 Nozzle Testing	38
4.4.1 Calorimeter Nozzle Testing	38
4.4.2 Transpiration Cooled Nozzle Testing	42
References:	54
Appendix A: Nomenclature and Unit Conversion Factors	A-1
B: Hardware Drawings	B-1
C: Equations	C-1
D: Design Summary	D-1
E: Test Data	E-1

LIST OF TABLES

Table No.		Page
1	Calorimetric Nozzle Summary	6
2	SINDA Channel Model Result (Mean Heat Flux)	7
3	Main Combustor Design Conditions	11
4	GO_2/GH_2 Igniter Operating Conditions	12
5	Fabrication Braze Experiments	26
6	Instrumentation List	34
7	Summary of Operating Conditions for Calorimeter Nozzle Hot Fire Tests	40
8	Calorimeter Channel Axial Location	41
9	Operating Conditions for RP-1 Transpiration Cooling Tests	46
10	Thermocouple Location	47
11	RP-1 Transpiration Coolant Flowrate Summary by Section for Test KEE4-D01-0A-125	48
12	Calculated RP-1 Coolant Flowrate Distribution for Test No. KEE4-D01-0A-125	49
13	New Baseline Specific Impulse Increase with RP-1 Cooling	53

LIST OF FIGURES

Figure		Page
1	Calorimetric Nozzle Assembly Drawing	5
2	Transpiration Cooled Throat Assembly Drawing	9
3	Carbon Deposition LOX/RP-1 Combustor Hardware	10
4	Main Chamber OFO Triplet Element Injector Pattern	14
5	Injector Body	15
6	Resonator/Fuel Film Cooling Manifold	16
7	Main Combustor Turbulence Ring	17
8	Calorimetric Barrel Section	18
9	Transpiration Platelet Pair	21
10	Washer Platelet	22
11	Instrumentation Platelets	23
12	Thermocouple Platelet Stack	24
13	Fabrication Cycle	28
14	Carbon Deposition Test Assembly Installed in Test Bay	30
15	Propellant System Schematic	32
16	Facility Instrumentation	36
17	Transpire Flowrate Control and Instrumentation Location	37
18	Axial Heat Flux Profile- Test No. KEE4 D01-OA-112	43
19	Throat Temperature History Test No. KEE4-D01-OA-125	51

1.0 INTRODUCTION

1.1 BACKGROUND

The development of a vehicle utilizing LOX/hydrocarbon propellant is one design approach for a launch vehicle, to economically deliver large payloads to orbit. High performance rocket engines designed to combust these propellants impose high heat loads on their components that can have detrimental impact on engine life, cost, and performance. Various engine thrust chamber cooling schemes are being considered to increase engine performance and/or life. A promising cooling approach which shows great performance and life benefits is to transpiration cool the high pressure drop throat region. The savings in throat pressure drop can be used to (1) increase chamber pressure and hence performance or (2) decrease pump output requirements and therefore increase turbopump life. Determination of the overall performance of a transpiration cooled throat rocket engine requires quantification of the performance loss due to transpiration cooling.

Aerojet has extensive experience in transpiration cooling. We have been actively designing and developing transpiration cooling systems since 1946. Transpiration cooling was successfully demonstrated in 1967 on the ARES 100,000 Lbf thrust, 3000 psi transpiration cooled chamber. The ARES and subsequent transpiration cooled chambers and nozzles were fabricated using platelets.

Platelets are thin sheets of metal individually photoetched and diffusion-bonded together or mechanically restrained to create a device with internal flow passages of literally any desired pattern. At the platelet surface, coolant is ejected through discrete pores as small as 0.001 in. Flow control in platelets is accomplished by providing discrete coolant passages for each pore, with primary coolant metering located away from the hot gas surface. Coolant flow profiles can be tailored to meet very severe requirements. Past experience with other porous materials, such as regimesh, sintered metals, and wound wire, do not provide adequate flow control. In these other porous materials, the coolant takes the path of least resistance and avoids hot spots by flowing toward the lower-pressure colder areas. Platelet designs are flexible; they have been fabricated from a number of wall materials: CRES, Copper, and Inconel. Platelets have been fabricated in a range of sizes and for a variety of discrete pore geometries.

1.0, Introduction (cont.)

1.2 OBJECTIVES

The objective of this program was to characterize the use of hydrocarbon fuels as transpiration coolants for rocket nozzle throats. The hydrocarbon fuels investigated in this program were RP1 and Methane. To adequately characterize the above transpiration coolants, a program was planned which consisted of five tasks. In Task 1, relevant full-scale transpiration cooled throat technology issues were addressed. Analytical models, anchored with available data were used to predict engine system performance and life enhancements due to transpiration cooling of the throat region. In Tasks 2 and 3, a versatile transpiration cooled subscale rocket nozzle was designed and fabricated. In Task 4, the subscale transpiration cooled nozzle was tested at very high throat heat flux levels. Finally, in Task 5, detailed data analyses were conducted on the data to determine the relationship between the key performance and life enhancement variables and to recommend a design approach for a larger-scale transpiration cooled throat design demonstration.

The end product of the program was a hydrocarbon transpiration cooling characterization that (1) was verified by hot fire testing and anchored thermal models, (2) provided performance and life enhancement data to support future booster studies and (3) created a computer program to assess system impacts when transpiration cooling is used.

2.0 SUMMARY

Transpiration cooling is an engine cooling scheme which can increase the life and performance of engine systems by eliminating the high pressure drops associated with regen cooling the combustion chamber throat. The pressure drop savings can be used to increase engine performance by increasing chamber pressure or to enhance engine life by reducing turbopump discharge pressure requirements.

To evaluate RP-1 and methane coolant, three subscale nozzles were built. The first nozzle was an all water cooled copper calorimeter nozzle. This nozzle was utilized to establish throat heat fluxes. The other two units were nozzles with transpiration cooled throat sections made from zirconium copper platelets. Each nozzle was capable of using RP-1 or liquid methane coolant. A number of fabrication problems were encountered; all were successfully resolved with the exception of the throat thermocouples. The 10 mil. thermocouples utilized to provide

2.0, Summary (cont.)

high resolution data experienced substantial attrition during the fabrication cycle, resulting in approximately 10% of the initial thermocouples still operational.

Calorimeter test results indicated a higher than predicted heat flux at the throat by approximately 25%. Due to the higher than predicted heat flux, transpire throat testing was performed at a chamber pressure (PC) of 1500 psi instead of the intended 2000 psi. Methane transpiration cooled nozzle testing was limited to one short duration test due to methane supply coolant limitations. RP-1 transpire testing was terminated during the second test, due to failure of the 12 inch water cooled L prime section.

3.0 CONCLUSIONS AND RECOMMENDATIONS

3.1 CONCLUSIONS

Analysis of the RP-1 transpiration cooled nozzle data indicates that subscale nozzle RP-1 transpiration flowrates can be reduced by 67% of the value predicted by previous models. Extrapolation of these results indicates that the RP-1 transpiration flowrates for the full scale baseline 750 Klbf engine are reduced by 35%. The maximum Isp increase for the full scale RP-1 engine is revised from 3 to 10 seconds over a complete regeneratively cooled nozzle.

The data obtained so far consists of only one high flowrate, low wall temperature test condition. Based on a single test point, the data should be considered promising but not conclusive. Full scale engine RP-1 flowrate predictions based on extrapolated test data should be treated as requiring further verification. Additional subscale nozzle testing would be prudent. The subscale nozzle is in good condition with no eroded areas or obstructed cooling slots, so future testing is possible.

3.2 RECOMMENDATIONS

1. Further RP-1 testing is recommended. At a minimum, several RP-1 flowrates should be tested.

2. If additional testing is funded, look into repairing inoperative thermocouples, especially those near the hot gas surface.

3.2, Recommendations (cont.)

3. Evaluate use of non-invasive measurement techniques to determine hot-gas wall temperature in transpire throats.

4.0 TECHNICAL DISCUSSION

4.1 HARDWARE DESCRIPTIONS

4.1.1 Component Descriptions

This sub-section describes the carbon deposition combustor test hardware in addition to the calorimeter and transpire cooled throat nozzles.

4.1.1.1 Calorimeter Nozzle

The high heat flux predicted for the throat area required the selection of copper for the liner material. The slots forming the coolant passages in the liner are machined perpendicular to the thrust axis. The liner contains 28 circumferential channels manifolded into 14 circuits as shown in Figure 1. Table 1 contains a summary of the calorimeter channel dimensions. Circuits 2-13 are single-channel calorimeter circuits located 0.66 in. upstream from the throat to 0.67 in. downstream. Circuits 1 and 14 are multi-channel circuits which are for cooling only and will not provide calorimeter measurements.

Table 2 lists thermal design data for the calorimeter circuits, including the mean heat flux, wall temperature, bulk temperature rise and pressure drop for each circuit. Heat flux is the primary simulation variable between the subscale bench-test and full-scale chamber, and is a required input to the analytical model which will be used to evaluate the transpire experimental data.

4.1.1.2 Long Transpire cooled throat nozzle

The nozzle design incorporates a water cooled calorimeter chamber section with 12 coolant passages machined perpendicular to the thrust axis. The circumferential channels are manifolded into 8 circuits. The transpire section of the nozzle starts at an axial distance 0.66 in. upstream from the throat and extends 0.18 in. downstream. It consists of four components which will be fed with separate external coolant flow lines. This feature allows the flowrates of the four compartments to be independently adjusted. The divergent nozzle section

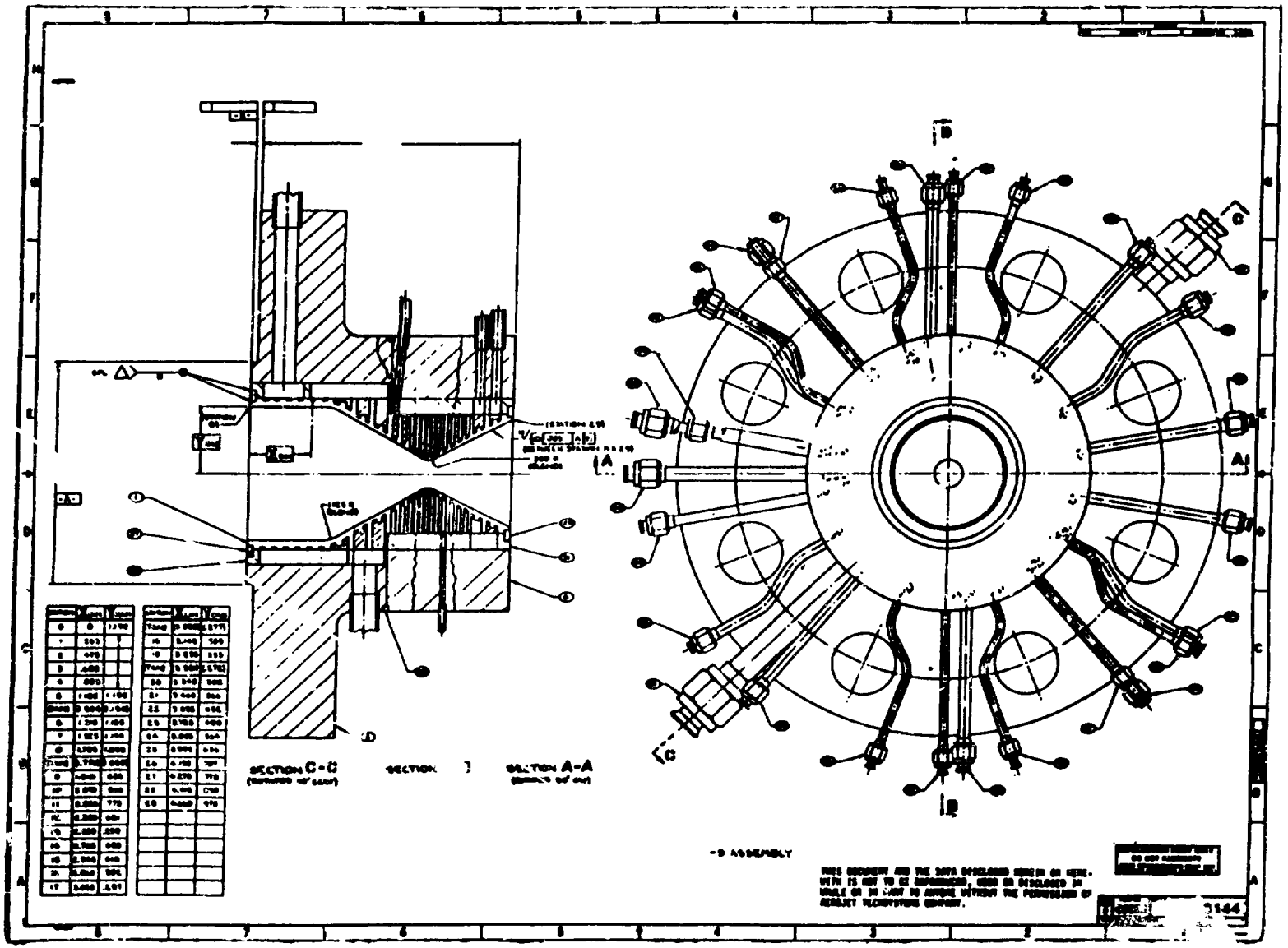

Figure 1. Calorimetric Nozzle Assembly Drawing

ORIGINAL PAGE IS
OF POOR QUALITY

TABLE 1

CALORIMETRIC NOZZLE SUMMARY

Circuit No.	Centerline Axial Location	No. of Channels	tw (in.)	L (in.)	W (in.)	D (in.)
1	-	12	.08/.12	.10/.12	.06/.09	.04
2	2.550	1	.045	.0015	.06	.04
3	2.705	1	.045	.085	.06	.04
4	2.845	1	.04	.065	.05	.04
5	2.960	1	.035	.05	.05	.04
6	3.055	1	.035	.05	.04	.04
7	3.145	1	.035	.05	.04	.04
8	3.235	1	.035	.05	.04	.04
9	3.340	1	.04	.05	.04	.04
10	3.465	1	.045	.08	.05	.04
11	3.595	1	.045	.08	.05	.04
12	3.725	1	.07	.08	.05	.04
13	3.855	1	.07	.08	.05	.04
14	-	4	.10	.09	.05	.04

TABLE 2

SINDA CH. .NNEL MODEL RESULT (MEAN HEAT FLUX)

Circuit No.	Mean Heat Flux	Wall Temp (°F)	Flowrate (lb/s)	Bulk Temp Rise (°F)	Pressure Loss (psi)	BOSF	Velocity (ft/s)
1	13.1	555	2.42	61	250	4.0	100
2	21.5	671	.22	66.1	264.3	2.51	106.1
3	31.0	794	.26	59.5	348.5	2.21	125.4
4	44.2	895	.27	55.8	515.0	1.96	156.3
5	59.4	1037	.31	47.5	625.7	1.79	176.5
6	74.7	1163	.30	40.3	922.6	1.70	217.0
7	78.4	1178	.32	34.6	1012.3	1.74	231.5
8	53.0	931	.28	30.0	778.1	2.27	202.5
9	26.5	719	.11	57.3	138.7	2.20	79.6
10	18.2	662	.11	62.0	98.1	2.44	63.7
11	13.4	558	.10	62.1	82.6	2.98	57.9
12	10.2	540	.075	72.9	52.4	3.26	43.4
13	10.2	540	.075	72.9	52.4	3.26	43.4
14	8.4	549	.27	86.8	44.0	3.44	39.9

consists of four calorimeter circuits immediately downstream of the throat to allow measurement of heat flux during the transpire testing. The nozzle assembly is shown in Figure 2.

4.1.1.3 Short transpire throat nozzle

The short transpire throat design is identical to the long throat with the exception of two additional upstream water flow passages and one less transpire coolant section. The transpire section of the throat begins at an axial distance 0.37 in. upstream from the throat and extends 0.18 in. downstream as shown on Figure 2.

4.1.1.4 Main Combustor

The main combustor assembly photo and sketch is shown in Figure 3. The combustor consists of an H_2/O_2 igniter assembly, an OFO triplet injector, a water-cooled copper acoustic cavity and fuel film coolant manifold, and two water-cooled cylindrical nickel liner L' sections. The water-cooled chamber sections are circumferentially cooled flow calorimeters. The components are designed to be interchangeable and utilize standard pipe flanges. Individual components are mechanically joined using self-energizing Teflon-coated Raco seals or O-rings for effective sealing at these pressures. The main combustor design requirements are summarized in Table 3. A detailed discussion of the main combustor components follows.

4.1.1.5 Igniter

A gaseous hydrogen/gaseous oxygen spark igniter is used for the main combustor assembly. This igniter was used on previous NASA-funded programs (NAS3-22647) and NASA program (NAS 9-15958) in addition to the present contract. The igniter assembly is bolted to the backside of the injector body such that the igniter fires thought the center of injector face. The igniter operating conditions are listed on Table 4.

4.1.1.6 Injector

The injector design was based on the triplet injector used on NASA Contract 9-15958. The injector was stable under most operating conditions, was in good condition at the end of testing and provided 97-99% efficiency.

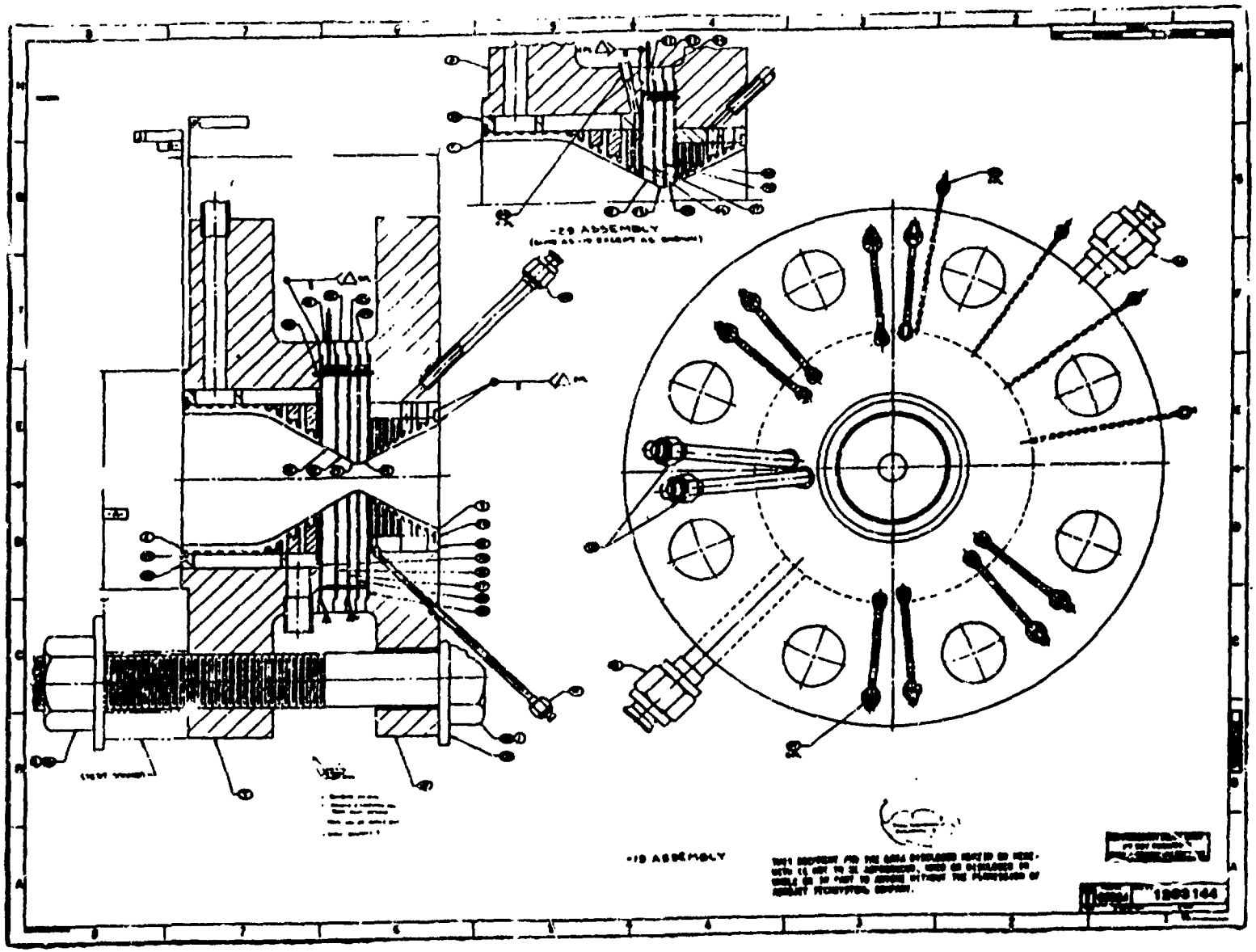

Figure 2. Transpiration Cooled Throat Assembly Drawing

ORIGINAL PAGE IS
OF POOR QUALITY

ORIGINAL PAGE
BLACK AND WHITE PHOTOGRAPH

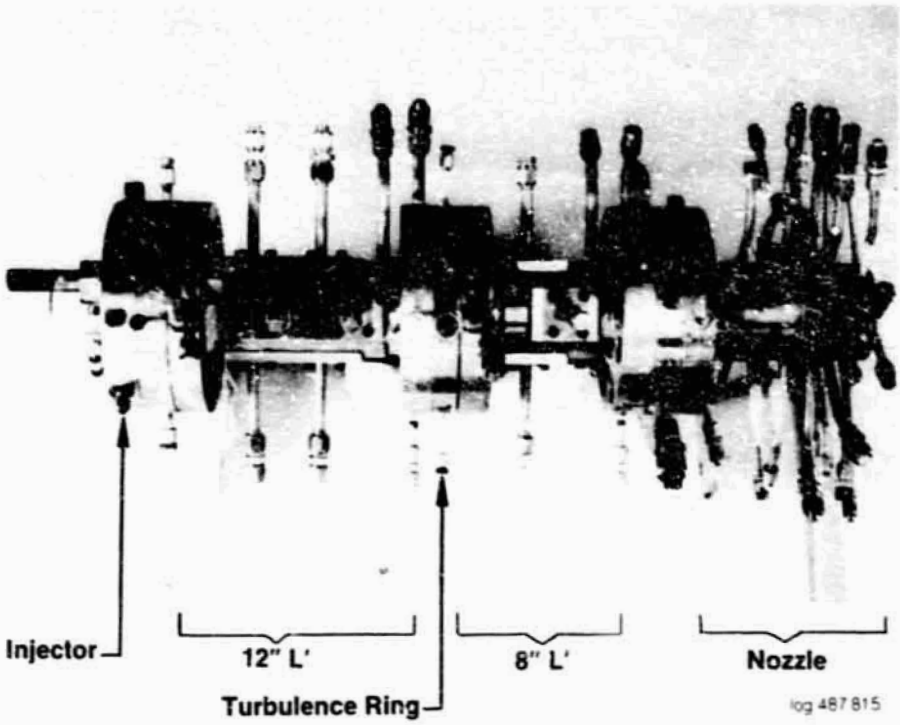

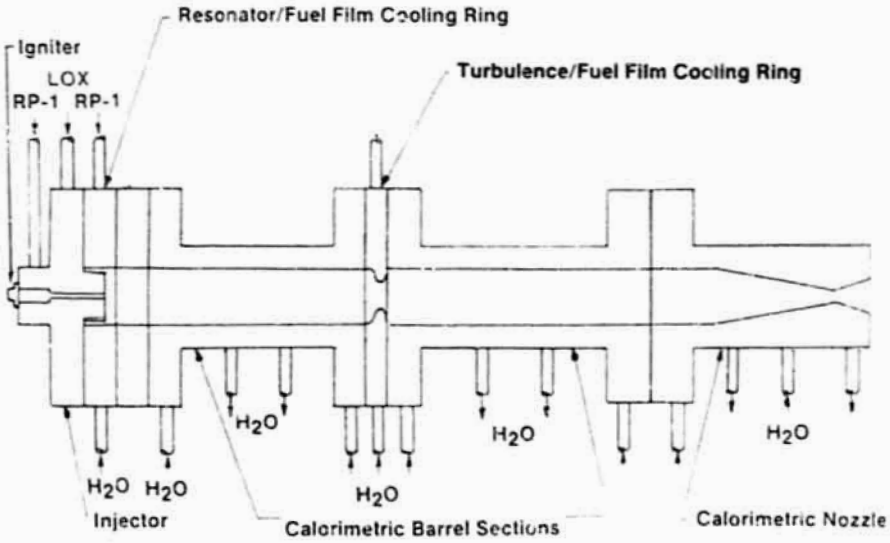

Figure 3. Carbon Deposition LOX/RP-1 Combustor Hardware

TABLE 3

MAIN COMBUSTOR DESIGN CONDITIONS

Design Paramters

P_c = 2,000 psia (1,500 - 2,000 psia) [13.78 MPa (10.34-13.78 MPa)]

MR = 3.0 (2.0 - 4.0)

W_f = 0.555 lb/sec (0.25 kg/sec)

W_o = 1.665 lb/sec (0.76 kg/sec)

A_t = 0.196 in2 (12.65 cm2)

D_t = 0.50 in (1.27 cm)

D_c = 2.38 in. (6.05 cm)

TABLE 4

GO_2/GH_2 IGNITER OPERATING CONDITIONS

P_c = 450 psia

MR = 1:1

$\dot{w}_f$ = 0.0471 lb/sec

$\dot{w}_o$ = 0.0471 lb/sec

Fuel orifice inlet pressure 1 250 psia

Oxidizer orifice inlet pressure 1,200 psia

Spark energy = 30 millihjoules

Spark rate = 500 spks/sec

Spark voltage = 40,000 volts

Maximum firing duration - 0.400 sec

4.1, Hardware Descriptions (cont.)

The injector has a 2.18 in. (5.54 cm) face diameter and contained 18 elements arranged in a single row. The oxidizer-rich OFO triplet had 0.024 in. (0.061 cm) oxidizer orifices and 0.021 in. (0.053 cm) fuel orifices. The element configuration is illustrated in Figure 4. The injector body is shown in Figure 5. The concentric ring manifold injector is a weldment consisting of nickel core body, a solid nickel face plate, and a stainless steel fuel inlet cover. Nickel was used as the face material for cooling purposes. All subcomponents were joined by electron beam welding. The oxidizer manifold is located in the injector flange, outboard of the injector channels. An oxidizer inlet line welded to the flange feeds the manifold via a drilled passage. The oxidizer manifold is machined eccentric to the injector axis to provide a constant velocity flow configuration. This manifold feeds three radial oxidizer manifolds which in turn feed the face ring through the axially-directed downcomers. The fuel manifold is located on the injector's back surface and has a single inlet which is offset to clear the central igniter. The fuel downcomers are fitted between the three radial oxidizer manifolds an connect the fuel manifold to the individual face rings.

The injector body also incorporates instrumentation for measuring propellant inlet pressures and temperatures. High frequency pressure transducers (Kistlers) ports are also located in each of the propellant inlet manifolds.

4.1.1.7 Acoustic Resonator and Film Coolant Manifold

A water-cooled quarter-wave acoustic resonator with an integral fuel-film coolant manifold is used to provide combustion stability (see Figure 6). The unit is made out of copper to provide maximum cooling margin when the fuel-film cooling circuit is not flowing. Eighteen 0.015 in. diameter (0.038 cm) holes directed the film coolant flow against the edge of the injector. These 18 atomized jets performed as splash plate elements to uniformly distribute the flow around the periphery of the chamber.

4.1.1.8 Turbulence Ring and film Coolant Injection Manifold

A water-cooled turbulence ring with an integral film coolant manifold is used to promote mixing. The copper liner is brazed into a stainless steel flange as shown in Figure 7. To promote mixing, the turbulence ring protruded approximately 0.44 in. (1.12cm) from the chamber wall into the flow field. The leading square-edge on the turbulence ring has

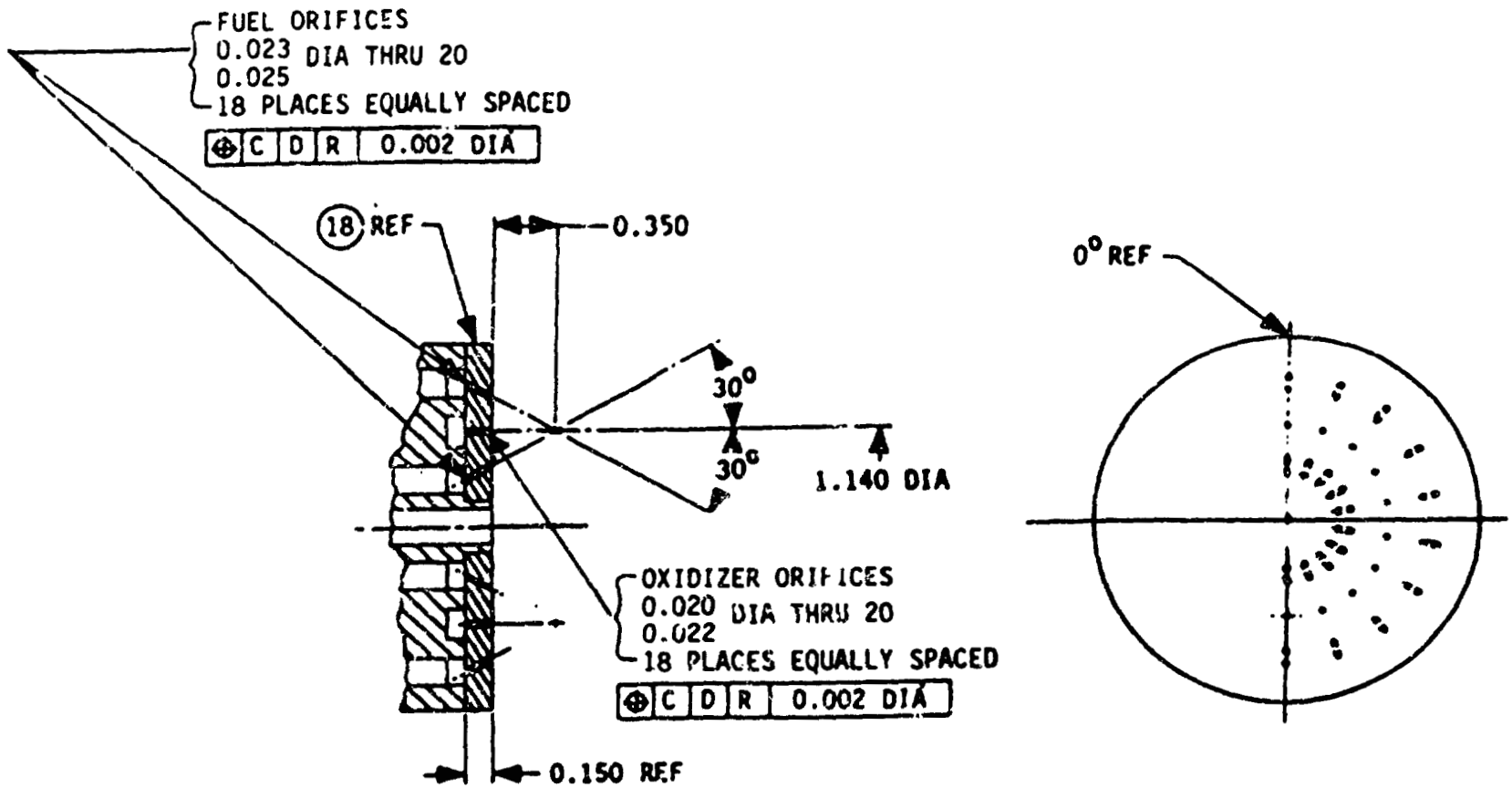

Figure 4. Main Chamber OFO Triplet Element Injector Pattern

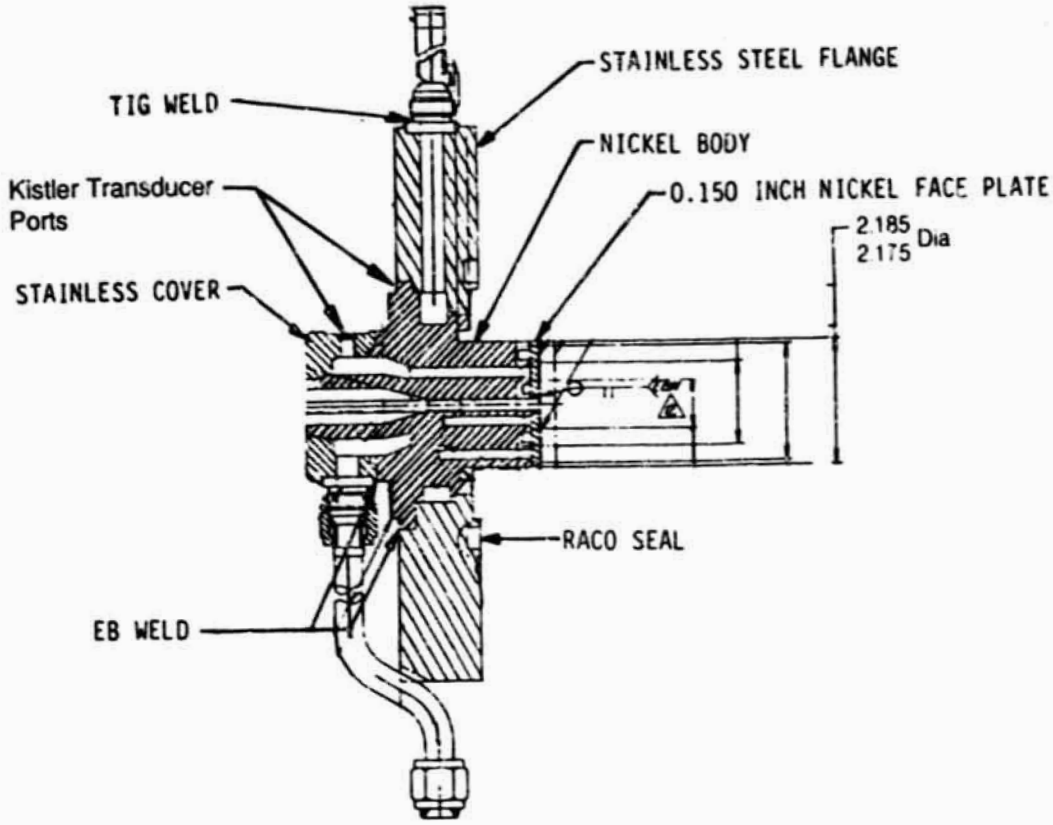

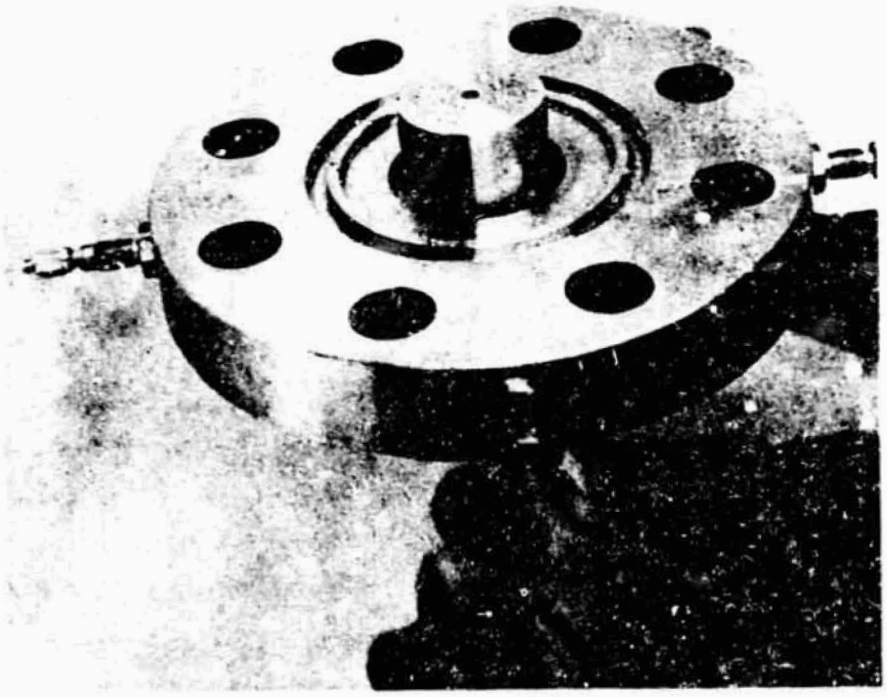

Figure 5. Injector Body

ORIGINAL PAGE
BLACK AND WHITE PHOTOGRAPH

ORIGINAL PAGE IS
OF POOR QUALITY

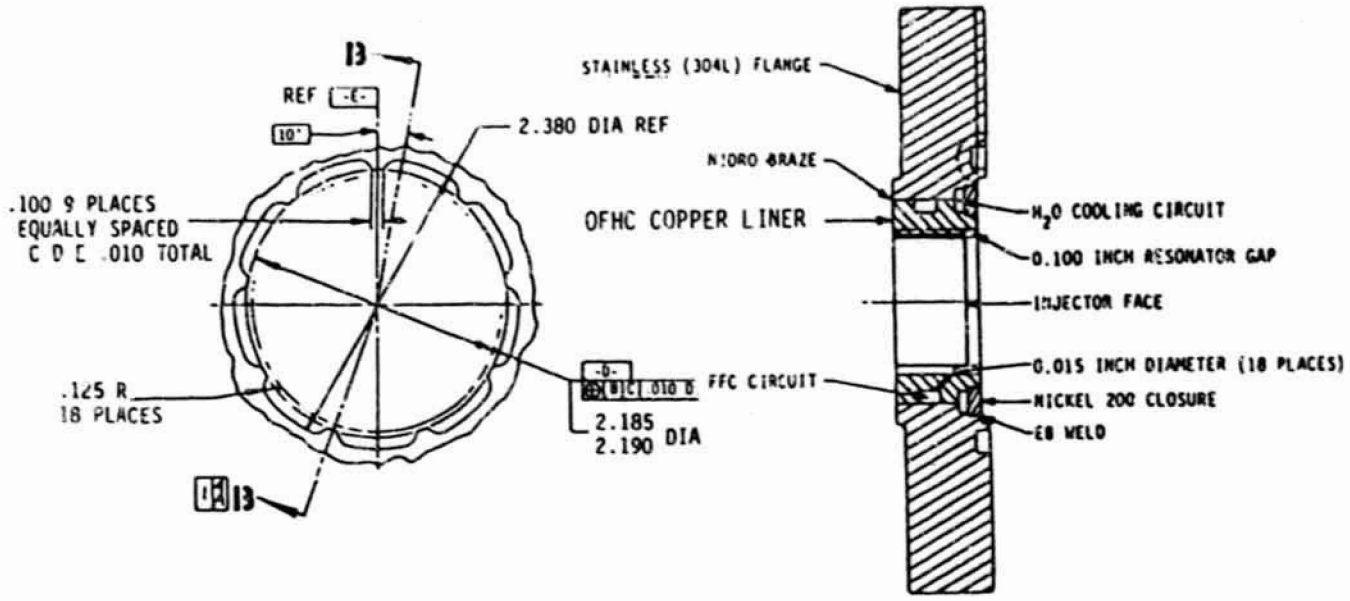

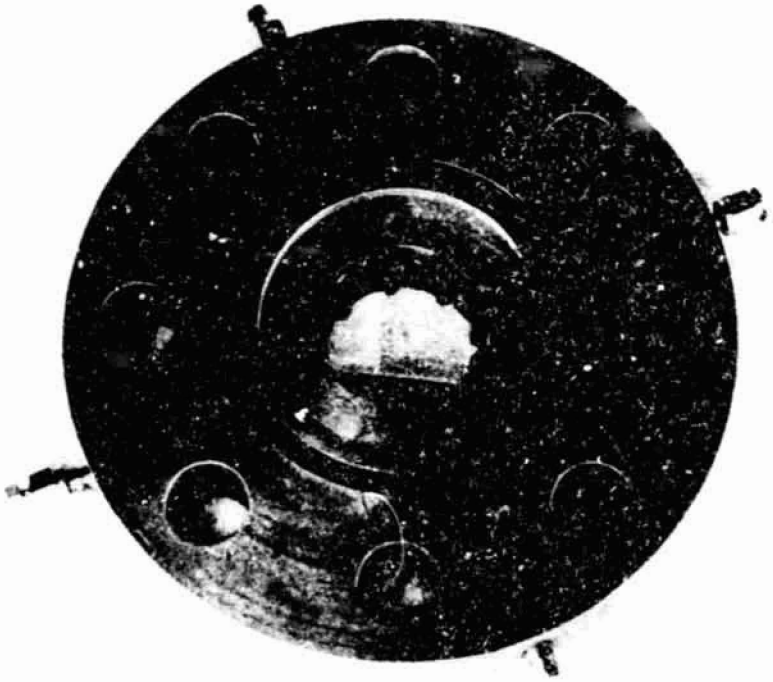

Figure 6. Resonator/Fuel Film Cooling Manifold

ORIGINAL PAGE
BLACK AND WHITE PHOTOGRAPH

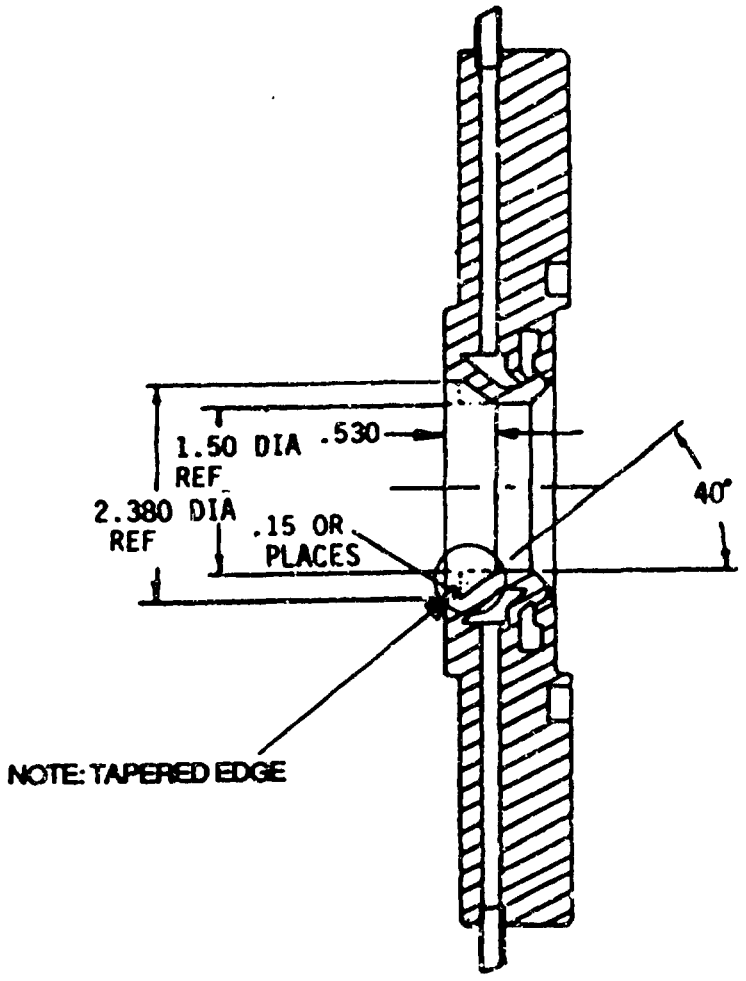

Figure 7. Main Combustor Turbulence Ring

been machined to a smooth, tapered edge for use in the higher temperature main chamber combustion gases. The ratio of turbulence ring area to chamber area (i.e. 0.58) is the same as was found most effective on previous Aerojet Propulsion Division programs. The integral film coolant manifold allows water or any other fluid to be injected at the start and/or end of the firing to clear the carbon off of the chamber walls.

4.1.1.9 Calorimetric Barrel Section

The combustion chamber consisted of two water-cooled cylindrical barrel or L' (Figure 8) sections which are bolted together. Each of the cylindrical chamber sections has a nickel liner designed to operate from 1500 to 1800° F (1090 to 1256K) surface temperature.

The cylindrical sections use a circumferential coolant flow scheme that allows the heat input to be measured at different axial locations.

The cylindrical chamber sections are designed as series flow calorimeter devices. With a series flow calorimeter, the discharge flow from one calorimeter section becomes the inlet flow for the next calorimeter section. The coolant temperature is measured between the adjoining flow sections. This approach minimized the number of coolant supply circuits and flow measurements required on the test stand.

The two cylindrical chamber sections fabricated are 8 in. (20.32 cm) long and 12 in. (30.48 cm) long. The sections are essentially identical except for length and can be used together or separately. The two different lengths provided flexibility in the selection of chamber L' section and in the location of the turbulence ring. Because they ar so similar, only the 8 in. (20,32 cm) long section is described.

The slots forming the coolant passages in the liners are machined perpendicular to the thrust axis. The cylindrical section contained 28 circumferential channels in the liner which are split into four coolant circuits in the 8 in. (20,32 cm) barrel section. The 12 in. barrel (30.48 cm) section contained 38 circumferential channels which are split into six coolant circuits. The calorimeter sections at the ends of the chamber were plumbed separately to provide added cooling capability. The middle of the chamber consists of one circuit which has three calorimeter sections in series and one circuit with two in series. Each inlet manifold, turnaround, and outlet is instrumented for temperature measurements and each outlet is instrumented

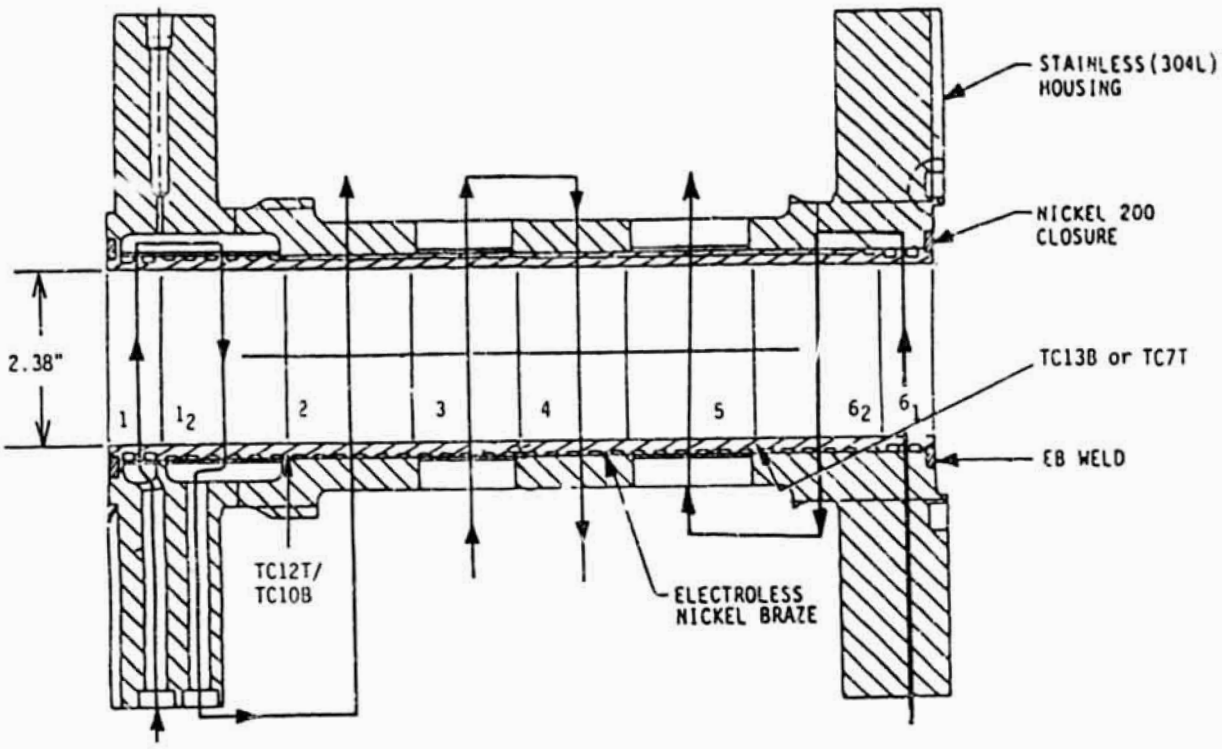

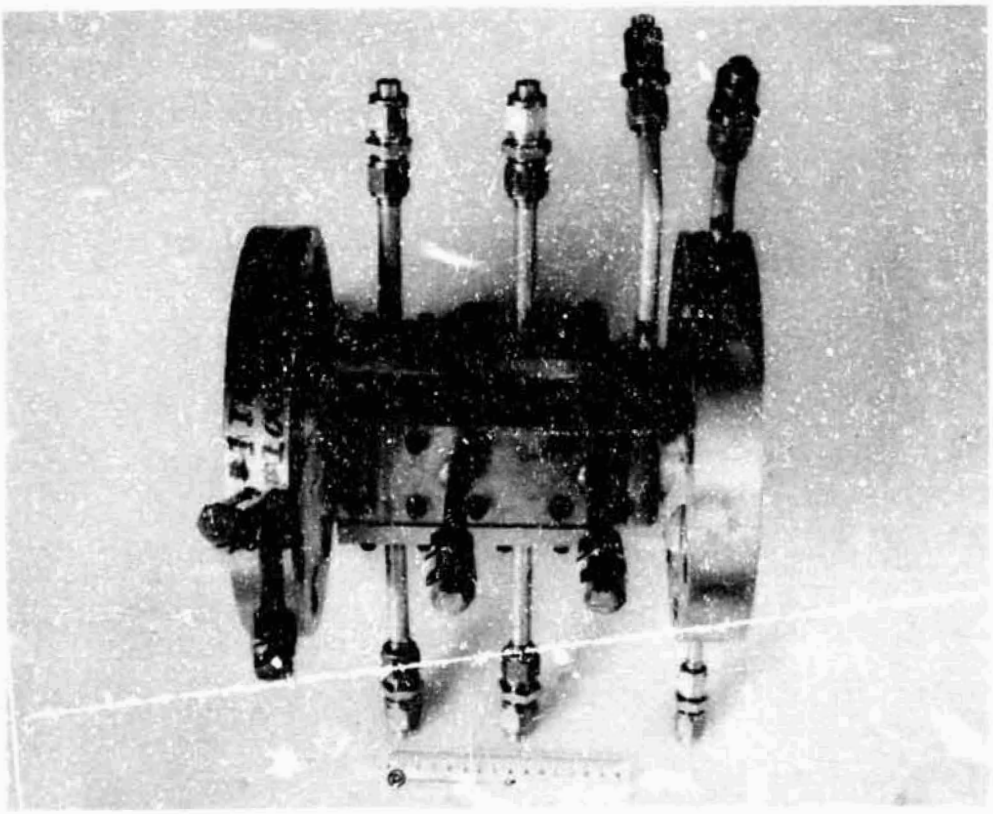

Figure 8. Calorimetric Barrel Section

ORIGINAL PAGE
BLACK AND WHITE PHOTOGRAPH

for pressure measurement. The cylindrical section is a three-piece brazed assembly. The inner liner is made out of nickel while the structural housing is make out of stainless steel. The circumferential cooling slots are lathe-turned into the nickel liner. Backside manifolding for the coolant channels is accomplished by machining axial passages 180° apart in the sleeve. The flame side of the cylindrical section is copper-plated to the thickness of 0.001 to 0.003 in. (0.0025 to 0.0076 cm) two in. (5.08 cm) on the downstream end of the [illegible] n (20.32 cm) calorimeter section.

4.2 COMPONENT FABRICATION

4.2.1 Platelets (Metering, Diffuser and Separator)

The transpire throats used were comprised of 4 and 8 mm thick photoetched ZrCu platelets of four different basic designs: metering, diffuser, separator and instrumentation. Platelets were stacked in a defined order to control the different coolant flowrate requirements at various points in the throat. Several different configuration platelets were required to comply with the design coolant flow requirements. The long transpire cooled throat required 106 platelets and the short 73 platelets. Typical platelet configurations are shown in Figures 9, 10 and 11.

4.2.2 Platelets (Thermocouple Assembly)

The thermocouple plate assembly consists of three photo etched platelets with twelve thermocouples brazed into the platelet stack. Several braze experiments were required to establish an acceptable procedure. The ideal braze for thermocouple installation is 360 degree contact between the thermocouple and platelets for the first 1/4 to 1/2 in. at the tip to ensure valid heat transfer during test. Seven thermocouple platelet stacks of four different configurations were required for fabrication of both the short and long transpire cooled nozzles. A photograph of a typical stack is shown in Figure 12. After assembly and braze, a random check of several thermocouples was made and all were found to be operative. It should be noted that the 10 mil. thermocouples create a major handling problem due to the delicate nature of the 1.5 mil. wires used in their fabrication.

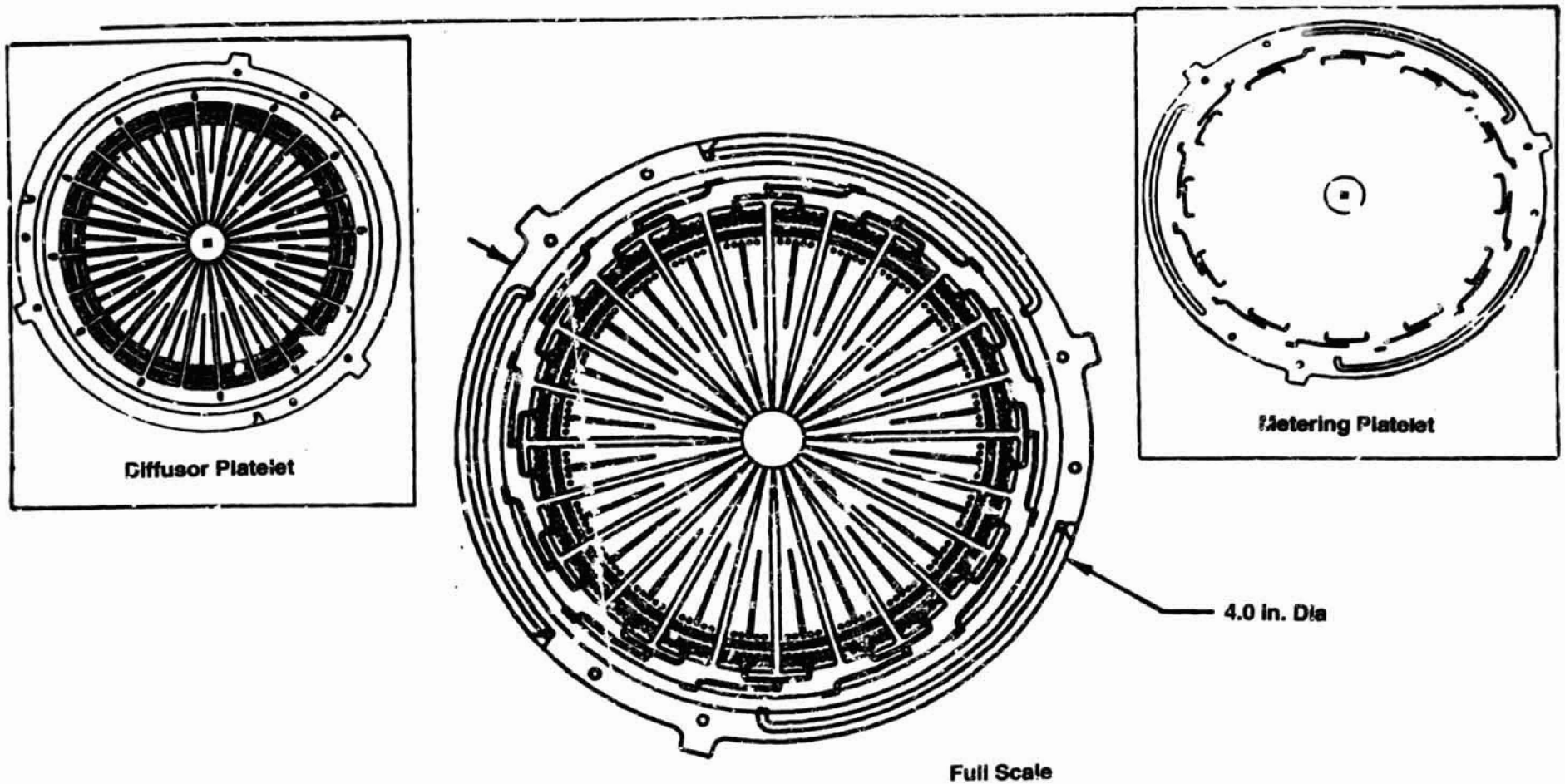

Figure 9. Transpiration Platelet Pair

Notes:

1. Dimension and Fabricate per 1203147-1 Except as Shown Here.
2. Mark per AS478-37 With 1203147-6.

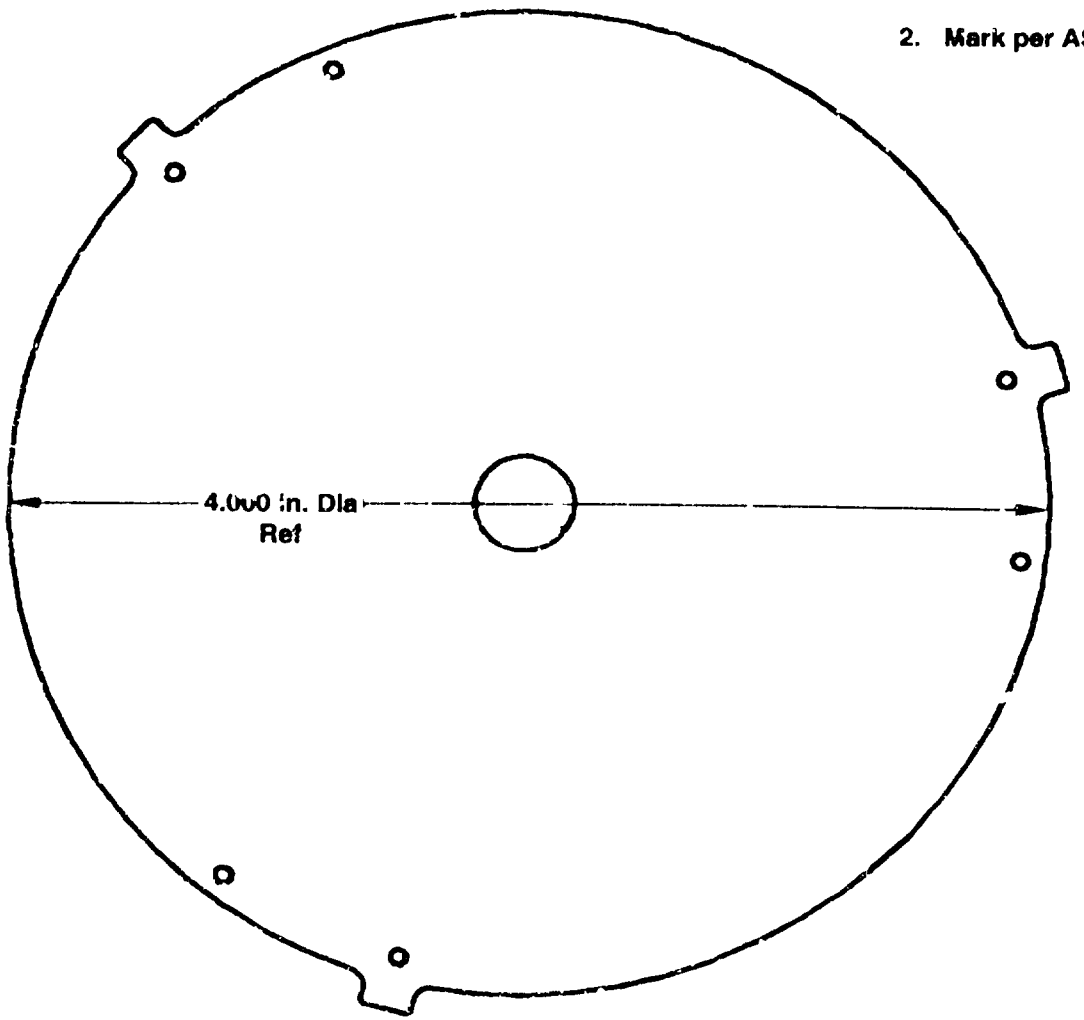

Figure 10. Washer Platelet

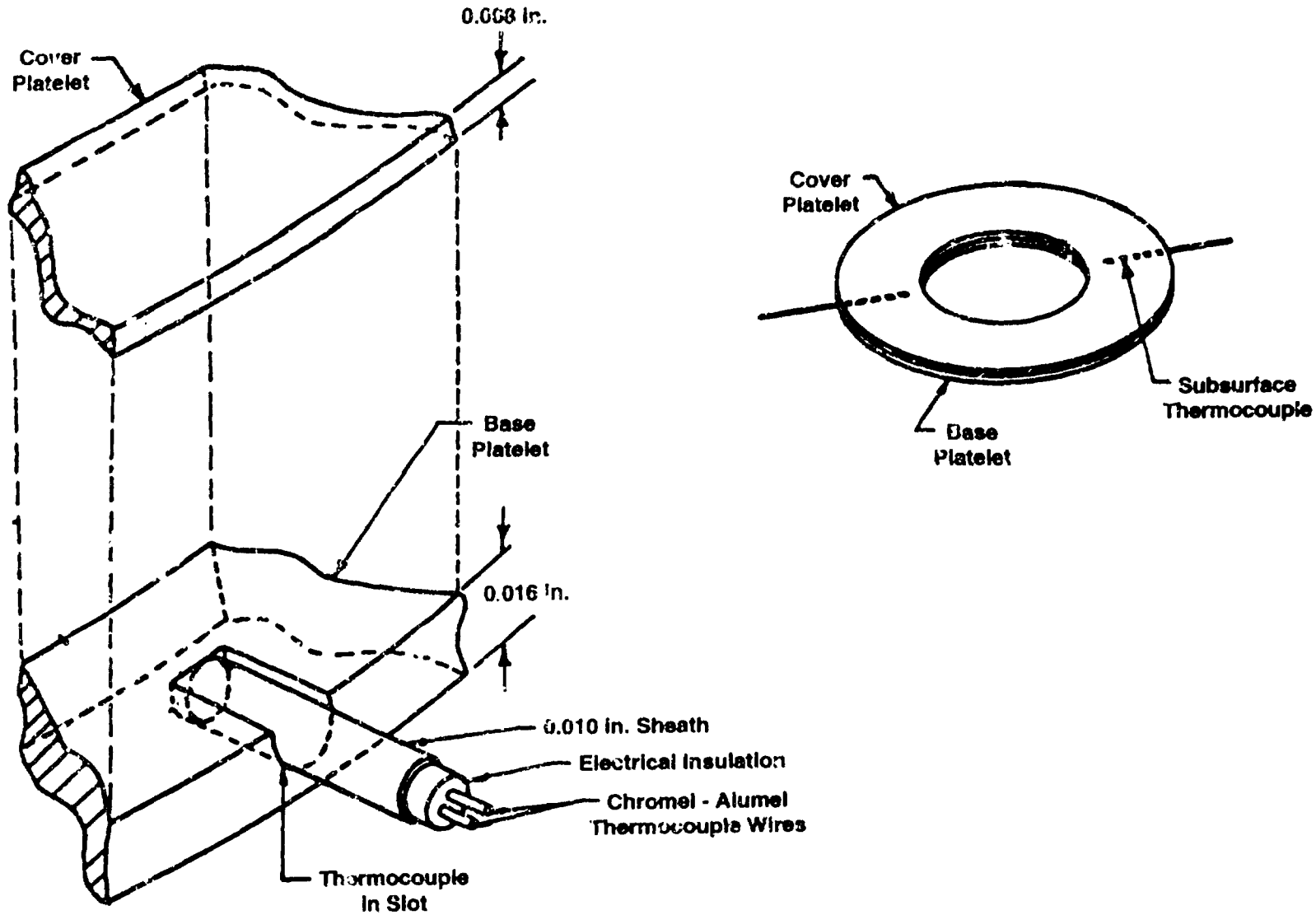

Figure 11. Instrumentation Platelets

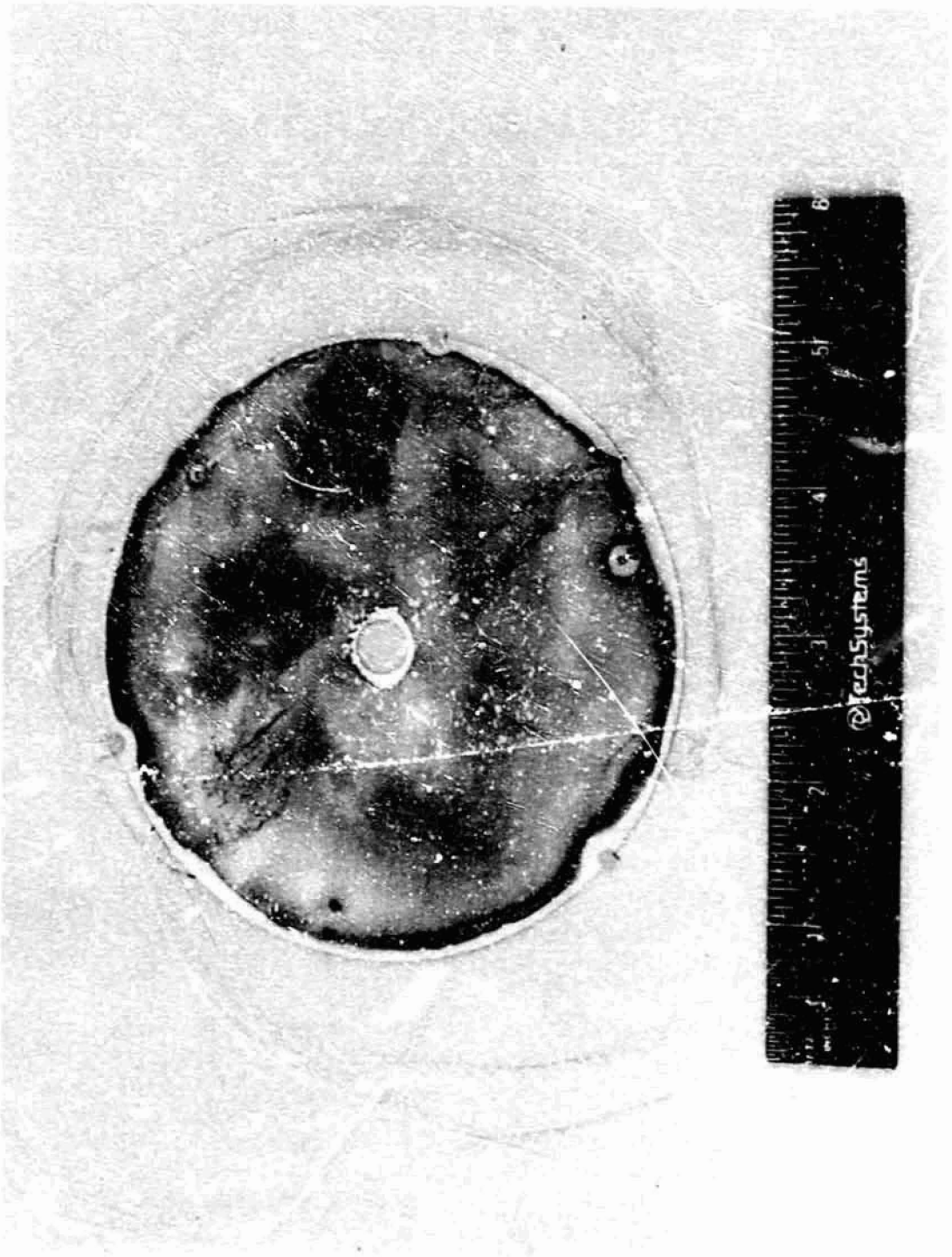

Figure 12. Thermocouple Platelet Stack

ORIGINAL PAGE
BLACK AND WHITE PHOTOGRAPH

4.2, Component Fabrication (cont.)

4.2.3 Liner Fabrication

The fab cycle starts by machining the coolant channels into the ZrCu liner. OHFC half rings are machined and brazed into the liner forming the calormeter coolant passages. During the first liner to half ring braze attempts porosity occurred in the braze bond. In an attempt to correct the porosity nicro braze 50 powder was added to the braze joint and the liner was subjected to an additional braze cycle. This resulted in the nicro braze 50 powder flowing through the braze joint and partially plugging the flow channel.

To resolve the braze procedures, a review of the past problems relating to brazing of copper and zirconium copper nozzle assemblies was conducted. The procedures used to machine, plate and braze nozzle assemblies (as shown in Table 1) were reviewed, and it was determined that the key to successful brazing for this type of assembly was (1) close tolerance control of ring thickness and nozzle slots, (2) control of nickel-phosphorus composition, (3) plating thickness and uniformity, and (4) machining sequence.

The first nozzle liner assembly attempted (S/N 1) experienced difficulty in ring insertion and channel spreading, however, working with a combination of custom fitted rings and a liner machining sequence solved the problem. S/N 2 liner nozzle employed essentially the same procedure as S/N 1, however, materials-of-construction altered the assembly procedure. Some leakage was noted on S/N 2 after brazing, however it was deemed usable. Note that the body was fabricated from Zr Cu.

It should be noted that Zr-Cu is extremely difficult to braze under either hard vacuum or dry hydrogen conditions. A tenacious oxide film forms during heating. The problem is further aggravated when electroless nickel plating is used as the braze filler metal in hard vacuum (due to critical vapor pressure for phosphorus). Dry hydrogen brazing of Zr-Cu (using electroless nickel) requires that all the Zr-Cu surfaces be plated unless the Zr-Cu is to be joined to material such as OFHC copper, then only the Zr-Cu surface requires plating.

The first prototype nozzle liner assembly (# 3, Table 5) vacuum furnace brazed by Thermo Electron leaked after brazing (note that the Zr-Cu liner was unplated). Attempts to repair braze the nozzle liner using a nickel phosphorus braze powder (W.C. 50) resulted in plugging the coolant channels. Destructive examination of nozzle samples at Aerojet revealed extensive unbonded areas between the Zr-Cu body and the OFHC copper brazed rings,

TABLE 5

FABRICATION BRAZE EXPERIMENTS

Nozzle Assembly #1

Body	OFHC Copper
Rings	OFHC Copper
Plating	*Electroless Nickel
Thickness	Nominal 0.0003"/Surface
Composition	90% Ni 10% P
M.P.	-1750°F (950°C)
Dry H_2	-80°F D.P.
Brazed	-1850° F/10 min. at temp
Fit-up	Light Press Fit

*OFHC Rings Plated

Nozzle Assembly #2

Body	Zr Copper
Rings	18-8 Stainless Steel
Plating	*Electroless Nickel
Thickness	0.0002" to 0.0004"/Surface
Composition	10-12% P Bal Ni
M.P.	Range Between 1700°-1750°F
Dry H_2	-80°F D.P.
Brazed	-1850° F/10 min. at temp
Fit-up	Light Press Fit/Interference

*S.S. Rings Plated

Nozzle Assembly #3

Body	Zr-Cu
Rings	OFHC Copper
Plating	*Electroless Nickel
Thickness	0.0003" Nominal
Composition	10-11% P Bal Ni
M.P.	-1750°F
Vac. Brazed	-1810°F (988°C)/5 min at temp
Vac Pressure	-1 x 10^{-5} Torr Range
Fit-up	Loose/Press Fit

*OFHC Copper Rings Plated

indicating the inability of the molten Ni-P to wet the unplated Zr-Cu. It was at this point that Aerojet recommended a series of tests that included plating of the Zr-Cu body and use of dry hydrogen brazing.

Samples prepared by Thermo Electron revealed what was previously conjectured. That is, Zr-Cu vacuum furnace brazed to Zr-Cu, plating one surface only did not result in a good braze. Hydrogen furnace brazed samples of Zr-Cu plated on one surface only revealed evidence of only partial bonding, and plating of Zr-Cu against unplated OFHC copper brazed completely.

These results conclusively indicated that in order to dry hydrogen furnace braze a Zr-Cu nozzle liner, the liner has to be electroless nickel plated. A test piece simulating the nozzle with the deep channels was satisfactorily plated, depositing an overall nominal plating thickness of 0.0003 in.

Utilizing the established machining, plating, fit up and braze procedure. all subsequent brazing on liner to half-rings was completed successfully.

4.2.4 Nozzle Assembly Fabrication

During the assembly of the transpire cooled throats, the platelets are stacked into flow sections with separator platelets isolating the flow sections. Each individual flow section has a separate manifold that is installed during the stacking operation. The manifold has .013 diameter through holes to accommodate the .010 diameter thermocouple leads. The twelve leads are fed simultaneously through the manifold as it is installed over the platelet stack. Due to the routing of the leads and the close tolerance in the feed holes, an extremely high stress load is placed on the leads. A majority of the thermocouple losses experienced are attributed to this operation. After completion of stacking, the transpire coolant manifolds are E B welded. The external bolts are installed and the liner to shell close outs are E B welded. The complete fabrication cycle is shown in Figure 13.

After completion of thermocouple terminations, 5 out of 48 thermocouples were functional on the long transpire throat nozzle and 3 out of 36 on the short transpire throat.

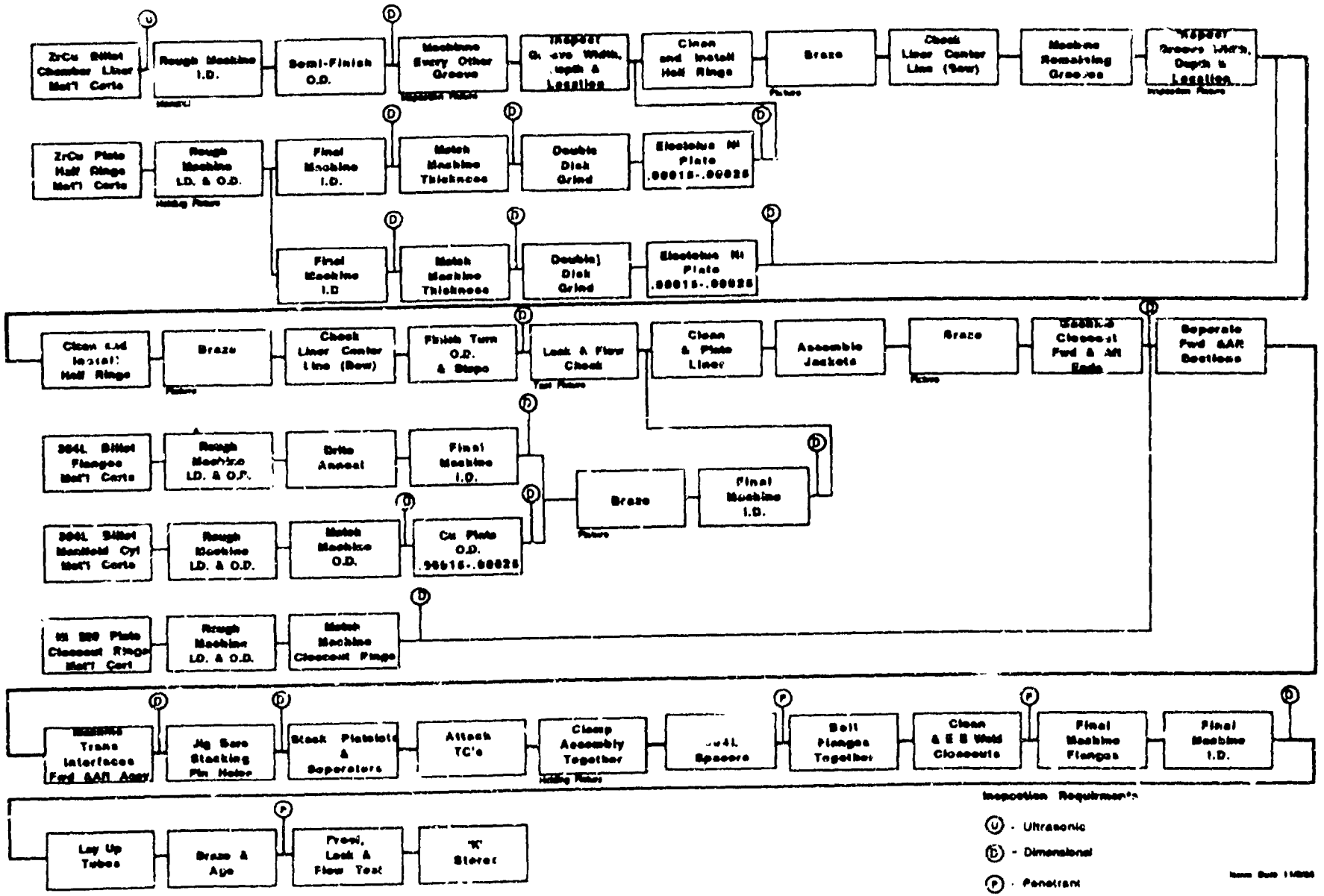

Figure 13. Fabrication Cycle

ORIGINAL PAGE IS OF POOR QUALITY

4.3 TEST FACILITIES

The hot-fire testing was conducted in Bay 6 of the Aerojet Research Physics Laboratory. The setup consisted of the fuel and oxidizer feedsystem, a water coolant feedsystem, a thrust stand, the hardware and igniter feedsystem and instrumentation The test bay with carbon deposition test assembly installed is shown in Figure 14. The facility has been checked out and used extensively to support testing on Contract NAS 8-34715.

4.3.1 Propellants

The propellants supplied to the injector conformed to the following.

4.3.2 Injector Oxidizer

The injector oxidizer was liquid oxygen (LOX) flowrates varied from 0.80 to 1.70 lb/sec.

4.3.3 Injector Fuel

The injector fuel was RP-1 (MIL-P-25576). The RP-1 was passed through a 10-micron filter before entering the igniter. The injector fuel feed system was capable of supplying ambient temperature RP-1 to the injector over a pressure range from 1500 to 3000 psig. The RP-1 flowrates varied from 0.50 to 1.70 lb/sec.

4.3.4 Igniter Fuel

The igniter fuel was gaseous hydrogen (GH_2) MIL-P-27202B. The GH_2 was passed through a 10-micron filter before entering the igniter. The igniter fuel feed system was capable of supplying ambient temperature GH_2 to the igniter inlet at approximately 2,500 psia. The GH_2 flowrate was 0.0074 lb/sec.

4.3.5 Transpire Nozzle Coolant (Methane)

The liquid methane (LCH_4) transpire coolant conformed to Propellant Methane Type 2 PC-44. The LCH_4 was passed through a 10-micron filter before entering the nozzle circuits. The coolant feed system was capable of supplying LCH_4 over a pressure range

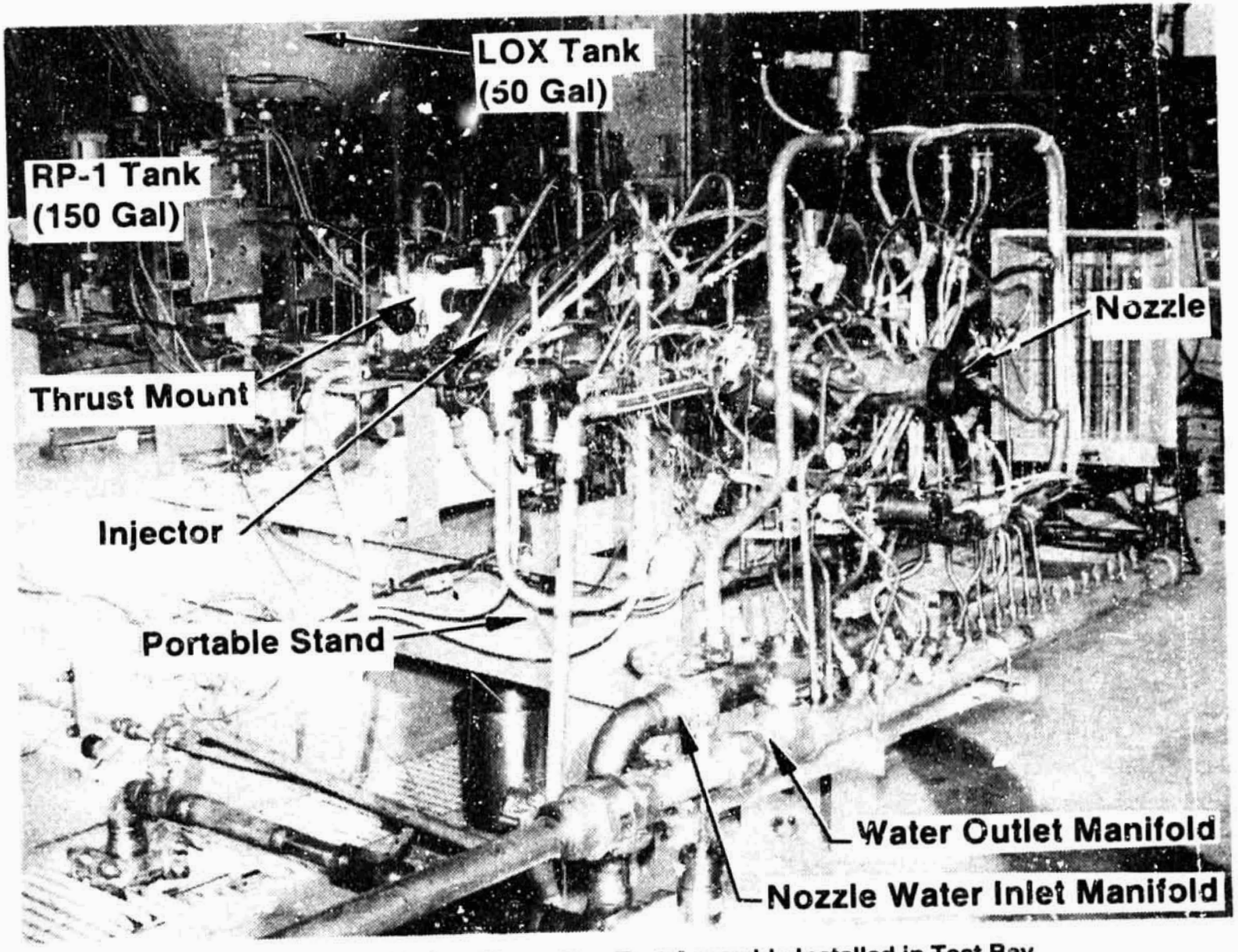

Figure 14. Carbon Deposition Test Assembly Installed in Test Bay

ORIGINAL PAGE
BLACK AND WHITE PHOTOGRAPH

from 1000 to 3000 psia and a temperature range of -250 to -270°F. The LCH_4 flowrate was 0.42 lbs/sec.

4.3.6 Transpire Nozzle Coolant (RP-1)

The RP-1 coolant conformed to MIL-P-25576 and was passed through a 10-micron filter before entering the nozzle circuits. The coolant feed system was capable of supplying ambient temperature RP-1 over a pressure range from 1000 to 3000 psia and a flowrate from 0.26 to 0.56 lbs/sec.

4.3.7 Propellant Feedsystem

A schematic of the propellant feedsystem is shown in Figure 15. The propellants were supplied to the engine from the pressurized tankage. The oxidizer is pressurized with helium and the fuel with nitrogen. Both the fuel and oxidizer tanks and lines are jacketed to provide temperature control with liquid nitrogen, as required to condition the propellants. The fuel tank capacity is 200 gal. and the oxidizer tank is 50 gal. capacity. Both tanks can be operated to 5,500 psia.

The GO_2/GH_2 igniter was fed propellant from high pressure 'K' bottles. Sonic verturies were used to control the flowrates. An existing GLA power supply was used to provide the required spark energy for ignition.

The liquid methane for nozzle throat transpire cooling was supplied from a 1500 gal supply tank to a 30 gal run tank. The 30 gal. run tank was pressurized with nitrogen to a maximum of 3000 psig. The methane was then supplied to the nozzle coolant circuits. The methane coolant circuit was provided with a GN_2 purge. The GN_2 conformed to MIL-P-27401 and was passed through a 10 micron filter before entering the coolant circuits.

Deionized water for cooling of the thrust chamber components (calorimeter chambers, resonators, etc.) was supplied from a 3,000 psi, 180 gallon tank situated adjacent to the test bay. This tank feeds an inlet manifold located next to the test stand. This manifold constitutes a common coolant supply plenum for all circuits in the cooled hardware. Each cooling circuit is supplied through its own individual high pressure (4000 psi) flex line leading from the manifold to the test hardware. The flow in each circuit is controlled by an orifice in the discharge side of the circuit. This location for the flow control orifices maintains high pressure in

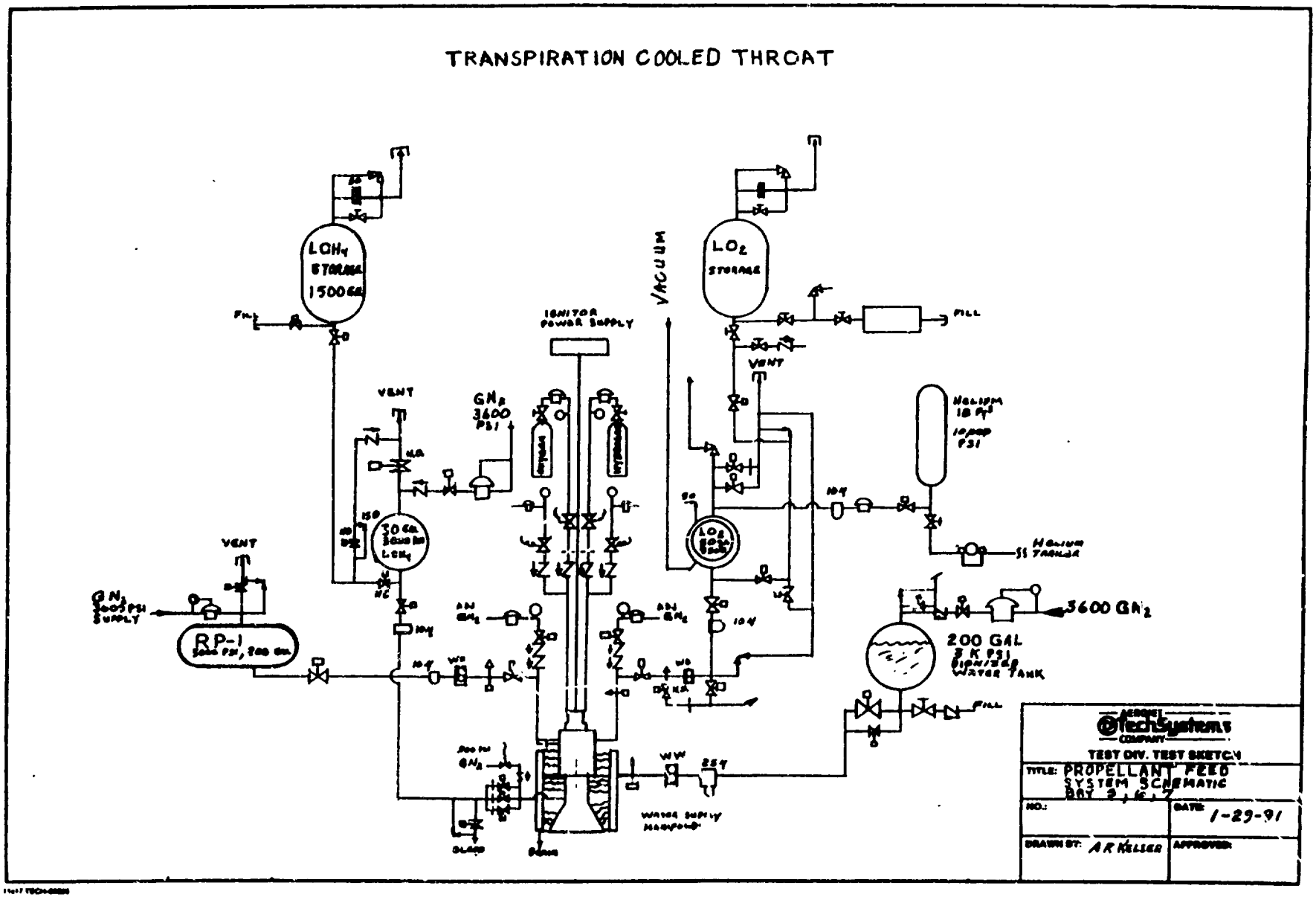

Figure 15. Propellant System Schematic

ORIGINAL PAGE IS OF POOR QUALITY

the cooling circuit and maximizes the burnout safety factor. The individual cooling circuits discharge through flex lines to a common discharge manifold and thence to a drain.

4.3.7.1 Purges

4.3.7.1.1 Oxidizer Purge

The oxidizer circuit was provided with a dry GN_2 purge. The GN_2 conformed to specification MIL-P-27401. It was passed through a 10-micron (nominal) filter before entering the oxidizer circuit. Maximum dew point requirement was -50°F. The purge pressure provided an oxidizer injector cold-flow pressure of 80 psia.

4.3.7.1.2 Fuel Purge

The fuel circuit was provided with a GN_2 purge. The GN_2 conformed to Specification MIL-P-27401. It was passed through a 10-micron (nominal) filter before entering the fuel circuit. The purge pressure provided a fuel injector cold-flow pressure of 80 psia.

4.3.7.1.3 Igniter Purge

The igniter fuel and oxidizer circuits were provided with GN_2 purges. The GN_2 conformed to Specification MIL-P-27401. The minimum purge pressure was 2,800 psia. This purge was activated during the testing such that there is no backflow of LO_2/RP-1 propellants or combustion products into the igniter.

4.3.8 Instrumentation

An instrumentation list is provided in Table 6. Figure 16 shows instrumentation location. The calorimeter instrumentation consisted of a pressure transducer and thermocouple probe in the coolant water supply manifold, an orifice plate, pressure transducer and thermocouple probe in each of the calorimeter channel outlets, and a pressure transducer in the coolant water outlet manifold. The bulk temperature rise and flowrate in each channel was used to calculate the average heat flux at that location.

The transpire flowrate instrumentation is illustrated in Figure 17. The manifold feeding the transpire cooled section contained three orificed circuits controlled by independent remote valves. This configuration allows three different flowrates during any single test.

TABLE 6

INSTRUMENTATION LIST

Parameter	Symbol	Transducer Type	Range	Accuracy ± % Reading	Recording Device FM	O'Graph	Digital
Oxidizer Tank Pressure	POT	Strain Gauge	0-3000 psi	.25		X	X
Oxidizer Flowmeter Pressure	POFM	Strain Gauge	0-3000 0psi	.25			X
Igniter Oxidizer Pressure	POSI	Strain Gauge	0-3000 psi	.25		X	X
Oxidizer Flowmeter Temperature	TOFM	Thermocouple	-300 to -200°F	.5			X
Igniter Oxidizer Temperature	TOS1	Thermocouple	0-200°F	.5			X
Oxidizer Flowrate	WO-1	Turbine	0-2#/sec	.5		X	X
Fuel Tank Pressure	PFT	Strain Gauge	0-3000 psi	.25		X	X
Fuel Flowmeter Pressure	PFFM	Strain Gauge	0-3000 psi	.25			X
Igniter Fuel Pressure	PFSI	Strain Gauge	0-3000 psi	.25		X	X
Fuel Flowmeter Temperature	TFFM	Thermocouple	50 to 100°F	.5			X
Igniter Fuel Temperature	TFS1	Thermocouple	50-100°F	.5			X
Fuel Flowrate	WF-1	Turbine	0-2#/sec	.5		X	X
Oxidizer Control Valve Trace	LTOCV	Potentiometer	0-100%	1.0		X	X
Fuel Control Valve Trace	LTFCV	Potentiometer	0-100%	1.0		X	X
Oxidizer Control Valve Signal	VOCV	Voltage	--	--		X	X
Fuel Control Valve Signal	VFCV	Voltage	--	--		X	X
Oxidizer Igniter Valve Trace	LTOIV	Potentiometer	0-100%	1.0		X	X
Fuel Igniter Valve Trace	LTFIV	Potentiometer	0-100%	1.0		X	X
Oxidizer Igniter Valve Signal	VOIV	Voltage	--	1.0		X	X
Fuel Igniter Valve Signal	VFIV	Voltage	--	--		X	X
Water Flow	WW-1	Turbine	0-20 lb/sec	.5			X
Water Inlet Temperature	TWI-1,-2	Thermocouple	50-100°F	.5			X
Water Inlet Pressure	PWI	Strain Gauge	0-3000 psia	.25		X	X
Water Outlet Pressure	PWC-1,-19	Strain Gauge	0-100 psia	.25			X
Water Outlet Manifold Pressure	PWOM-1,-2	Strain Gauge	0-2000 psia	.25			X
Water Outlet Temperature	TWC-1,-19	Thermocouple	100-300°F	.5			X
Water Outlet Manfiold Temperature	TWOM-1,-2	Thermocouple	100-300°F	.5			X

TABLE 6 (cont.)

INSTRUMENTATION LIST

Parameter	Symbol	Transducer Type	Range	Accuracy ± % Reading	Recording Device FM	O'Graph	Digital
Oxidizer Injection Pressure	POJ	Strain Gauge	0-3000 psi	0.25		X	X
Igniter Ox Injection Pressure	POJI	Strain Gauge	0-3000 0psi	0.25		X	X
Oxidizer Injection Temperature	TOJ	Strain Gauge	-300 to -200°F	0.5			X
Fuel Injection Pressure	PFJ	Strain Gauge	0-300 psi	0.25		X	X
Igniter Fuel Injection Pressure	PFJJ	Strain Gauge	0-3000 psi	0.25		X	X
Fuel Injection Temperature	TFJ	Thermocouple	50-160°F	0.5			X
Igniter Chamber Pressure	PCI	Strain Gauge	0-3000 psi	0.25		X	X
Chamber Pressure	PC-1	Strain Gauge	0-3000 psi	0.25		X	X
*High Frequency Ox Injection	KOJ	Piezoelectric	0-3000	5.0	X		
*High Frequency Fuel Injection	KFJ	Piezoelectric	0-3000	5.0	X		
Transpire Throat Temperature	TTT-1 → 24	Thermocouple	0-2000°F	0.5			X
Transpire Throat Coolant Pressure	TTCP-1,-4	Strain Gauge	0-3000 psi	0.25			X

*AC Component Only – Range for 500 psi PK-PK. 40 IPS Play Back Required.

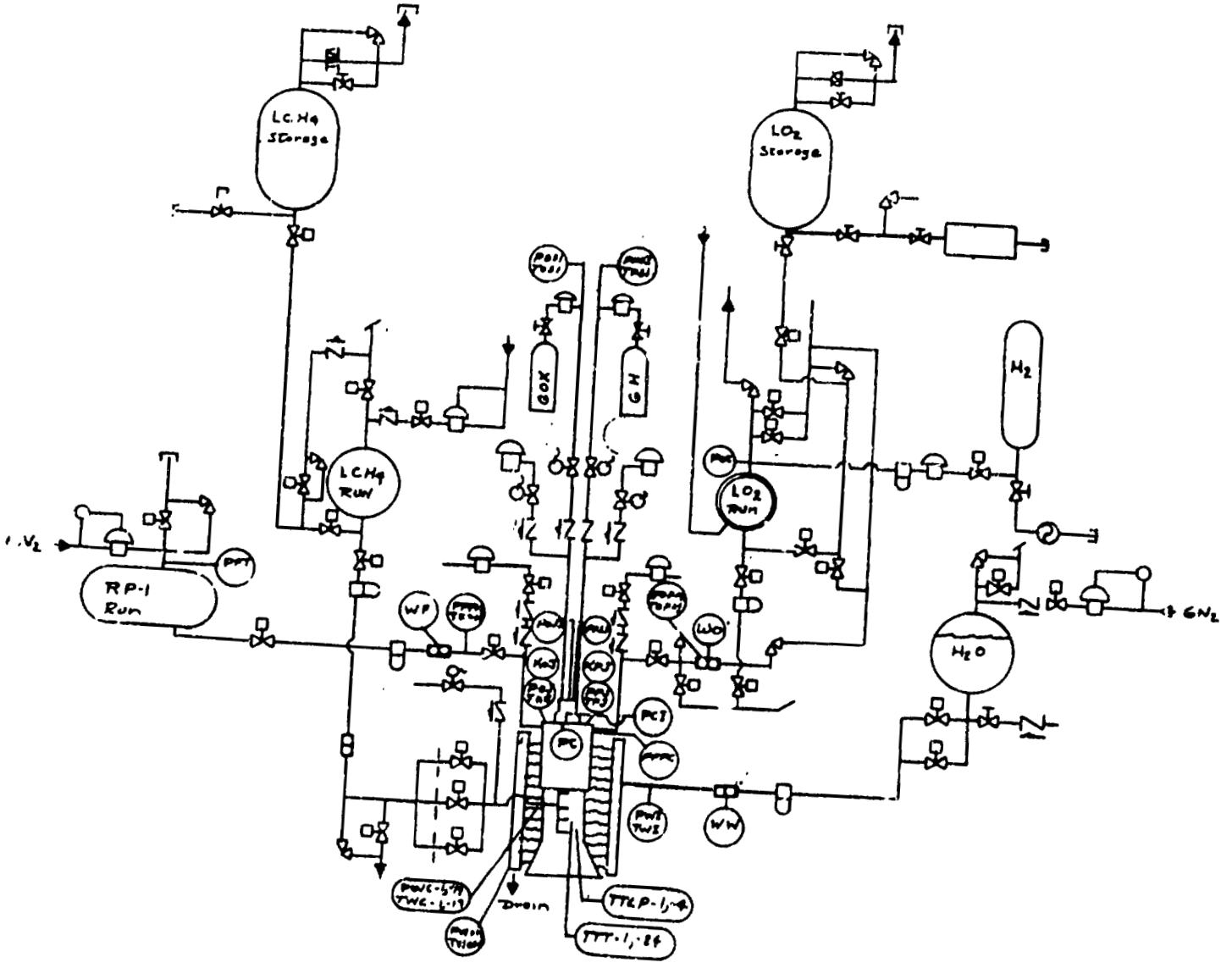

Figure 16. Facility Instrumentation

ORIGINAL PAGE IS
OF POOR QUALITY

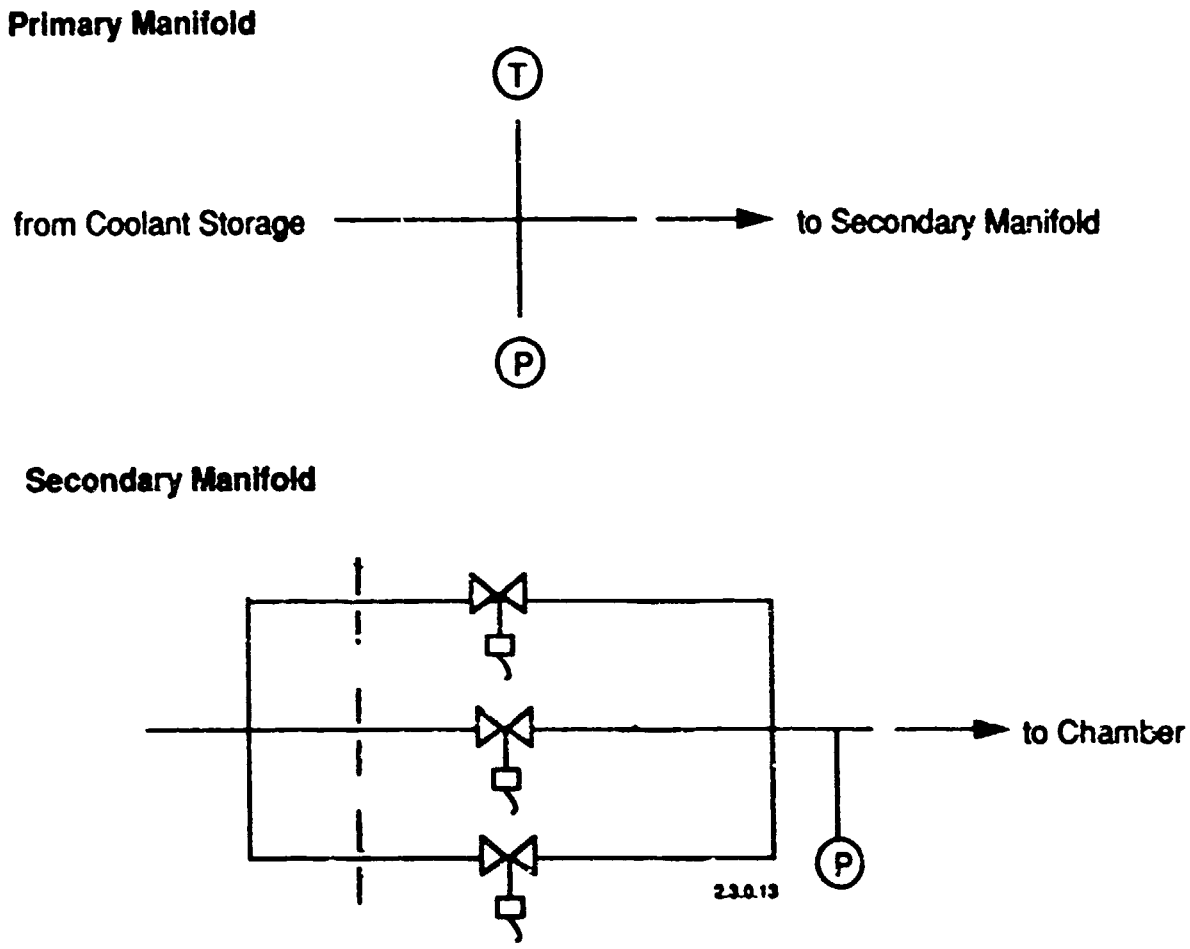

Figure 17. Transpire Flowrate Control and Instrumentation Location

4.3, Test Facility (cont.)

The instrumentation in the existing hardware, viz., the injector and barrel calorimeter sections, was the same as that used on the Carbon Deposition (NAS 8-34715) tests.

The test hardware was instrumented to measure the injector manifold pressures, the injector face pressure, and the chamber wall temperatures. The steady-state pressures are measured with Taber transducers.

High frequency injector manifold pressure oscillations were measured using Kistler pressure transducers. The Kistler output is recorded on magnetic tape and played back on the oscillograph at reduced speed for data analysis.

Calibration of the test instrumentation was maintained in accordance with MIL-C-45662 and standard Aerojet calibration procedures. The instrumentation recording system was calibrated and ranged prior to and after conducting the tests and at any other time required in order to ensure data accuracy. The calibration steps was of sufficient number and magnitude to fully define deviations of the instrumentation system and was identified by parameter and sequence.

4.4 NOZZLE TESTING

4.4.1 Calorimeter Nozzle Testing

4.4.1.1 Cold Flow Water Tests

The calorimeter circuits were water flowed to establish a Kw value for each independent circuit. This Kw data compared to the predicted valves within expected results. The measured Kw circuit values were used to compute flowrate during hot fire testing.

4.4.1.2 Calorimeter Hot Fire Testing

The combustor consisted of an H_2/O_2 igniter assembly, an OFO LOX/RP-1 triplet injector, a water cooled copper acoustic cavity and fuel film coolant manifold, and two water cooled cylindrical nickel sections, as described in section 4.1 of this report. This hardware, designed for the ongoing Carbon Deposition program, had been run previously at main chamber conditions and was considered to be a well characterized, non-streaking injector. The injector

propellant flowrate was about 1.7 lb/s at 1500 psi. The heat transfer characteristics of the injector are discussed in Ref 2.

Twelve calorimeter tests were run, as summarized on Table 7. Four tests were run at 1000 psi chamber pressure to check out the rig and to provide low chamber pressure heat flux data. The remaining tests were run at 1500 psi chamber pressure and oxygen to RP-1 fuel mixture ratios of 2.4 to 3.8. Throat heat fluxes varied from 60 to 82 BTU/in^2-s. Since the throat cooling circuits were designed for a maximum mean heat flux of 78 BTU/in^2-s, per Ref. 3, it was decided not to test at 2000 psi chamber pressure as originally planned. The extrapolated heat flux for 2000 psi chamber pressure is 103 BTU/in^2-s assuming heat flux varies as the 0.8 power of chamber pressure. The planned test duration was 20 seconds per test, but several tests were shut down by the CSM (combustion stability monitor). Similar CSM shut downs occurred on the Carbon Deposition program. On test no. 114, there was a loud hum, but no CSM shut down, at 14 seconds until end of test. During the hum, throat and convergent section heat fluxes increased 20 percent.

The maximum throat heat flux at 1500 psi chamber pressure was 82.3 B/in^2-s on test no 111. Throat heat fluxes are listed for both start and end of test, where "start" is 3 to 5 seconds into the test, and "end" is the last data point prior to shut down. On test nos. 107 to 114 there was a 2 to 13 percent increase in heat flux from beginning to end of test. On test nos. 115 to 117 this trend reversed itself and the heat flux went down about 15 percent from beginning to end of test.

Calorimeter channel axial locations and area ratios are listed in Table 8.

The axial distance of a channel was defined at the intersection of a line normal to hot gas side channel wall and the hot gas surface. Calorimeter design detail was taken from drawing nos. 1203144 and 1203145. The surface area is the hot gas wall area cooled by the circuit.

Heat fluxes were calculated from the measured cooling water bulk temperature rises and flowrates using eq. (1) below.

$$Q/A = w \quad Cp \ (T_{out} - T_{in}) \qquad (1)$$

TABLE 7

SUMMARY OF OPERATING CONDITIONS FOR CALORIMETER NOZZLE HOT FIRE TESTS

Test No.	Dur (s)	PC (psia)	O/F MR	Start Q/A *BTU/in^2-s*	End Q/A	Comment
106	2.0	967	2.4			Check out test
107	20.0	990	3.8	40.6	45.7	
108	20.0	978	2.7	50.0	56.3	
109	2.0	1520	2.5			Check out test
110	2.8	1498	3.2		78.6	Shut down on 1L
111	13.6	1500	3.2	80.1	82.3	Shut down on 1L
112	20.0	1505	3.2	75.5	77.2	
113	8.1	1519	2.8	75.1	76.3	Shut down on 1L
114	20.0	1487	2.6	71.8	72.9	Loud hum @ 14 sec
115	20.0	1486	3.8	67.6	60.0	
116	20.0	970	3.3	56.2	49.9	
117	20.0	1507	3.4	80.6	68.3	

TABLE 8

CALORIMETER CHANNEL AXIAL LOCATION

Circuit No.	Axial Dist. (in)	Dist. to Throat (in)	Wall Radius (in)	Area Ratio	Surface Area (in^2)
2	2.527	-.653	.602	5.80	.691
3	2.682	-.498	.512	4.19	.569
4	2.825	-.355	.430	2.96	.393
5	2.940	-.240	.364	2.12	.284
6	3.035	-.145	.309	1.53	.202
7	3.145	-.035	.255	1.04	.180
8	3.235	.055	.255	1.04	.177
9	3.343	.163	.304	1.48	.233
10	3.470	.290	.368	1.47	.337
11	3.600	.420	.434	3.01	.438
12	3.742	.562	.506	4.10	.465
13	3.872	.692	.572	5.23	.547

Frictional heating and water inlet temperature variation effects were negligible. Water flowrates were calculated from the measured pressure drops across the individual circuits using pre-test cold flow data. Surface areas were obtained from Table 7. Reference wall temperatures were not calculated.

4.4.1.3 Calorimeter Hot Fire Test Data Analysis

A review of the appended calorimeter data plots reveals that heat fluxes upstream from the throat, measured by circuits 02 to 06, show beginning to end of test variation, similar to the throat heat flux, circuit 07. Heat fluxes downstream from the throat, circuits 08 to 13, did not vary from beginning to end of test, nor did they increase during the hum on test no. 114.

Figure 18 shows a comparison of measured and predicted heat flux versus axial position for test no. 112. Predicted heat fluxes were obtained from Ref. 3, calculated using the SCALE integral boundary layer model with Cg correction factors based on Carbon Deposition calorimeter heat flux data. The measured throat heat flux is 20 percent greater then the SCALE prediction, but convergent section heat fluxes are up to 50 percent less than predicted. The low convergent section heat fluxes may indicate unburned propellant. These propellants could be burning in the throat, which accounts for the high throat heat flux.

4.4.2 Transpiration Cooled Nozzle Testing

4.4.2.1 Cold Flow Water Test

The calorimeter and transpire circuits were flowed independently to establish a Kw value for each circuit. These Kw values were within predicted values and were used to calculate flowrates during hot fire testing.

4.4.2.2 Methane Transpiration Cooled Hot Fire Testing

On the initial attempts to hot fire the main combustor, ignition was not obtained. This resulted in the major share of the methane coolant being expended during the bleedin/chilldown cycle for the attempted tests. The lack of ignition was attributed to the ignitor assembly. To correct the problem, the spark plug was replaced and propellant inlet pressures adjusted to reduce ignitor chamber pressure.

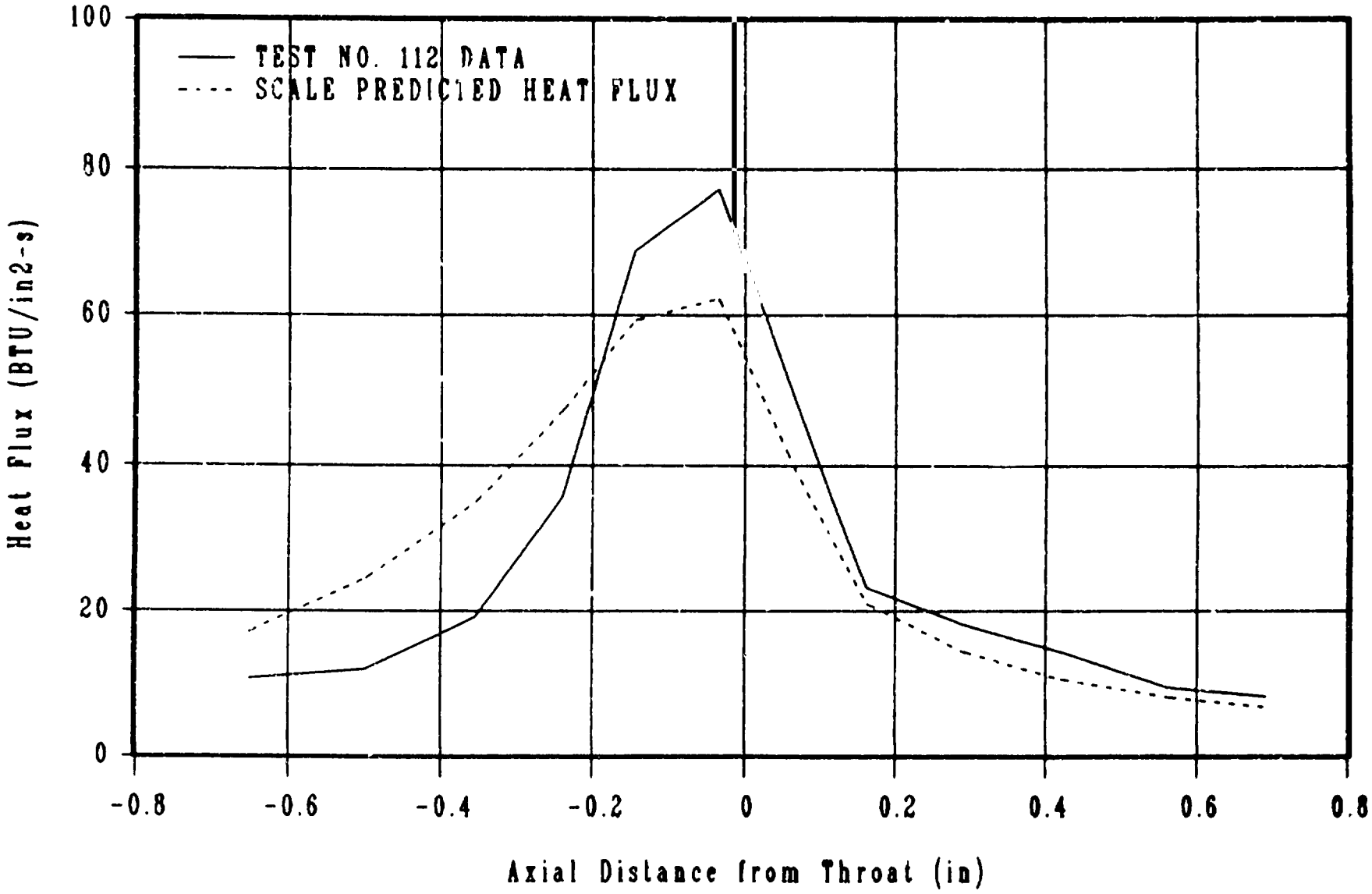

Figure 18. Axial Heat Flux Profile - Test No. KEE4 - D01 - 0A - 112

4.4, Nozzle Testing (cont.)

A single five second short duration test was completed before the methane was expended. The primary purpose of this test was for system and nozzle check out. Coolant flowrate was purposefully set high at 0.27 lbs/sec. This flowrate resulted in a throat wall temperature of -169°F, compared to a design allowable temperature of 900°F. The methane data plot from test 119 is appended. This data was insufficient to perform meaningful analysis.

4.4.2.3 RP-1 Transpiration Cooled Hot Fire Testing

After the methane tests, RP-1 transpiration cooling tests were begun. On the second test, the 12 in. calorimeter nickel barrel section burned through and the test program was terminated. The post test condition of the nozzle was excellent. There were no eroded areas or plugged slots. The throat wall temperature was about 200° F on both tests. The RP-1 transpiration flowrate was 0.21 lb/s, or 11 percent of total propellant flowrate. Of this total, about 0.15 lb/s or 8 percent of total propellant flowrate came from the first three compartments covering -0.7 in. just upstream from the throat. This is the relevant transpiration flowrate for analytical anchoring and extrapolation to full scale. The .06 lb/s flowrate in the fourth section downstream from the throat is a feature of the bench test design. A full scale engine would probably be regen cooled in this section.

For a 0.15 lb/s RP-1 transpiration flowrate, the TRANSP2 predicted throat wall temperature is about 900° F, compared to 200° F measured. The difference between the predicted and actual wall temperature is attributed to an RP-1 liquid layer at the wall not accounted for in the TRANSP2 one-dimensional gaseous analytical model. The data was correlated by a two-dimensional liquid layer heat sink model, but the lack of additional flowrate data points makes extrapolation uncertain. If the liquid layer heat sink model correlation is assumed accurate, the throat flowrate can be reduced to .05 lb/s with a coking limited design allowable wall temperature of 550° F. This is a 67% reduction in RP-1 transpiration flowrate compared to the flowrate tested.

Using the liquid layer heat sink model further, the RP-1 transpiration flowrates for a full scale 750 Klbf LOX/RP-1 engine were recalculated. The new transpiration flowrates are about 35% less than the flowrates in Ref. 1. The revised maximum Isp increase for an RP-1 engine is 10.2 seconds at 2804 psi chamber pressure, compared to 3.0 seconds in Ref. 1 over a pure regen cooled design. The following discussion is based on a review of the RP-1 cooling data from test nos. 124 and 125. Both the methane and RP-1 data plots are appended.

4.4, Nozzle Testing (cont.)

Operating conditions for the two RP-1 tests are listed on Table 9. The planned test duration was 60 seconds. During this run time, three different coolant flowrates were to be tested, starting with maximum flowrate, then throttling down at 20 and 40 seconds. However, on test no. 124, an operating limit kill was encountered after the first 20 seconds, and on test no. 125 the 12 in. barrel section failure shut down the test at 13 seconds. Therefore, only one flowrate was run on each test.

There were three operational thermocouples which provided wall temperature data. Their axial and radial thermocouple placement is listed in Table 10.

The thermocouple of primary interest is TNC10C since it is closest to the hot gas wall in the throat where the maximum heat flux occurs. On test no. 124 the maximum temperature at TNC10C was 169° F. The RP-1 transpiration coolant flow was 0.26 lb/s. On test no. 125, the maximum temperature at TNC10C was 177°F and the RP-1 transpiration flowrate was 0.21 lb/s. There were other thermocouples installed in the nozzle, but only the three listed above were operational.

The RP-1 transpiration coolant distribution for test no. 125 is shown in Table 11.

In this report, the flow sections are numbered in the hot gas flow direction, i.e., section 01 is closest to the injector. For clarity, the upstream axial distance for each section is given. There was 0.15 lb/s of RP-1 injected from sections 01, 02 and 03, which cover -0.7 in. upstream from the throat. This flowrate maintains the throat temperature as measured by thermocouple TNC10C. The RP-1 flowrate from section 04 is injected downstream from the throat and therefore does not affect throat temperature.

Since only the total RP-1 coolant flowrate was measured, the RP-1 flowrate distribution had to be determined analytically. The calculation was made using the Ref. 5 hydraulic model modified by a 0.7 flowrate correction factor based on cold flow data. A complete summary of flowrate by platelet is given in Table 12.

The TRANSP2 predicted wall temperature for an RP-1 transpiration flowrate of 0.15 lb/s RP-1 is 900° F. Thus, the analytical model appears to contain a significant error. One possible explanation for the difference between measured and predicted wall

TABLE 9

OPERATING CONDITIONS FOR RP-1 TRANSPIRATION COOLING TESTS

	Test No. 124	Test No. 125
Chamber Pressure	1538	1536 PSIA
Mixture Ratio	3.5	3.5
OX Flowrate	1.35	1.34 LB/S
RP-1 Fuel Flowrate	0.38	0.38 LS/S
RP-1 Transpire Flowrate	0.26	0.21 LB/S
Duration	20	13 SEC
Throat Temperature	169	176 F

TABLE 10

THERMOCOUPLE LOCATION

T/C No.	Axial Dist. from Throat (in)	Radial Dist. from Hot Gas (in)	Test No. 124 Temperature (F)	Test No. 125 Temperature (F)
TNC10C	0	0.05	169	177
TNC11C	0	0.15	115	122
TNC13D	0.180	0.05	112	113

TABLE 11

RP-1 TRANSPIRATION COOLANT FLOWRATE SUMMARY

BY SECTION FOR TEST KEE4-D01-0A-125

Section No.	Axial Dist. (in)	Cooled Length (in)	Manifold Pressure (PSIA)	Flowrate (lb/s)
1	-0.70	0.27	1966.	0.0434
2	-0.43	0.23	1966.	0.0498
3	-0.20	0.20	1966.	0.0533
4	0.20	0.20	1966.	0.0600
TOTAL				0.21

Table 12. Calculated RP - 1 Coolant Flowrate Distribution for Test No. KEE4 - D01 - 0A - 125

METER NO	AXIAL DIST (IN)	AREA RATIO	MANIFOLD PRESS (PSI)	WALL PRESS (PSI)	DELTA PRESS (PSI)	FLOW RATE (LB/S)
SECTION 01						
1	2.482	6.31	1966.0	1508.4	457.5	0.00418
2	2.502	6.08	1966.0	1507.7	458.3	0.00419
3	2.530	5.76	1966.0	1506.9	459.1	0.00419
4	2.558	5.46	1966.0	1505.4	460.6	0.00420
5	2.586	5.16	1966.0	1504.6	461.3	0.00420
6	2.614	4.87	1966.0	1503.1	462.8	0.00421
7	2.642	4.59	1966.0	1501.6	464.4	0.00422
8	2.670	4.32	1966.0	1499.3	466.6	0.00423
9	2.698	4.05	1966.0	1497.1	468.9	0.00425
10	2.726	3.80	1966.0	1494.8	471.1	0.00555
SECTION 02						
11	2.762	3.48	1966.0	1490.2	475.7	0.00428
12	2.790	3.24	1966.0	1486.4	479.5	0.00430
13	2.818	3.01	1966.0	1481.1	484.8	0.00564
14	2.846	2.79	1966.0	1475.1	490.9	0.00560
15	2.874	2.58	1966.0	1468.2	497.7	0.00573
16	2.902	2.38	1966.0	1459.2	506.8	0.00579
17	2.930	2.18	1966.0	1447.8	518.2	0.00767
18	2.958	1.99	1966.0	1432.6	[illegible]3.4	0.01068
SECTION 03						
19	2.994	1.77	1966.0	1408.4	557.6	0.00801
20	3.022	1.60	1966.0	1381.1	584.9	0.00824
21	3.050	1.44	1966.0	1343.2	622.8	0.00856
22	3.078	1.29	1966.0	1287.8	678.1	0.00690
23	3.106	1.17	1966.0	1216.6	749.3	0.00732
24	3.134	1.08	1966.0	1116.5	849.4	0.00606
25	3.162	1.04	1966.0	1059.7	906.3	0.00820
SECTION 04						
26	3.198	1.00	1966.0	877.0	1089.0	0.00914
27	3.226	1.04	1966.0	686.0	1279.9	0.00772
28	3.254	1.10	1966.0	582.1	1383.8	0.00809
29	3.282	1.18	1966.0	495.0	1470.9	0.00838
30	3.310	1.32	1966.0	397.2	1568.7	0.00870
31	3.338	1.46	1966.0	332.8	1633.1	0.00891
32	3.366	1.62	1966.0	279.7	1686.2	0.00908

temperatures is that the TRANSP2 calculation did not include RP-1 liquid layer effects. This hypothesis is examined in the data correlation section below.

A transient analysis of the thermocouple temperature data from test no. 125 indicates a throat heat flux of about 2.5 BTU/in^2-s. This is a 97% reduction compared to 80 BTU/in^2-s without RP-1 cooling. The transient analysis was performed using the IMPL fin model. Several combinations of heat transfer coefficient and hot gas temperature fit the data, as shown if Figure 19. Thus, although the wall heat flux can be calculated from the data, it is not possible to separate the wall recovery temperature and heat transfer coefficient.

Data Correlation

Ref. 5 used a modified porous wall analytical model, TRANSP2, to predict transpiration flowrates for the subscale nozzles. In this model, the hot gas side heat flux is reduced from the no blowing value using a blockage correlation derived from sintered wall gaseous cooling data. On the coolant side, a fin model is used to calculate the coolant blowing core gas recovery temperature. In other words, all heat flux reductions are lumped into the heat transfer coefficient.

RP-1 is injected as a liquid, and probably forms a liquid layer next to the wall. Thus, as in liquid film cooling, the primary wall protection mechanism may be wall film temperature reduction. This would be especially likely for high coolant flowrates where most of the liquid carries over from upstream injection. For thin liquid layers there are several analytical methods. Ref. 6 assumes a diffusing coolant vapor at the surface which reduces the wall heat flux in the same manner as in transpiration. Ref. 7 treats the liquid layer as an isothermal heat sink and imposes an empirically derived efficiency methods assume an adiabatic wall.

Neither of the above methods fully describe the present case. Because the nozzle wall is not adiabatic, it is necessary to predict both the hot gas side heat transfer coefficient as well as the RP-1 layer temperature to perform a wall energy balance. The heat transfer coefficient cannot be easily calculated since it requires an estimate of the velocity and temperature boundary layer profile in the liquid layer. No such information is readily available.

It is possible to calculate the RP-1 layer bulk temperature if an energy balance with the core gas is assumed wherein the heat flux to the annular liquid RP-1 layer is equal

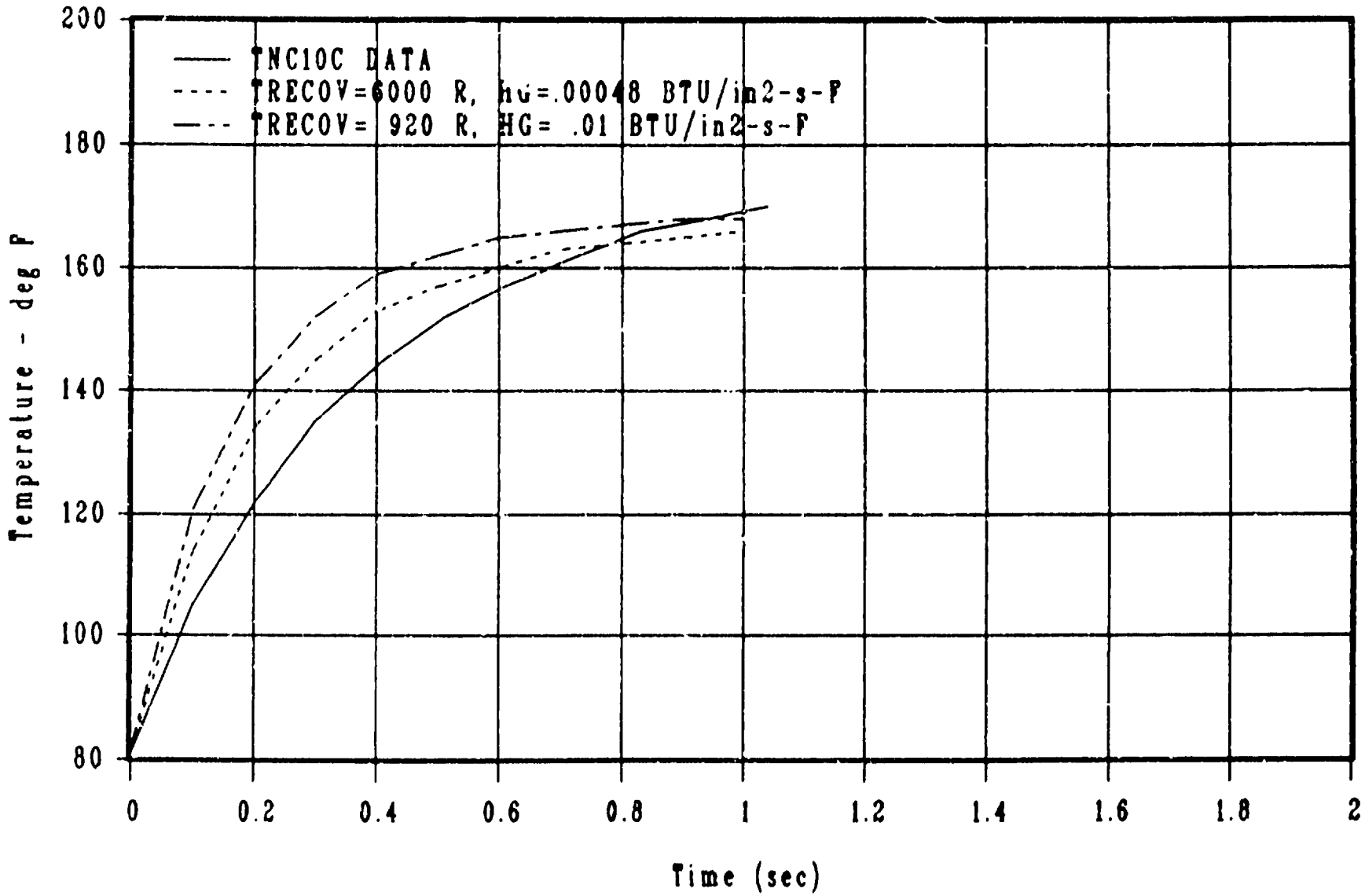

Figure 19. Throat Temperature History - Test No. KEE4 - D01 - 0A - 125

to the heat flux to a solid wall. The heat load can then be taken directly from the calorimeter nozzle heat load data. For test no. 117, where the injector mixture ratio was 3.4, the heat load up to the throat was 31.4 BTU/s. This heat load is assumed for test no. 125 since the chamber pressure and mixture ratio were about the same. For test no. 125, the RP-1 flowrate up to the throat was 0.15 lb/s. Thus the calculated energy balance RP-1 layer bulk temperature at the throat is 460° F, using an average specific heat of 0.55 BTU/lb-F. The RP-1 temperature is higher than the wall temperature because the wall is internally cooled by RP-1 forced convection. If the 460° F bulk temperature is used as the driving temperature for heat transfer, a heat transfer coefficient of .01 BTU/in^2-s-F is inferred from the transient data. Now, if the heat transfer coefficient is assumed constant, and the above method is repeated, the predicted flowrate for a 550° F wall is .05 lb/s, or about 67% less than the 0.15 lb/s throat flowrate on test no. 125.

The liquid layer model used above is a simple model which does not treat any of the gas and liquid dynamics. It is unlikely that such a model would correlate data obtained over a wide range of coolant flowrates. If future tests are conducted and the data is not correlated by the heat sink approach, it may be useful to modify TRANSP2 to account for liquid layer effects. These include: (1) liquid layer build up similar to downstream cooling in the gaseous model; (2) heat transfer reduction at the core gas interface due to RP-1 vapor, similar to the current gaseous blockage model; and (3) liquid layer boundary layer analysis to determine the wall heat transfer coefficient.

Full Scale Engine Cooling

RP-1 transpiration flowrates for a 750 Klbf engine were reported in Ref 1, Table 8. Flowrate requirements varies from 32.2 lb/s to 211 lb/s, or 1.2 to 8.5 percent of total propellant, depending on cooled length. A coking limited 550° F wall temperature was assumed for the hot gas wall with RP-1 transpiration. RP-1 flowrates were recalculated using the liquid layer heat sink approach described above and were found to be reduced by about 35%, as shown in Table 13. The new RP-1 flowrates are 0.8 to 5.9 percent of total propellant flowrate. The maximum sea level Isp increase is 10.2 seconds when the cooled length is 32 in. The previous maximum Isp increase was 3 seconds. The reason for the large change in Isp increase is that RP-1 transpiration is assumed to make no contribution to thrust. Therefore a reduction in RP-1 transpiration flowrate causes a proportional increase in Isp. In the above calculations, the liquid

TABLE 13

NEW BASELINE SPECIFIC IMPULSE INCREASE WITH RP-1 COOLING

PC (psi)	L Prime (in)	Cooled Length (in)	Transpiration Flowrate (lb/s)	% Total Propellant	ISP (sec)	Delta ISP (sec)
1000	31.0	0	0.	0.	275.2	
1192	29.5	7	22.	0.8	276.5	1.3
1604	27.2	17	59.	2.3	279.3	4.1
2004	25.6	25	101.	4.0	282.0	6.8
2804	23.2	32	135.	5.9	285.4	10.2

layer heat transfer coefficient to the wall was set equal to the core gas wall heat transfer coefficient from the SCALE computer program.

For the case where RP-1 chamber pressure is maintained at 1000 psi, the turbopump discharge pressure can be reduced from 8000 psi to 4010 psi with an associated RP1 transpiration flowrate of 80 lb/s, compared to 120 lb/s previously. The new performance loss for this case is 8 seconds.

A note of caution needs to be added in regards to the use of the above data. Although these preliminary RP-1 data appear promising, the single data point and the lack of a verified analytical model makes extrapolation highly uncertain. The predictions for the full scale engine should therefore be regarded as preliminary and further investigations undertaken to enlarge the available database.

REFERENCES:

1. Sieger, S. N., "Interim Report for Task I- Engine Analysis," Contract NAS 8-36952, July 1989.

2. Hernandez, R., et. al, "Carbon Deposition Model for Oxygen Hydrogen Combustion," Interim Final Report 2427-IFR, Contract NAS 8-34715, September 1987.

3. Kim, D., "Thermal Analysis for Subscale Regerative Cooled Nozzle", Presented at Preliminary Design Review, 7 November 1988.

4. May, L.R., "Subscale Hardware Hot Fire Testing Test Plan", Contract NAS 8-36952, February 1991.

5. Sieger, S.N., "Thermal Analysis for Transpiration Cooled Throat Platelet Bench Test Nozzles", EAR No. 9986:2589.

6. Rosenhow, Warren M. ed., "Handbook of Heat Transfer Applications," McGraw-Hill Book Company, 2nd Edition, 1985, pp. 1-48 to 1-51.

7. Huzel, Dieter K., and Huang, David H., "Design of Liquid Propellant Rocket Engines," NASA SP-125, 1971, pp. 115-116.

APPENDIX A

SYMBOLS, NOMENCLATURE

AND UNIT CONVERSION FACTORS

LIST OF SYMBOLS

B	λ/St_o, blowing parameter
B′	λ/St, reduced blowing parameter
Cp	specific heat
F	thrust
h	enthalpy
I_{SL}	sea-level specific impulse
k	thermal conductivity
m	molecular weight
M	Mach no.
MW	molecular weight
Pc	chamber pressure
Pr	Prandtl number
q	heat flux
r	fin equation coefficient
Re	Reynolds number
St	Stanton number
T	temperature
u	velocity
w	flowrate
λ	$(\rho u)c/(\rho u)e$, injection ratio
ε	exit area ratio
ρ	density
Subscripts	
c	coolant
cm	coolant manifold
cr	critical
e	boundary layer edge
o	without blowing
r	recovery
T	total
TC	transpiration coolant
w	wall

NOMENCLATURE

AN	Air Force/Navy Standard fitting
A_t	Throat area
APD	Aerojet Propulsion Division
BOSF	Burn Out Safety Factor
C_DA	effective area for fluid flow
Cg	h_g (experimental/h_g (theoretical)
Cg, in	h_g (experimental/h_g (theoretical)
C_p	specific heat at constant pressure
CC*	characteristic velocity
C^*_{gas}	gas characteristic velocity
C^*_{test}	characteristic velocity from test data
C^*_{ODE}	characteristic velocity from ODE
C/H	carbon to hydrogen mole ratio
CH_4	chemical formula for methane
C_2H_2	chemical formula for acetylene
C_2H_4	chemical formula for ethylene
C_2H_6	chemical formula for ethane
C_3H_6	chemical formula for propylene
C_3H_8	chemical formula for propane
$C_{12}H_{26}$	chemical formula for RP-1
D_c	chamber diameter
Dia	diameter
D_o	oxidizer injector orifice diameter
D_f	fuel injector orifice diameter
D_t	throat diameter
EB	Electron Beam Welding
EDM	Electro Discharge Machining
FFC	fuel film cooling
FOF	fuel-oxidizer fuel injector pattern
FRCM	Fuel Rich Combustion Model
FTY	yield strength
g_c	gravitational constant
GG, gg	gas generator

GH_2, gH_2	gaseous hydrogen
GN_2	gaseous nitrogen
GOX	gaseous oxygen
H_2	hydrogen
H_2O	water
HC	hydrocarbon
h_g	heat transfer coefficient
Isp	specific impulse
JANNAF	Joint Army, Navy, NASA, Air Force
KOJ	Kistler high-frequency pressure transducer-oxidizer
KFJ	Kistler high-frequency pressure transducer-fuel
Kw	hydraulic admittance
L/D	length-to-diameter ratio
LH_2	liquid hydrogen
LNG	liquified natural gas
L'	chamber length
LOX, LO_2	liquid oxygen
1L	first longitudinal mode instability
M_{inner}	momentum through inner circle of injection elements
M_{outer}	momentum through outer circle of injection elements
MR	mixture ratio
MR_{gas}	gas mixture ratio
MRGG	gas generator mixture ratio
MW	molecular weight
NASA/LeRC	NASA Lewis Research Center
NBP	normal boiling point
Ni	chemical symbol for nickel
nom	nominal
O_2	chemical formula for oxygen
O/F, w_{ox}/w_f	mixture ratio
ODE	One Dimensional Equilibrium
OFHC	oxygen-free high-conductivity copper
OFO, O-F-O	oxidizer-fuel-oxidizer injector pattern
OMS	Orbital Maneuvering System
ox, OXID	oxidizer
P_c or PC	chamber pressure

$P_{c\ cav}$	pressure in acoustic cavity (Taber transducer)
P_{cav} HF	pressure in acoustic cavity (Kistler transducer)
$P_{coolant\ in}$	coolant inlet pressure
$P_{coolant\ out}$	coolant outlet pressure
PCTSD	chamber pressure downstream of turbine simulator
PCTSU	chamber pressure upstream of turbine simulator
Pk-to-Pk	peak-to-peak
PFJ	fuel injection pressure
P_{gas}	gas pressure
P_{in}	inlet pressure
$P_{manifold\ out}$	manifold outlet pressure
POJ	oxidizer injection pressure
PRTSC	PCTSD/PCTSSU
PWC	pressure of water coolant
PWI	inlet pressure of water coolant
R	gas constant
RAD	radius
RP-1	hydrocarbon fuel similar to kerosene
SINDA	Systems Improved Numerical Differencing Analyzer
T_{gas}	gas temperature
TC or T/C	thermocouple
TCA	thrust chamber assembly
$T_{coolant\ in}$	coolant inlet temperature
$T_{coolant\ out}$	coolant outlet temperature
TCR	thermocouple reading
TIG	Tungsten Inert Gas Welding
$T_{manifold\ out}$	manifold outlet temperature
TRAN72	computer program to calculate thermodynamic and transport properties of complex mixtures
TWC	temperature of water coolant
V_c	chamber volume
w_f	fuel flow rate
w_{ox} or w_o	oxidizer flow rate
w_t, WTOT	total flow rate

Zr-Cu, ZrCu	zirconium-copper alloy
ΔH	enthalpy
ΔP	pressure drop
η_c^*	c^*_{test}/c^*_{ode}
ε_c	area ratio in convergent section
ε_e	area ratio in divergent section
γ	gas specific heat ratio, c_p/c_v
φ_g	gas side heat flux
ρ	fluid denisty
τ	gas residence time

UNIT CONVERION FACTORS (ENGLISH TO SI)

1 Btu/in.^{2}-s	=	0.163 kW/cm^2
1°F	=	32 + 1.8 (°K - 273)
1 ft/s	=	30.48 cm/s
1 in.	=	2.54 cm
1kcal/mol	=	4.184 kJ/mol
1 lbm/s	=	0.45359 kg/s
1 psi	=	0.006895 MPa

APPENDIX B

HARDWARE DRAWINGS

Hardware Drawings

Drawing No.	Title
1203144	Transpiration and Calorimetric Cooled Nozzle Assy
1202345	Liner Assembly and Details
1203147	Housing
1203148	Platelet Stack Assy
1203149	Platelet Separator Assy
1203151	Ring, Platelet Manifold
1203153	Tube Assy
1203146	Manifold Cylinder
1204604	Adaptor, Fitting Instrumentation

Carbon Deposition Hardware

1195815	Thrust Chamber Assembly
1195813	Chamber Barrel Section
1195777	Injector Assembly (Fine Pattern)
1195812	Resonator Ring Fuel Film Cooling Assy
1195851	Turbulence Ring Fuel Film Cooling Assy
1195852	Resonator Tuning Ring

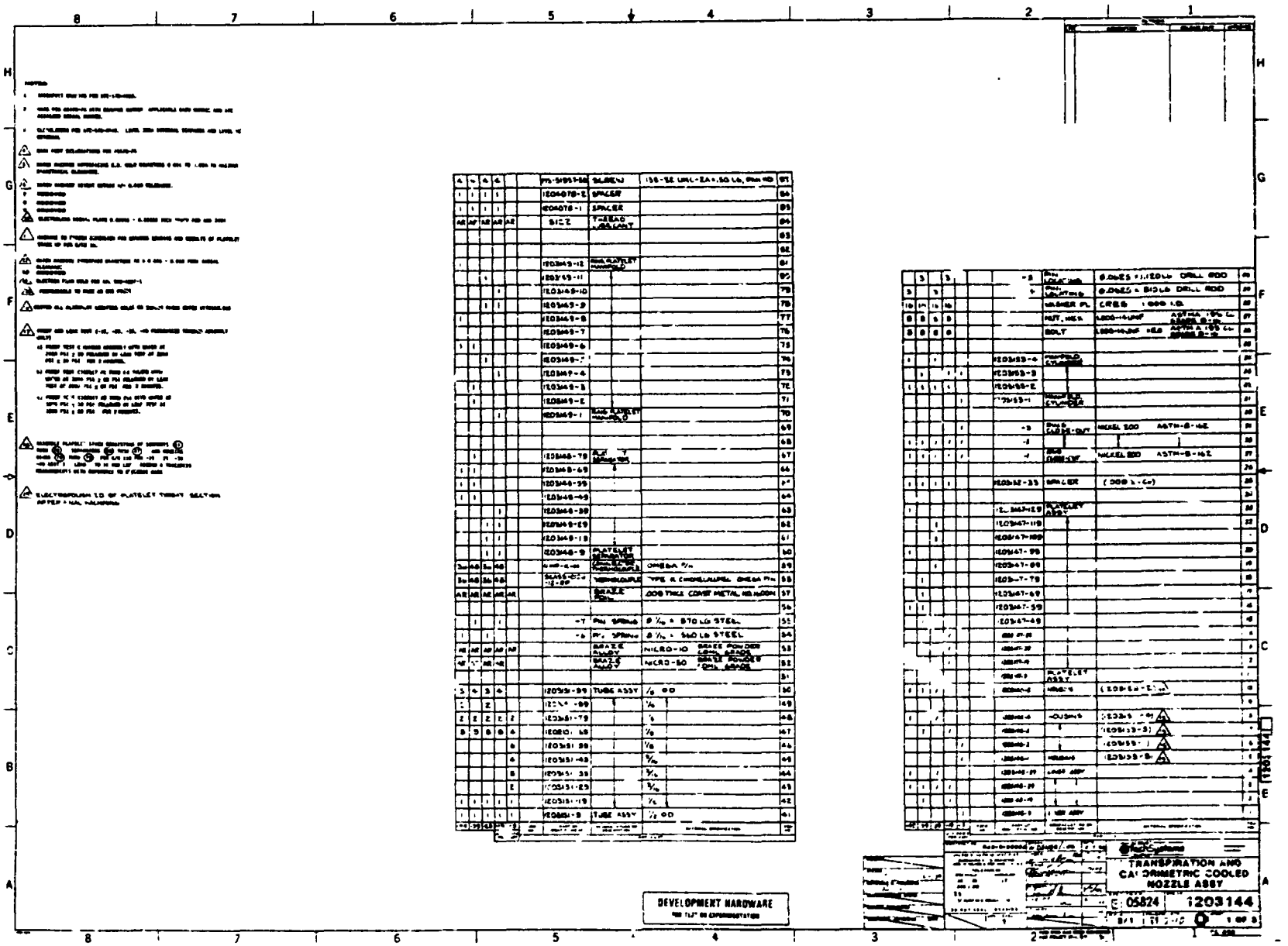

Figure B - 1

ORIGINAL PAGE IS
OF POOR QUALITY

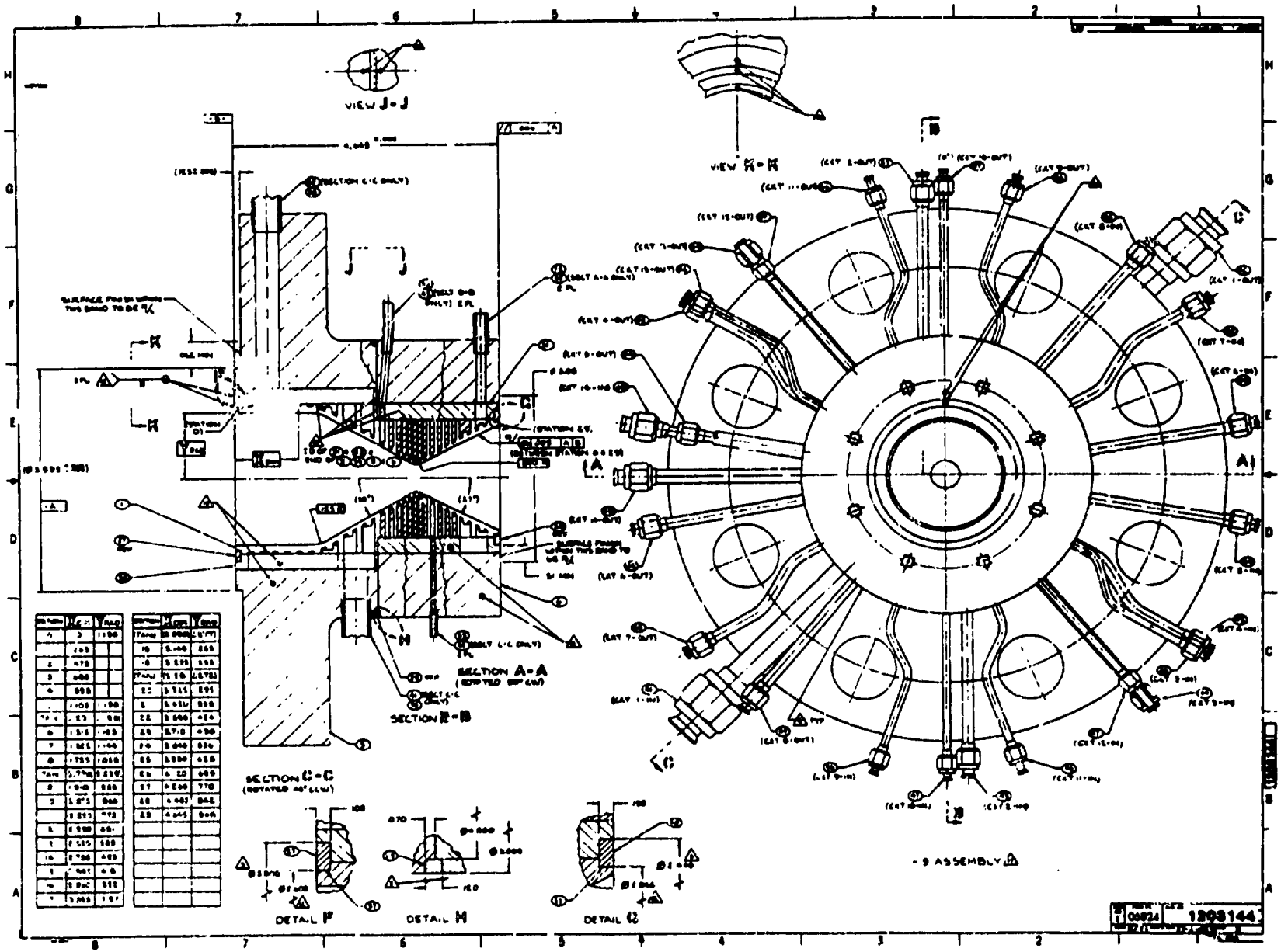

Figure B - 1 (Cont)

ORIGINAL PAGE IS
OF POOR QUALITY

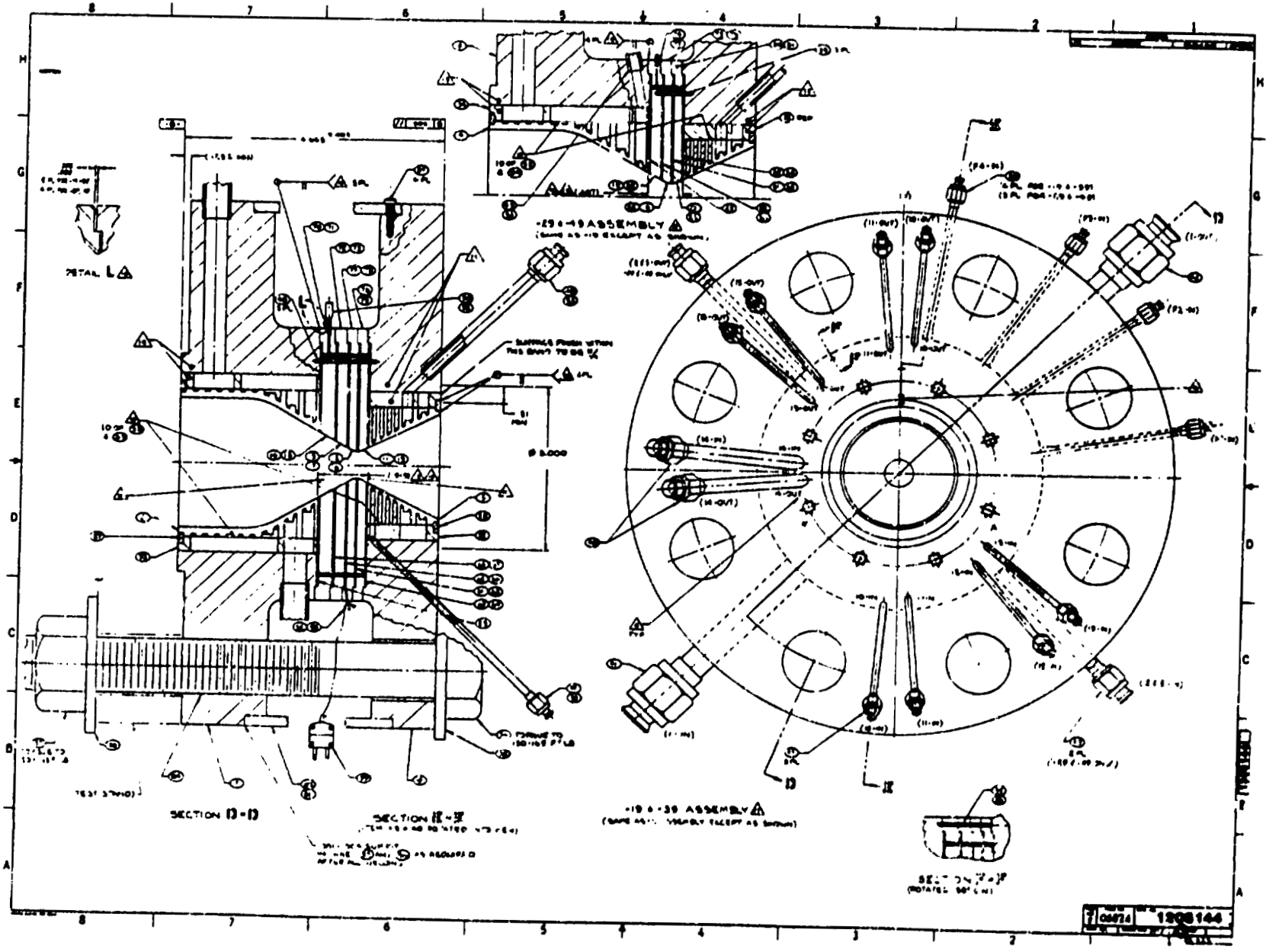

Figure B - 1 (Cont)

ORIGINAL PAGE IS
OF POOR QUALITY

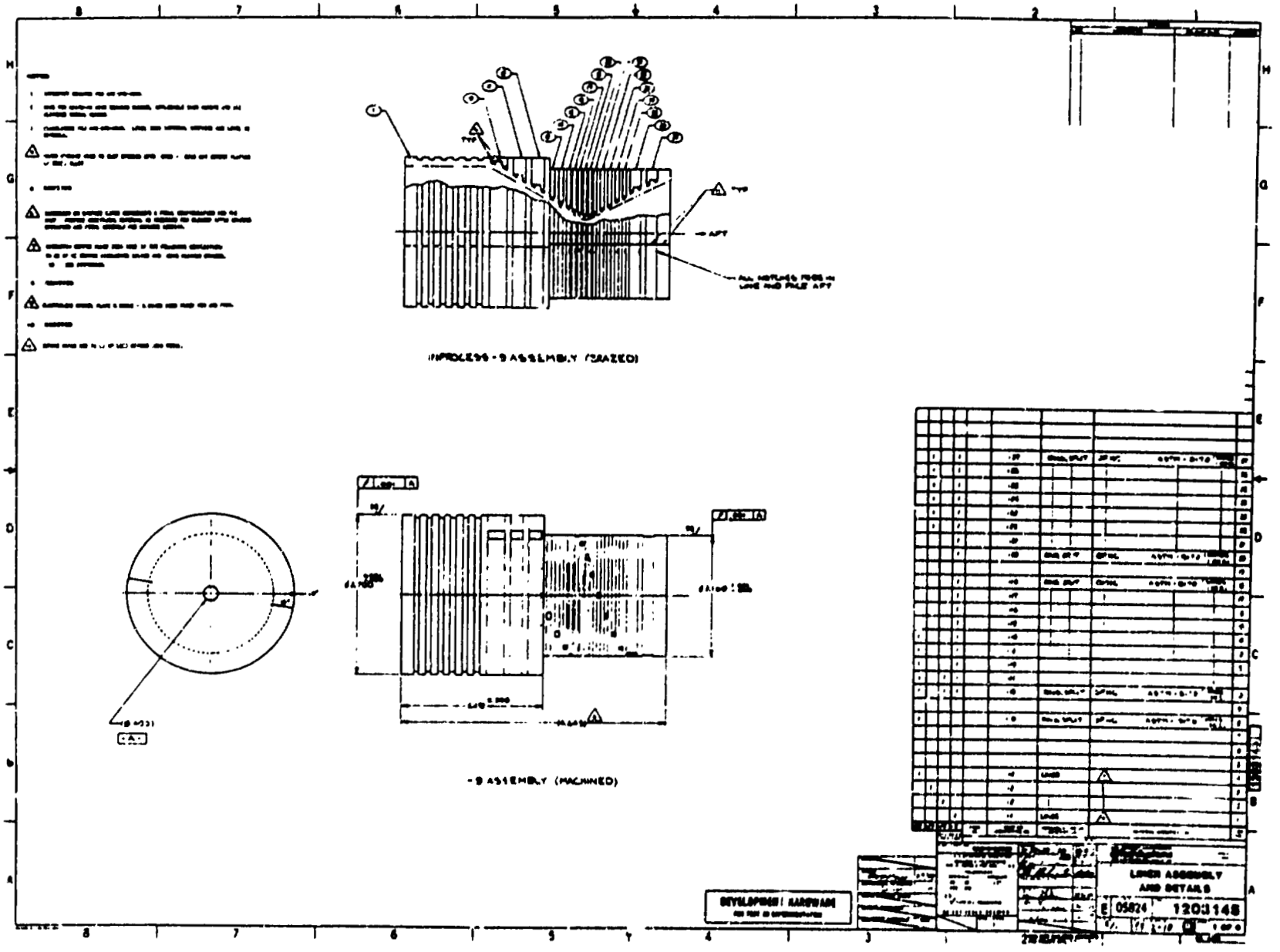

Figure B - 2

ORIGINAL PAGE IS
OF POOR QUALITY

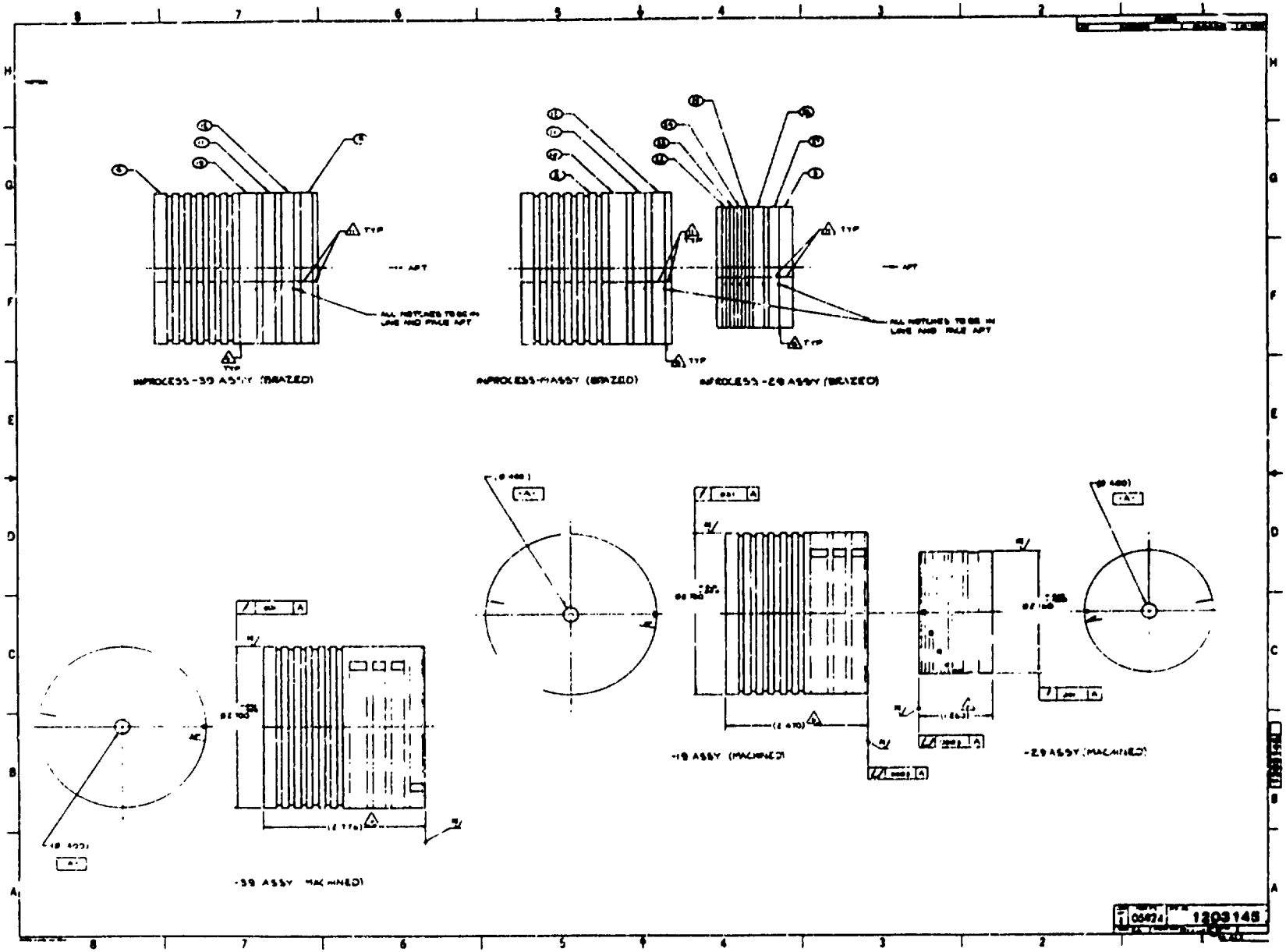

Figure B - 2 (Cont)

ORIGINAL PAGE IS
OF POOR QUALITY

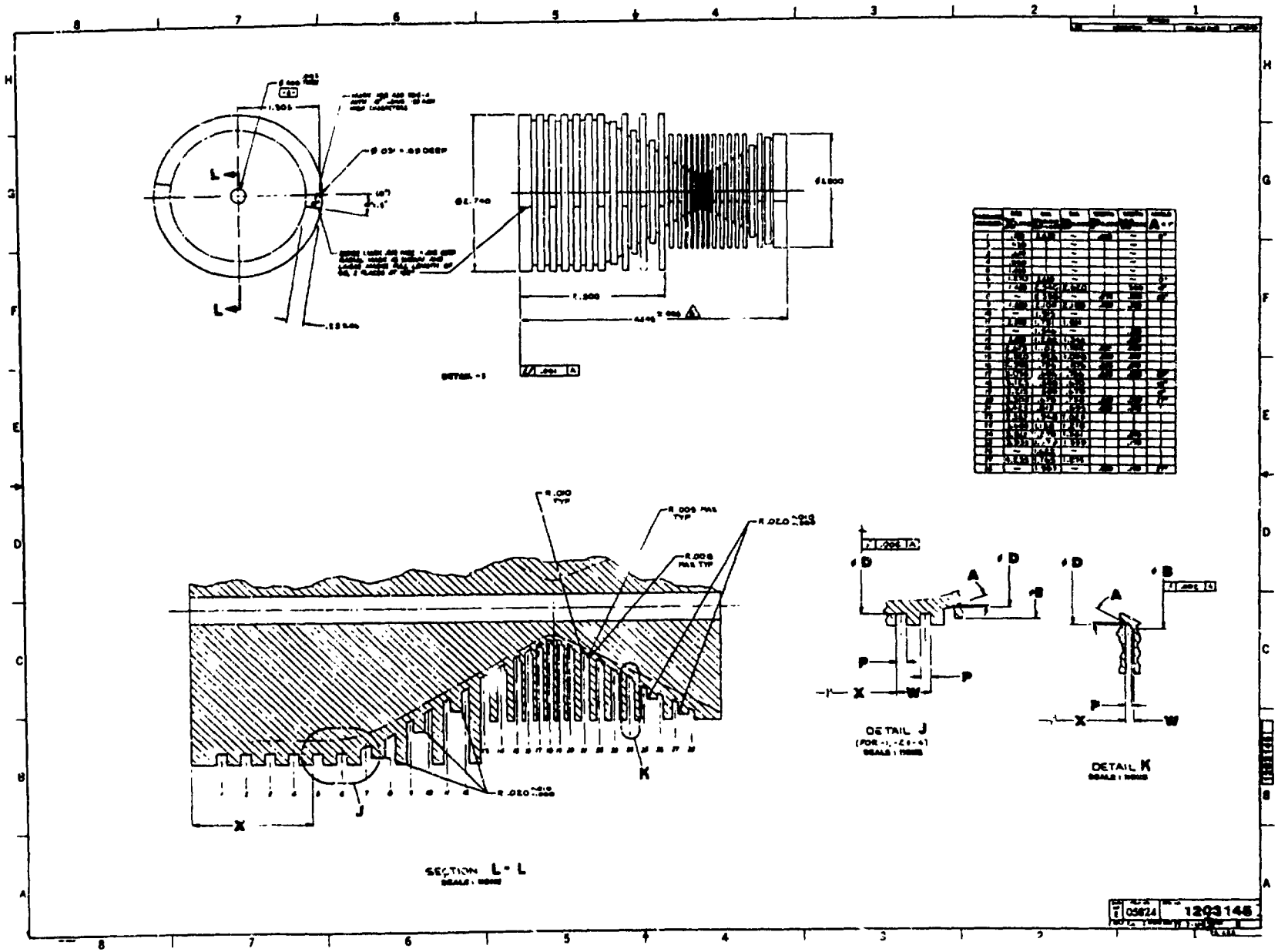

Figure B - 2 (Cont)

ORIGINAL PAGE IS
OF POOR QUALITY

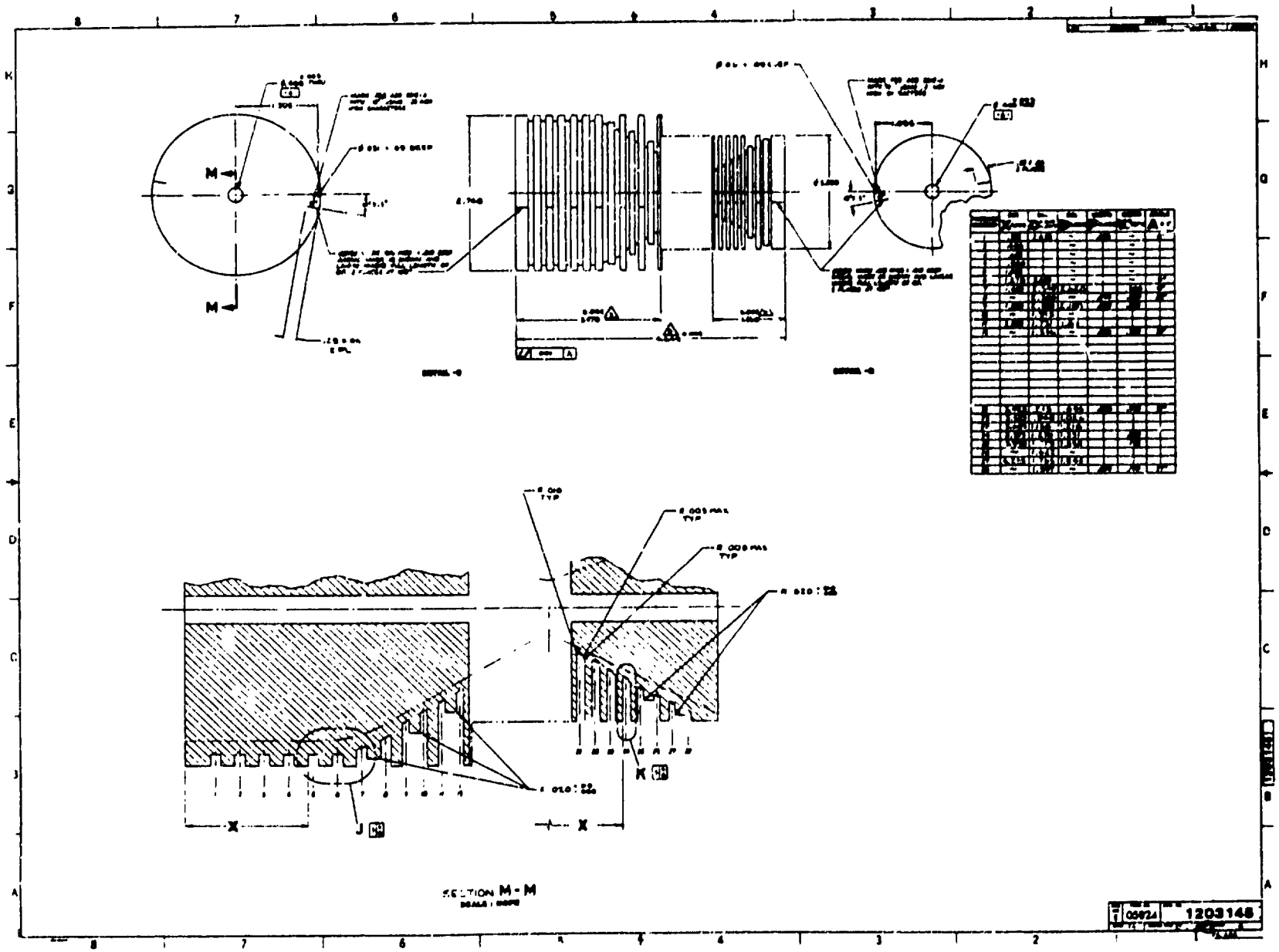

Figure B - 2 (Cont)

THIS PAGE IS OF POOR QUALITY

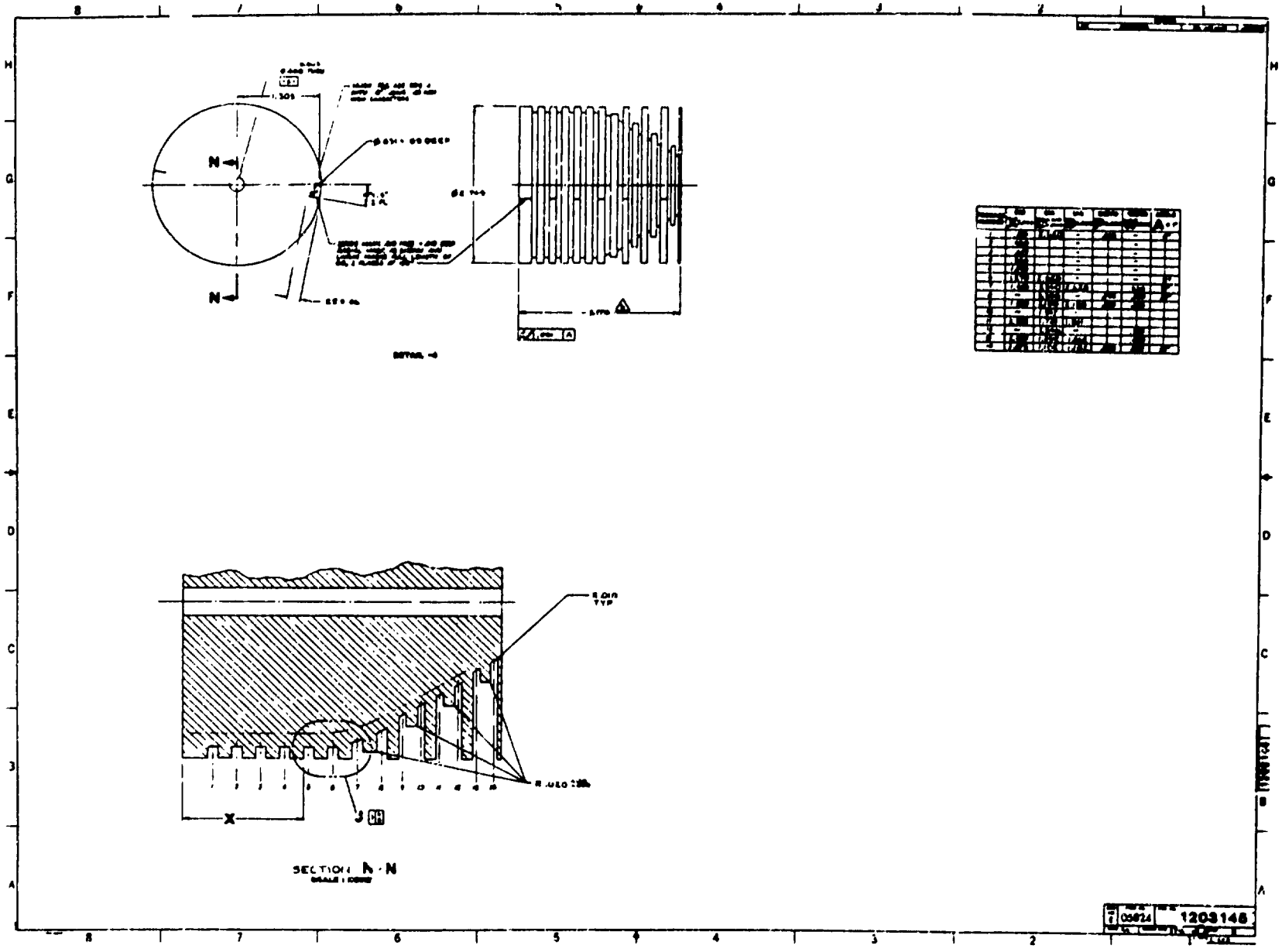

Figure B - 2 (Cont)

ORIGINAL PAGE IS
OF POOR QUALITY

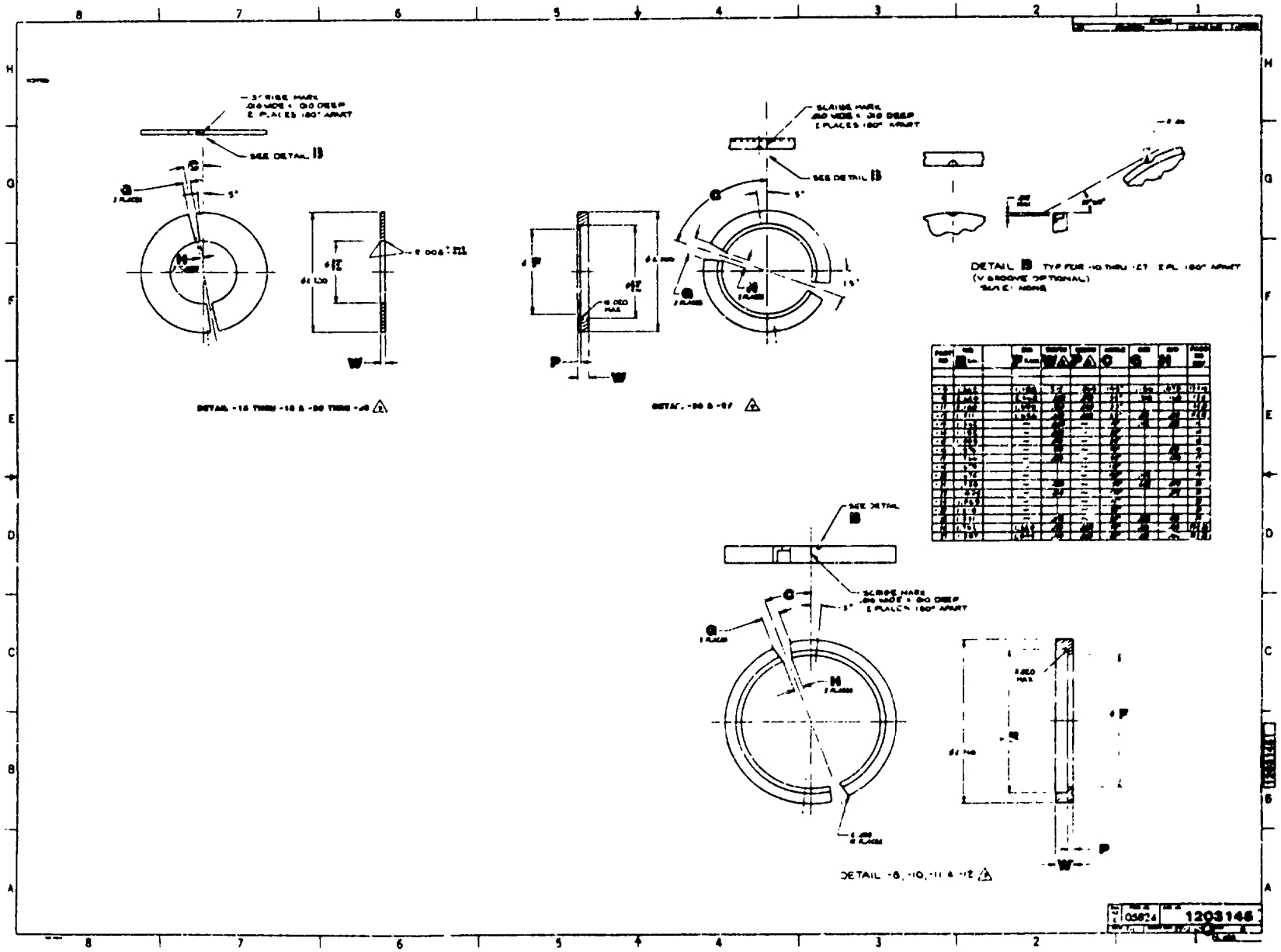

Figure B - 2 (Cont)

ORIGINAL PAGE IS
OF POOR QUALITY

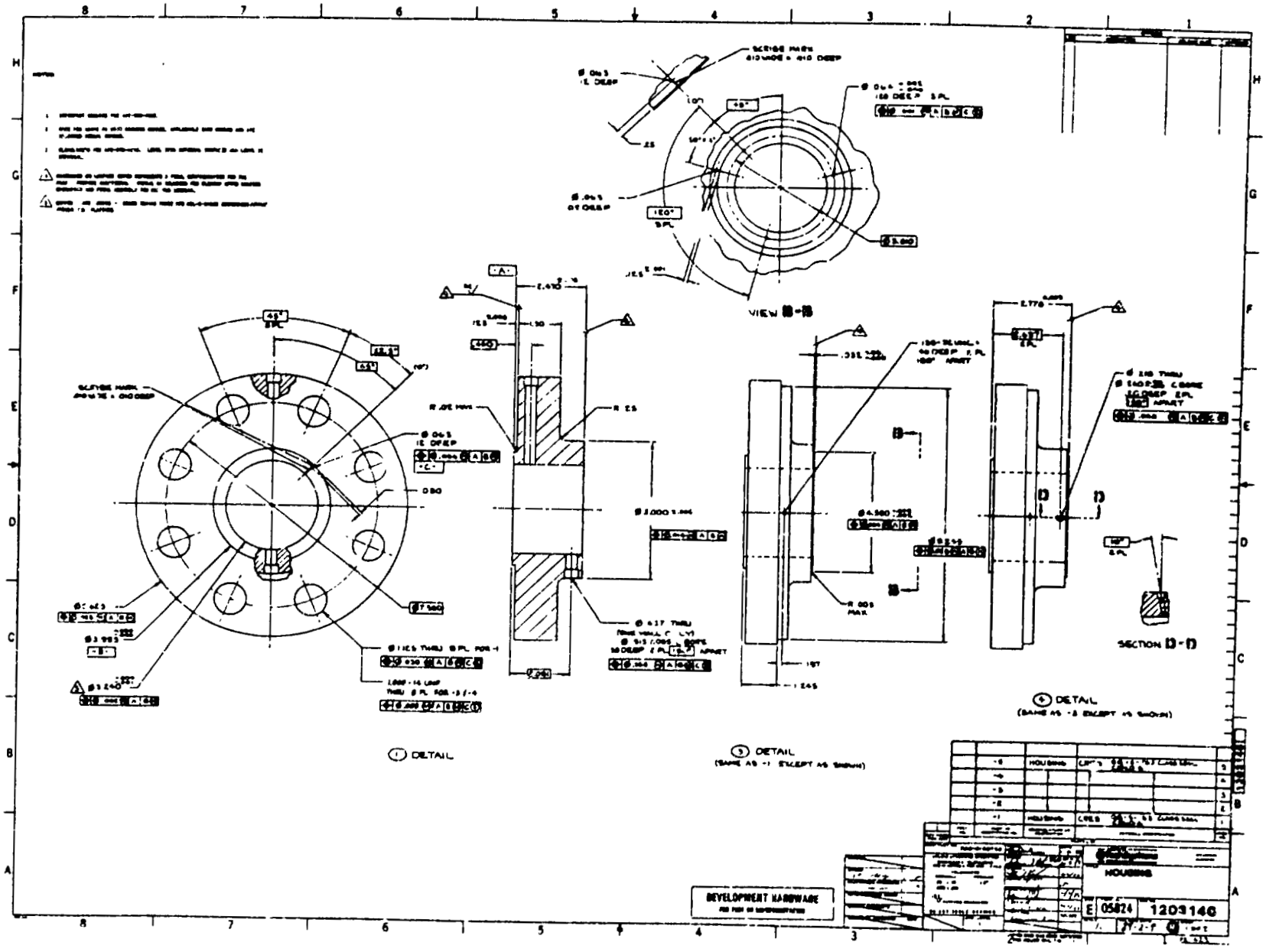

Figure B - 3

ORIGINAL PAGE IS
OF POOR QUALITY

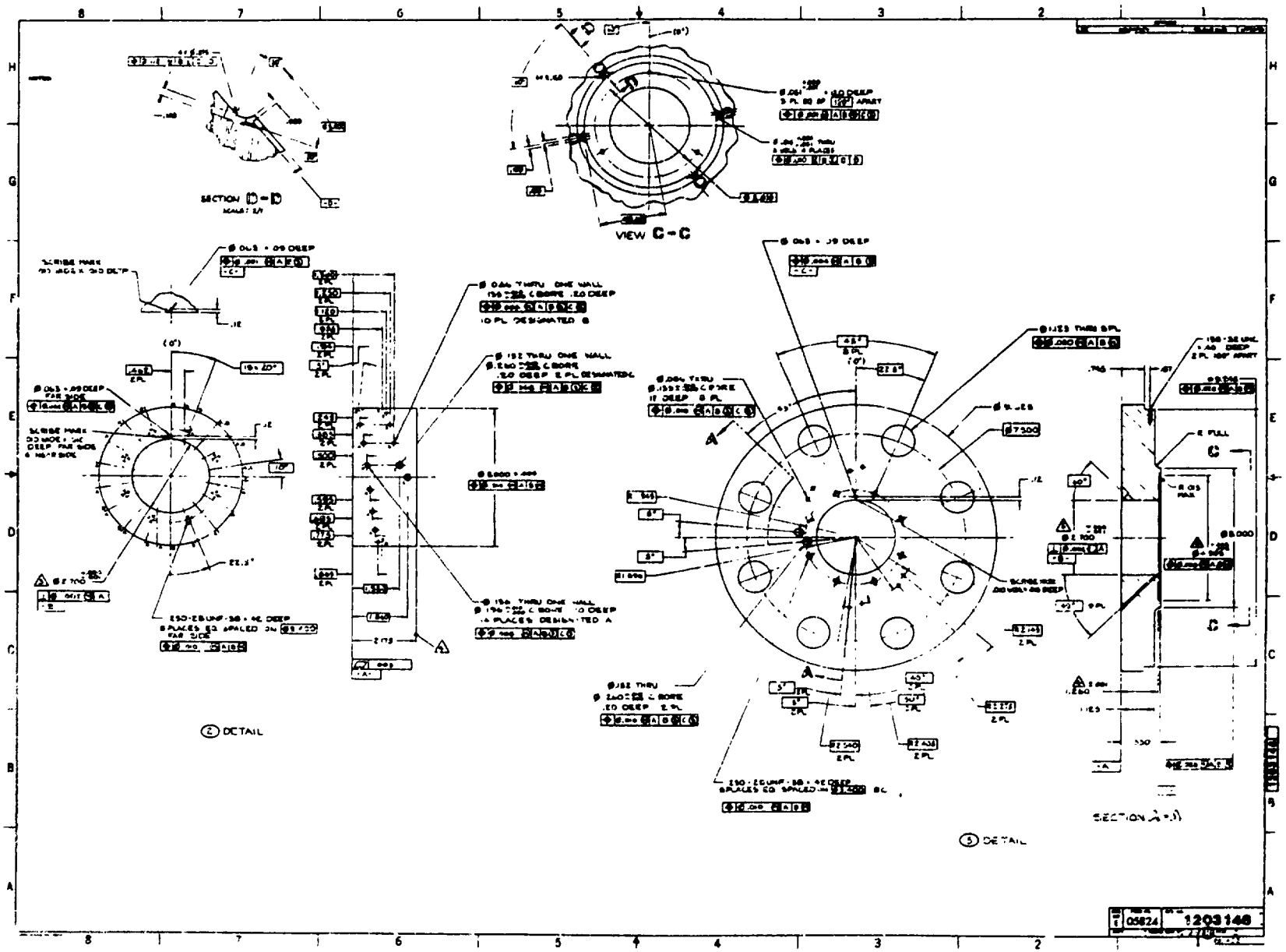

Figure B - 3 (Cont)

OF POOR QUALITY

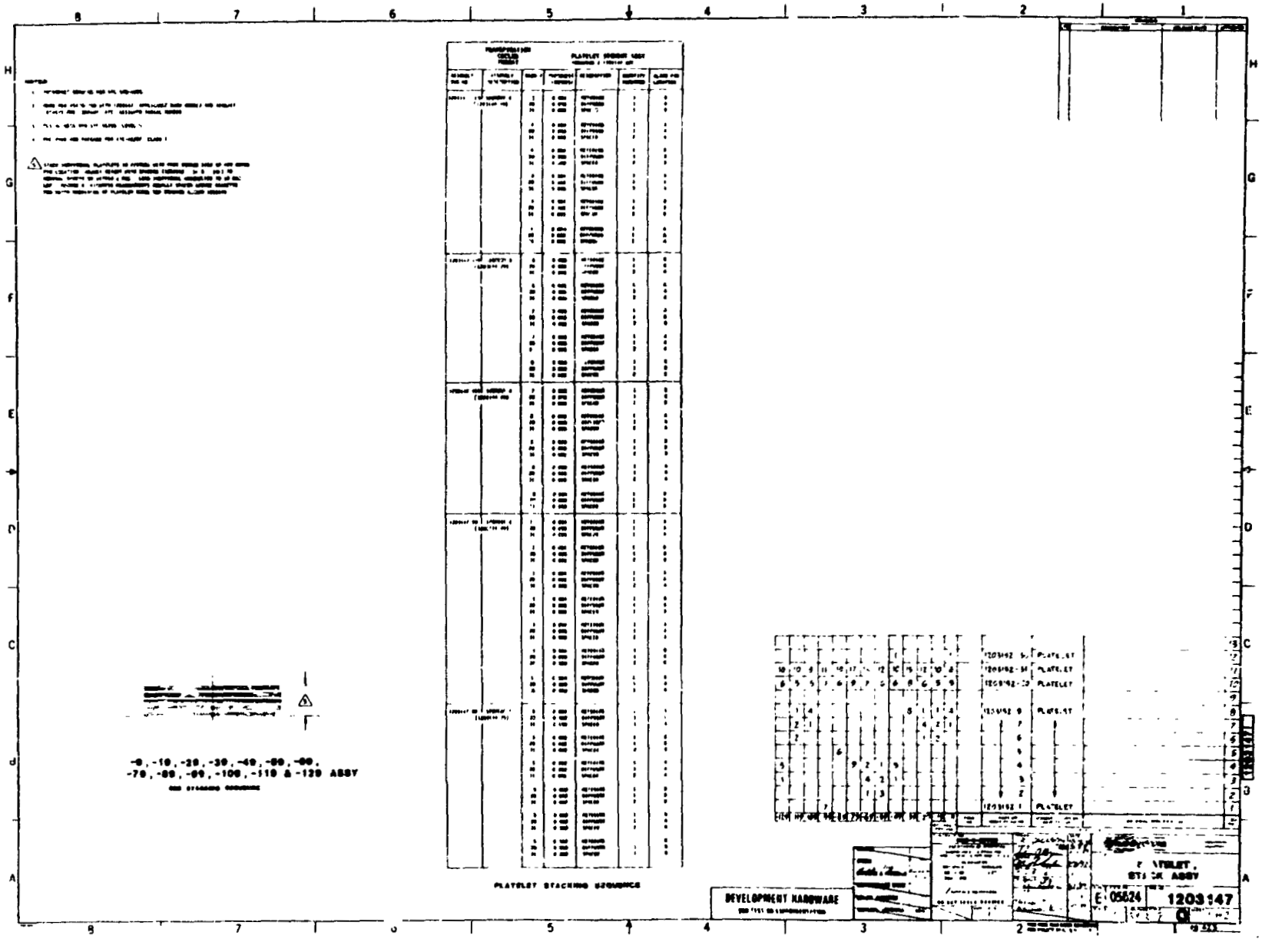

Figure B - 4

ORIGINAL PAGE IS
OF POOR QUALITY

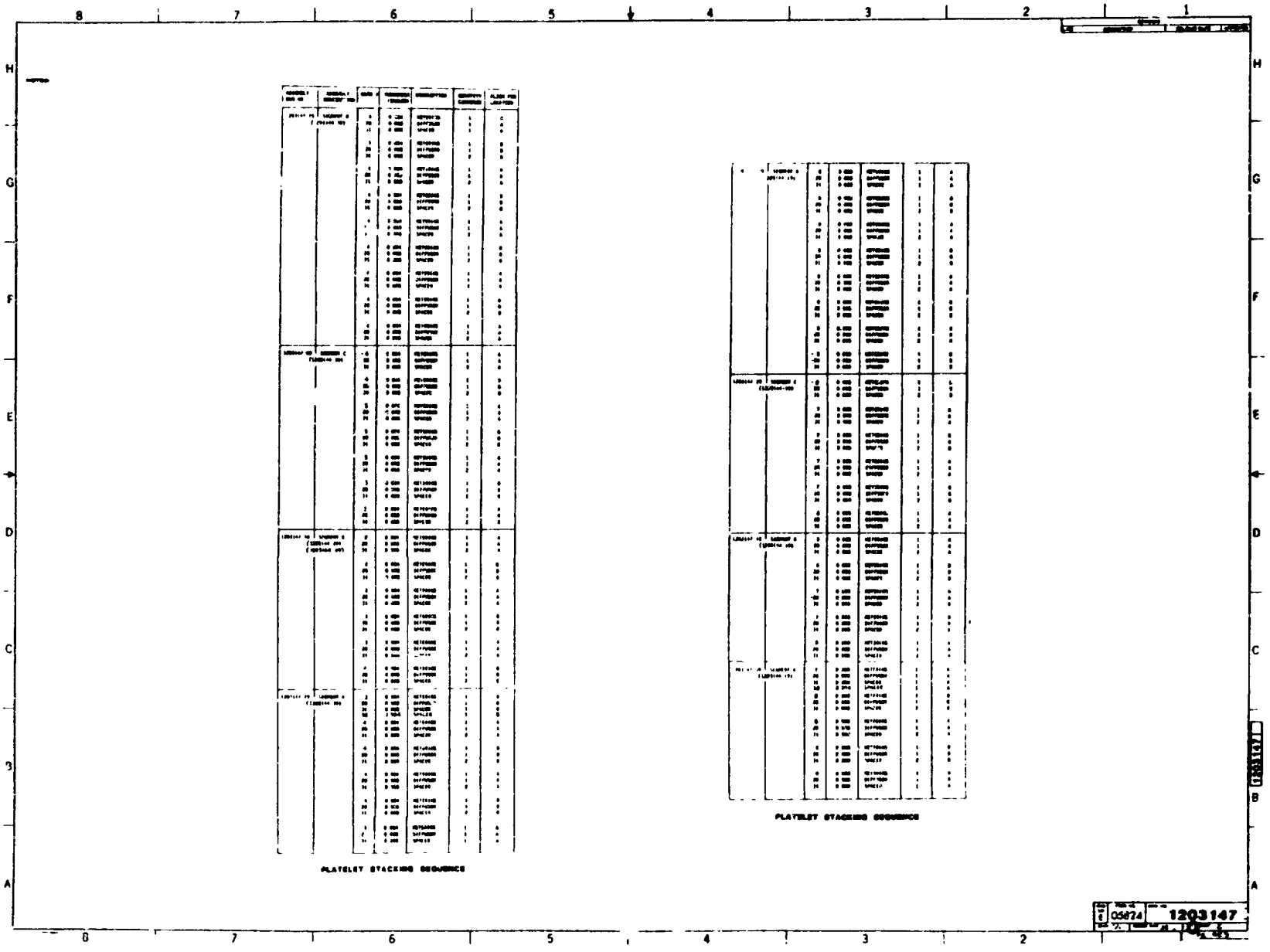

Figure B - 4 (Cont)

ORIGINAL PAGE IS
OF POOR QUALITY

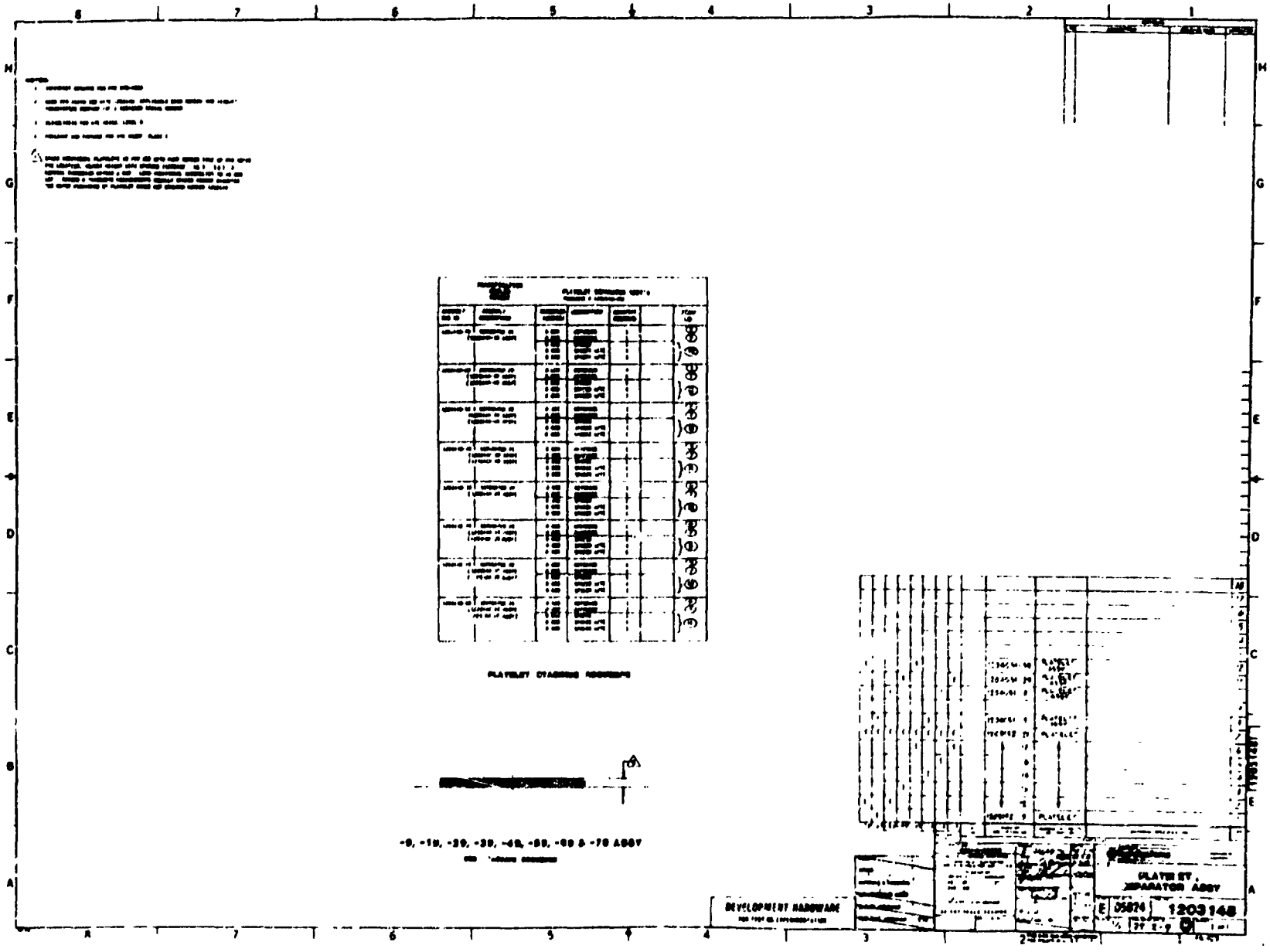

Figure B - 5

ORIGINAL PAGE IS
OF POOR QUALITY

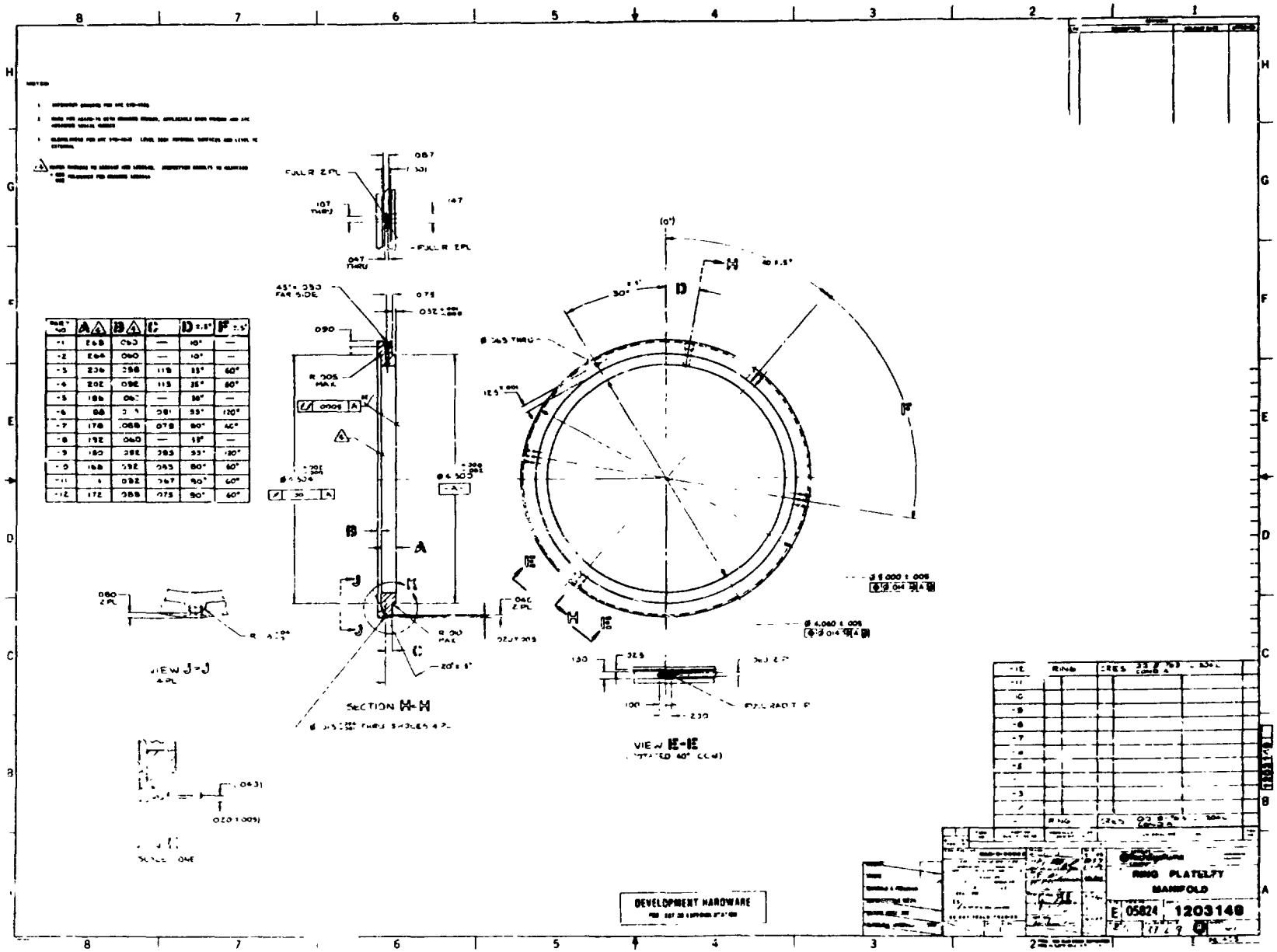

Figure B - 6

ORIGINAL PAGE IS
OF POOR QUALITY

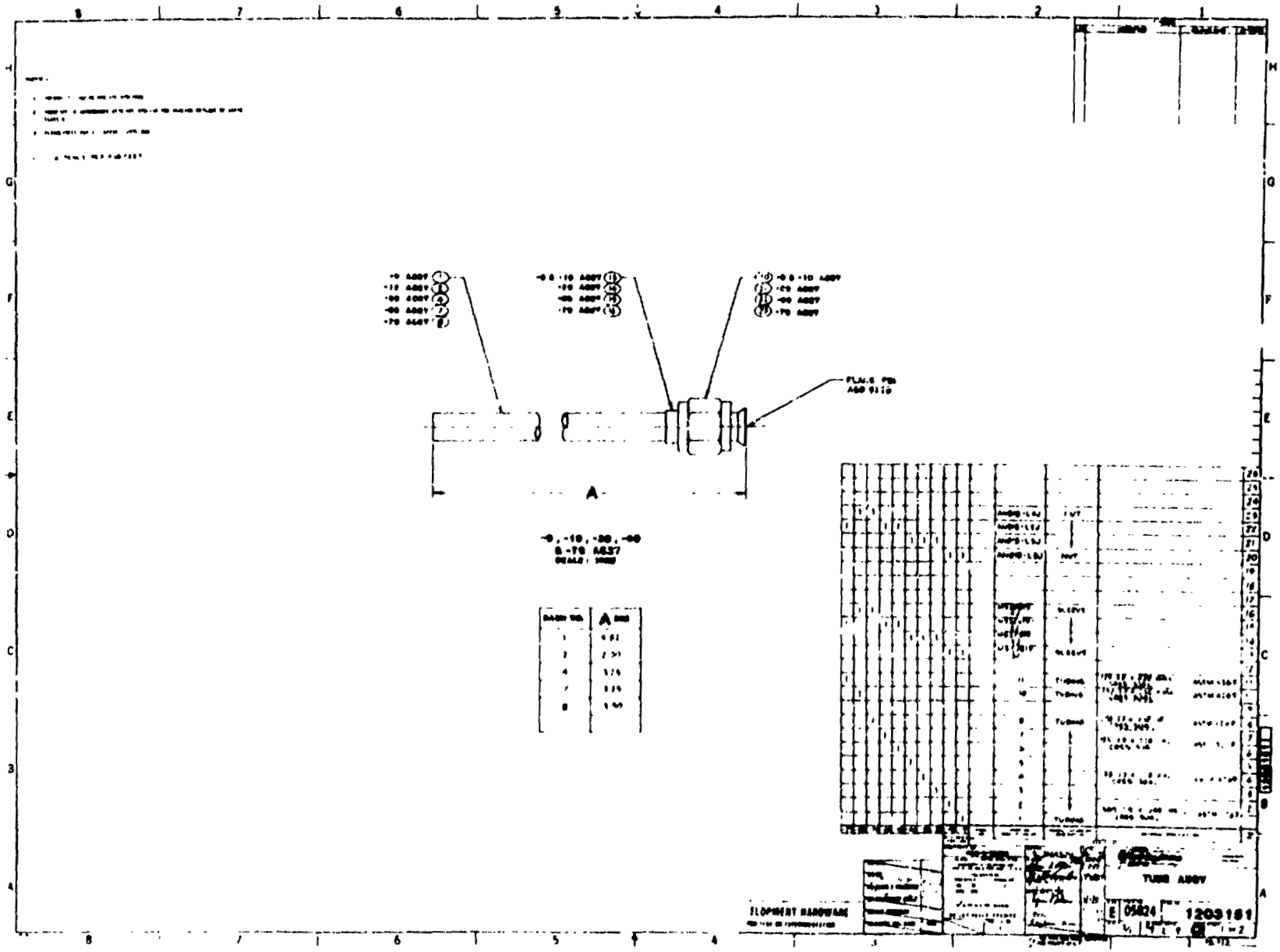

Figure B - 7

ORIGINAL PAGE IS
OF POOR QUALITY

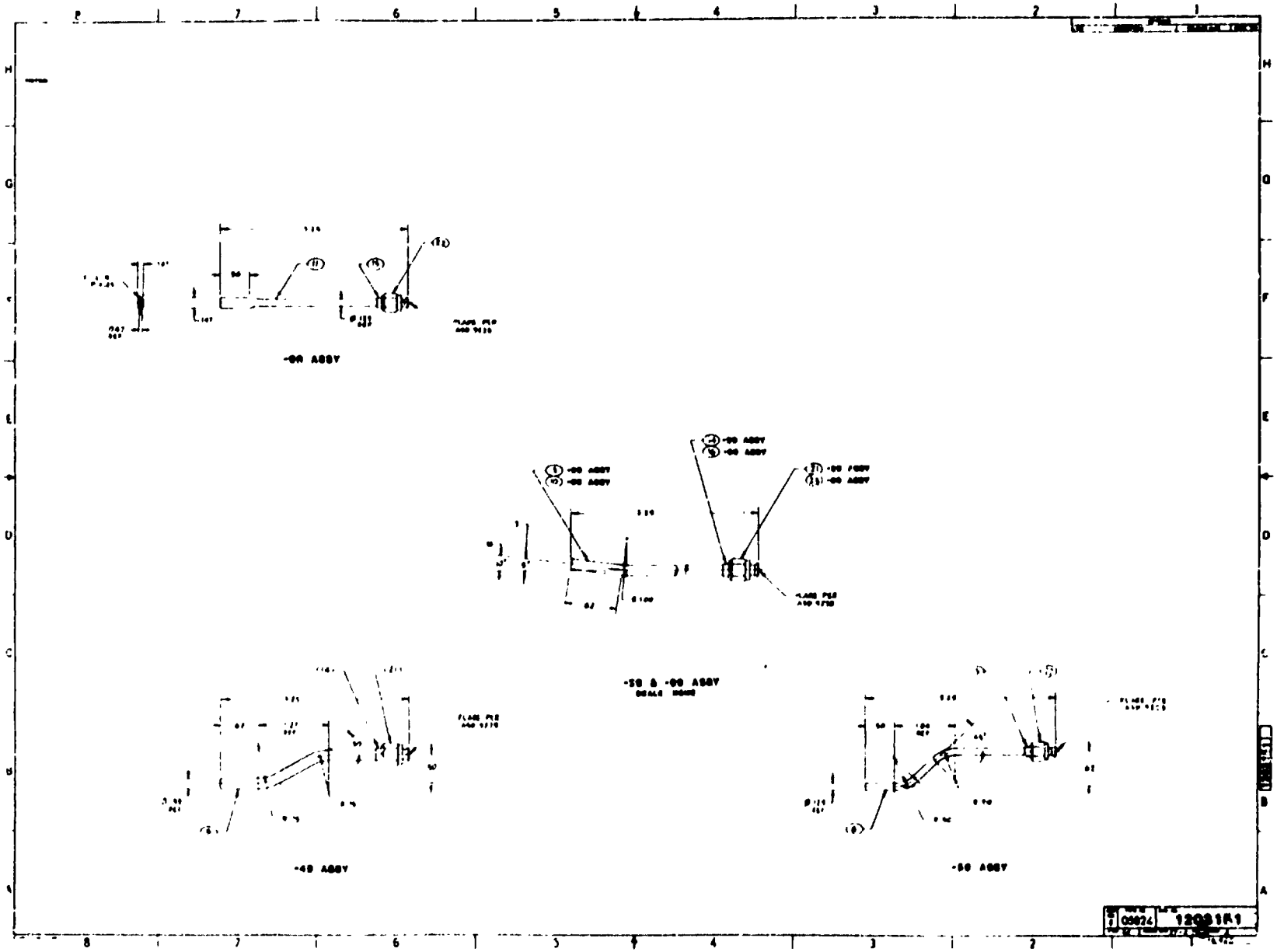

Figure B - 7 (Cont)

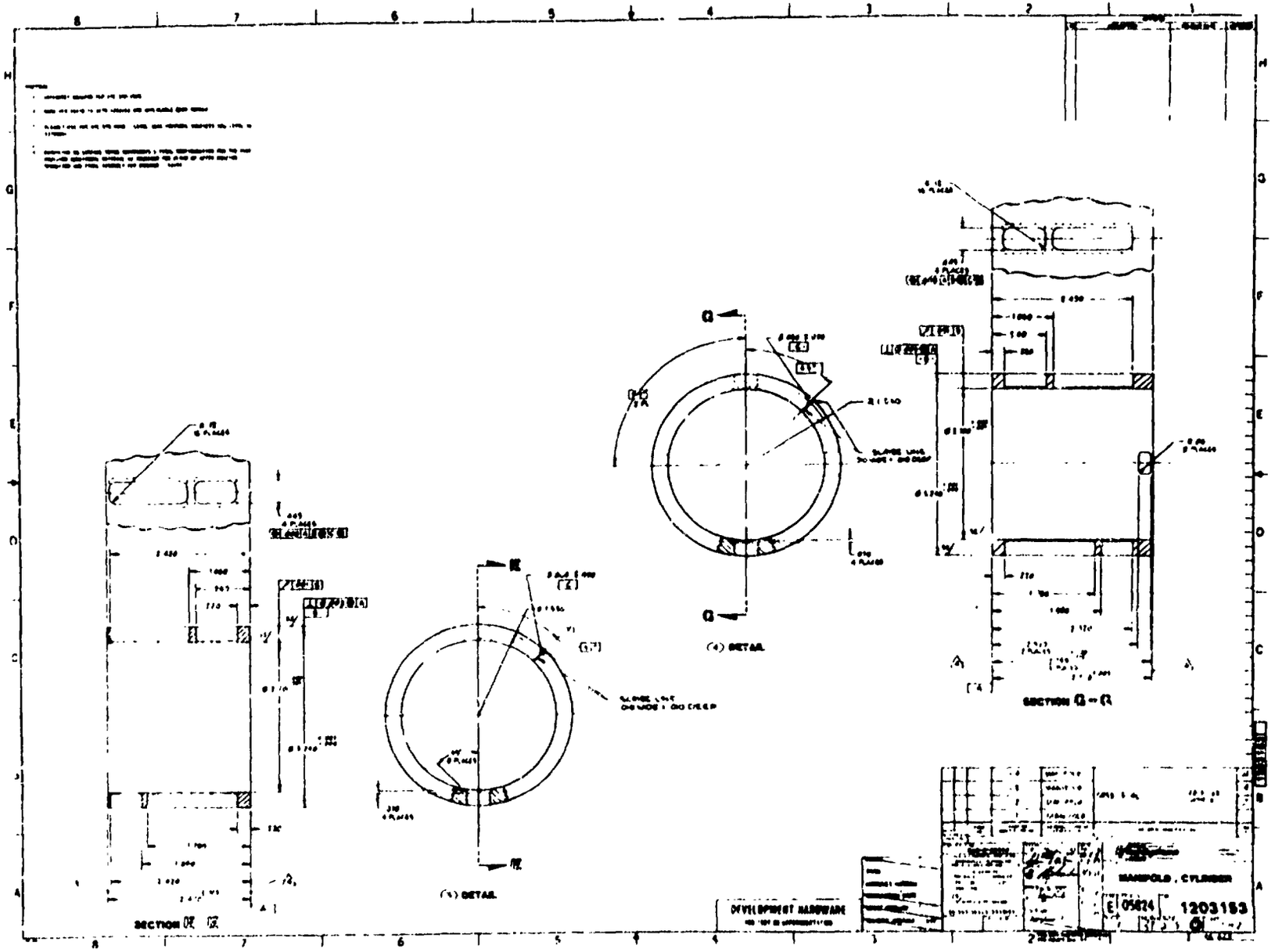

Figure B - 8

ORIGINAL PAGE IS
OF POOR QUALITY

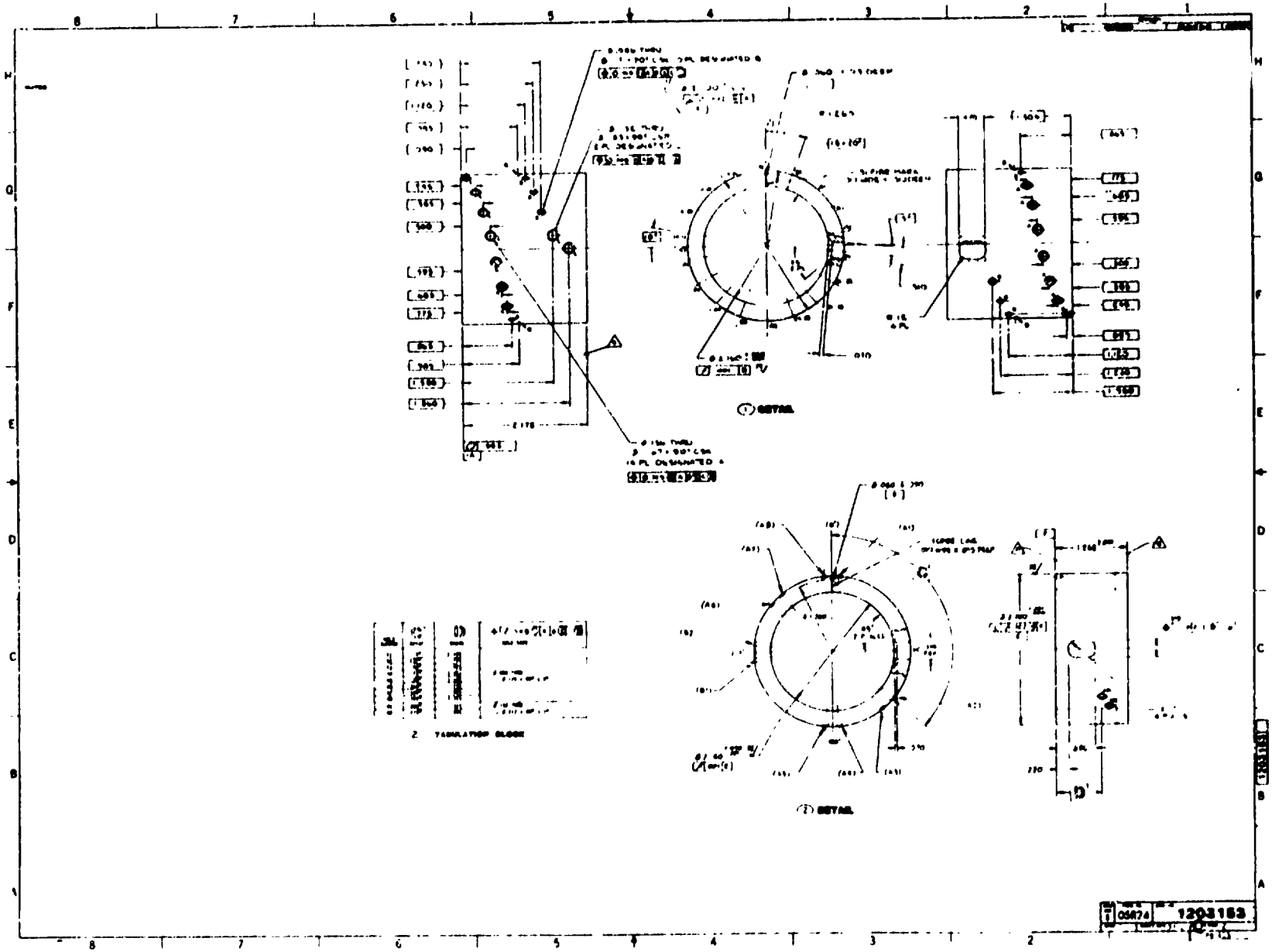

Figure B - 8 (Cont)

ORIGINAL PAGE IS
OF POOR QUALITY

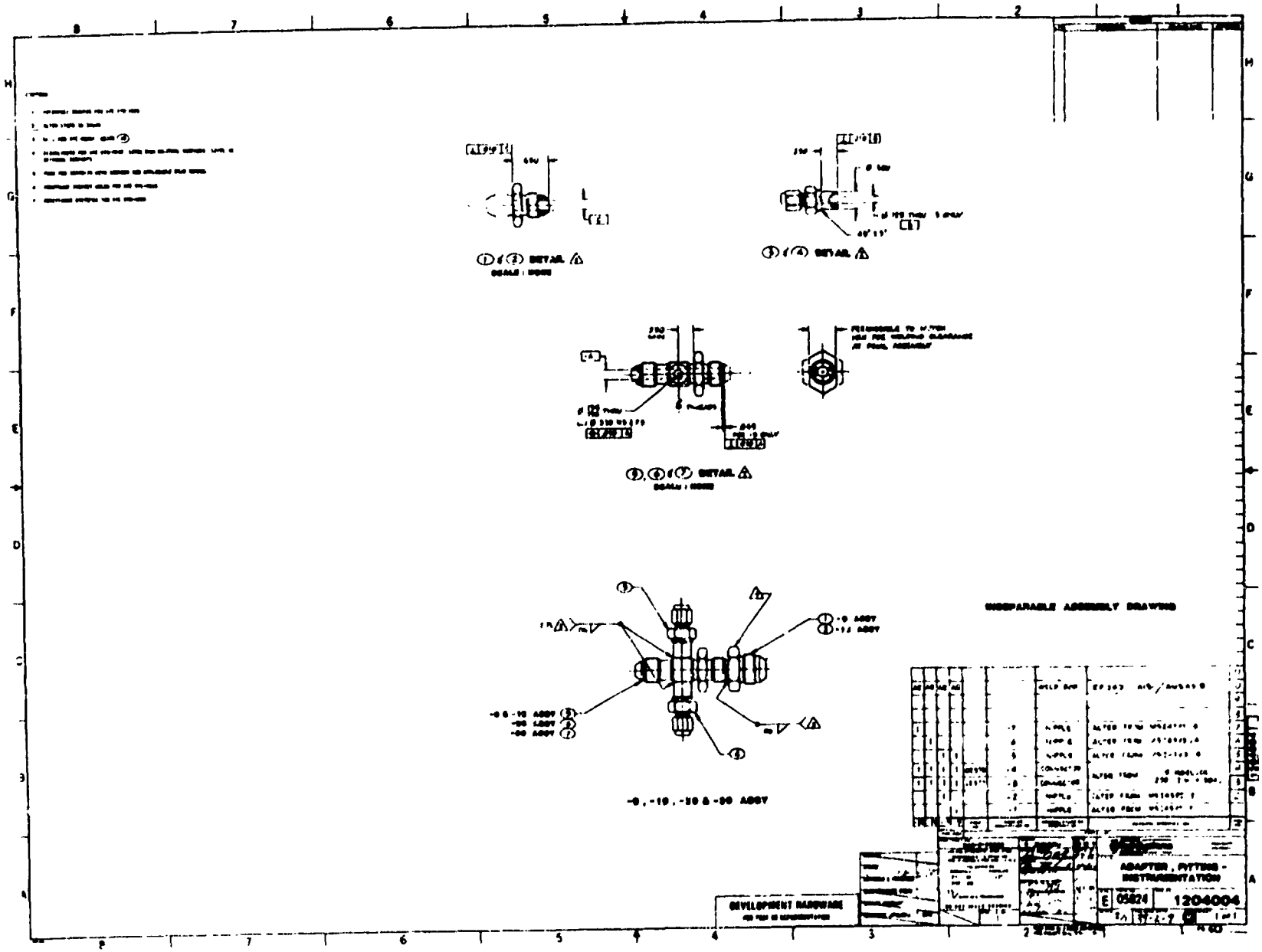

Figure B - 9

ORIGINAL PAGE IS
OF POOR QUALITY

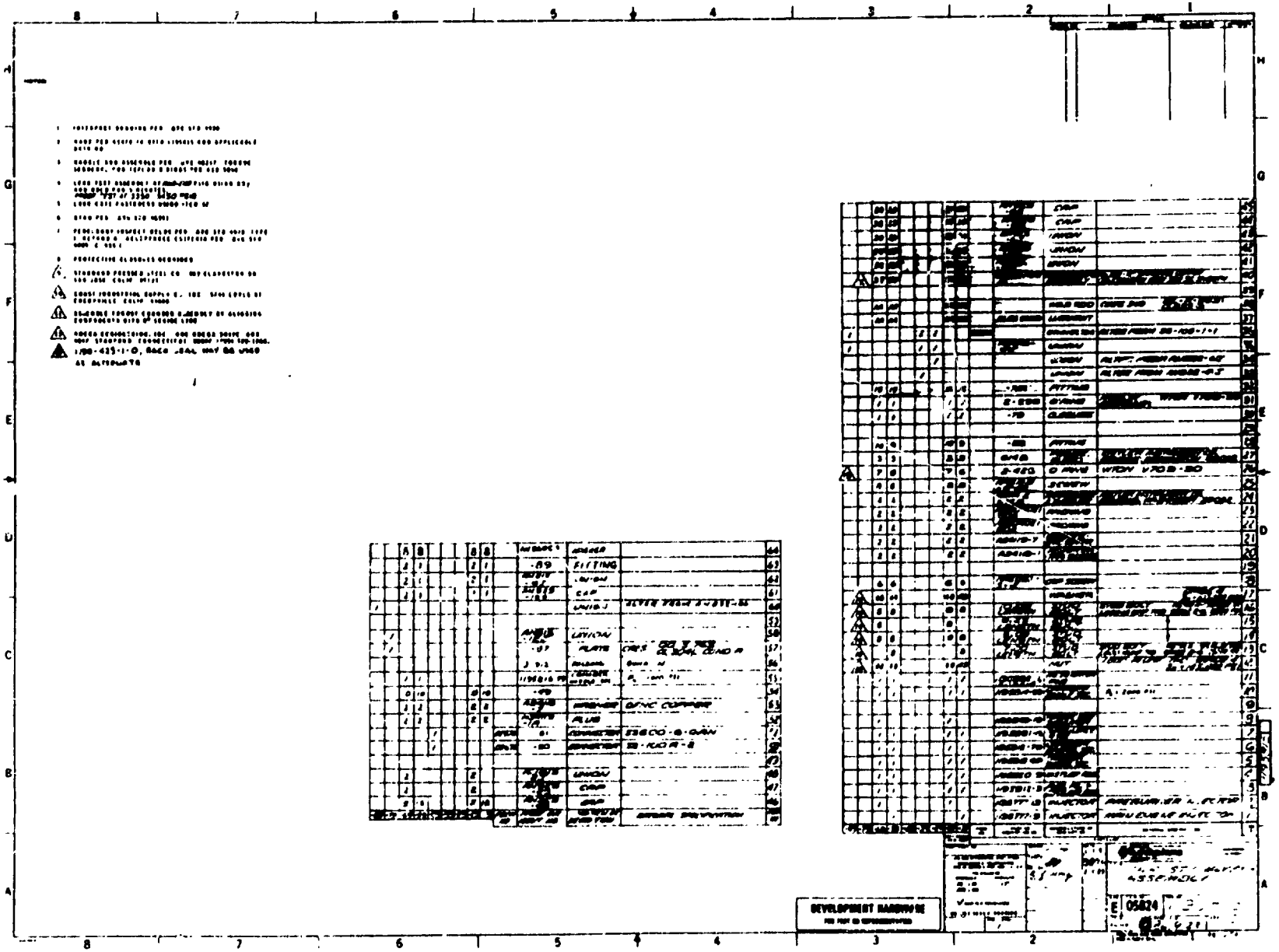

Figure B - 10

ORIGINAL PAGE IS
OF POOR QUALITY

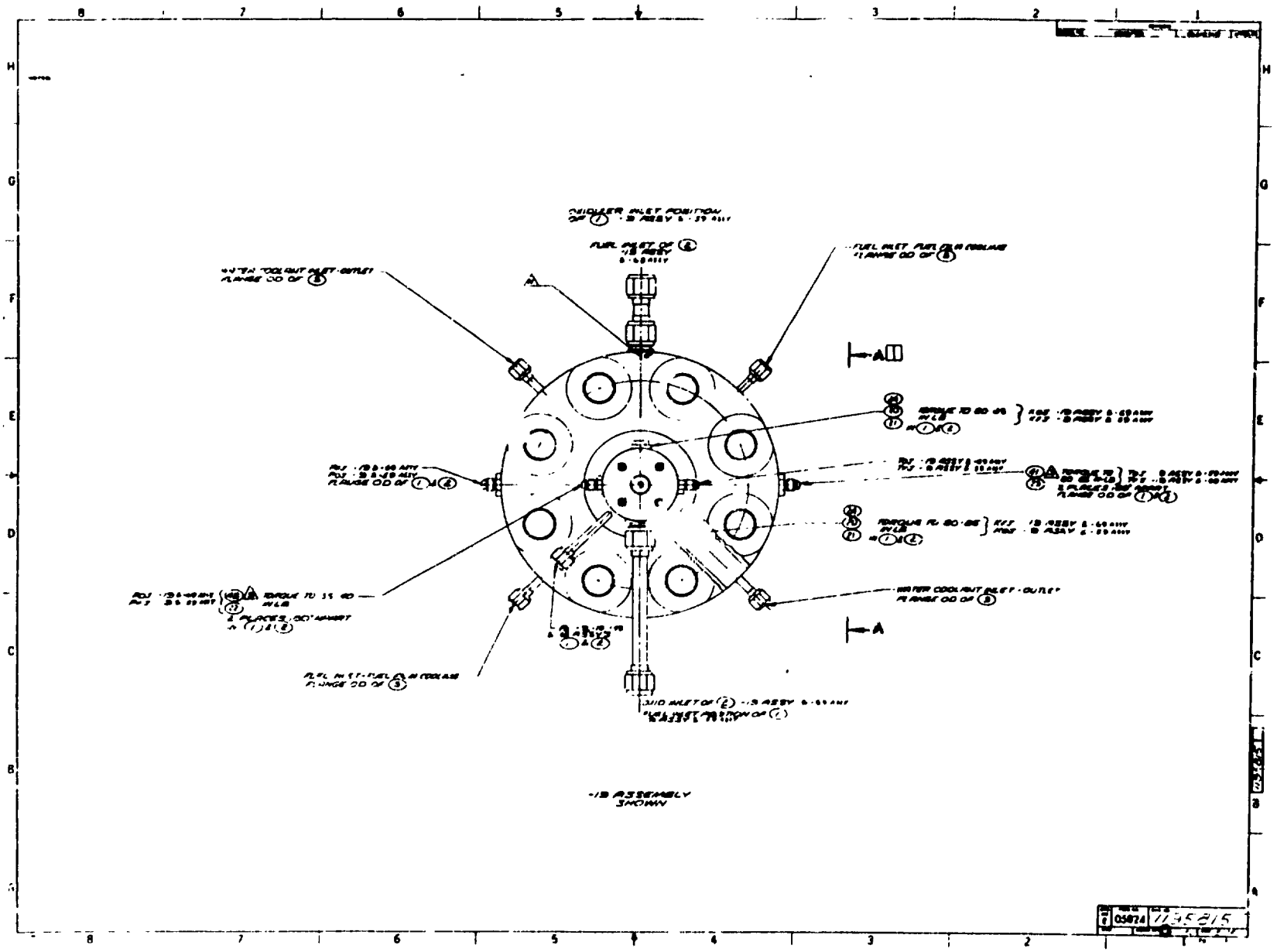

Figure B - 10 (Cont)

ORIGINAL PAGE IS
OF POOR QUALITY

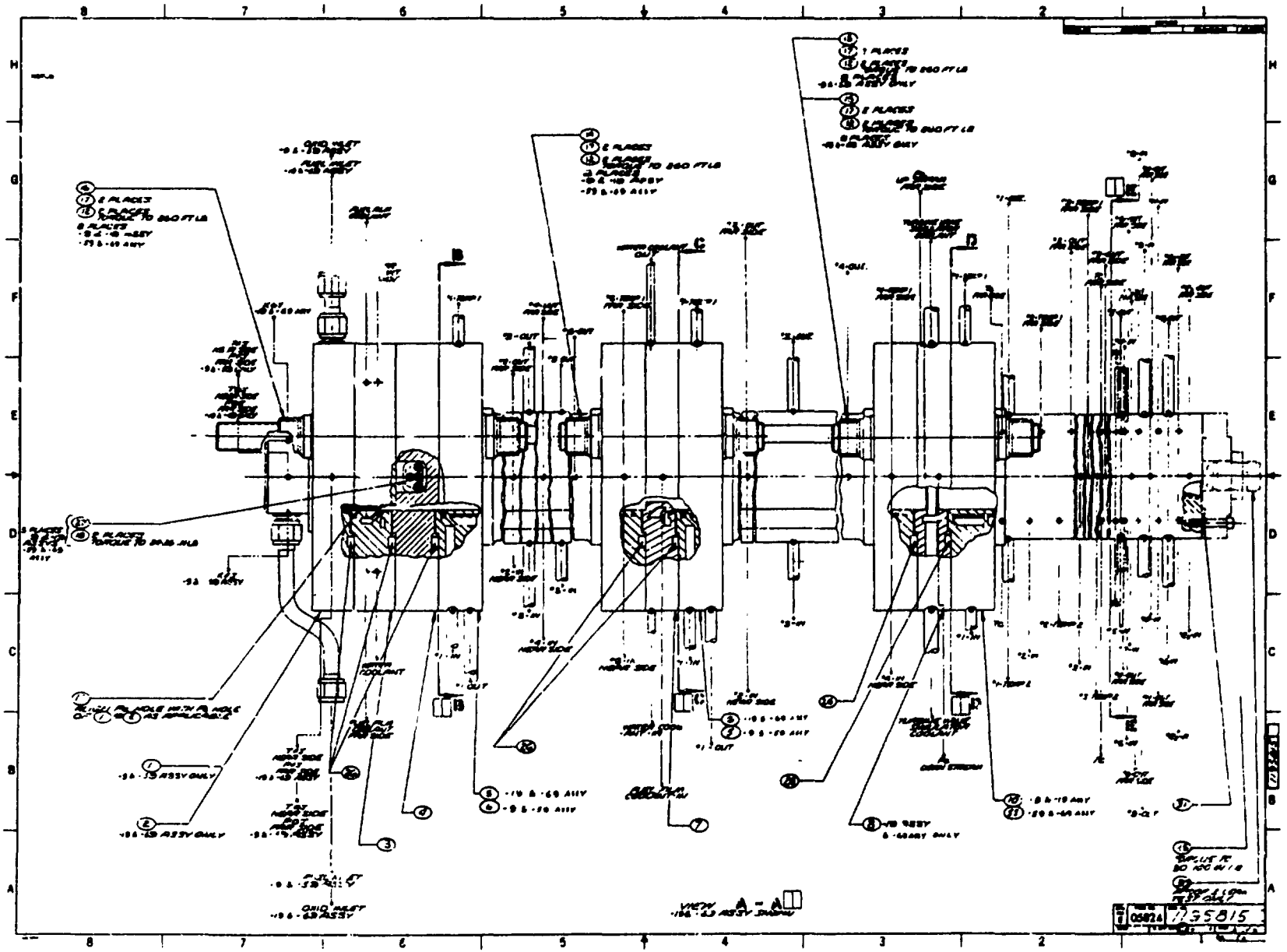

Figure B - 10 (Cont)

ORIGINAL PAGE IS
OF POOR QUALITY

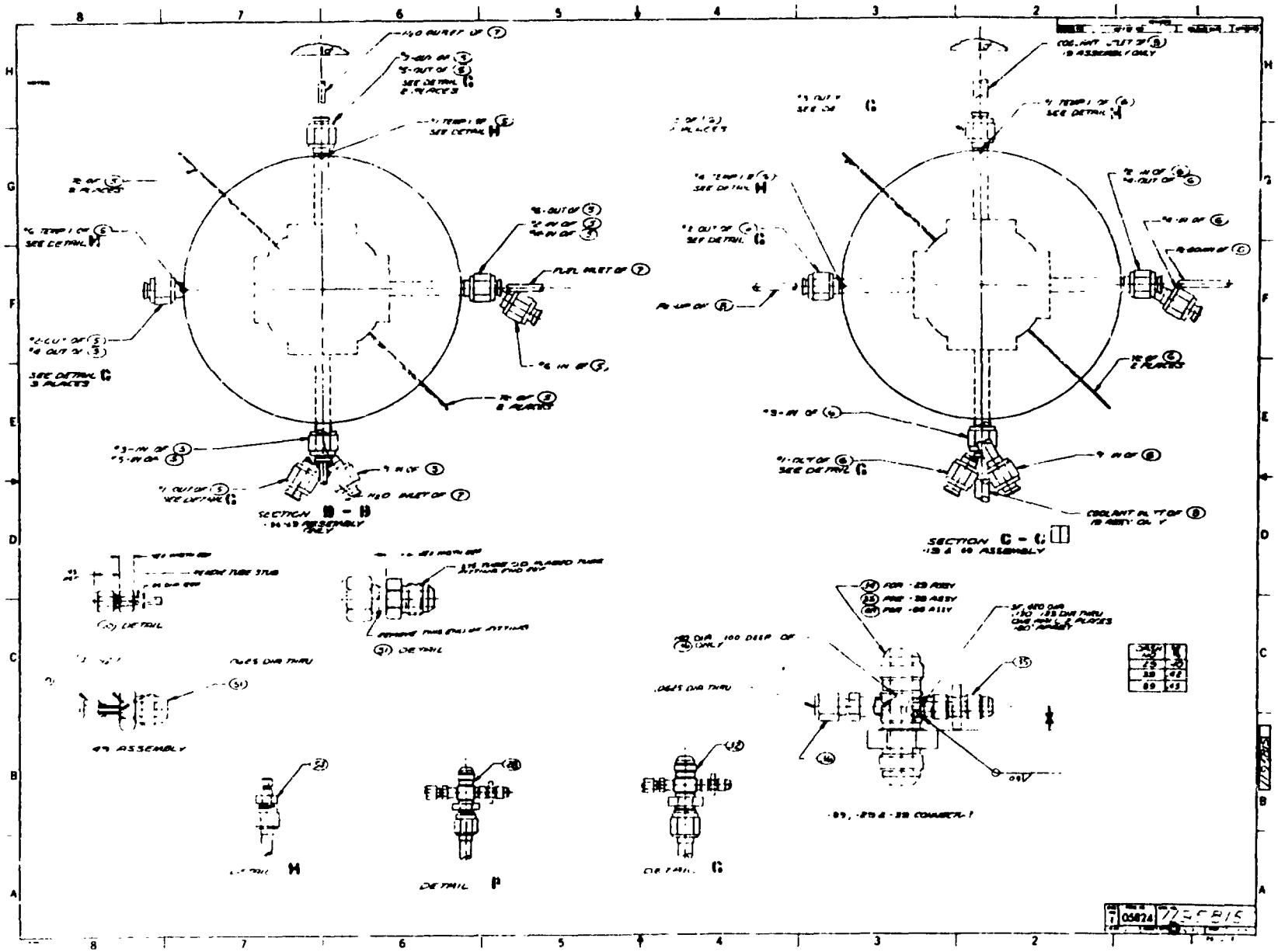

Figure B - 10 (Cont)

ORIGINAL PAGE IS
OF POOR QUALITY

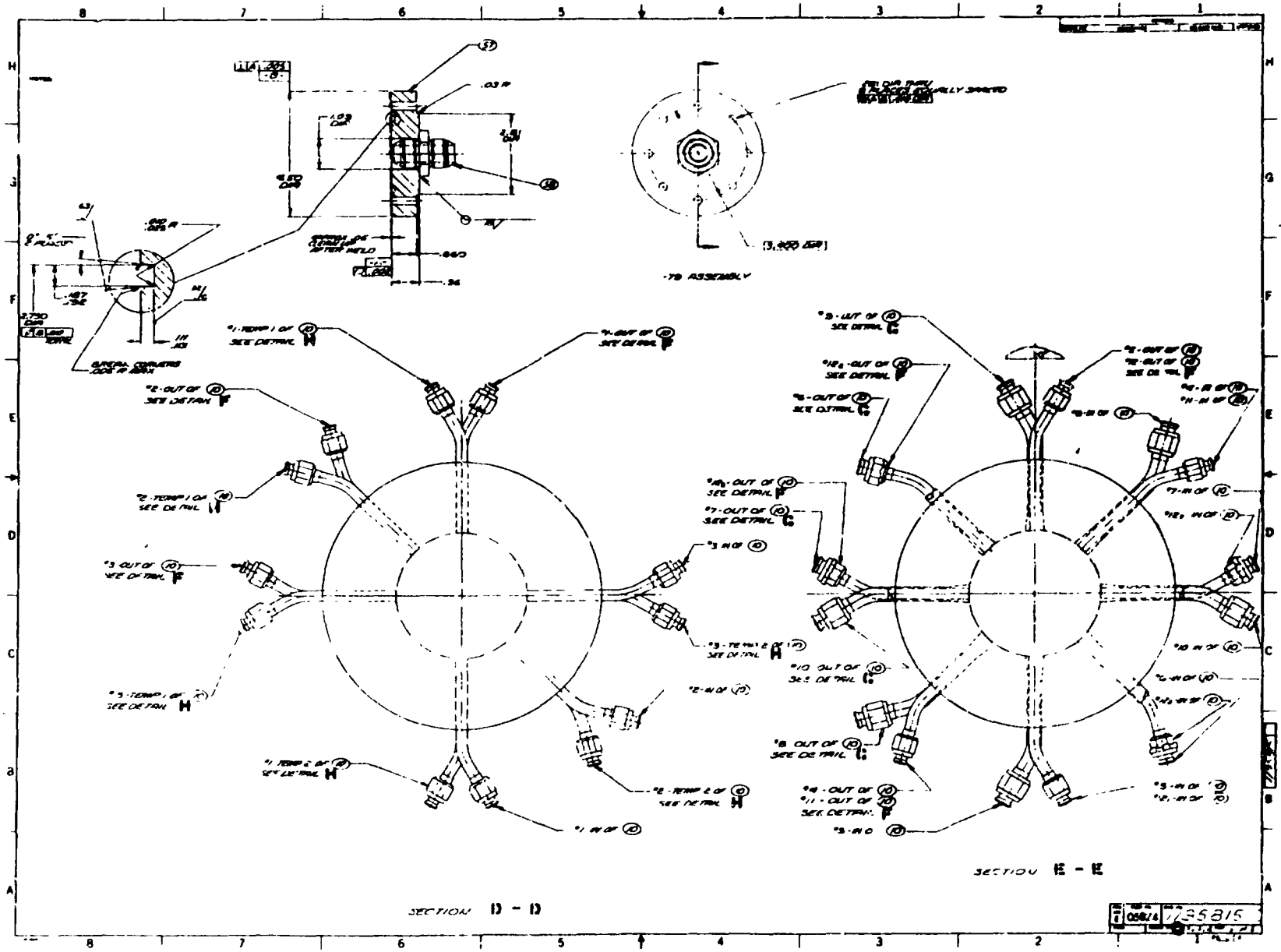

Figure B - 10 (Cont)

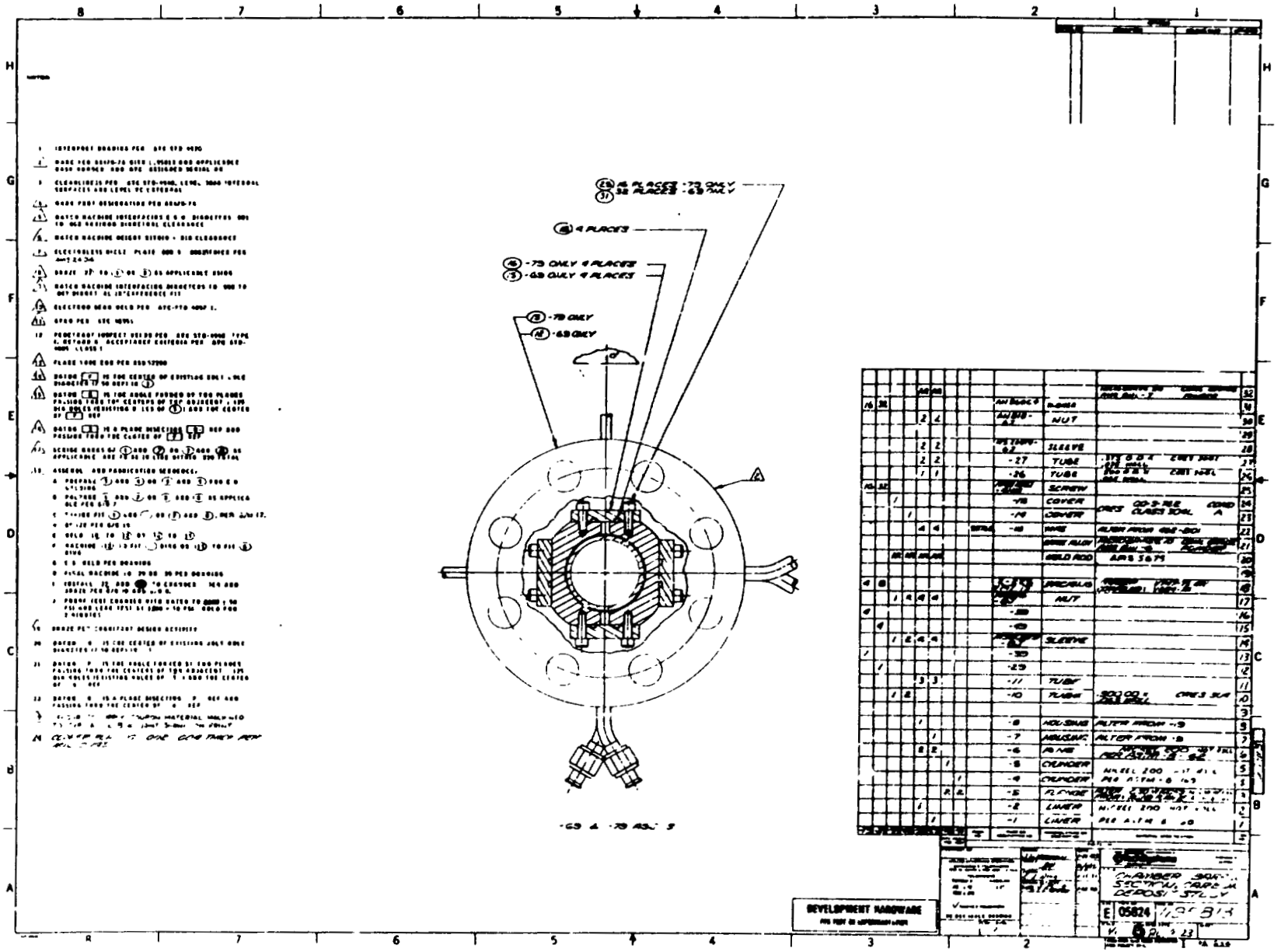

Figure B - 11

ORIGINAL PAGE IS
OF POOR QUALITY

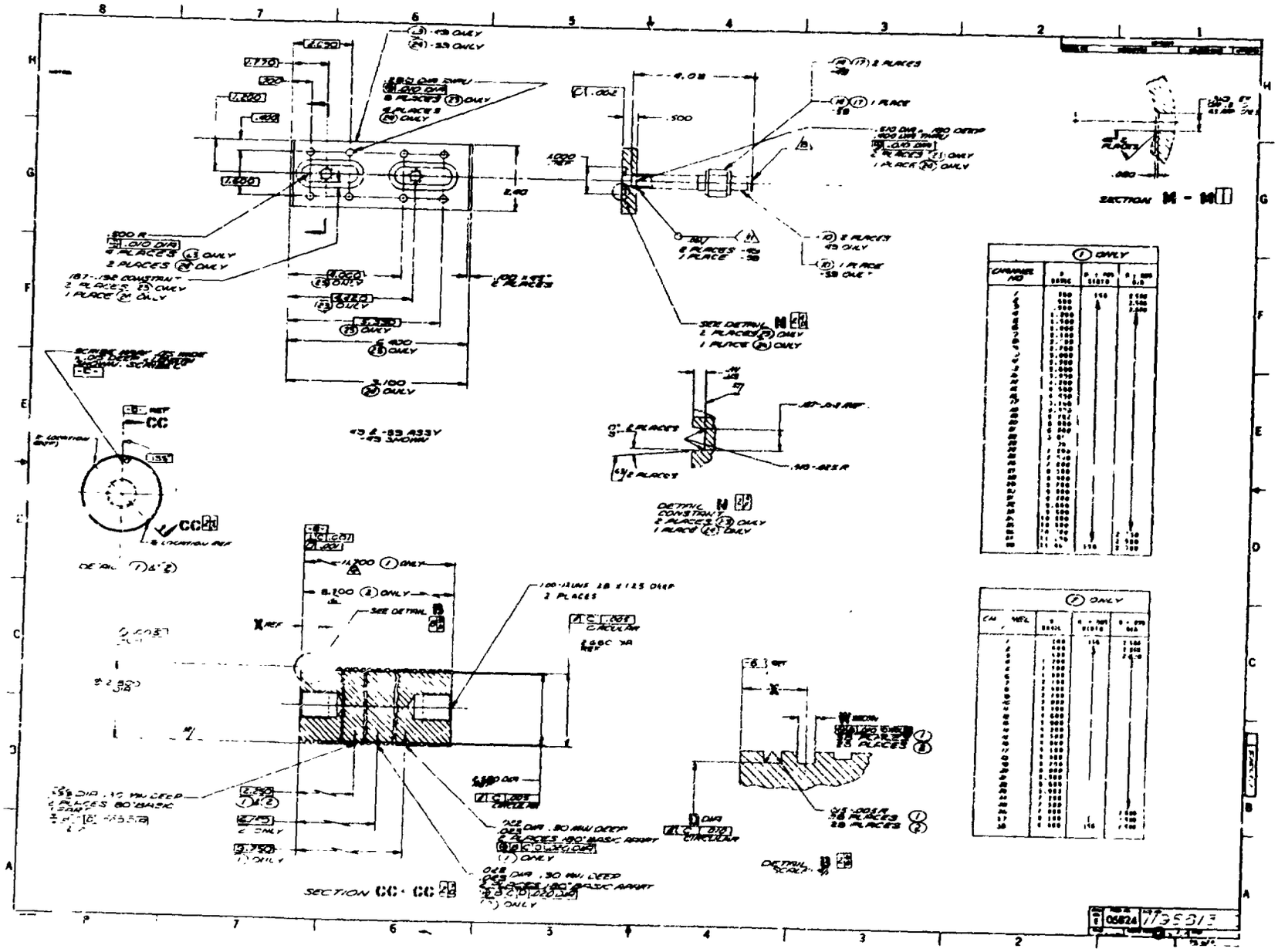

Figure B - 11 (Cont)

OF POOR QUALITY

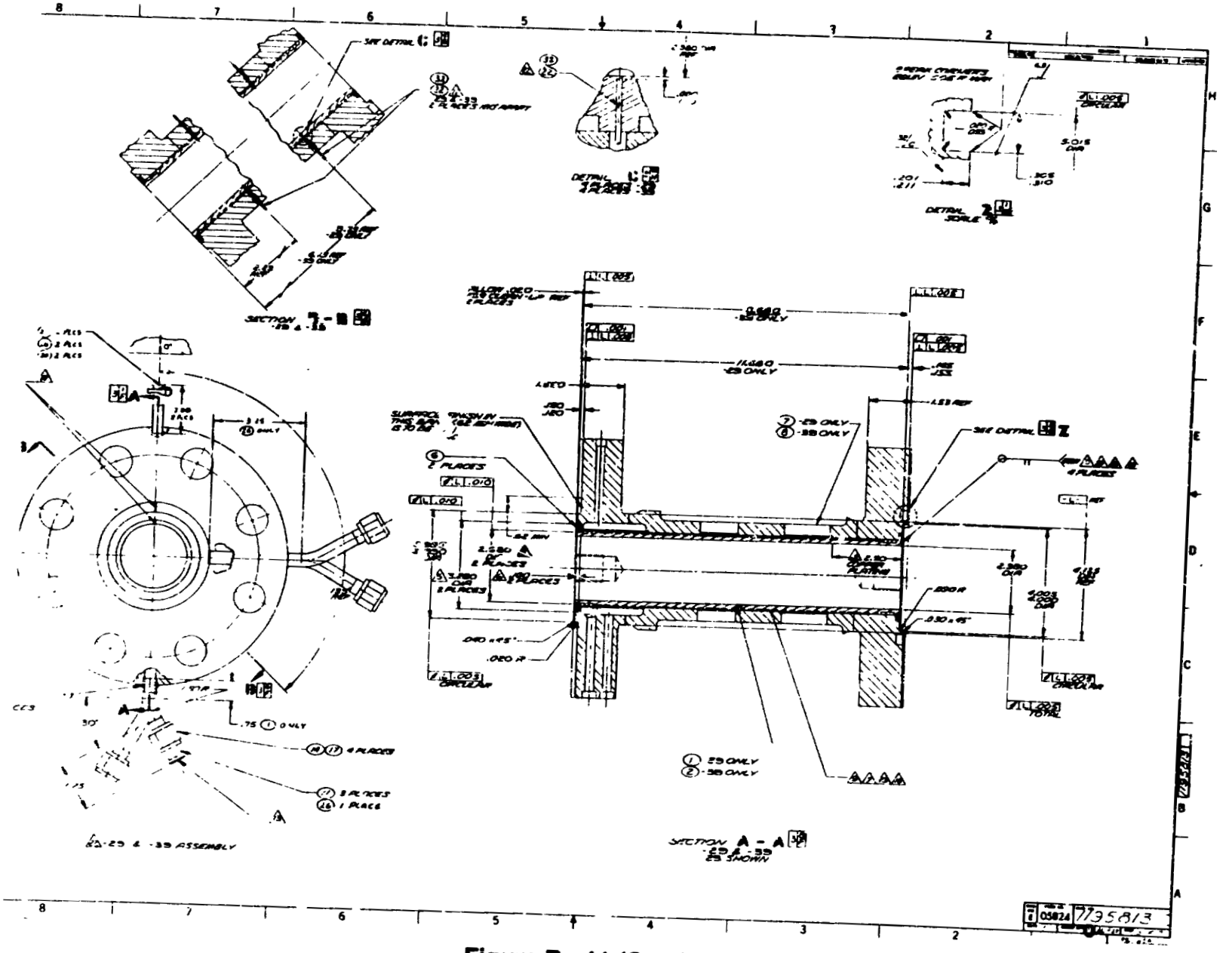

Figure B - 11 (Cont)

ORIGINAL PAGE IS
OF POOR QUALITY

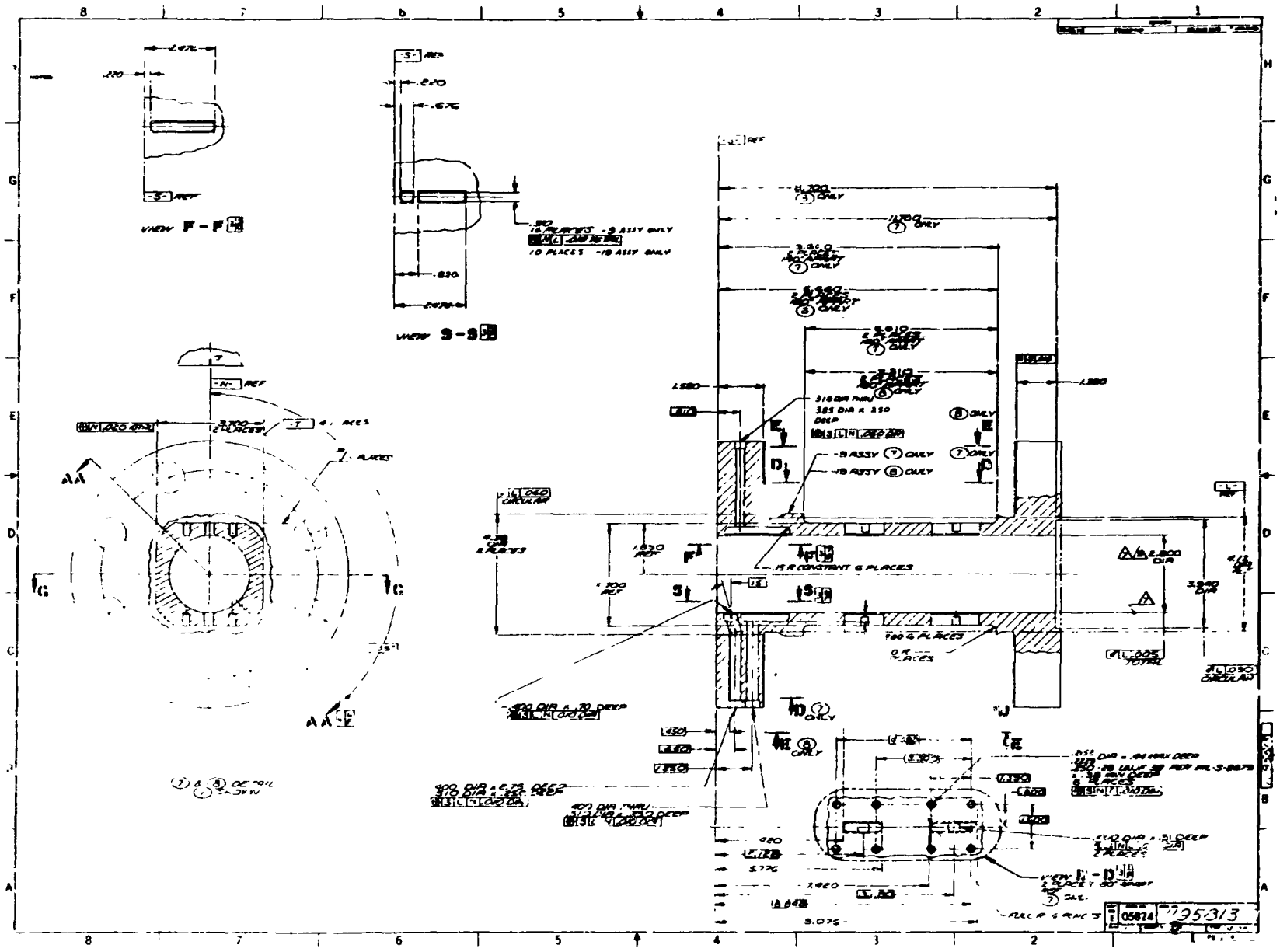

Figure B - 11 (Cont)

ORIGINAL PAGE IS
OF POOR QUALITY

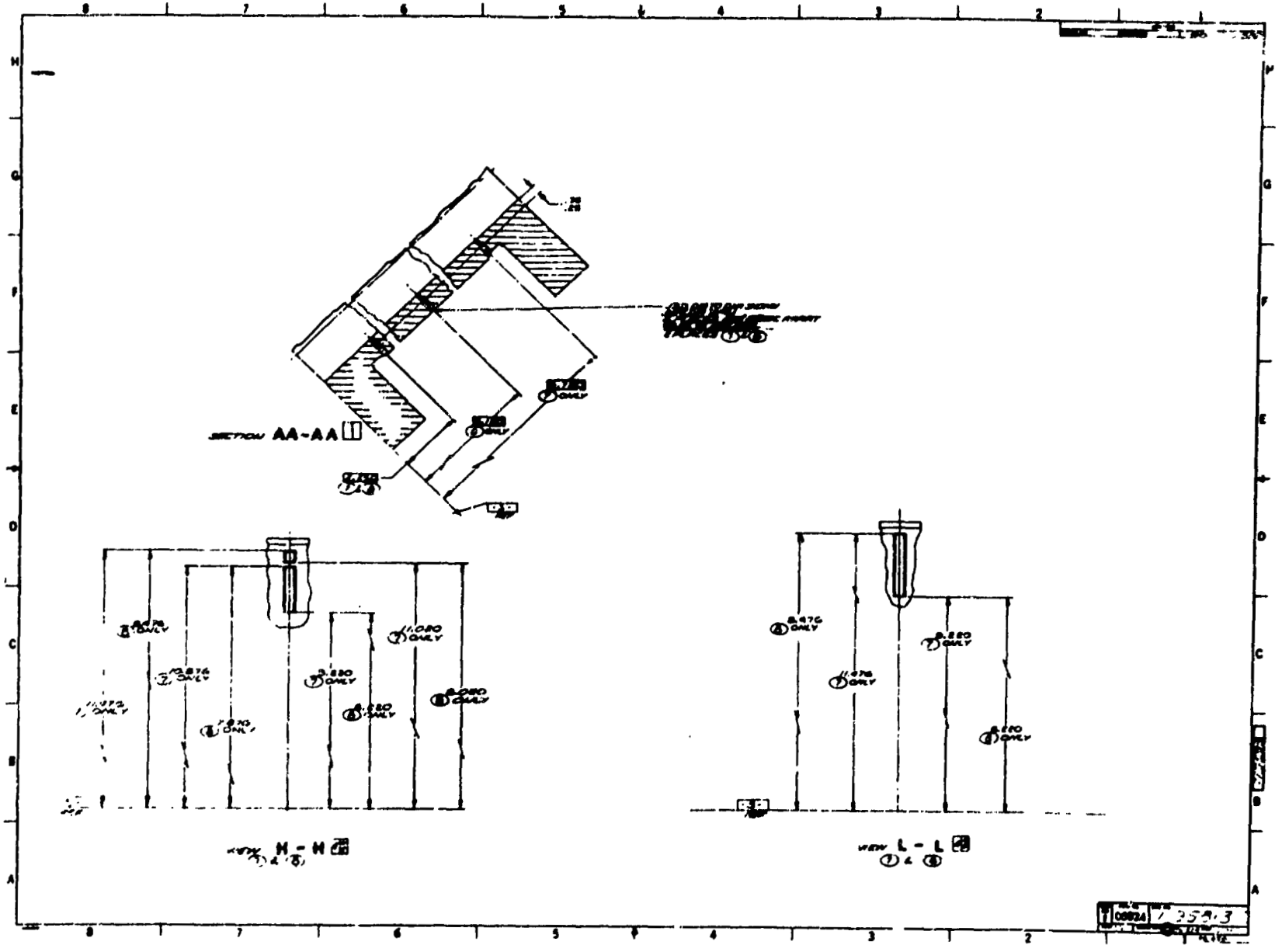

Figure B - 11 (Cont)

ORIGINAL PAGE IS
OF POOR QUALITY

C-2

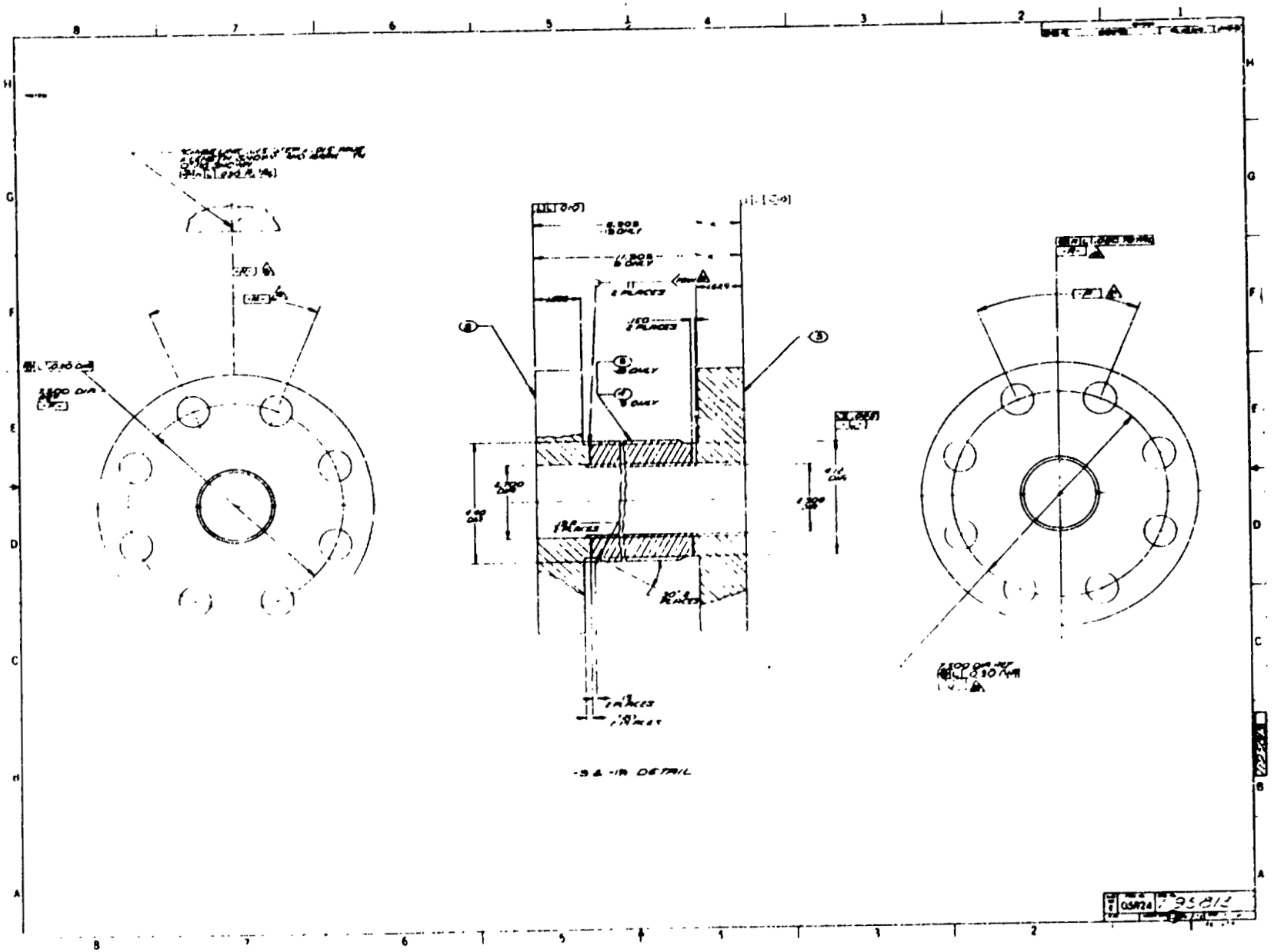

Figure B - 11 (Cont)

ORIGINAL PAGE IS
OF POOR QUALITY

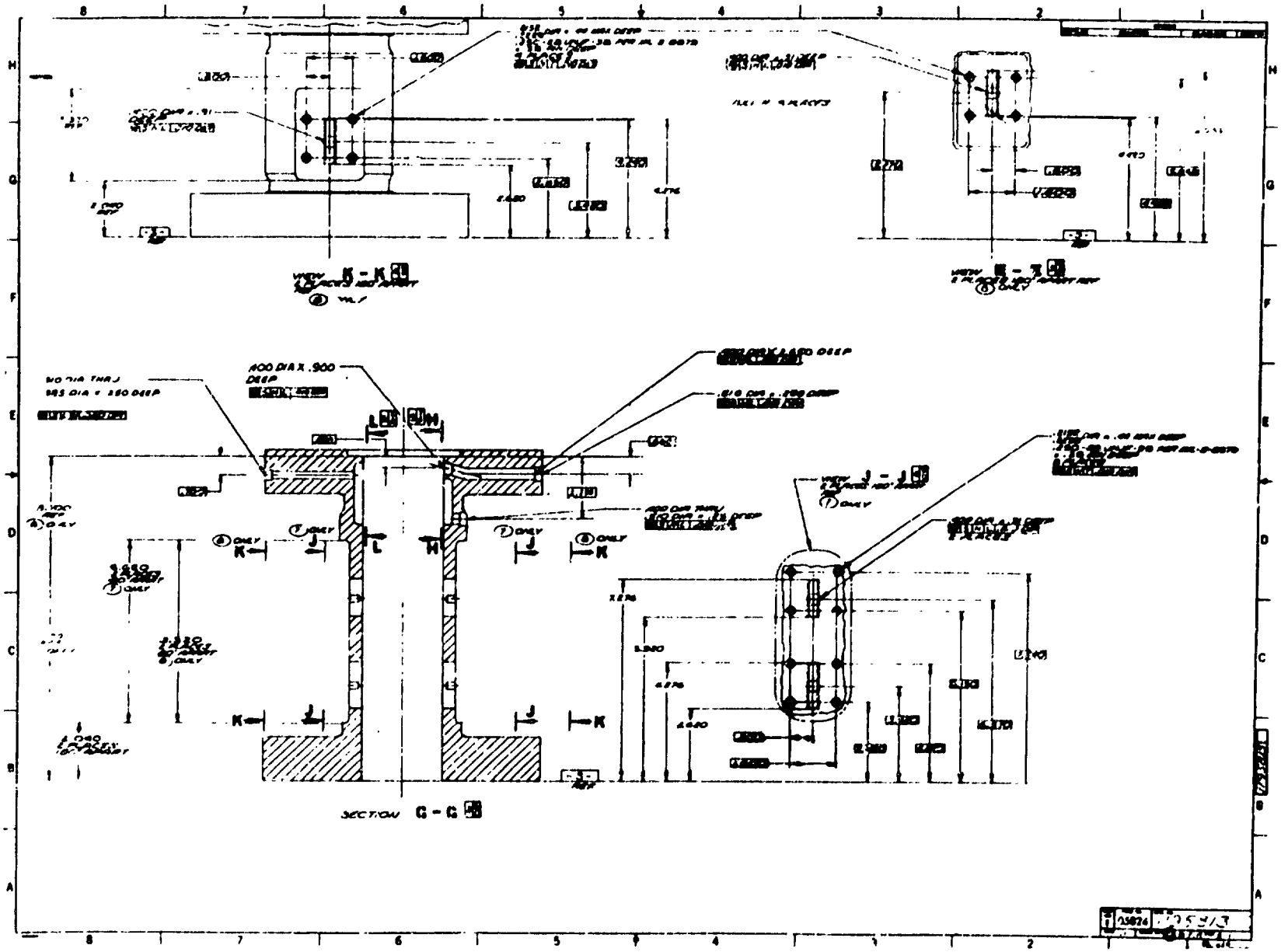

Figure B - 11 (Cont)

ORIGINAL PAGE IS
OF POOR QUALITY

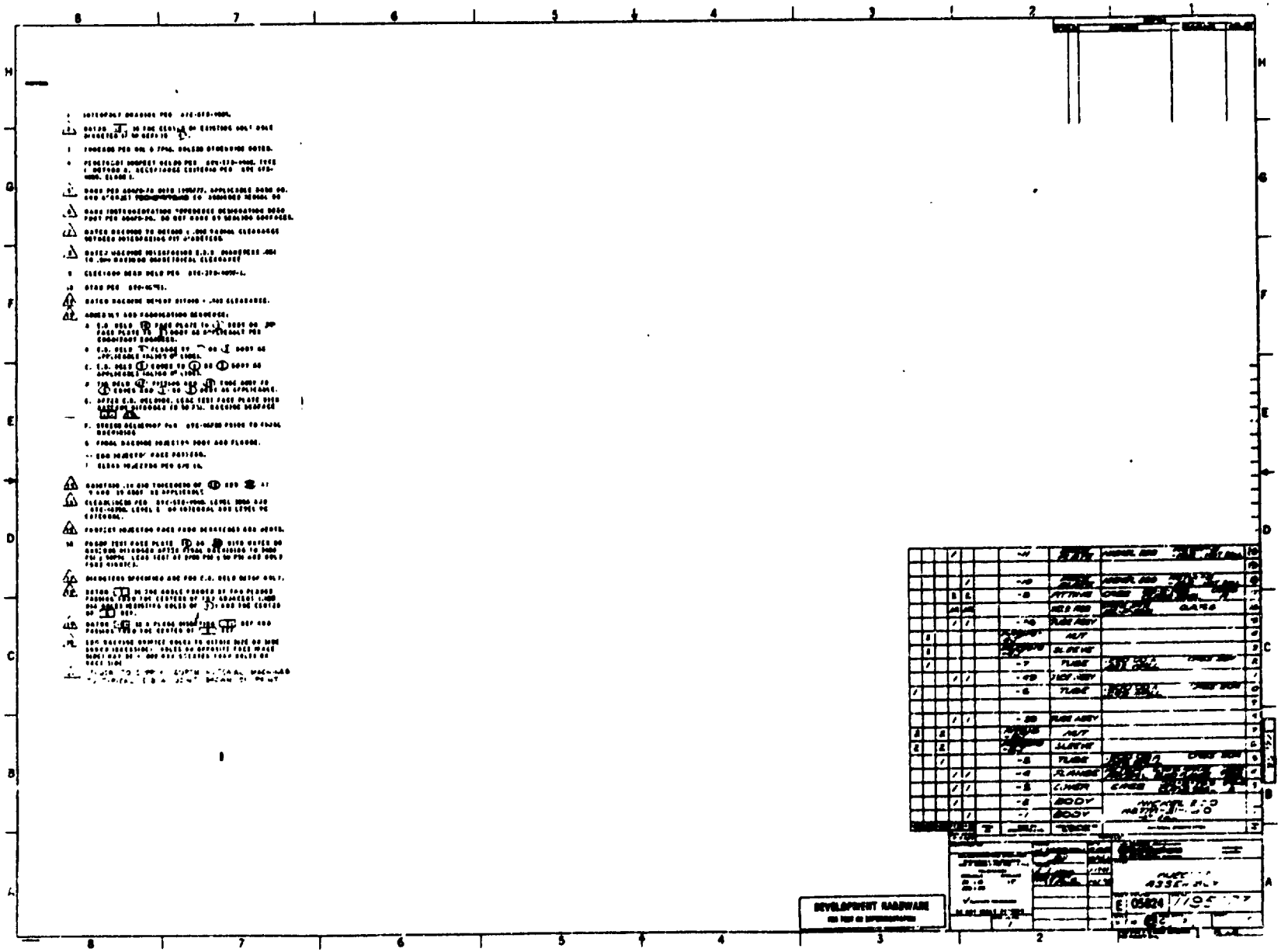

Figure B - 12

ORIGINAL PAGE IS
OF POOR QUALITY

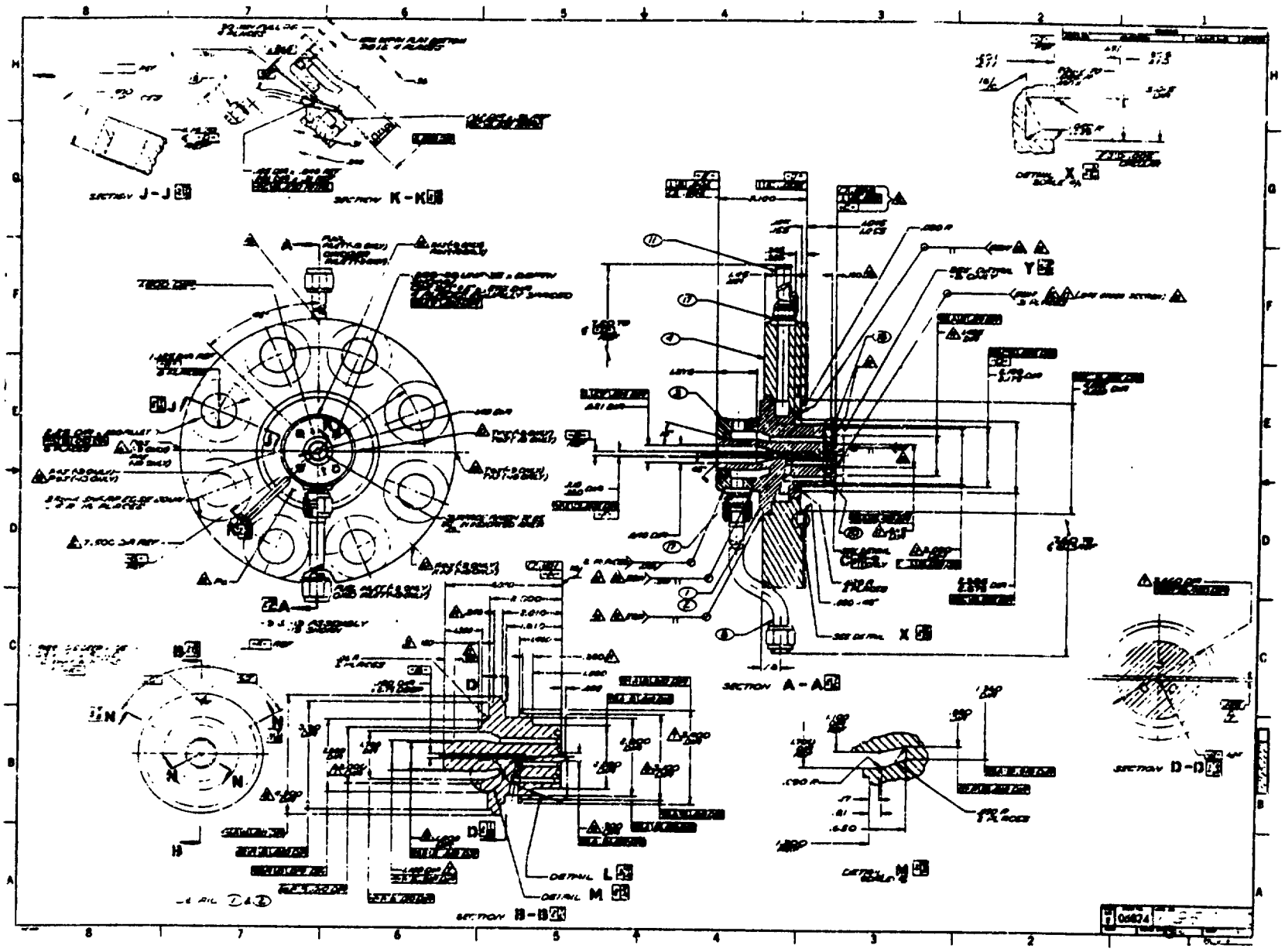

Figure B - 12 (Cont)

ORIGINAL PAGE IS
OF POOR QUALITY

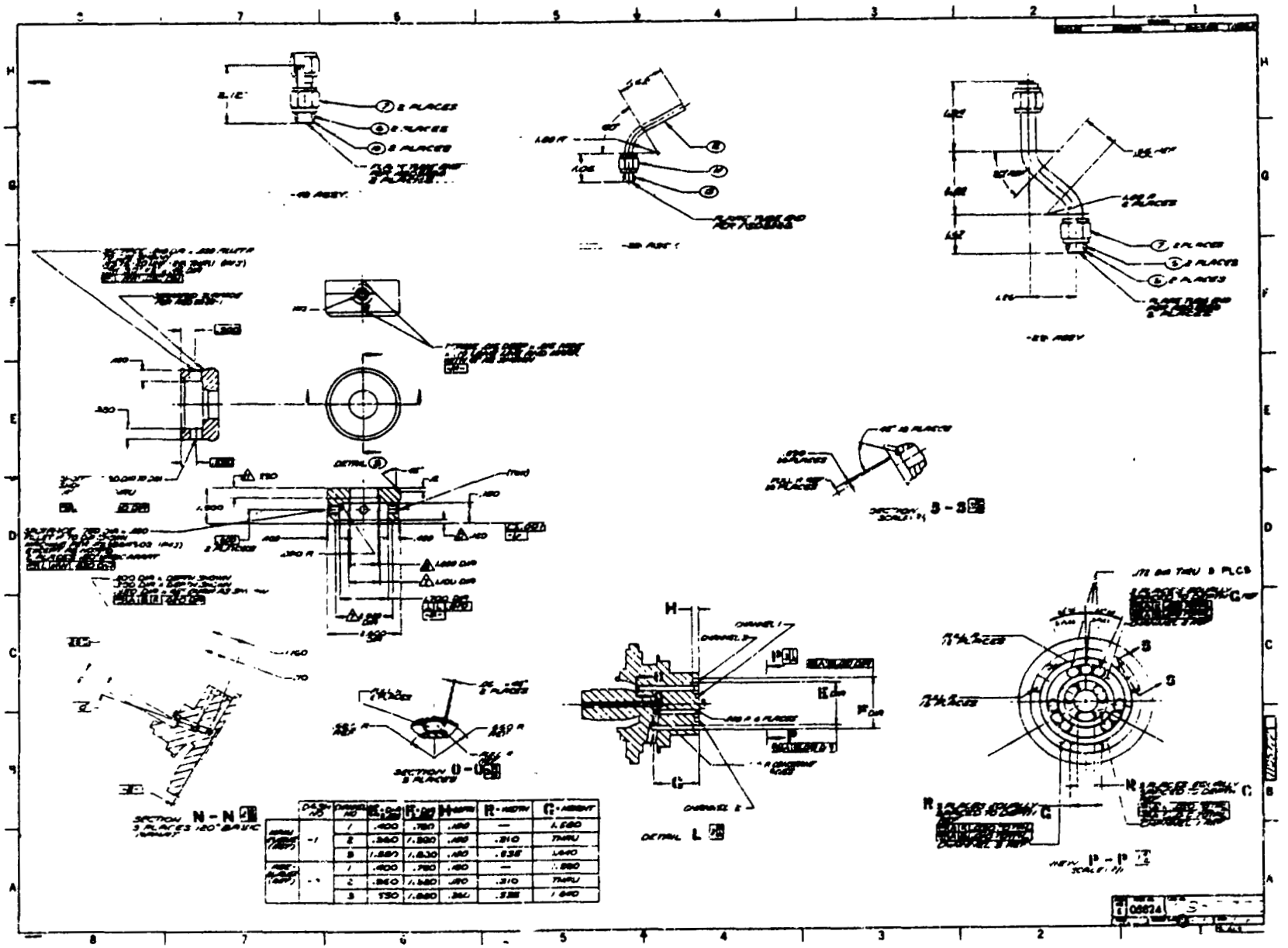

Figure B - 12 (Cont)

ORIGINAL PAGE IS
OF POOR QUALITY

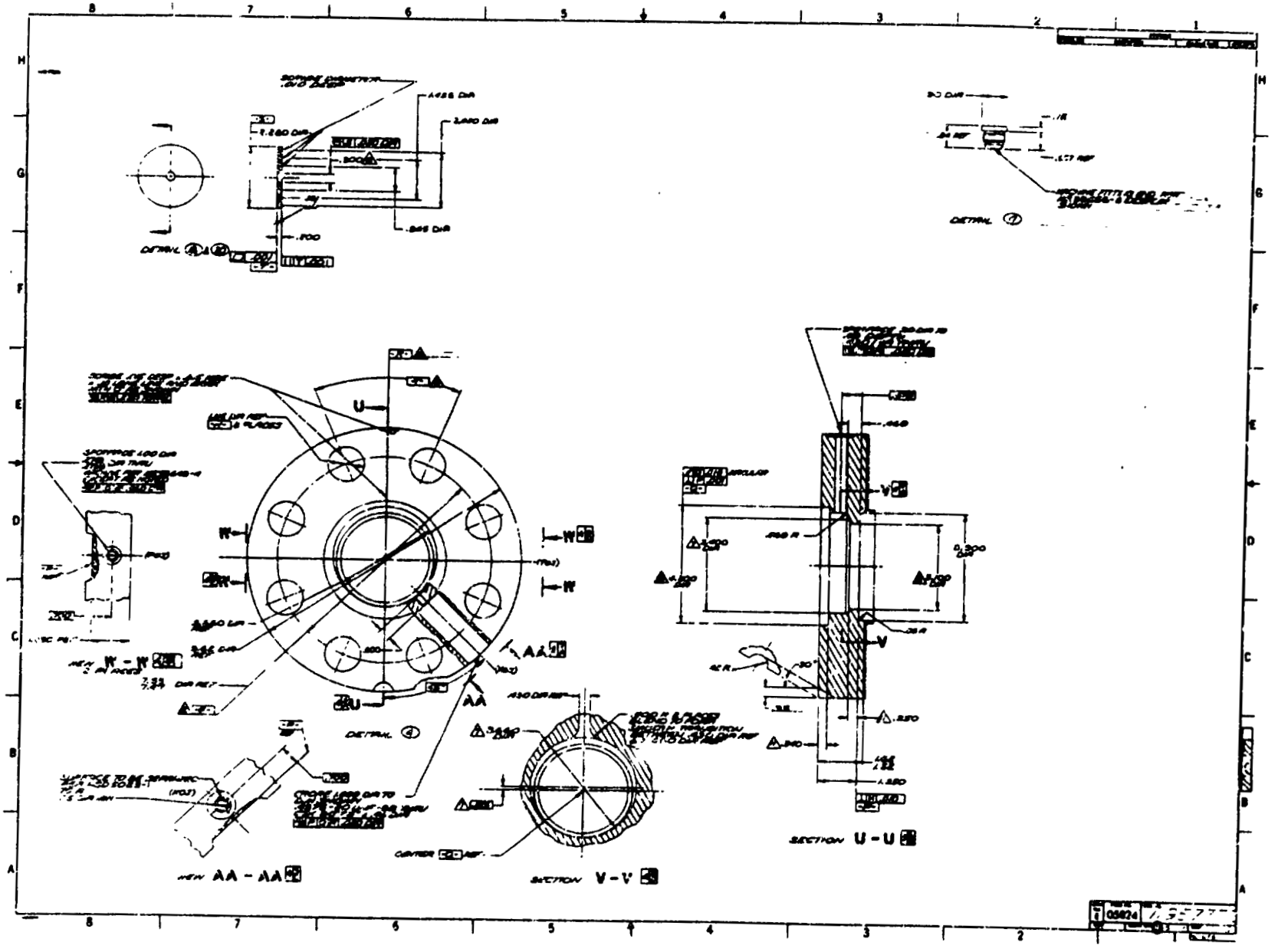

Figure B - 12 (Cont)

ORIGINAL PAGE IS
OF POOR QUALITY

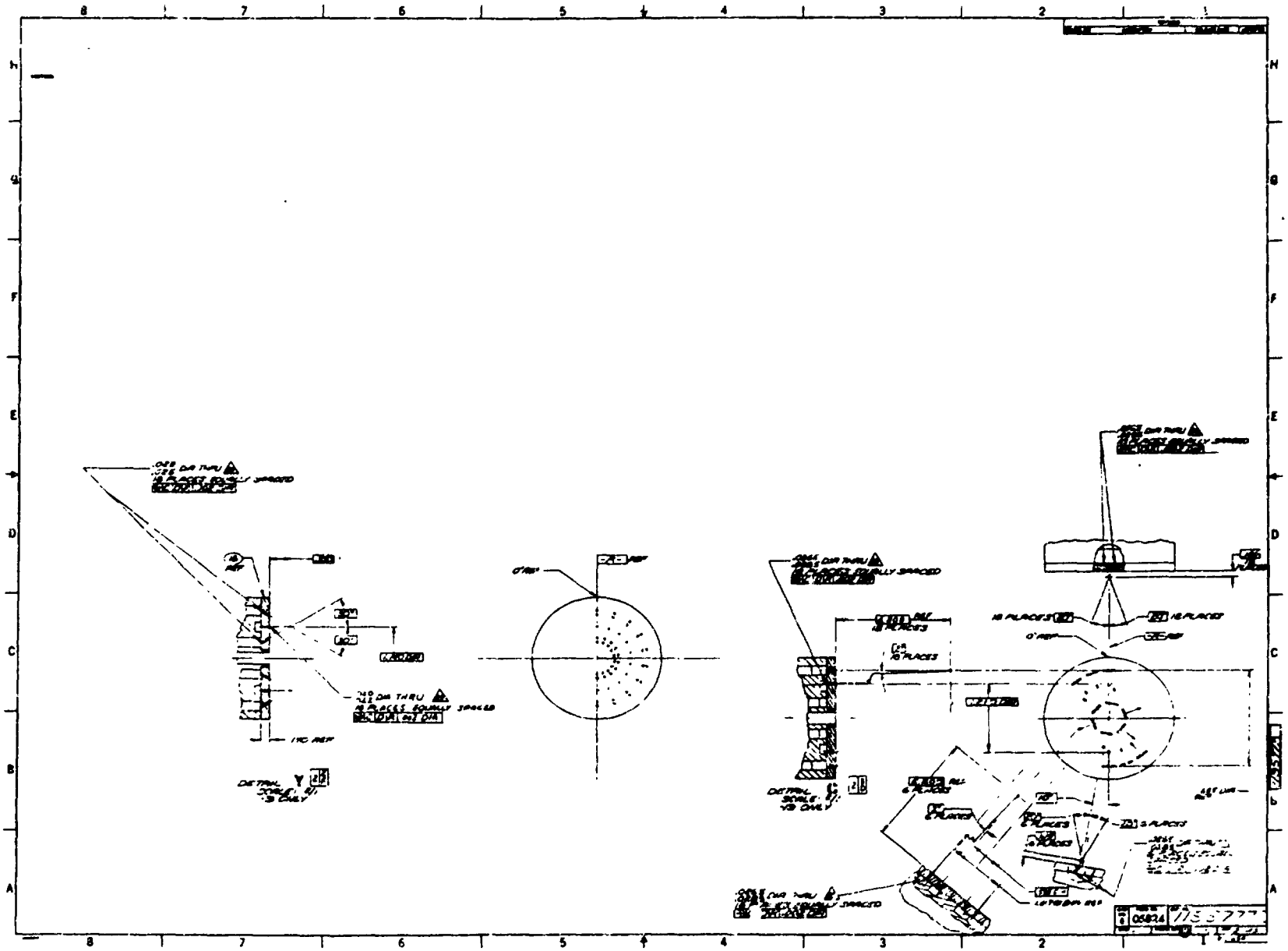

Figure B - 12 (Cont)

ORIGINAL PAGE IS
OF POOR QUALITY

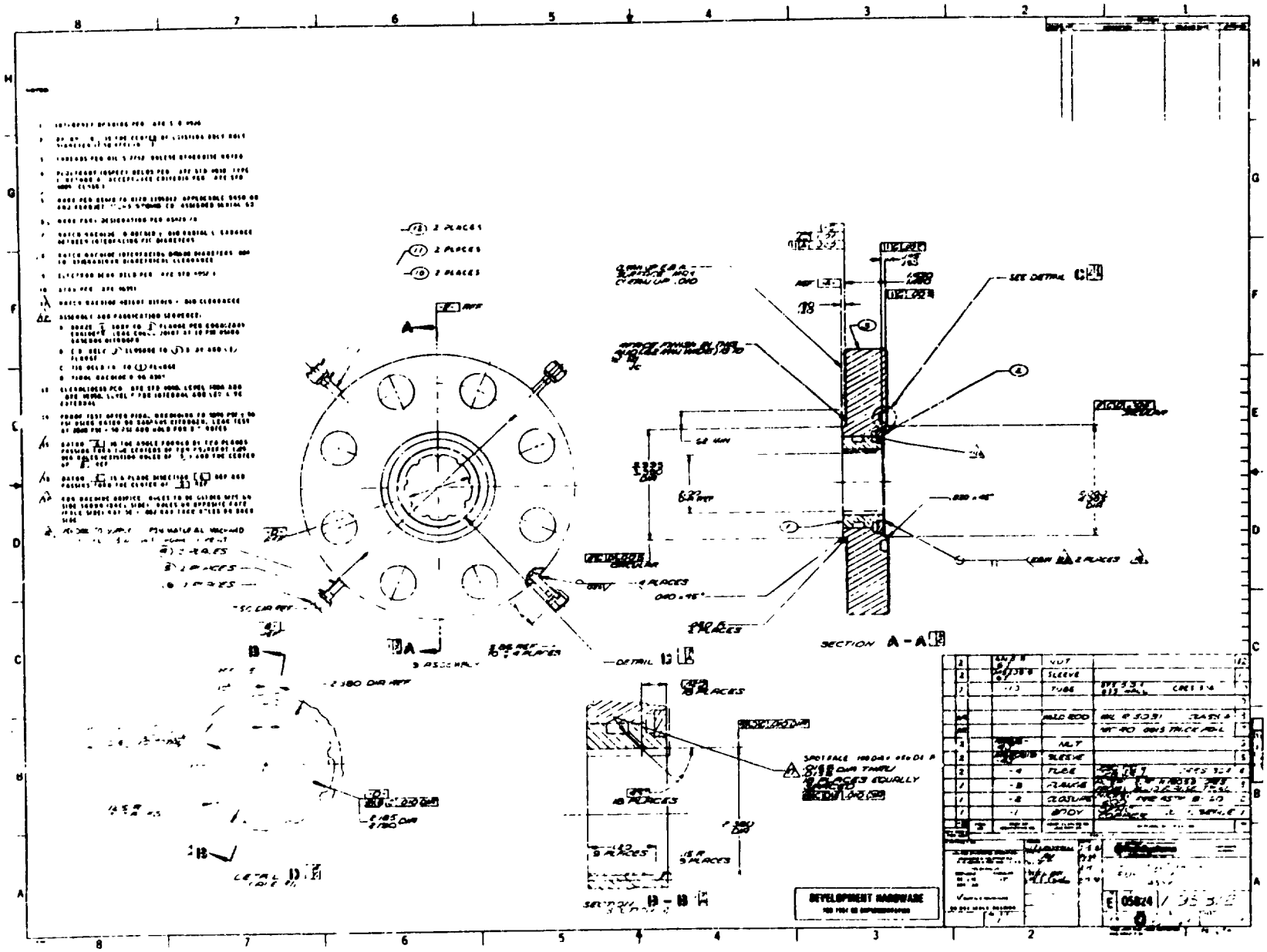

Figure B - 13

OF POOR QUALITY

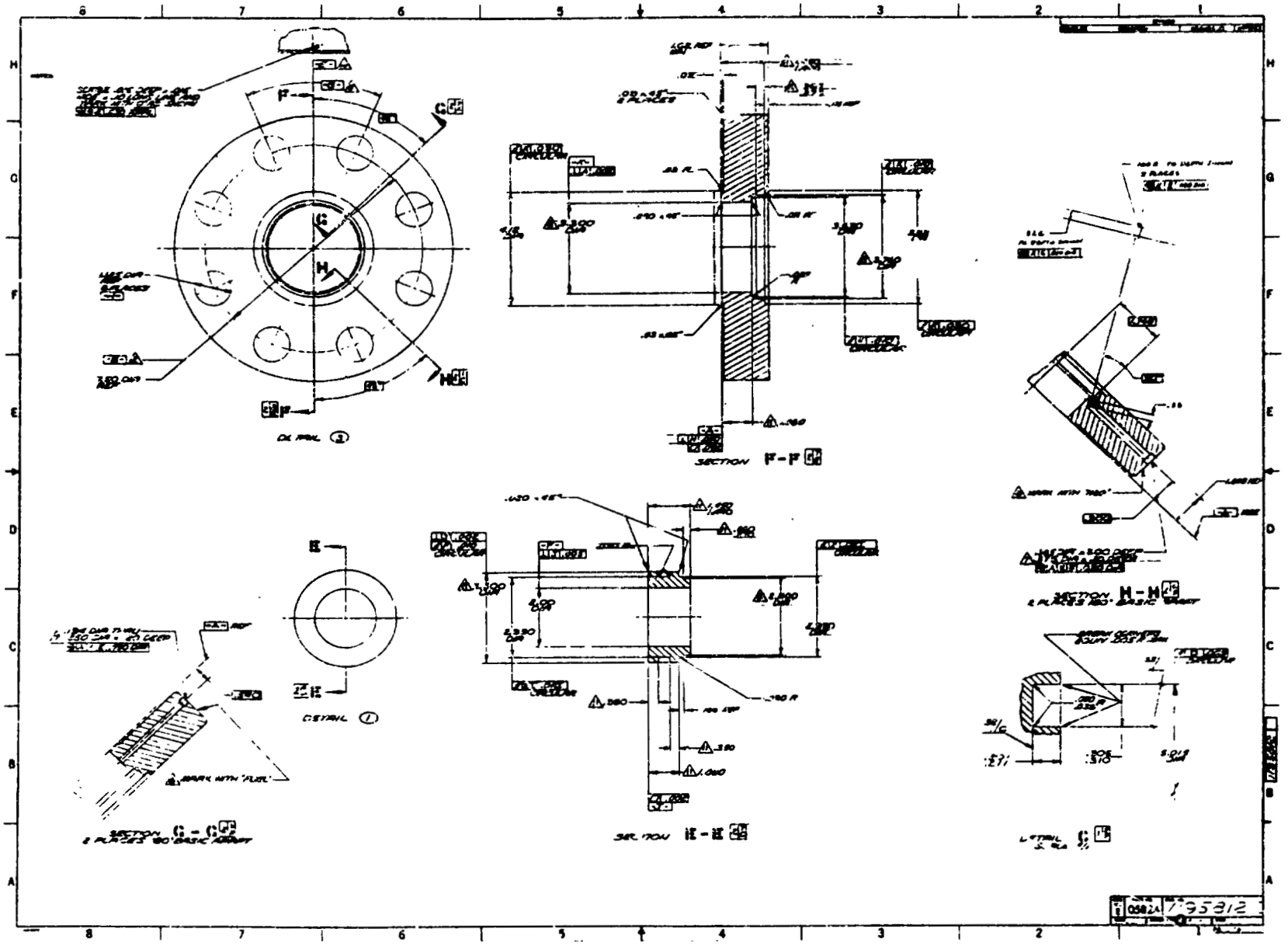

Figure B - 13 (Cont)

ORIGINAL PAGE IS
OF POOR QUALITY

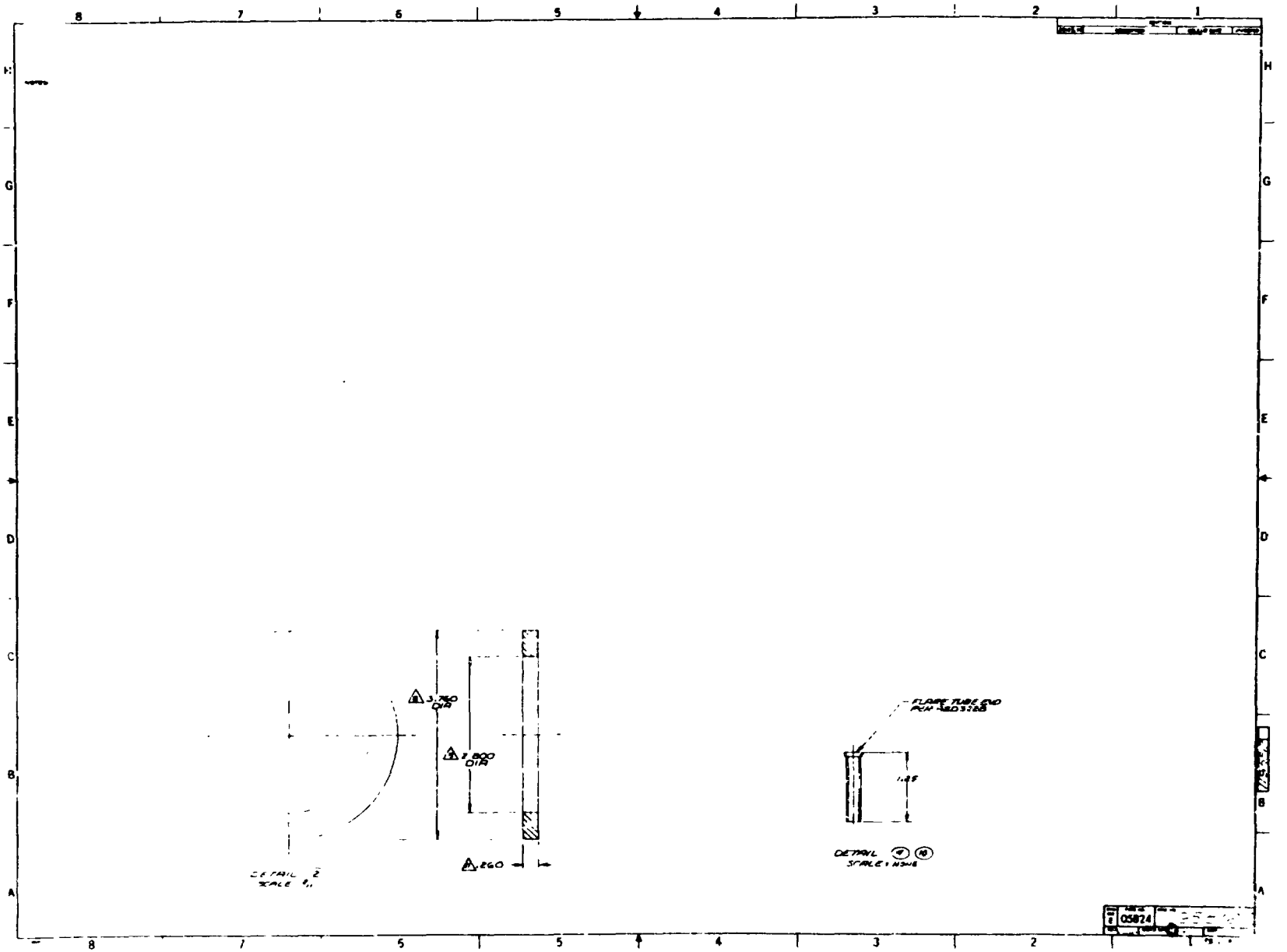

Figure B - 13 (Cont)

ORIGINAL PAGE IS
OF POOR QUALITY

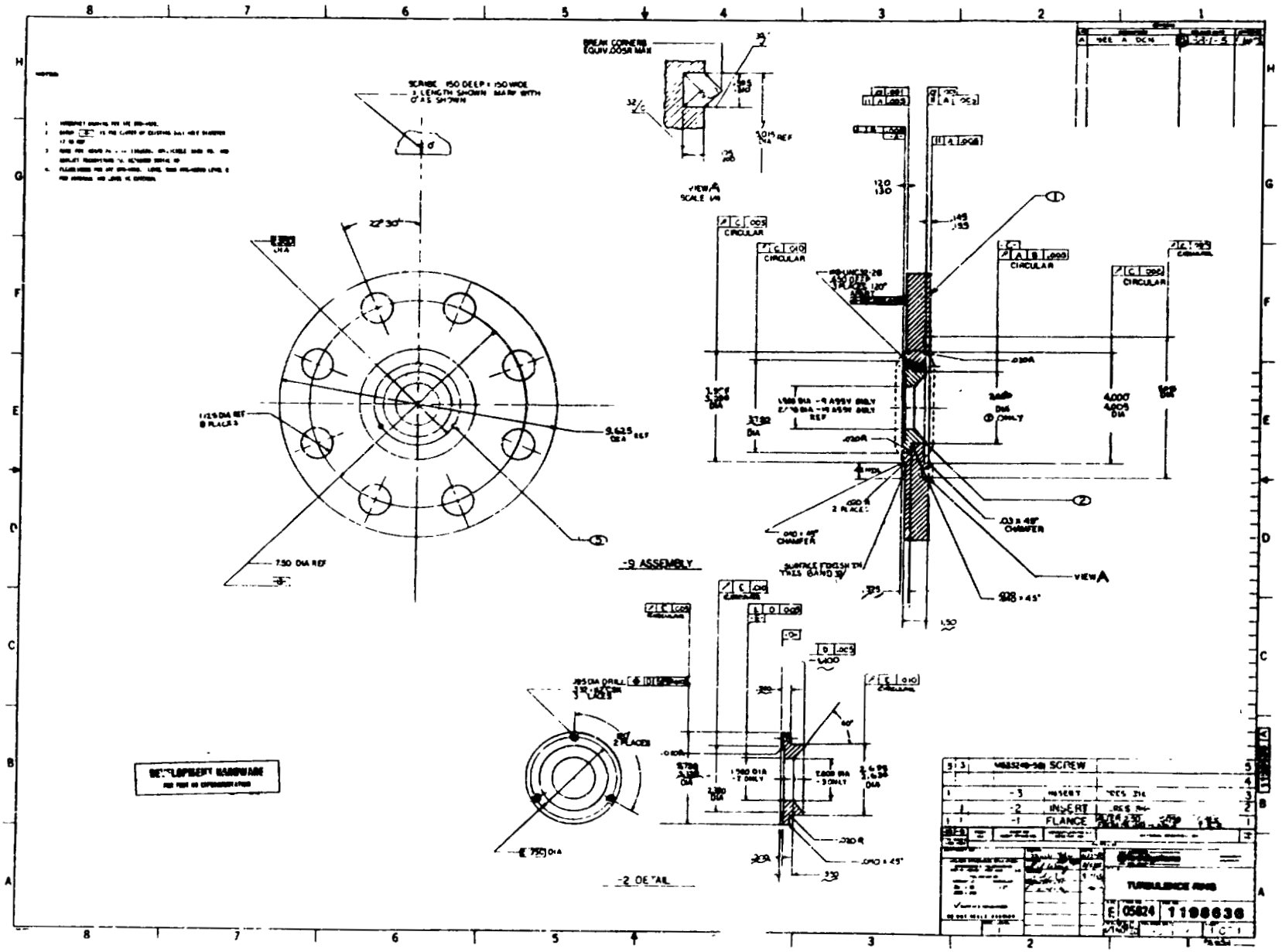

Figure B - 14

ORIGINAL PAGE IS
OF POOR QUALITY

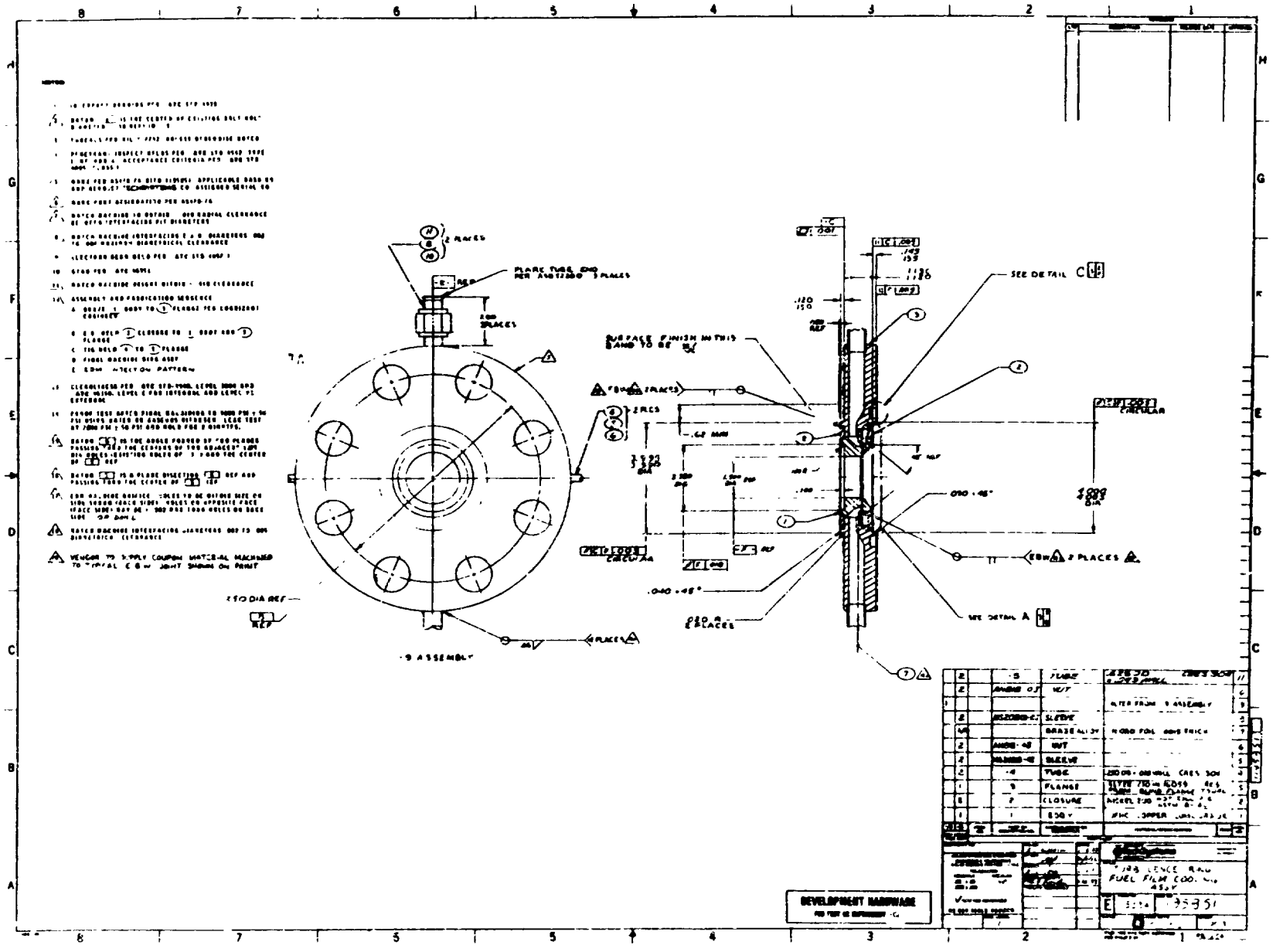

Figure B - 15

ORIGINAL PAGE IS
OF POOR QUALITY

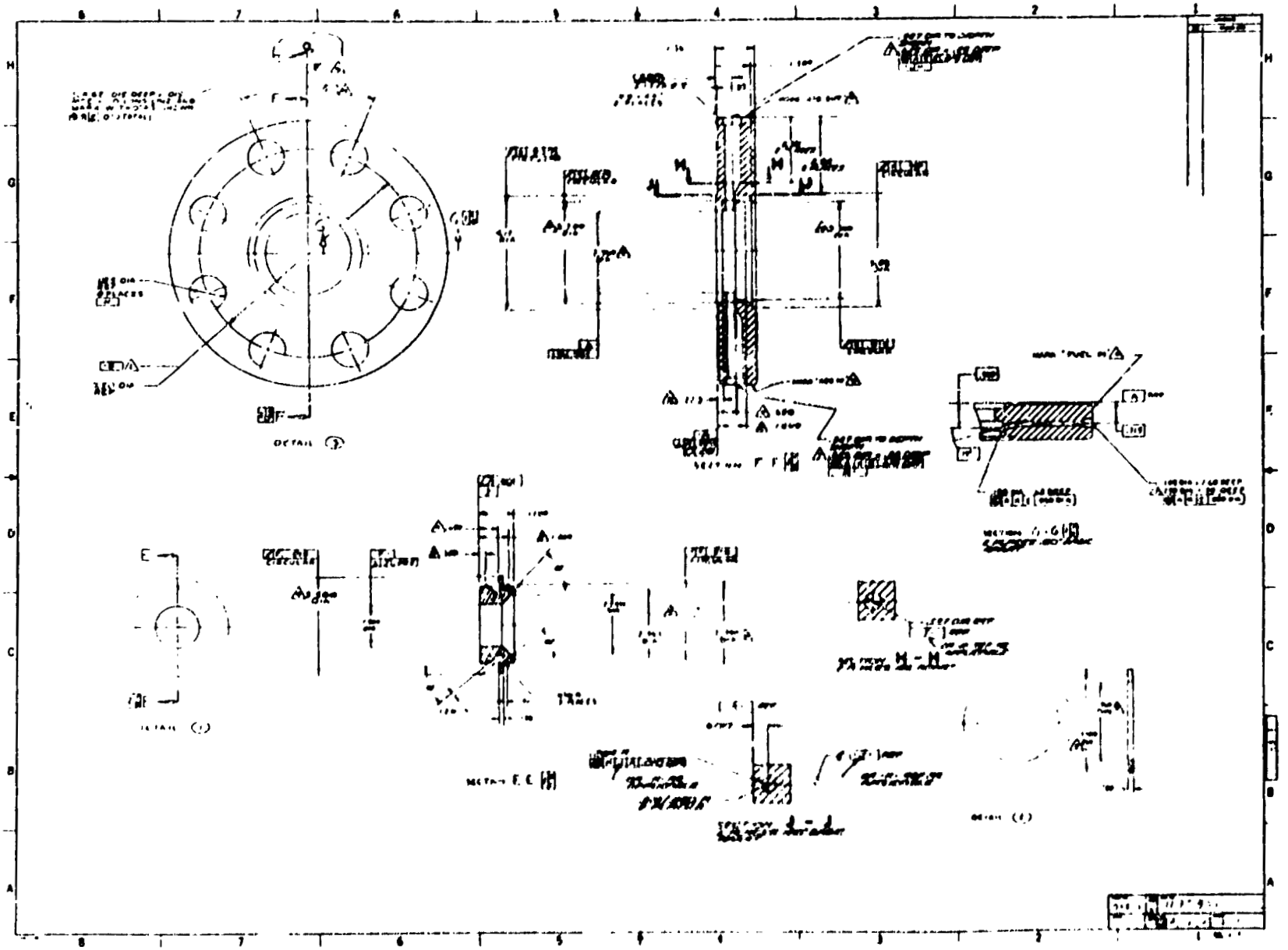

Figure B - 15 (Cont)

ORIGINAL PAGE IS
OF POOR QUALITY

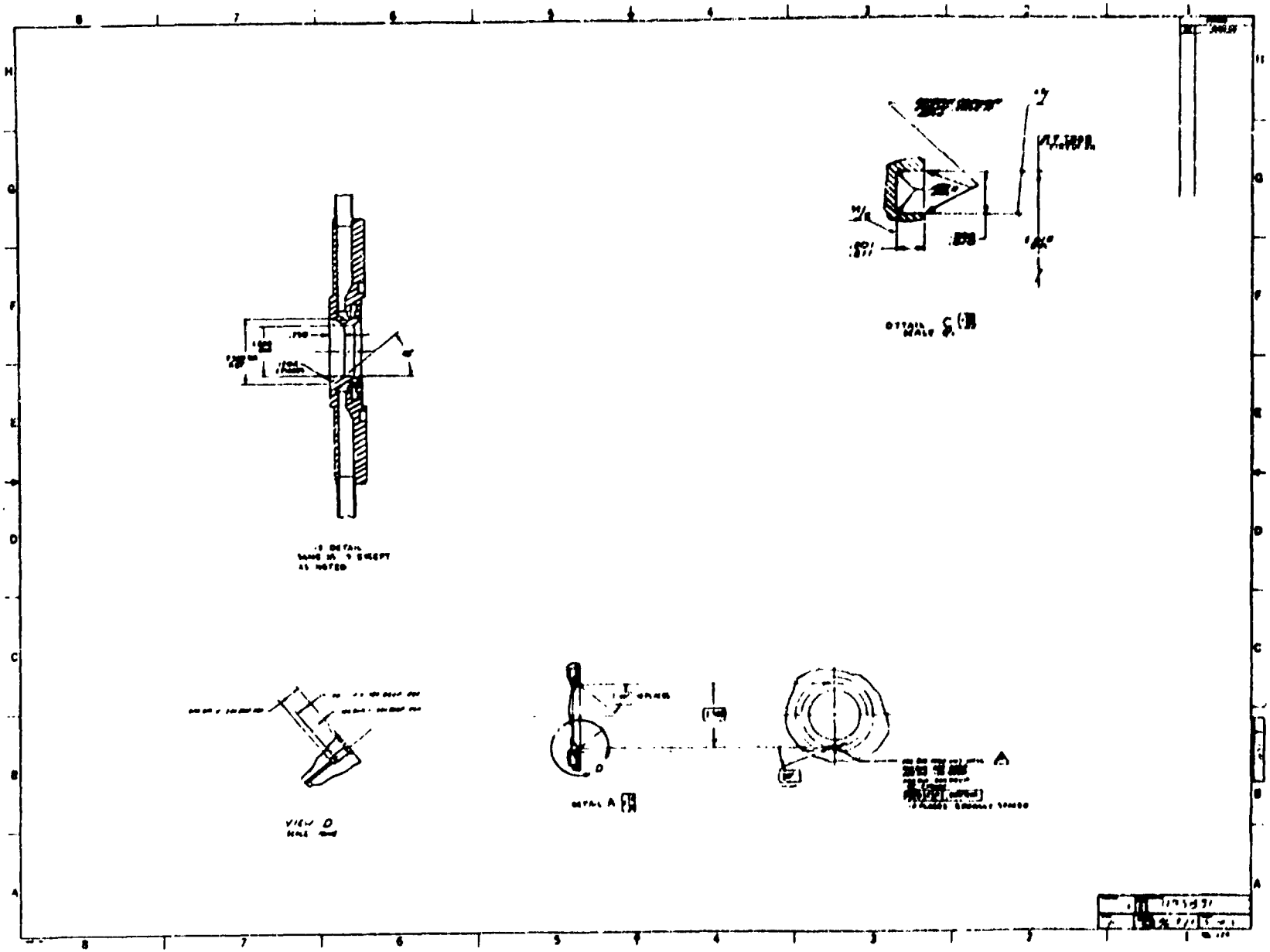

Figure B - 15 (Cont)

ORIGINAL PAGE IS
OF POOR QUALITY

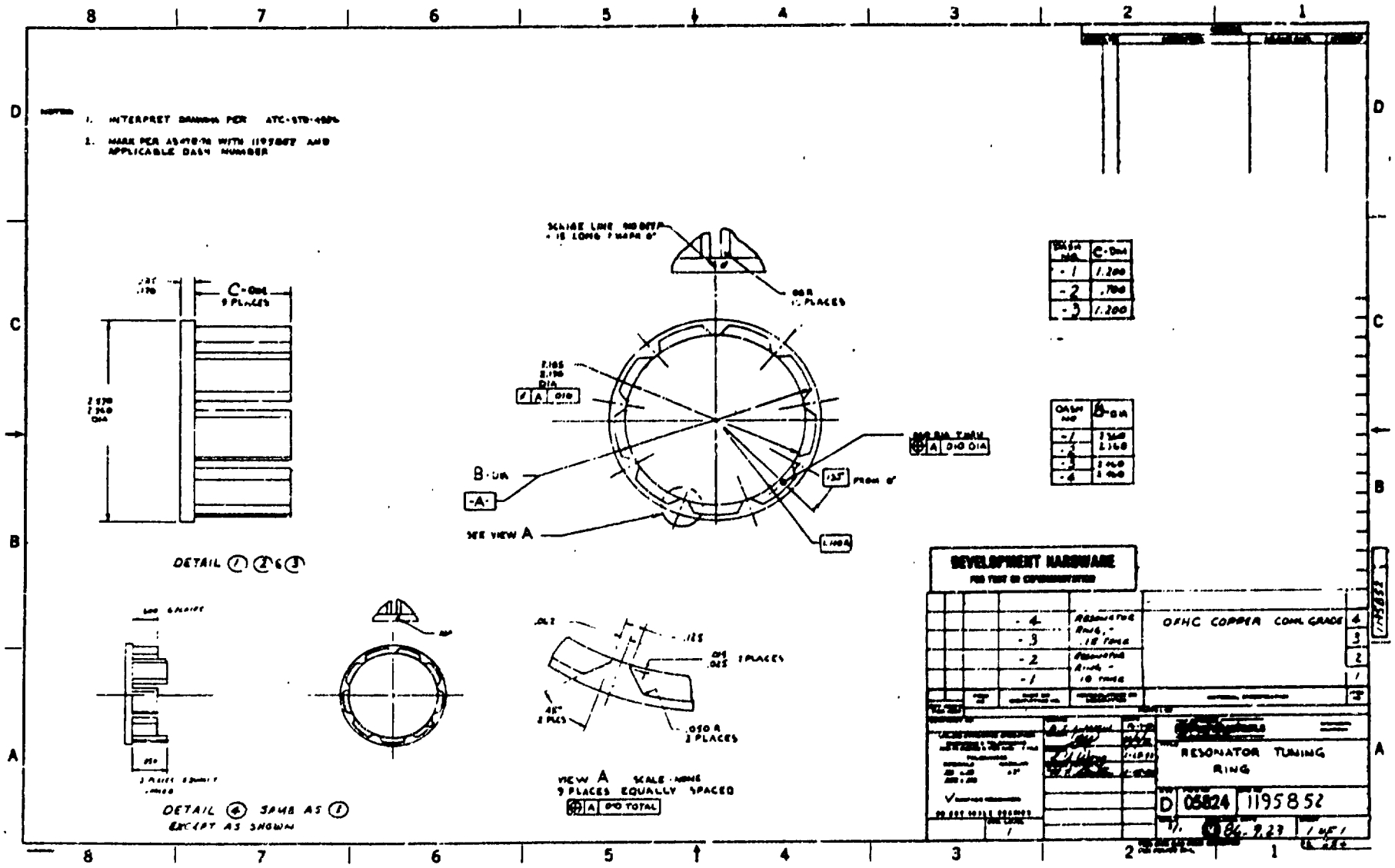

Figure B - 16

ORIGINAL PAGE IS OF POOR QUALITY

APPENDIX C

HOT FIRE TEST DATA PLOTS

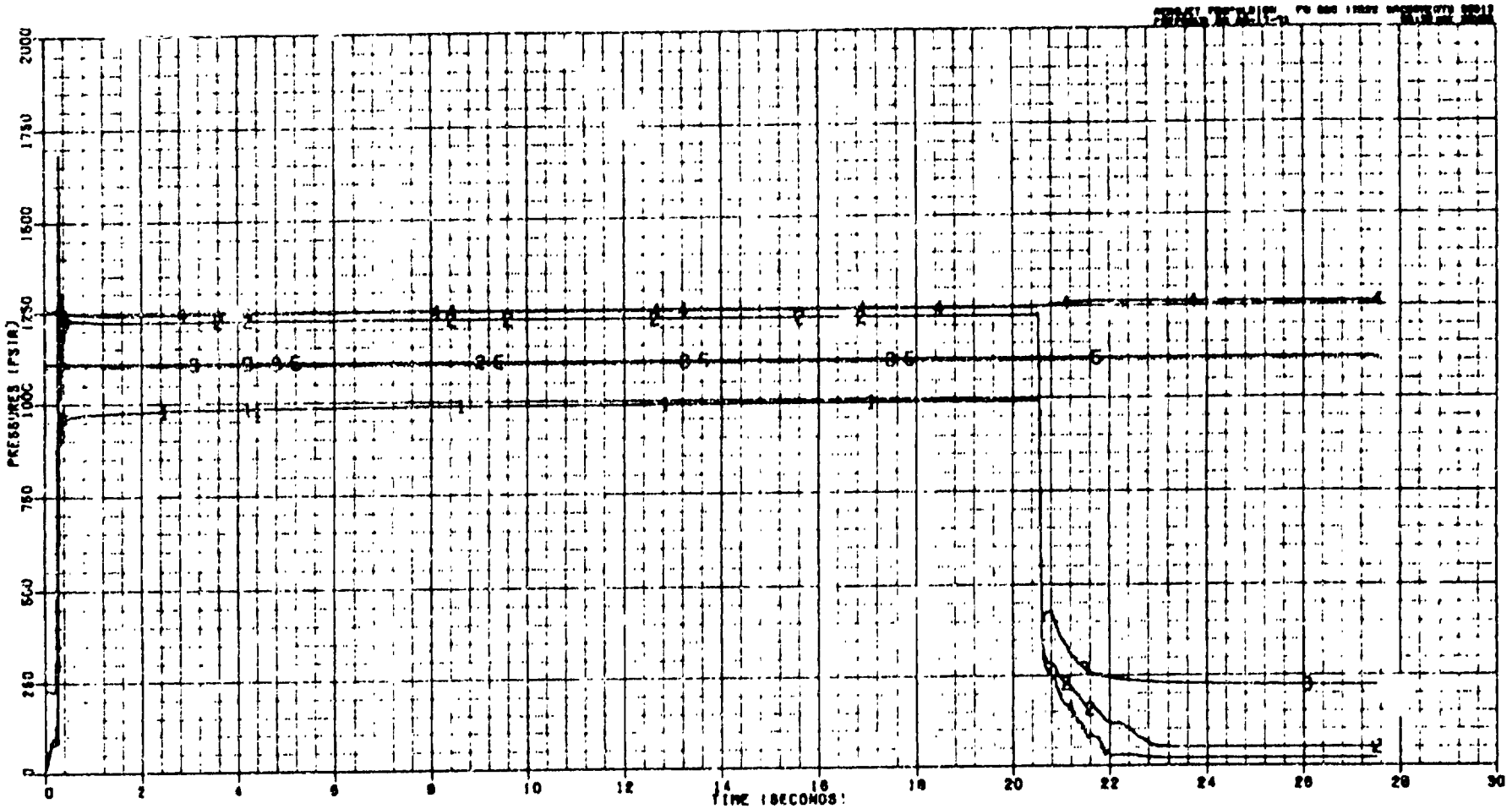

1 PC-1 PSIA
2 POJ PSIA
3 PFJ PSIA
4 POT PSIA
5 PFT PSIA

MEASURED PRESSURES VS TIME PLOT 1
TEST NO. KEE4-D01-09-107

TEST DATE 05-07-91 1325 HOURS 20.410 SEC.DUR

GENCORP
AEROJET

Figure C - 1

ORIGINAL PAGE IS
OF POOR QUALITY

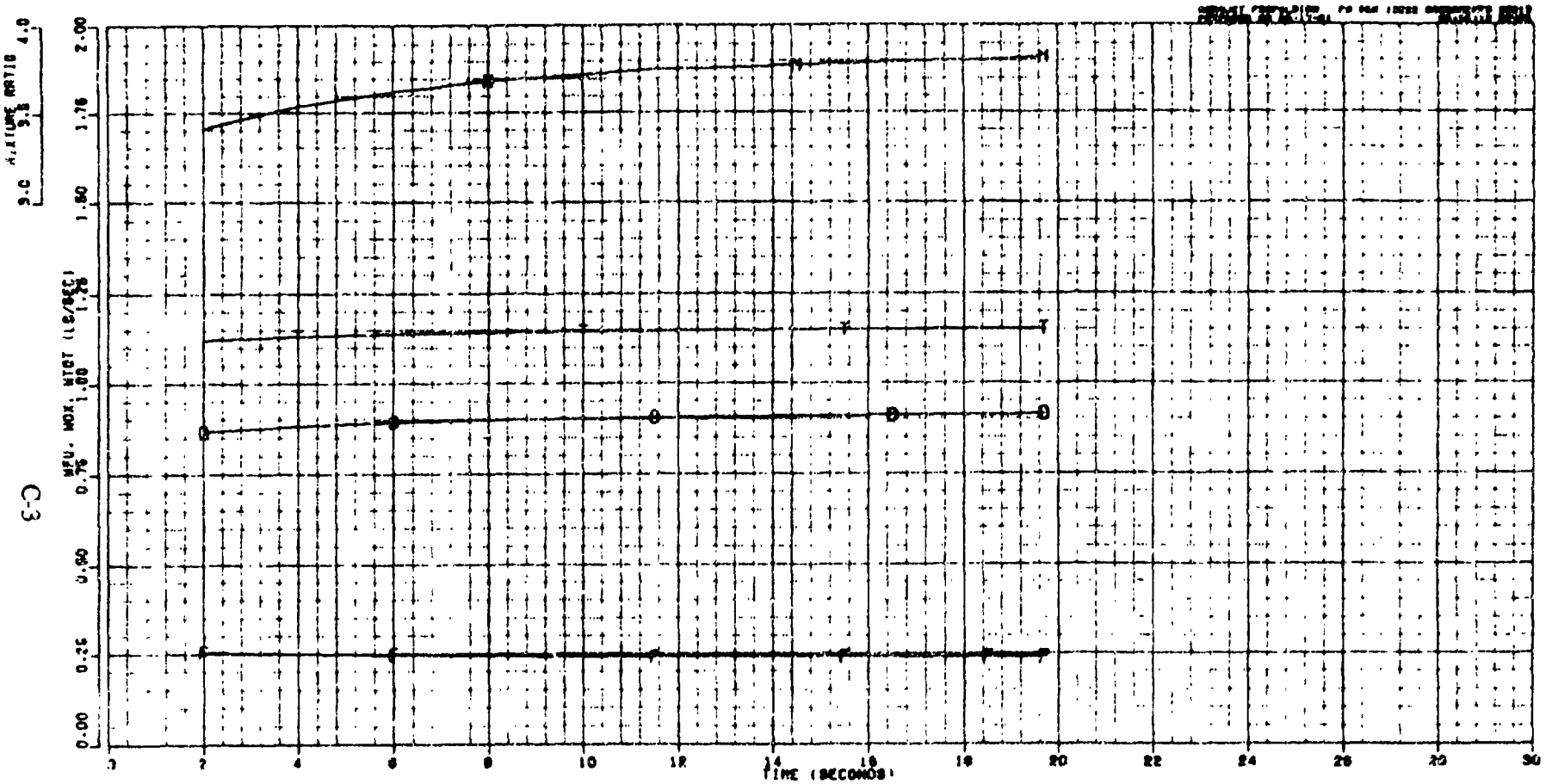

GENCORP
AEROJET

Figure C - 2

ORIGINAL PAGE IS
OF POOR QUALITY

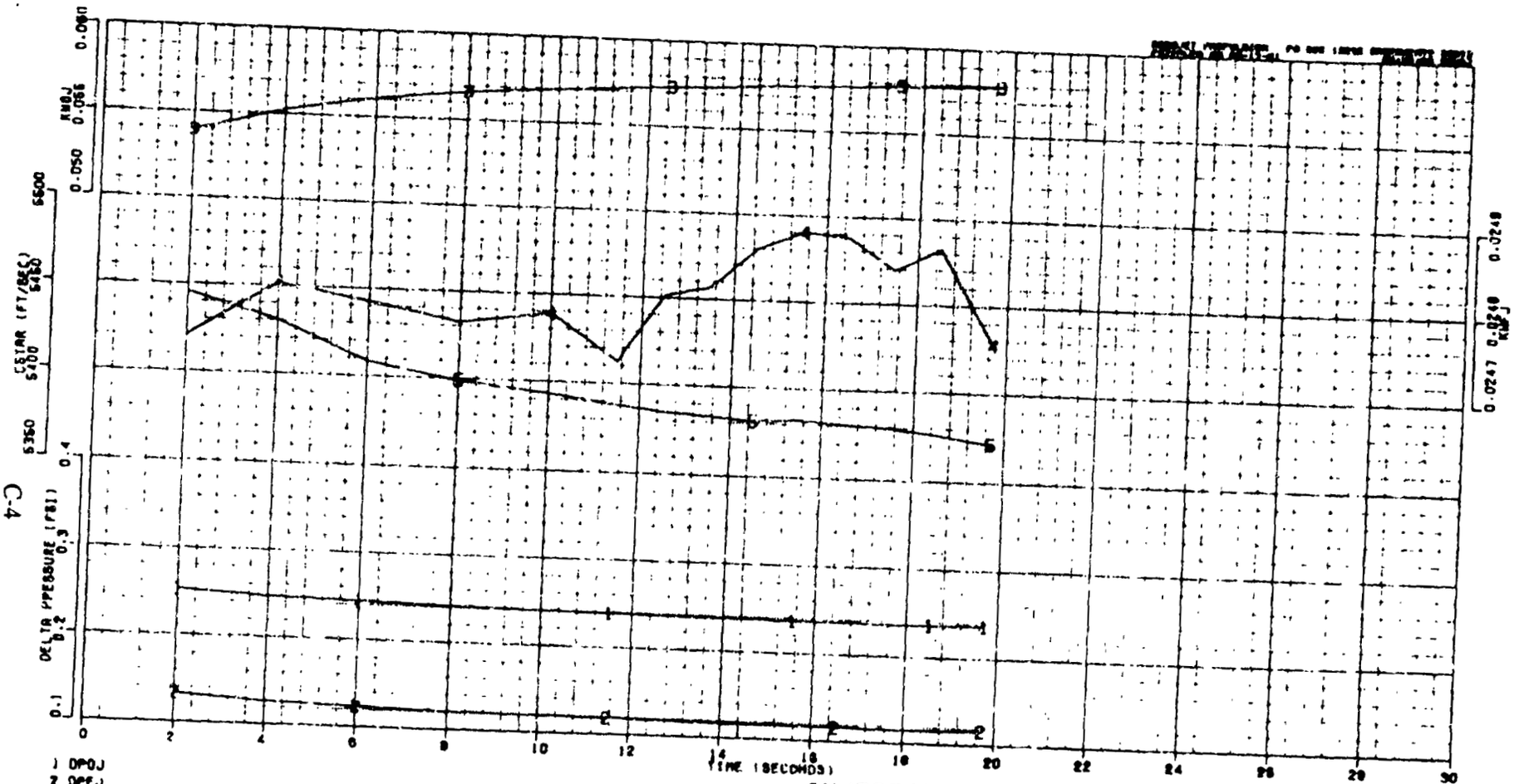

FT/SEC

INJECTOR CALCULATIONS VS TIME PLOT 3
TEST NO. KEE4-DD1-DA-107

TEST DATE 06-07-91 1326 HOURS 20.410 SEC.DUR

GENCORP
AEROJET

Figure C - 3

ORIGINAL PAGE IS
OF POOR QUALITY

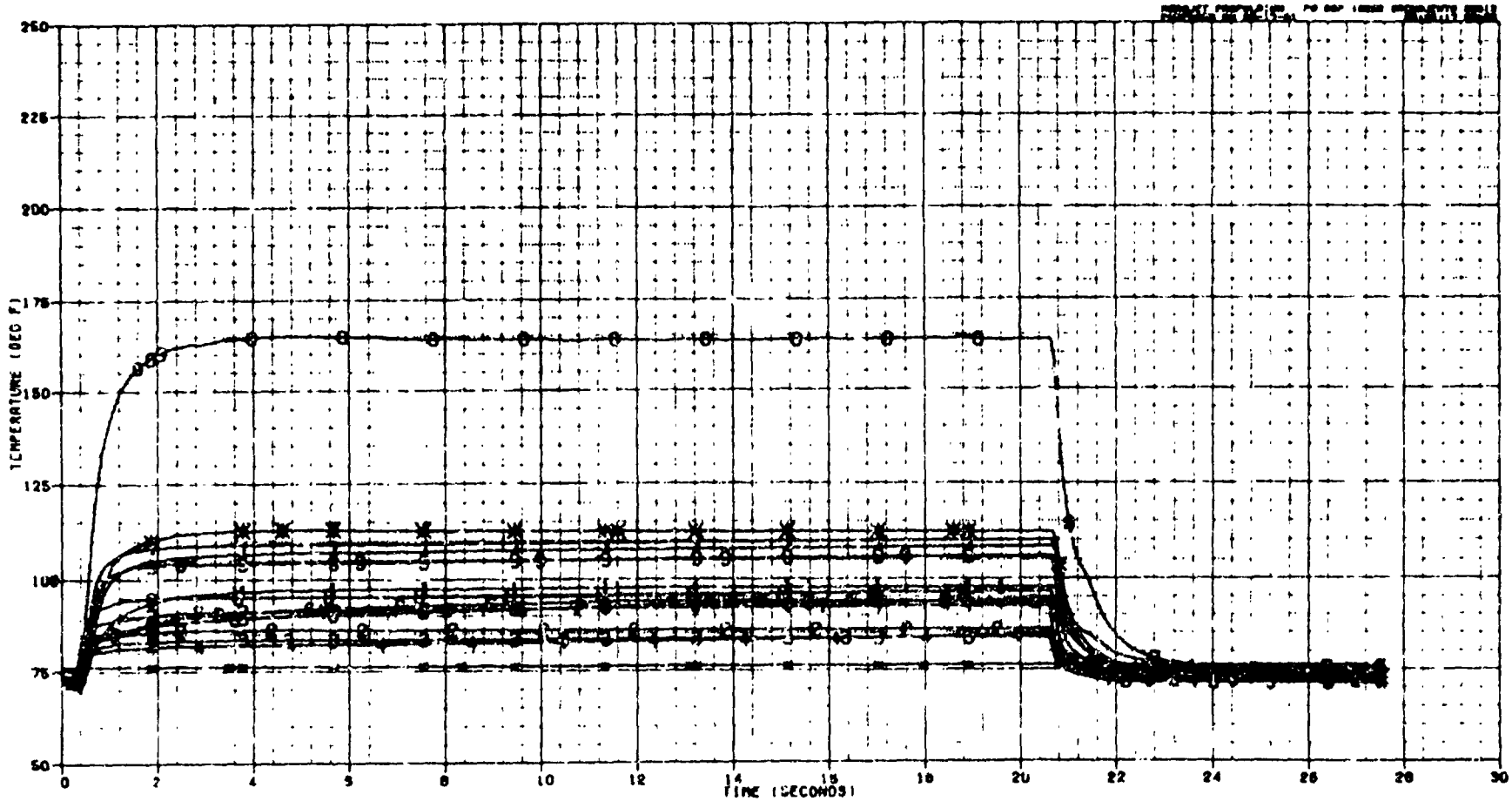

0 TNO-1 DEG F
1 TNO-2 DEG F
2 TNO-3 DEG F
3 TNO-4 DEG F
4 TNO-5 DEG F
5 TNO-6 DEG F
6 TNO-7 DEG F
7 TNO-8 DEG F
8 TNO-9 DEG F
9 TNO-10 DEG F
+ TNO-11 DEG F
■ TNO-12 DEG F
• TNO-13 DEG F
■ TNO-14 DEG F

GENCORP AEROJET

WATER TEMPERATURES VS TIME PLOT 4
TEST NO. KEE4-D01-DA-107

TEST DATE 05-07-91 1926 HOURS 20.410 SEC.DUR

Figure C - 4

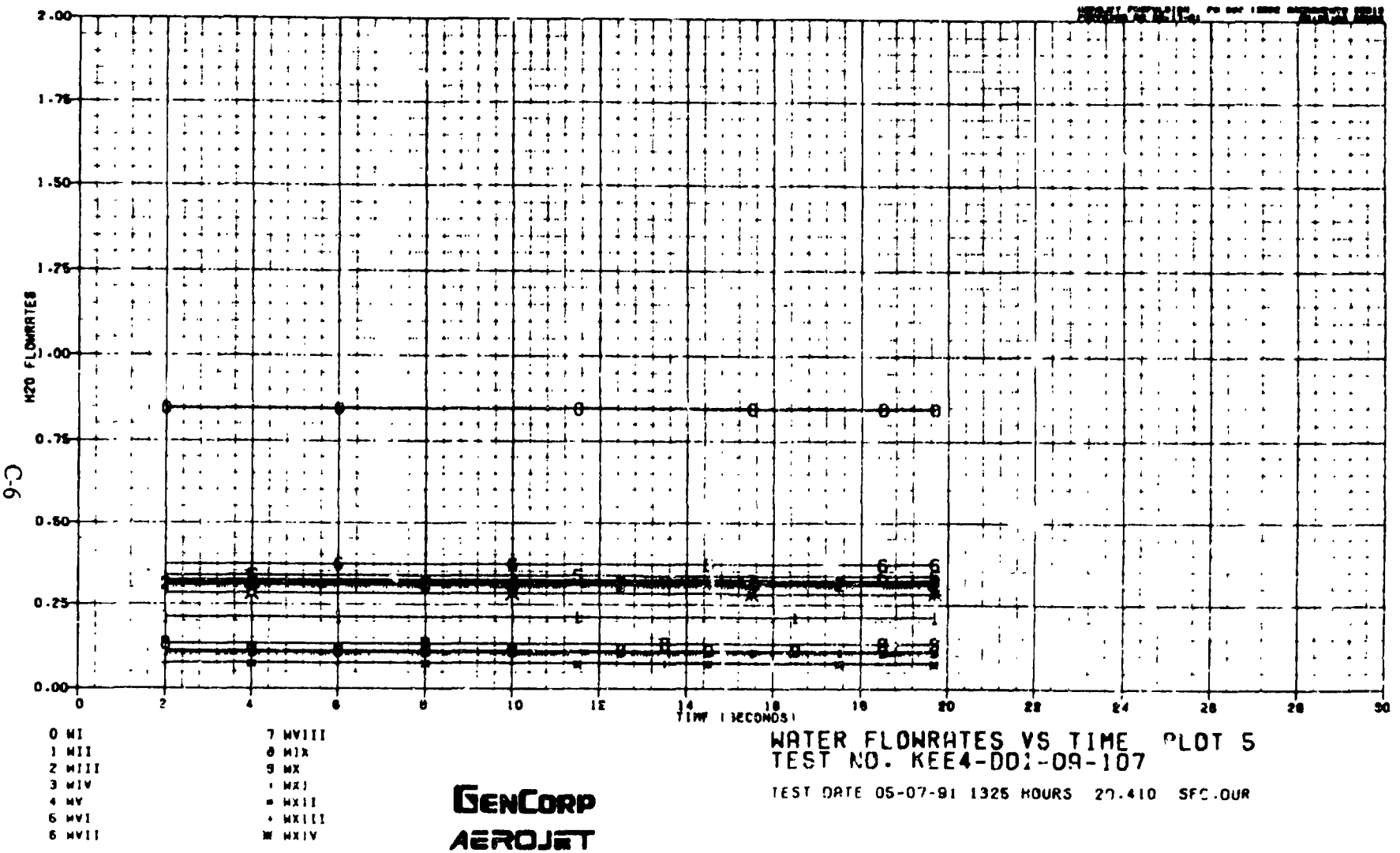
H2O FLOWRATES
2.00
1.75
1.50
1.25
1.00
0.75
0.50
0.25
0.00
0
2
4
6
8
10
12
14
16
18
20
22
24
26
28
30
TIME (SECONDS)
0 WI
1 WII
2 WIII
3 WIV
4 WV
5 WVI
6 WVII
7 WVIII
8 WIX
9 WX
WXI
WXII
WXIII
WXIV
GENCORP
AEROJET
WATER FLOWRATES VS TIME PLOT 5
TEST NO. KEE4-DD1-09-107
TEST DATE 05-07-91 1325 HOURS 20.410 SEC.DUR

Figure C - 5

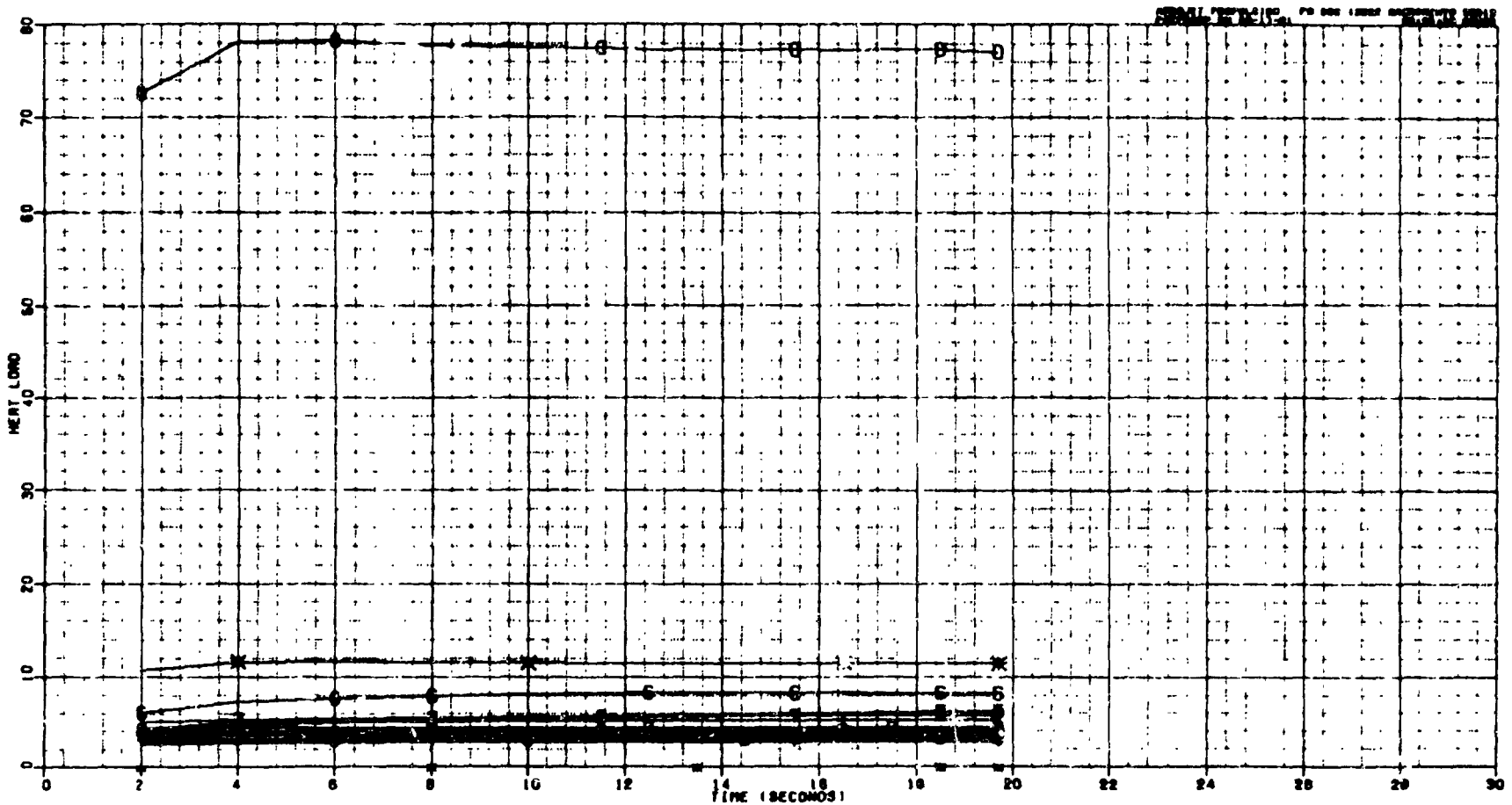

HEAT LOAD VS TIME PLOT 6
TEST NO. KEE4-D01-DA-107

TEST DATE 05-07-91 1325 HOURS 20.410 SEC.DUR

GENCORP AEROJET

Figure C - 6

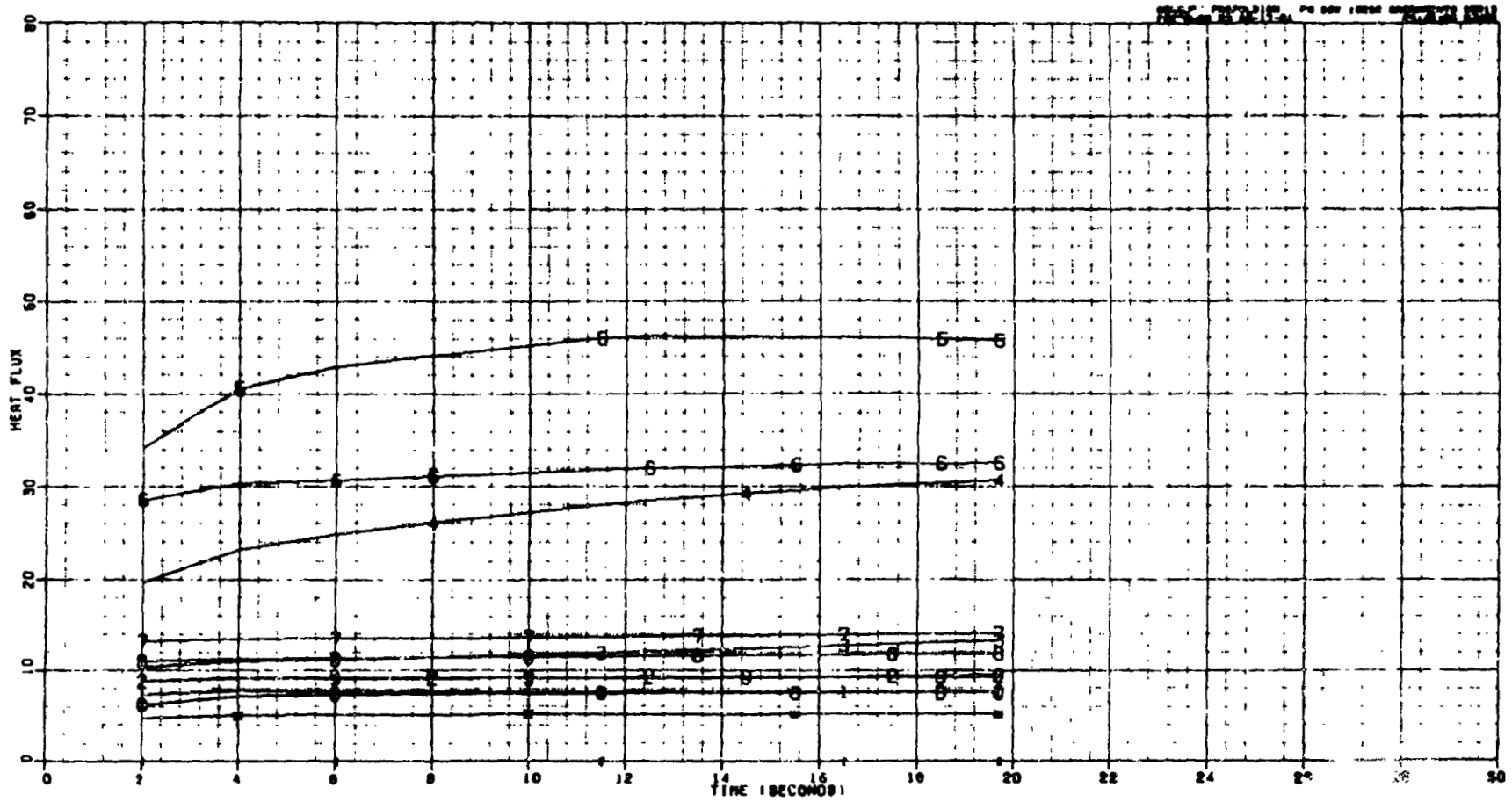

HEAT FLUX VS TIME PLOT 7
TEST NO. KEE4-DDI-OR-107

TEST DATE 05-07-91 1325 HOURS 20.410 SEC.DUR

GENCORP
AEROJET

Figure C - 7

ORIGINAL PAGE IS
OF POOR QUALITY

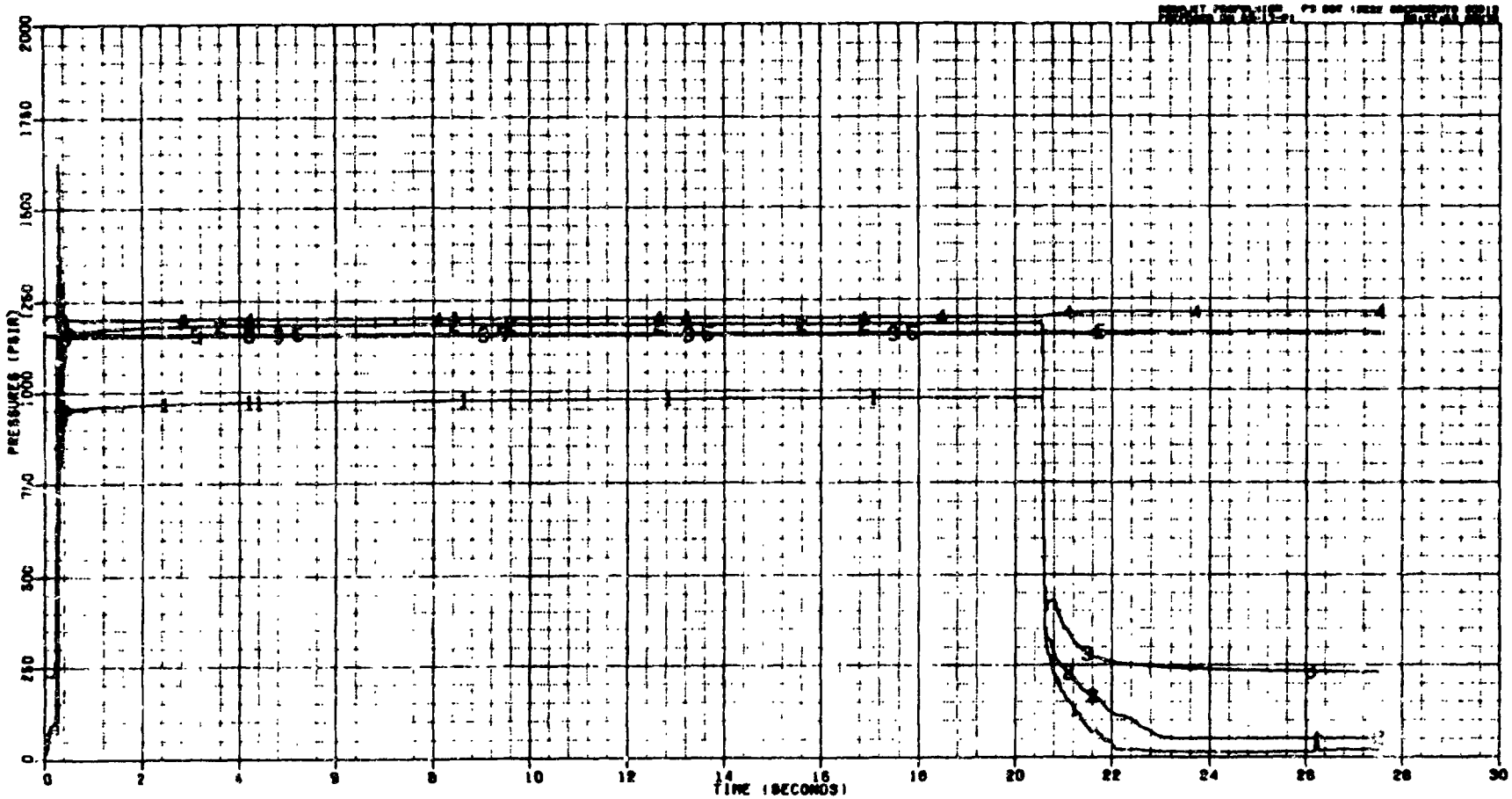

1 PC-1 PSIA
2 PDJ PSIA
3 PFJ PSIA
4 POT PSIA
5 PFT PSIA

MEASURED PRESSURES VS TIME PLOT 1
TEST NO. KE24-D01-DA-108

TEST DATE 05-07-91 1417 HOURS 20.423 SEC.DUR

GenCorp
AEROJET

Figure C - 8

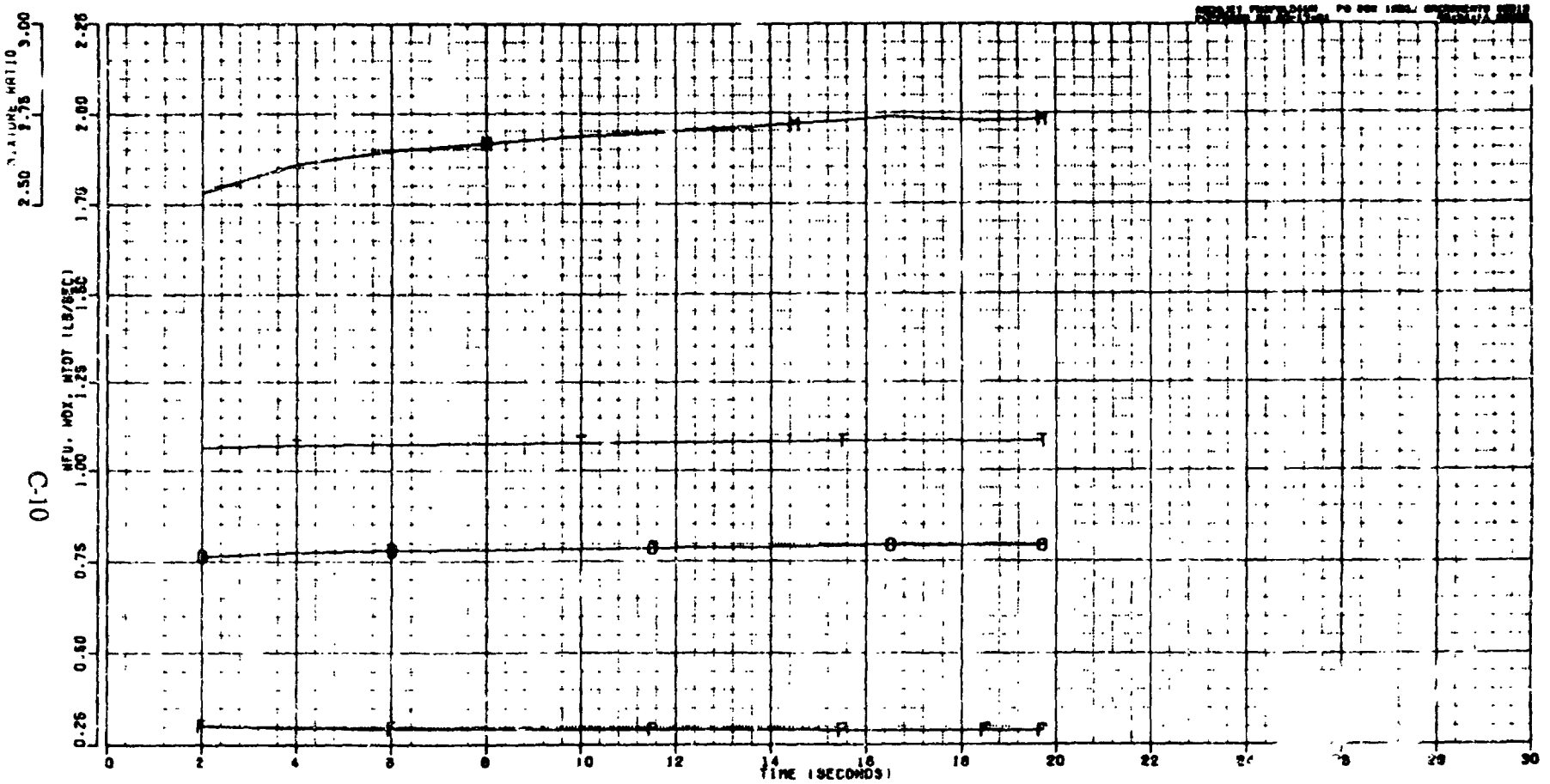

INJECTOR FLOW VS TIME PLOT 2
TEST NO. KEE4-D01-OR-108

TEST DATE 05-07-91 1417 HOURS 20.423 SEC.DUR

GENCORP
AEROJET

Figure C - 9

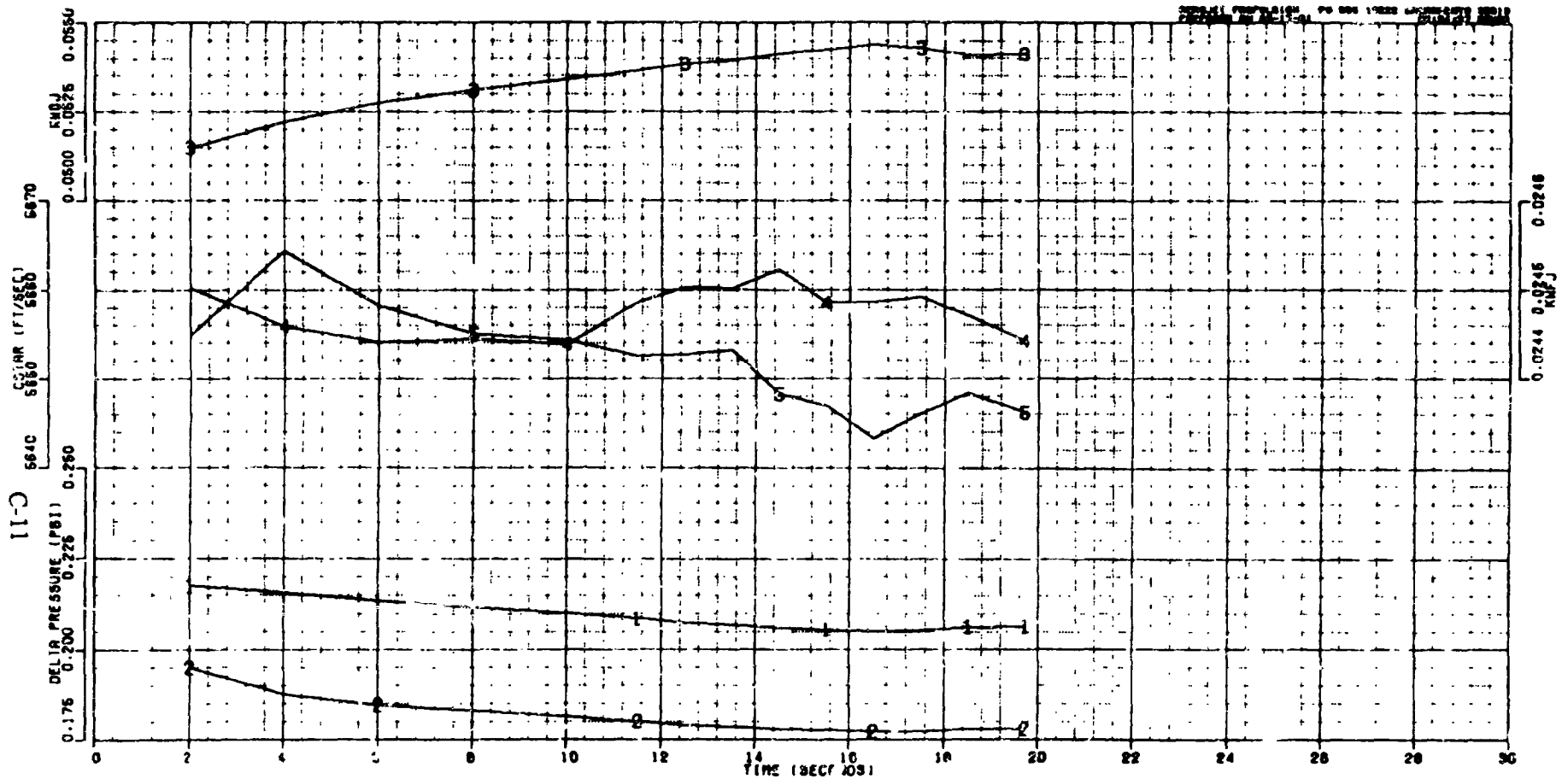

INJECTOR CALCULATIONS VS TIME PLOT 3
TEST NO. KEE4-D01-0A-108

TEST DATE 06-07-91 1417 HOURS 20.423 SEC.DUR

GENCORP AEROJET

Figure C - 10

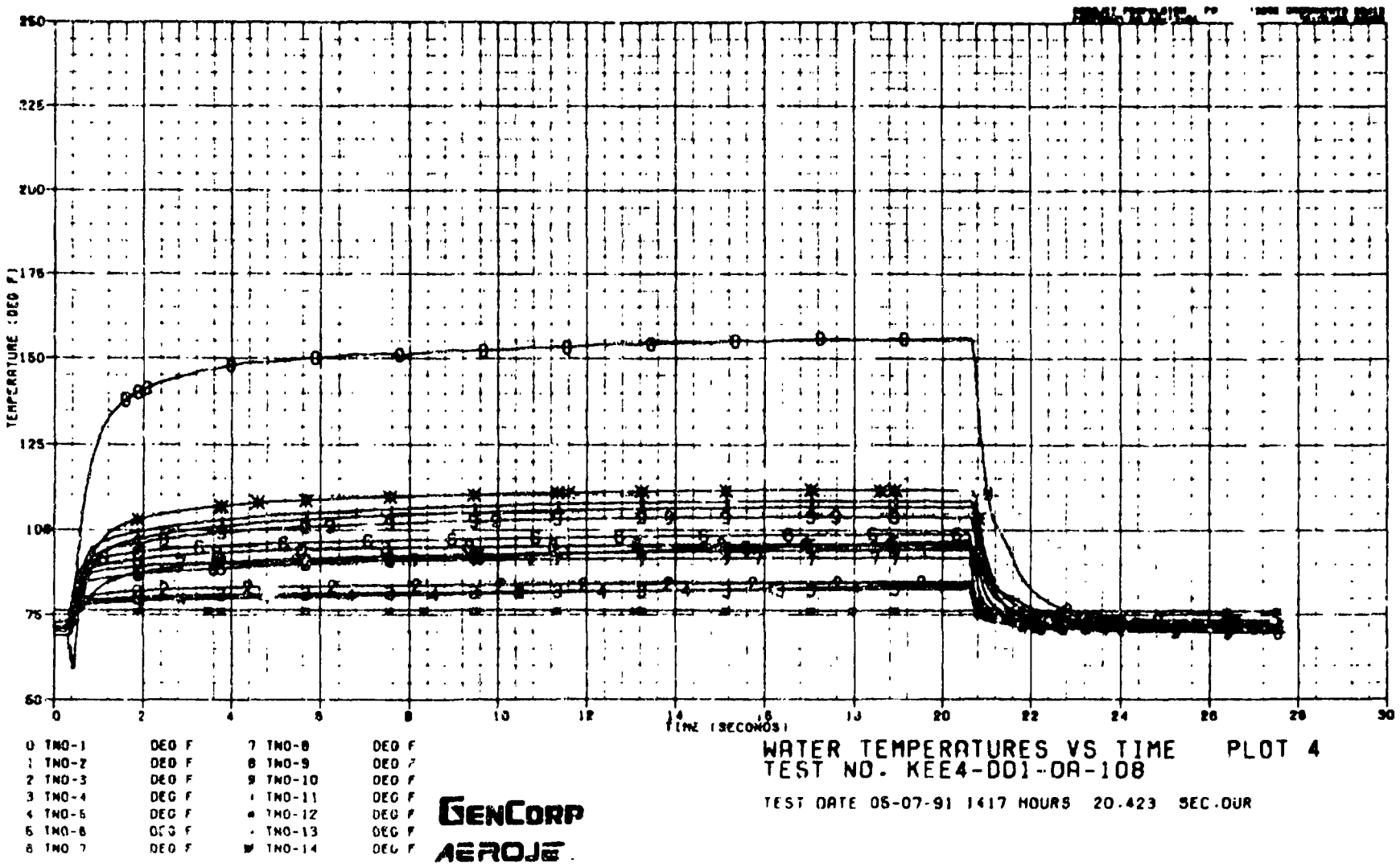
TEMPERATURE (DEG F)
TIME (SECONDS)
WATER TEMPERATURES VS TIME PLOT 4
TEST NO. KEE4-DD1-DA-108
TEST DATE 05-07-91 1417 HOURS 20.423 SEC.DUR
0 TNO-1 DEG F
1 TNO-2 DEG F
2 TNO-3 DEG F
3 TNO-4 DEG F
4 TNO-5 DEG F
5 TNO-6 DEG F
6 TNO-7 DEG F
7 TNO-8 DEG F
8 TNO-9 DEG F
9 TNO-10 DEG F
TNO-11 DEG F
TNO-12 DEG F
TNO-13 DEG F
TNO-14 DEG F
GENCORP
AEROJET

Figure C - 11

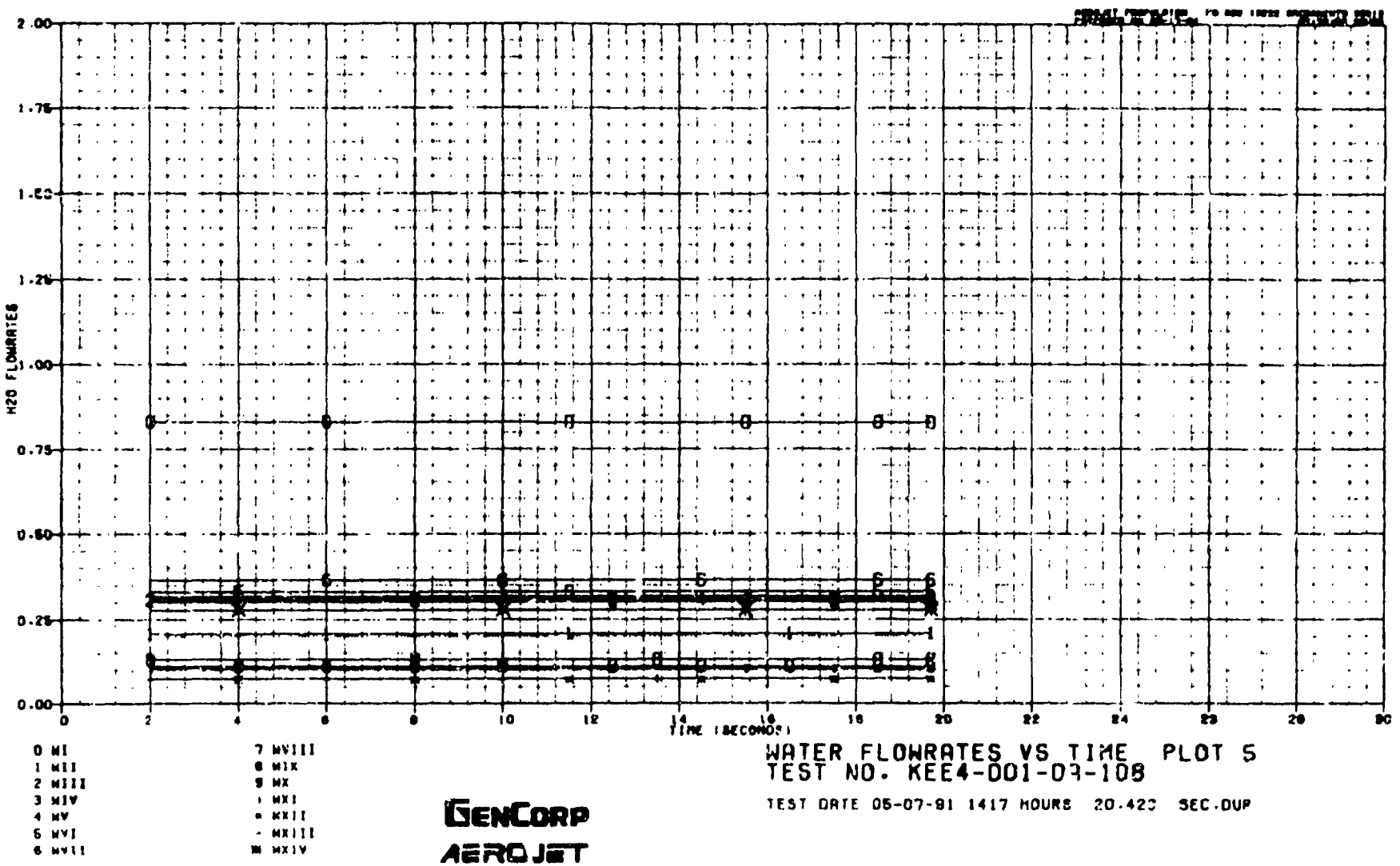
H2O FLOWRATES
TIME (SECONDS)
0 MI
1 MII
2 MIII
3 MIV
4 MV
5 MVI
6 MVII
7 MVIII
8 MIX
9 MX
MXI
MXII
MXIII
MXIV
WATER FLOWRATES VS TIME PLOT 5
TEST NO. KEE4-001-03-108
TEST DATE 05-07-91 1417 HOURS 20.420 SEC.DUR
GENCORP
AEROJET

Figure C - 12

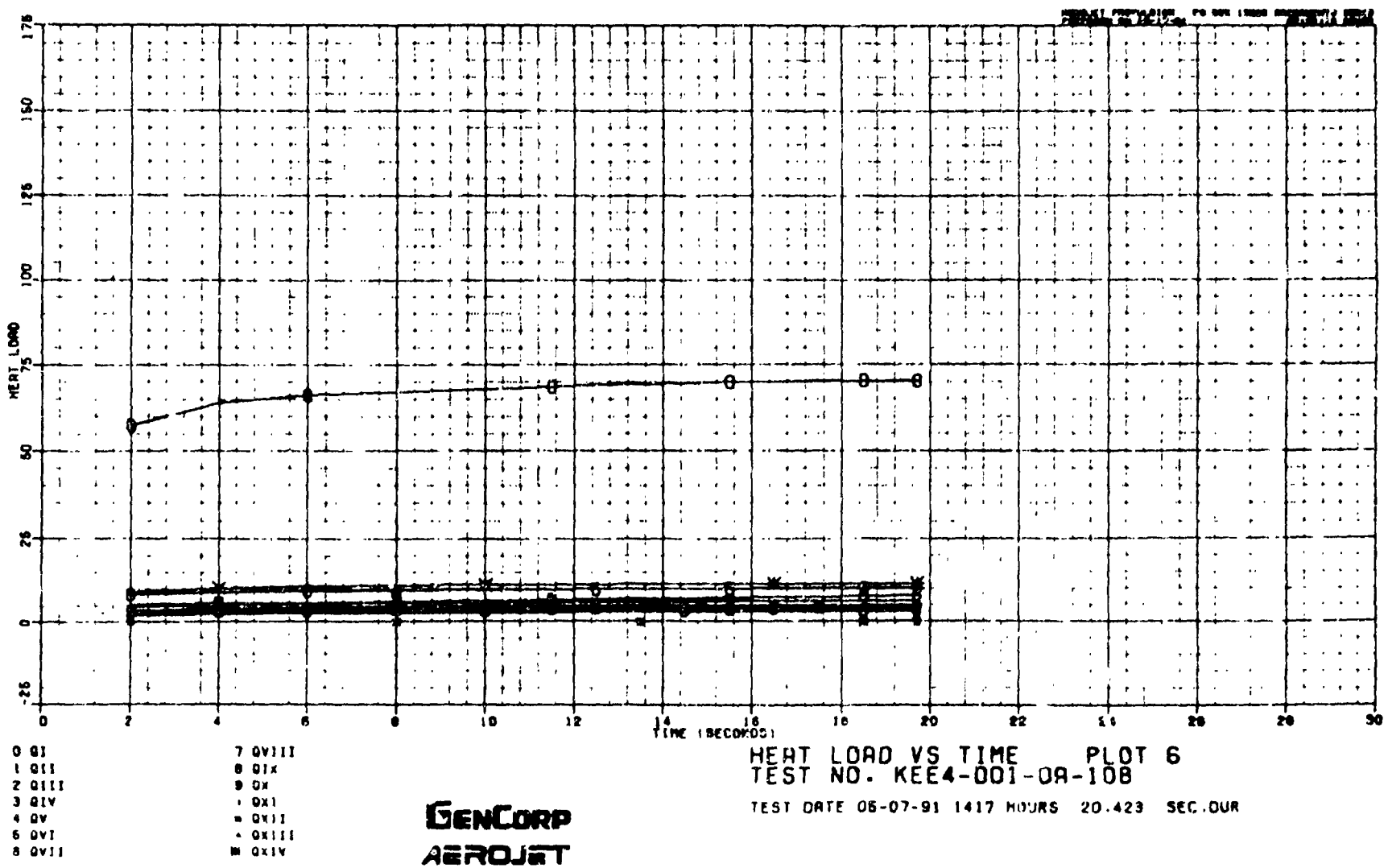
HEAT LOAD
TIME (SECONDS)
0 QI
1 QII
2 QIII
3 QIV
4 QV
6 QVI
8 QVII
7 QVIII
8 QIX
9 QX
QXI
QXII
QXIII
QXIV
HEAT LOAD VS TIME PLOT 6
TEST NO. KEE4-001-OA-108
TEST DATE 05-07-91 1417 HOURS 20.423 SEC.DUR
GENCORP
AEROJET

Figure C - 13

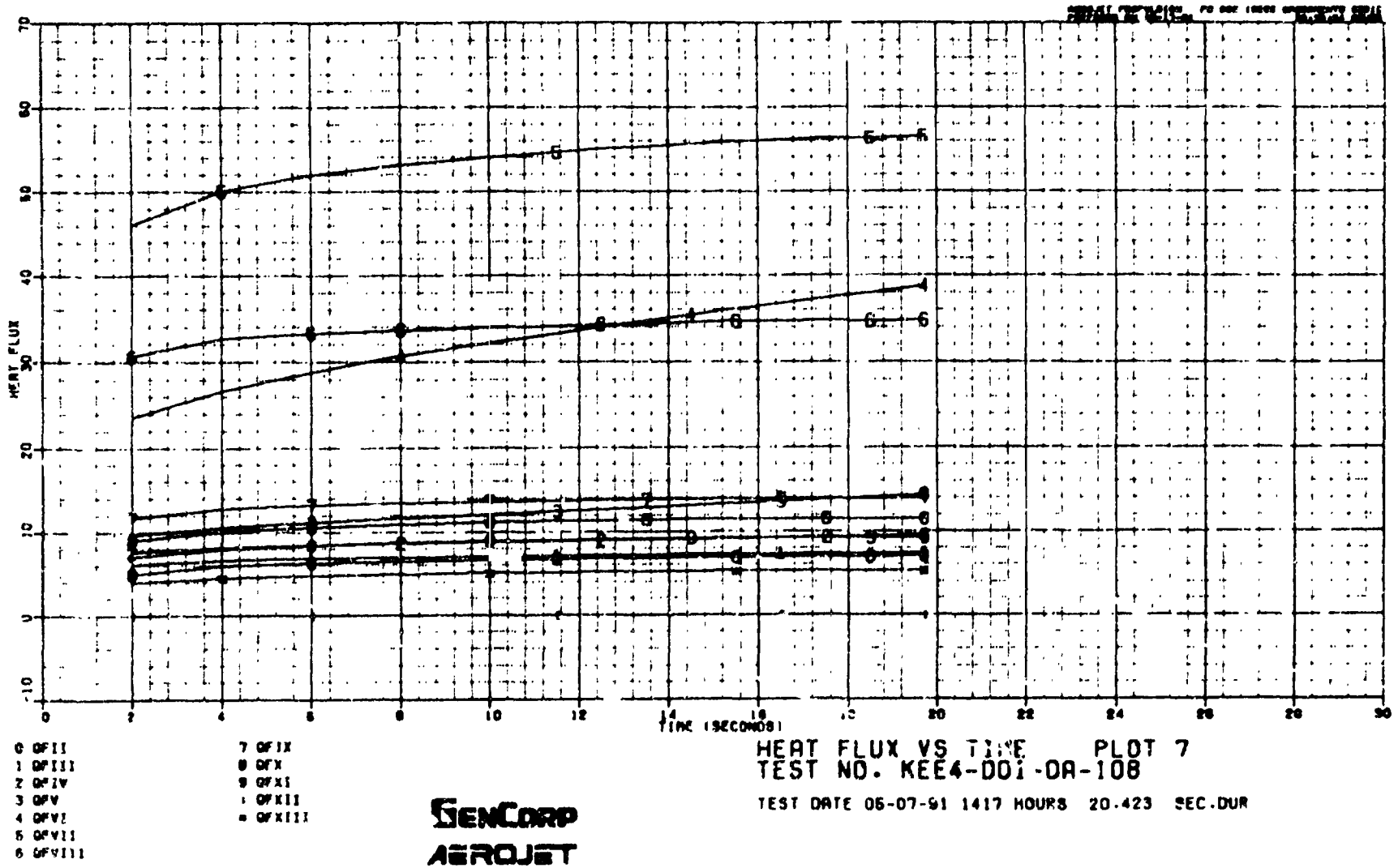
HEAT FLUX
TIME (SECONDS)
0 QFII
1 QFIII
2 QFIV
3 QFV
4 QFVI
5 QFVII
6 QFVIII
7 QFIX
8 QFX
9 QFXI
: QFXII
= QFXIII
HEAT FLUX VS TIME PLOT 7
TEST NO. KEE4-D01-DA-108
TEST DATE 05-07-91 1417 HOURS 20.423 SEC.DUR
GENCORP
AEROJET

Figure C - 14

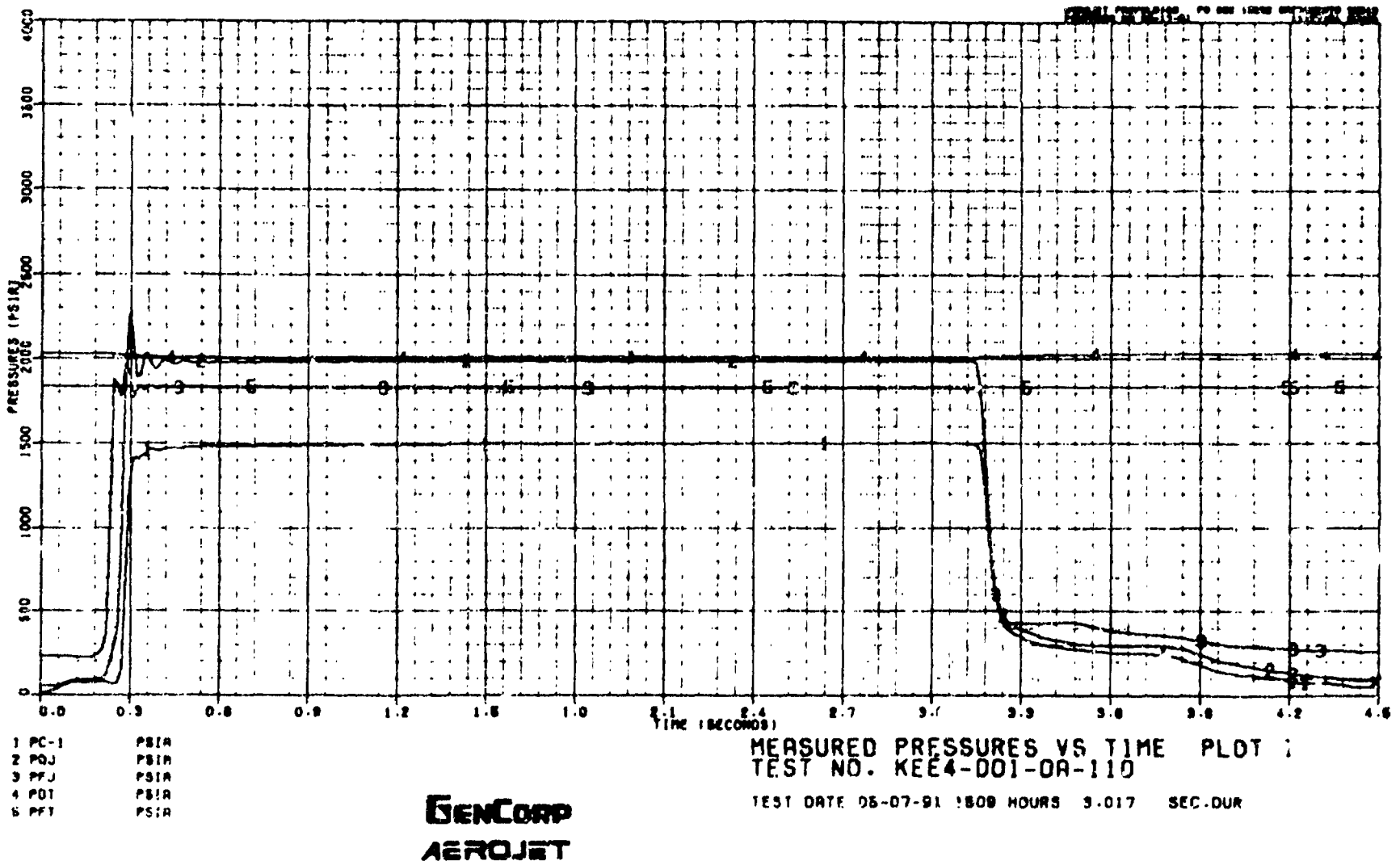
PRESSURES (PSIA)
TIME (SECONDS)
1 PC-1 PSIA
2 POJ PSIA
3 PFJ PSIA
4 POT PSIA
5 PFT PSIA
MEASURED PRESSURES VS TIME PLOT
TEST NO. KEE4-001-DA-110
TEST DATE 05-07-91 1809 HOURS 3.017 SEC.DUR
GENCORP
AEROJET

Figure C - 15

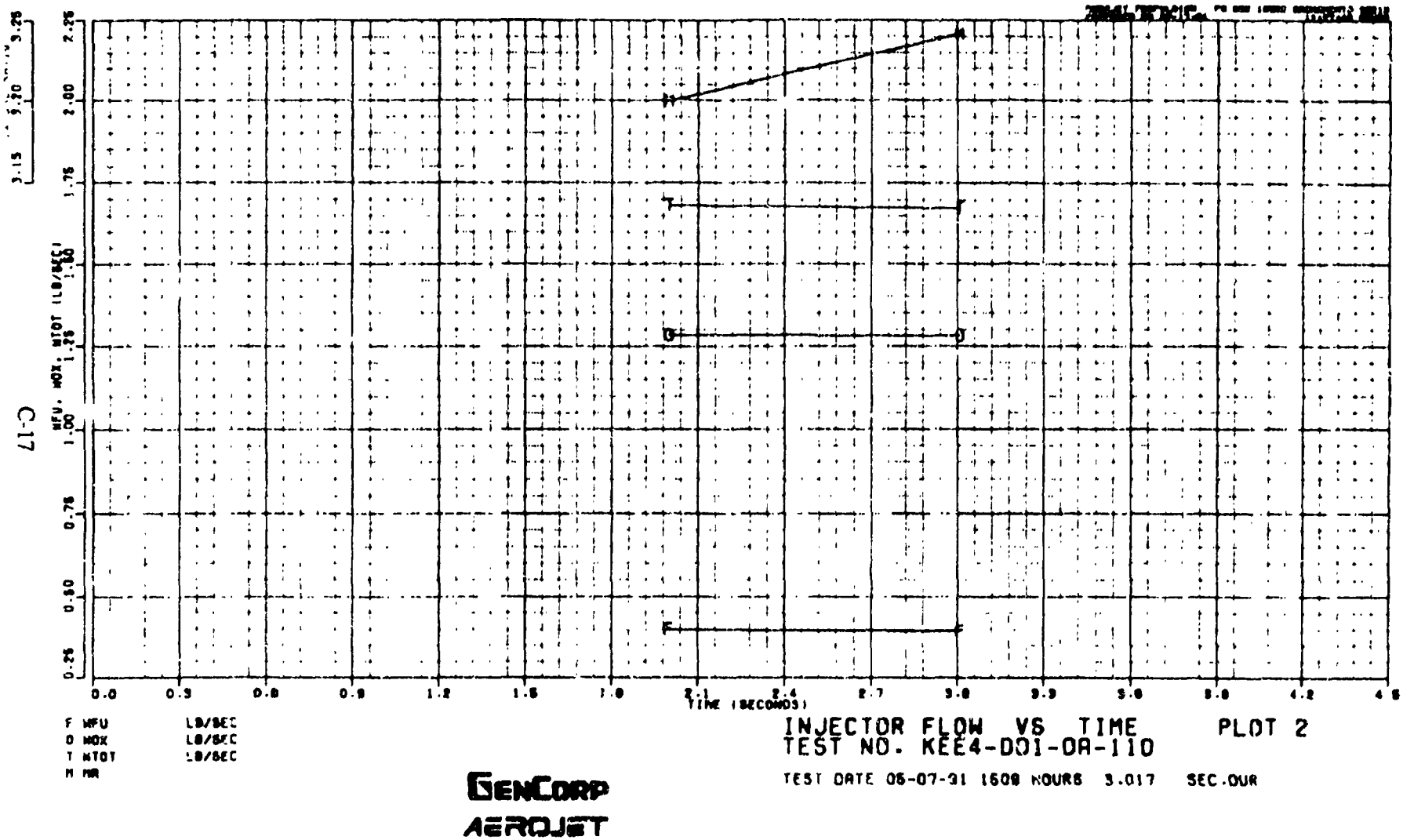
WFU, WOX, WTOT (LB/SEC)
0.25
0.50
0.75
1.00
1.25
1.50
1.75
2.00
2.25
2.50
0.0
0.3
0.6
0.9
1.2
1.5
1.8
2.1
2.4
2.7
3.0
3.3
3.6
3.9
4.2
4.5
TIME (SECONDS)
F WFU LB/SEC
O WOX LB/SEC
T WTOT LB/SEC
H MR
INJECTOR FLOW VS TIME PLOT 2
TEST NO. KEE4-D01-DR-110
TEST DATE 05-07-31 1509 HOURS 3.017 SEC.DUR
GENCORP
AEROJET

Figure C - 16

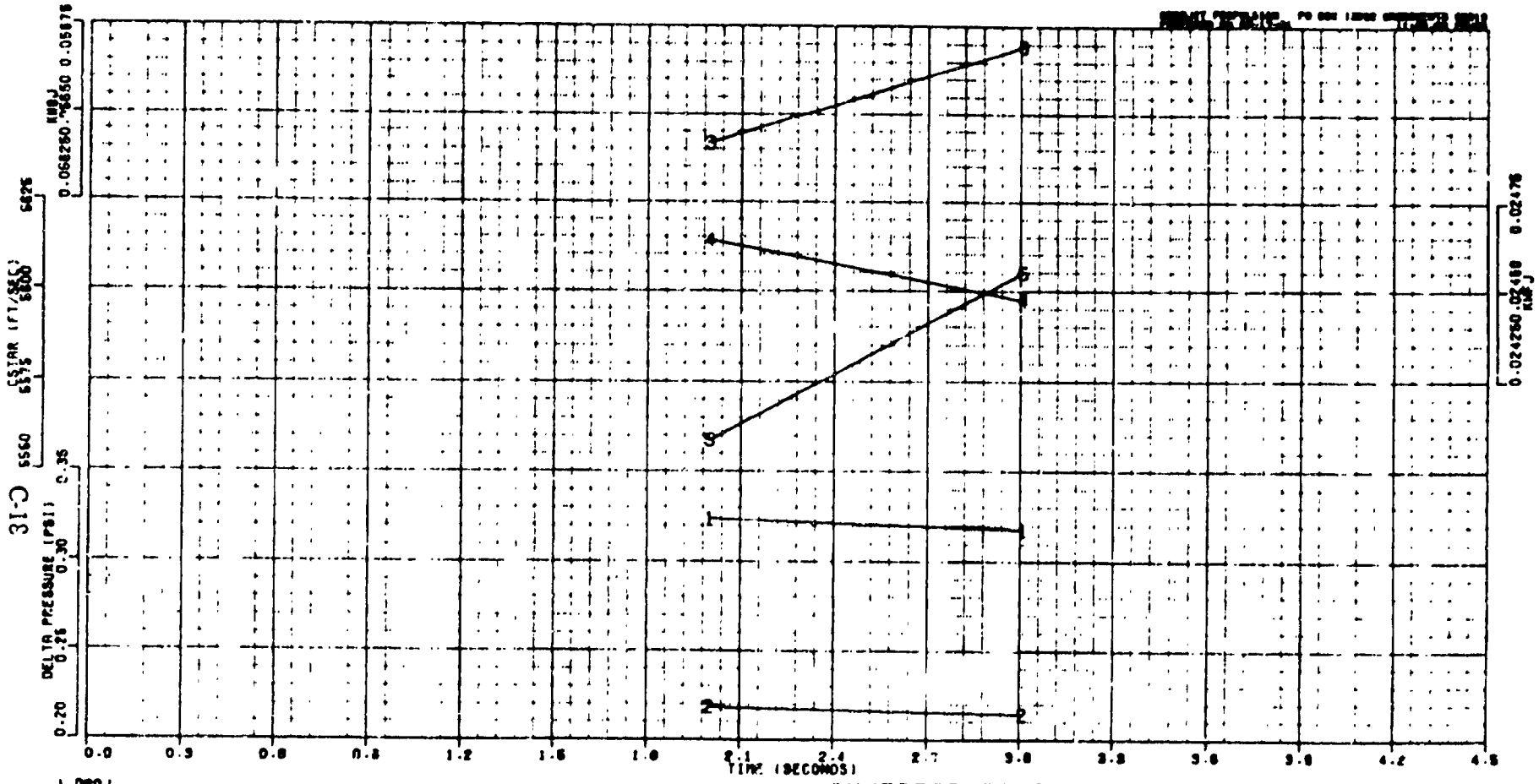

1 DPOJ
2 DPFJ
3 KWOJ
4 KWFJ
5 CSTAR FT/SEC

INJECTOR CALCULATIONS VS TIME PLOT 3
TEST NO. KEE4-DD1-DA-110

TEST DATE 06-07-91 1509 HOURS 3.017 SEC.DUR

GenCorp Aerojet

Figure C - 17

ORIGINAL PAGE IS
OF POOR QUALITY

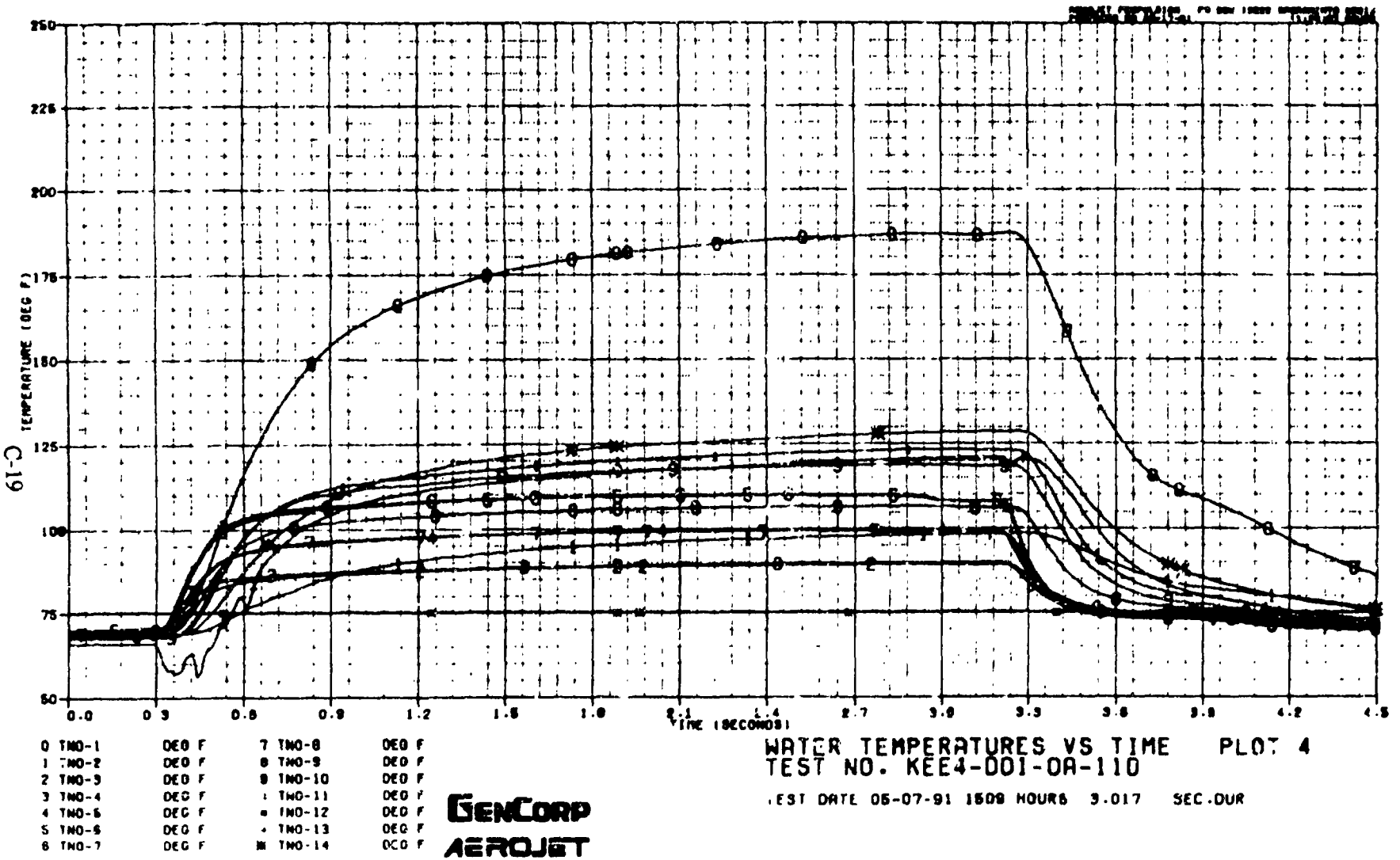
TEMPERATURE (DEG F)
250
225
200
175
150
125
100
75
50
0.0
0.3
0.6
0.9
1.2
1.5
1.8
2.1
2.4
2.7
3.0
3.3
3.6
3.9
4.2
4.5
TIME (SECONDS)
0 TWO-1 DEG F
1 TWO-2 DEG F
2 TWO-3 DEG F
3 TWO-4 DEG F
4 TWO-5 DEG F
5 TWO-6 DEG F
6 TWO-7 DEG F
7 TWO-8 DEG F
8 TWO-9 DEG F
9 TWO-10 DEG F
TWO-11 DEG F
TWO-12 DEG F
TWO-13 DEG F
TWO-14 DEG F
GENCORP
AEROJET
WATER TEMPERATURES VS TIME PLOT 4
TEST NO. KEE4-001-0A-110
TEST DATE 05-07-91 1509 HOURS 3.017 SEC.DUR

Figure C - 18

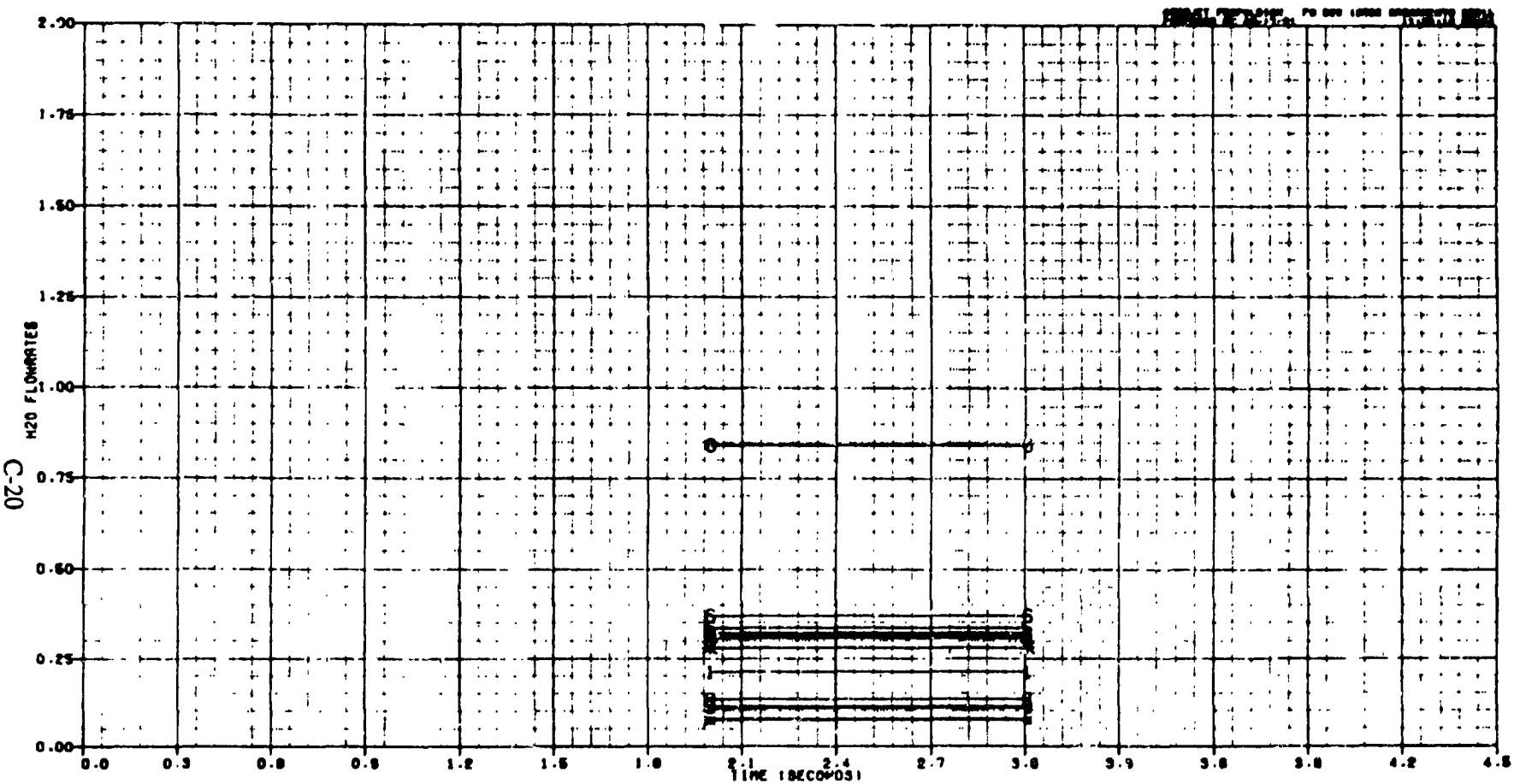

WATER FLOWRATES VS TIME PLOT 5
TEST NO. KEE4-DM1-OA-110

TEST DATE 06-07-91 1509 HOURS 3.017 SEC.DUR

GENCORP AEROJET

Figure C - 19

ORIGINAL PAGE IS
OF POOR QUALITY

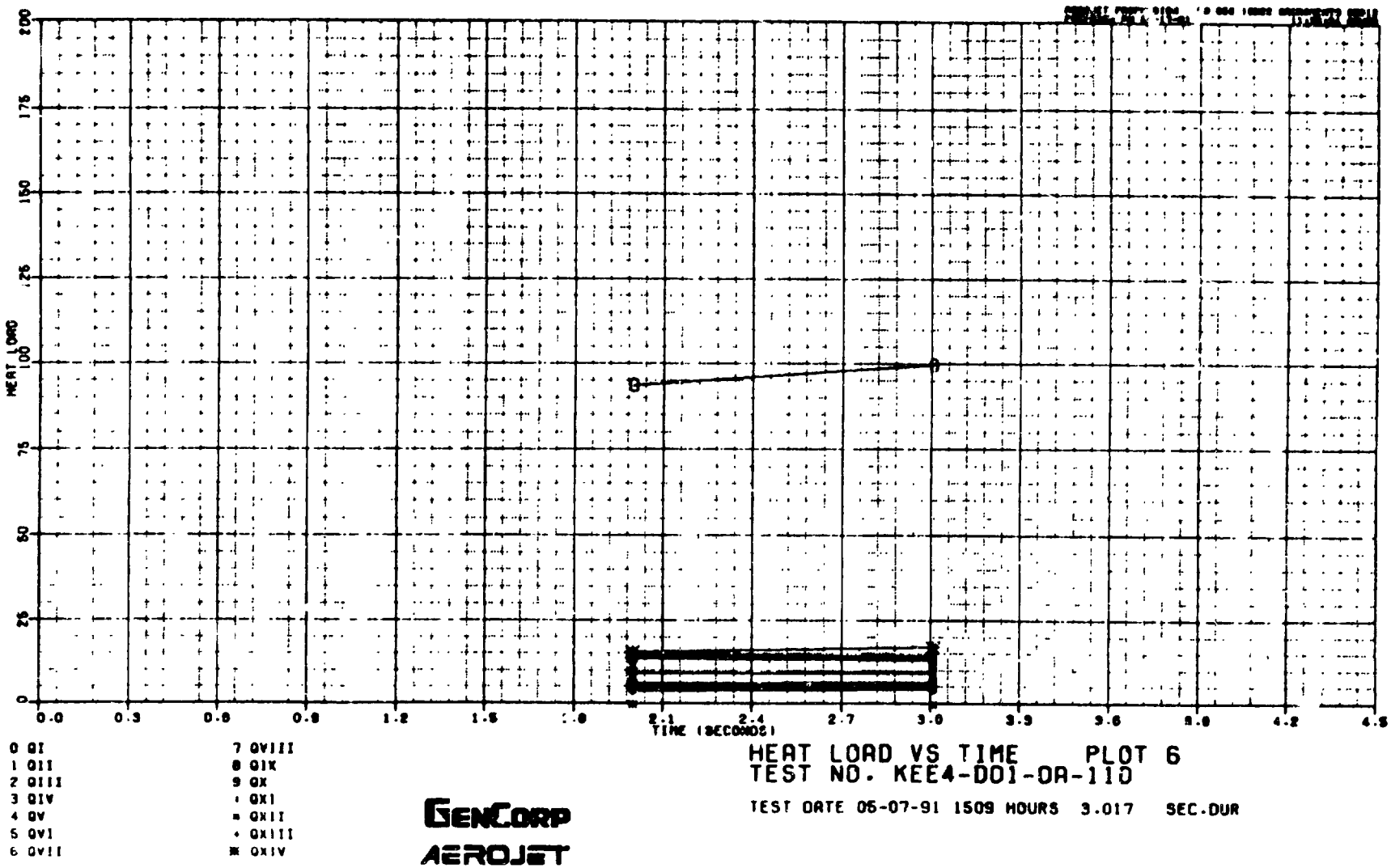
HEAT LOAD
TIME (SECONDS)
0 QI
1 QII
2 QIII
3 QIV
4 QV
5 QVI
6 QVII
7 QVIII
8 QIX
9 QX
QXI
QXII
QXIII
QXIV
GENCORP
AEROJET
HEAT LOAD VS TIME PLOT 6
TEST NO. KEE4-D01-DA-11D
TEST DATE 06-07-91 1509 HOURS 3.017 SEC.DUR

Figure C - 20

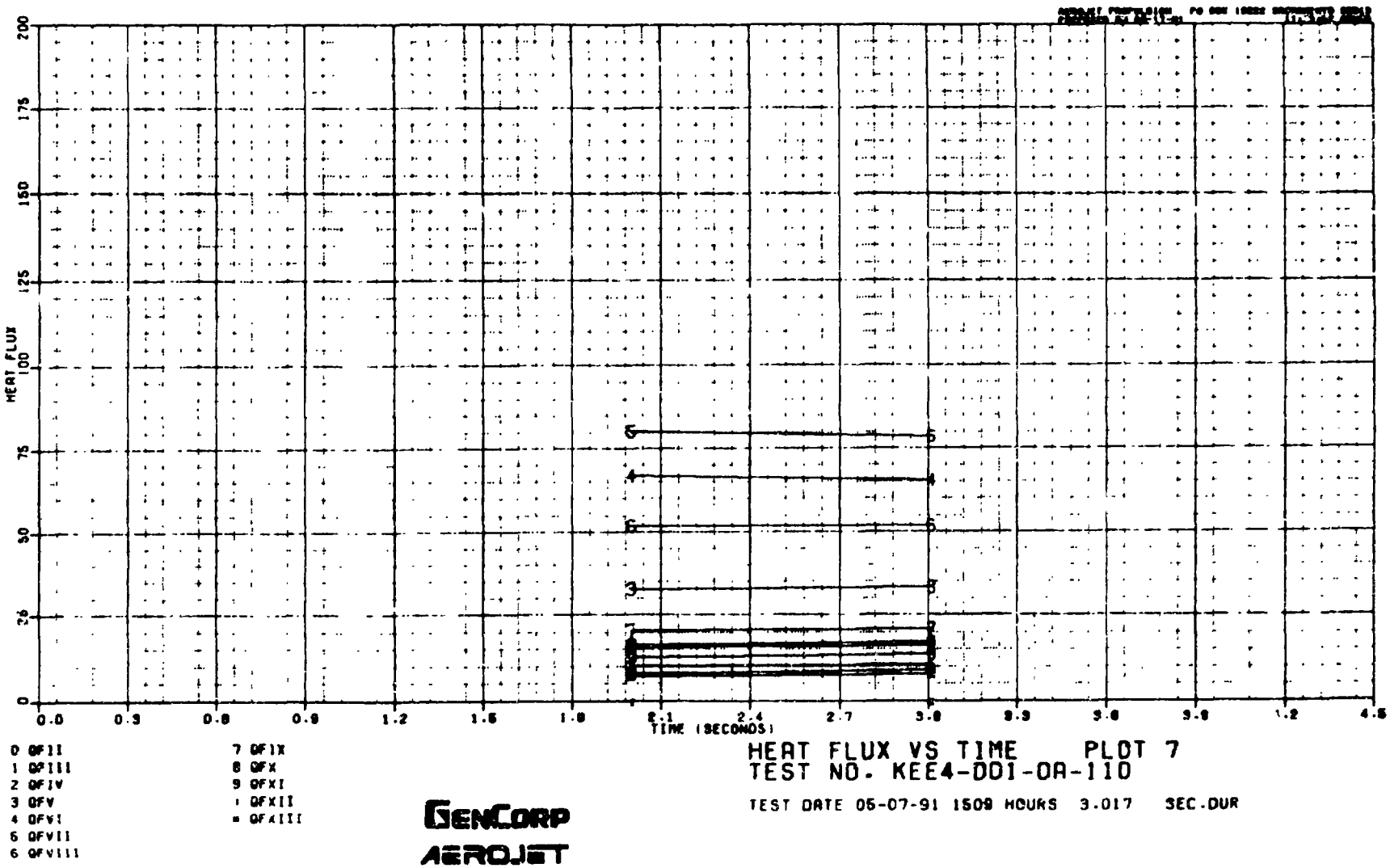

GENCORP AEROJET

Figure C - 21

ORIGINAL PAGE IS OF POOR QUALITY

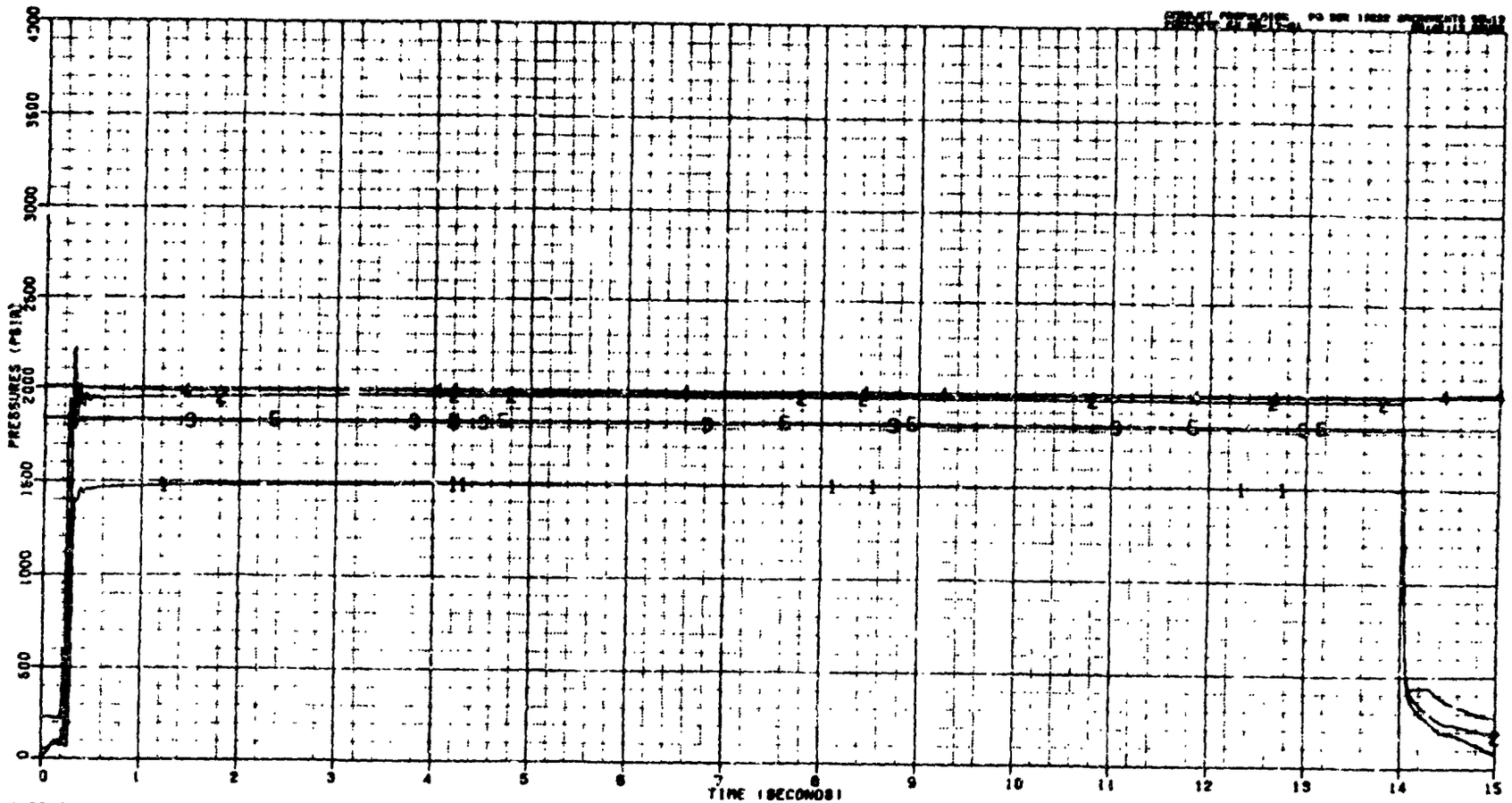

1 PC-1 PSIA
2 POJ PSIA
3 PFJ PSIA
4 POT PSIA
6 PFT PSIA

MEASURED PRESSURES VS TIME PLOT 1
TEST NO. KEE4-D01-DA-111

TEST DATE 05-07-91 1526 HOURS 13.867 SEC DUR

GenCorp
AEROJET

Figure C - 22

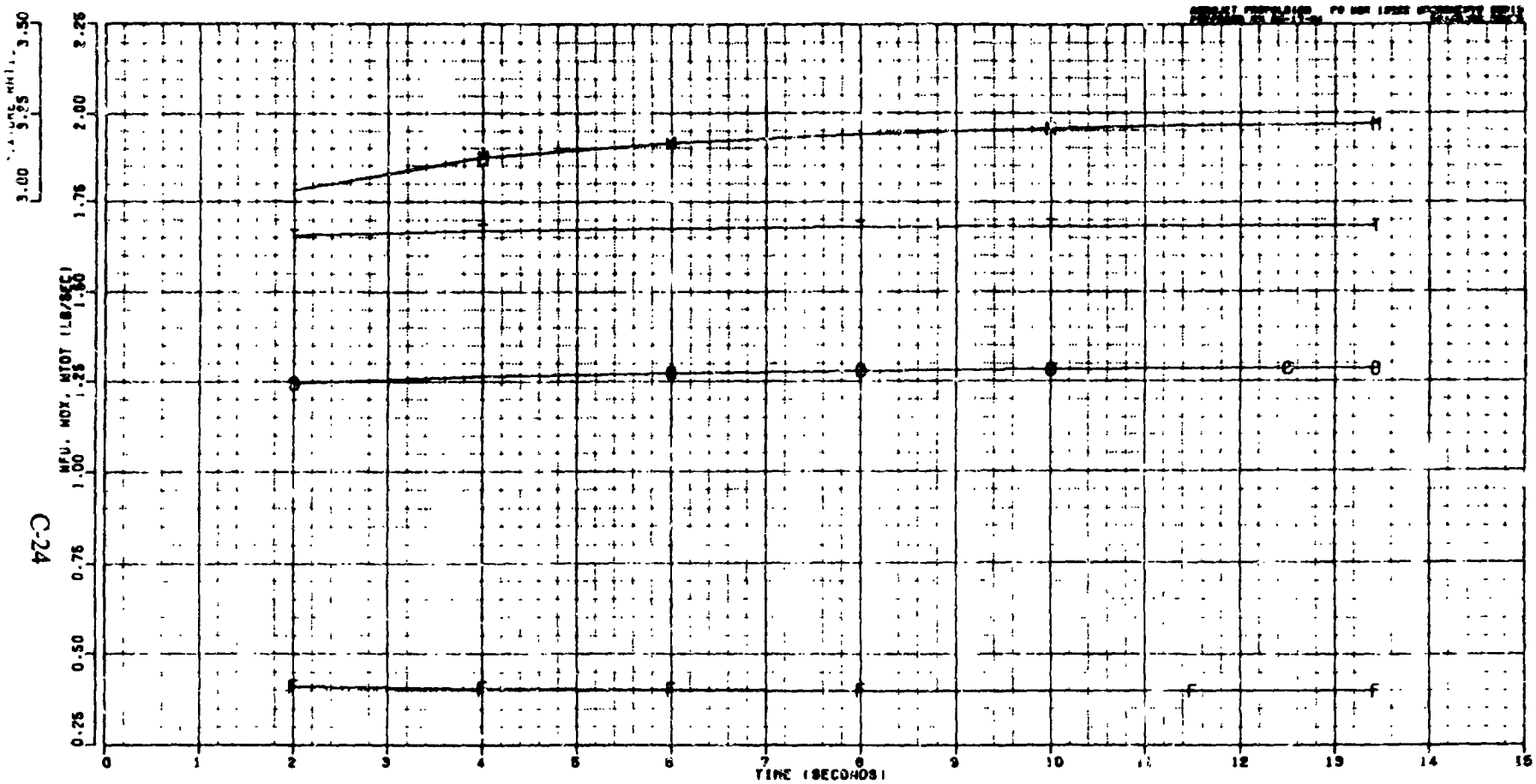

GENCORP
AEROJET

Figure C - 23

ORIGINAL PAGE IS
OF POOR QUALITY

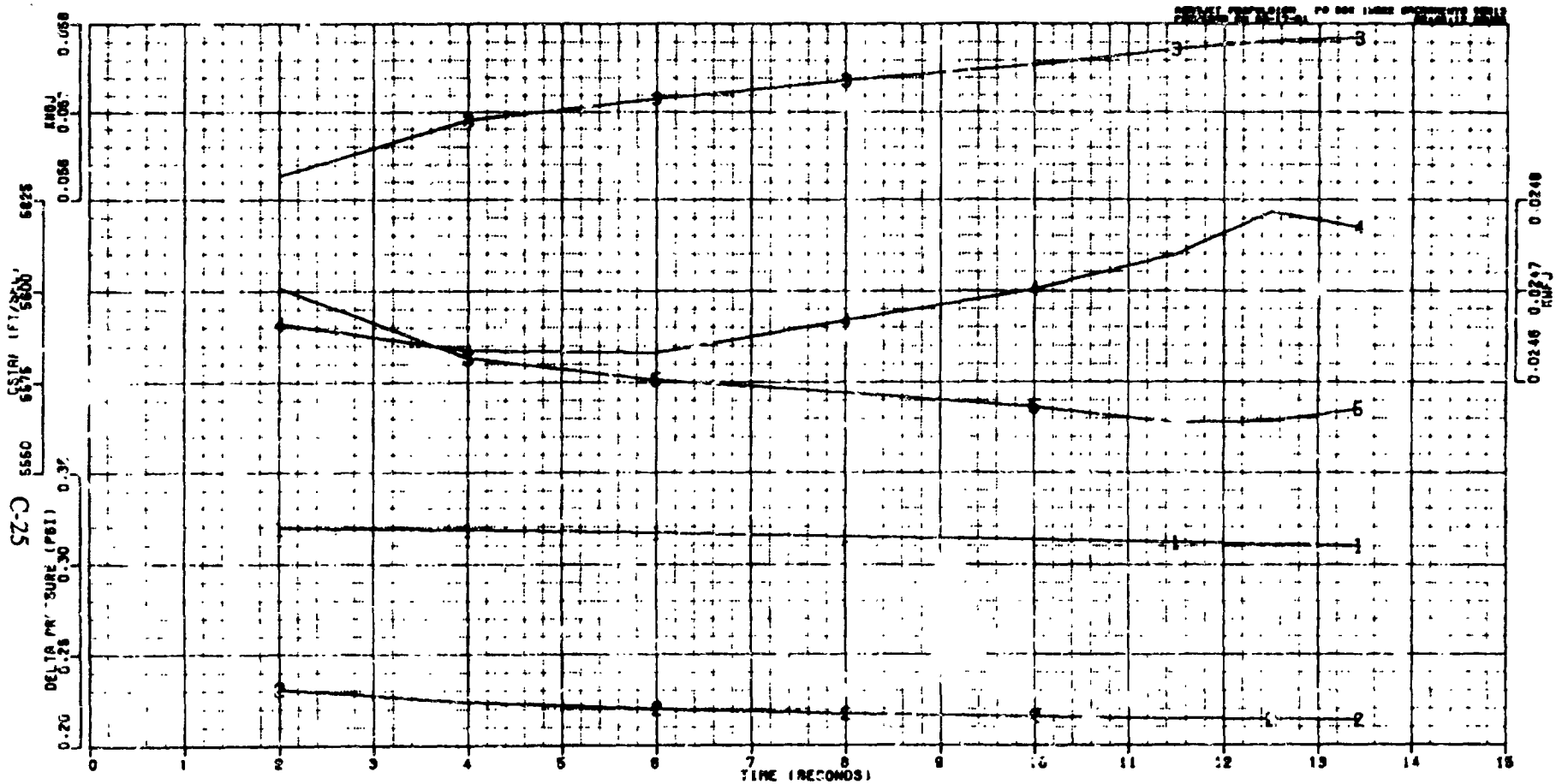

INJECTOR CALCULATIONS VS TIME PLOT 3
TEST NO. KEE4-001-OA-111
TEST DATE 05-07-91 1525 HOURS 13.067 SEC.DUR

GENCORP AEROJET

Figure C - 24

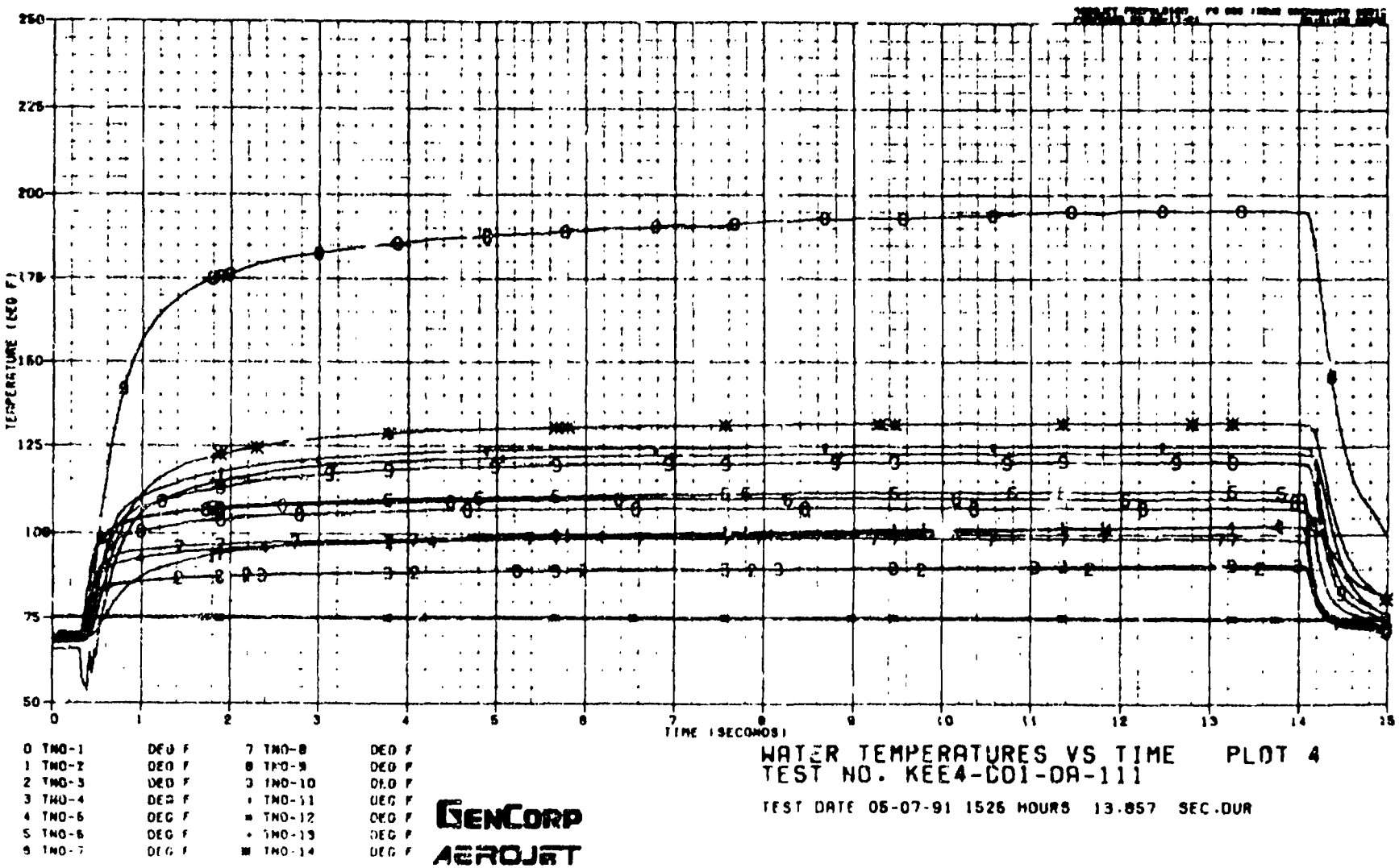

Figure C - 25

ORIGINAL PAGE IS
OF POOR QUALITY

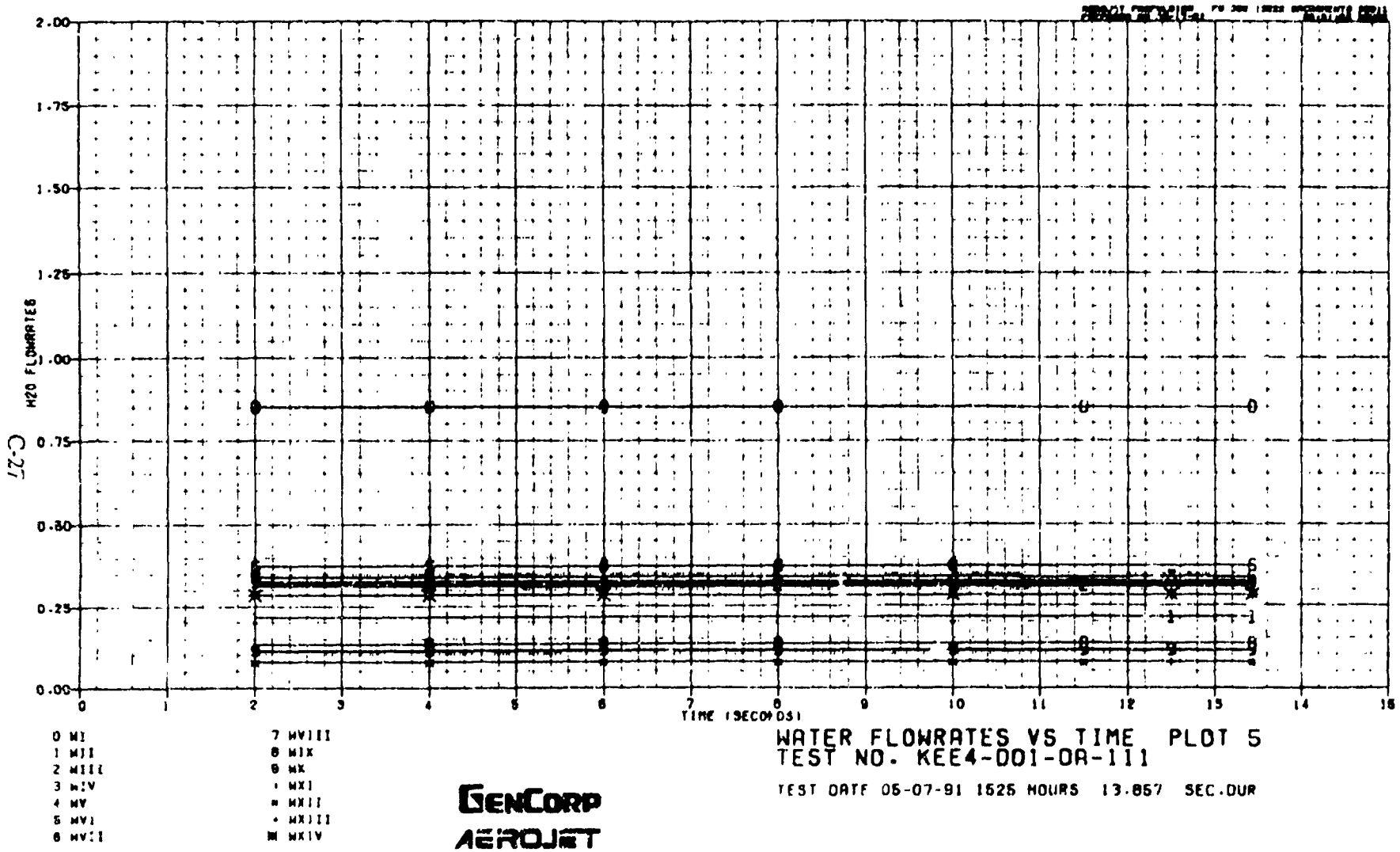
H2O FLOWRATES
2.00
1.75
1.50
1.25
1.00
0.75
0.50
0.25
0.00
0
1
2
3
4
5
6
7
8
9
10
11
12
13
14
15
TIME (SECONDS)
0 WI
1 WII
2 WIII
3 WIV
4 WV
5 WVI
6 WVII
7 WVIII
8 WIX
9 WX
WXI
WXII
WXIII
WXIV
WATER FLOWRATES VS TIME PLOT 5
TEST NO. KEE4-001-OR-111
TEST DATE 05-07-91 1525 HOURS 13.857 SEC.DUR
GENCORP
AEROJET

Figure C - 26

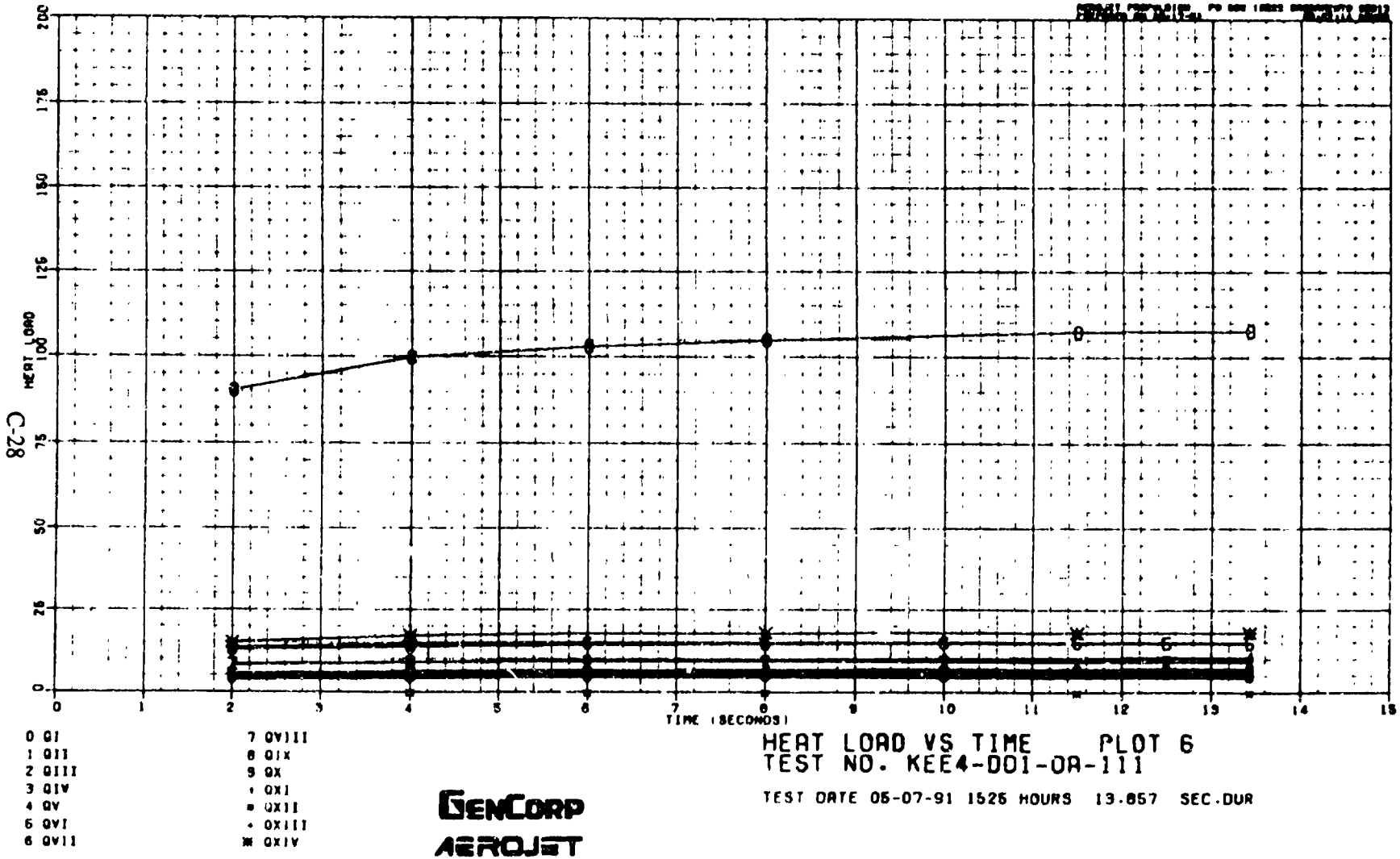
HEAT LOAD
TIME (SECONDS)
0 QI
1 QII
2 QIII
3 QIV
4 QV
5 QVI
6 QVII
7 QVIII
8 QIX
9 QX
+ QXI
■ QXII
• QXIII
✱ QXIV
GENCORP
AEROJET
HEAT LOAD VS TIME PLOT 6
TEST NO. KEE4-DOI-OA-111
TEST DATE 05-07-91 1525 HOURS 13.857 SEC.DUR

Figure C - 27

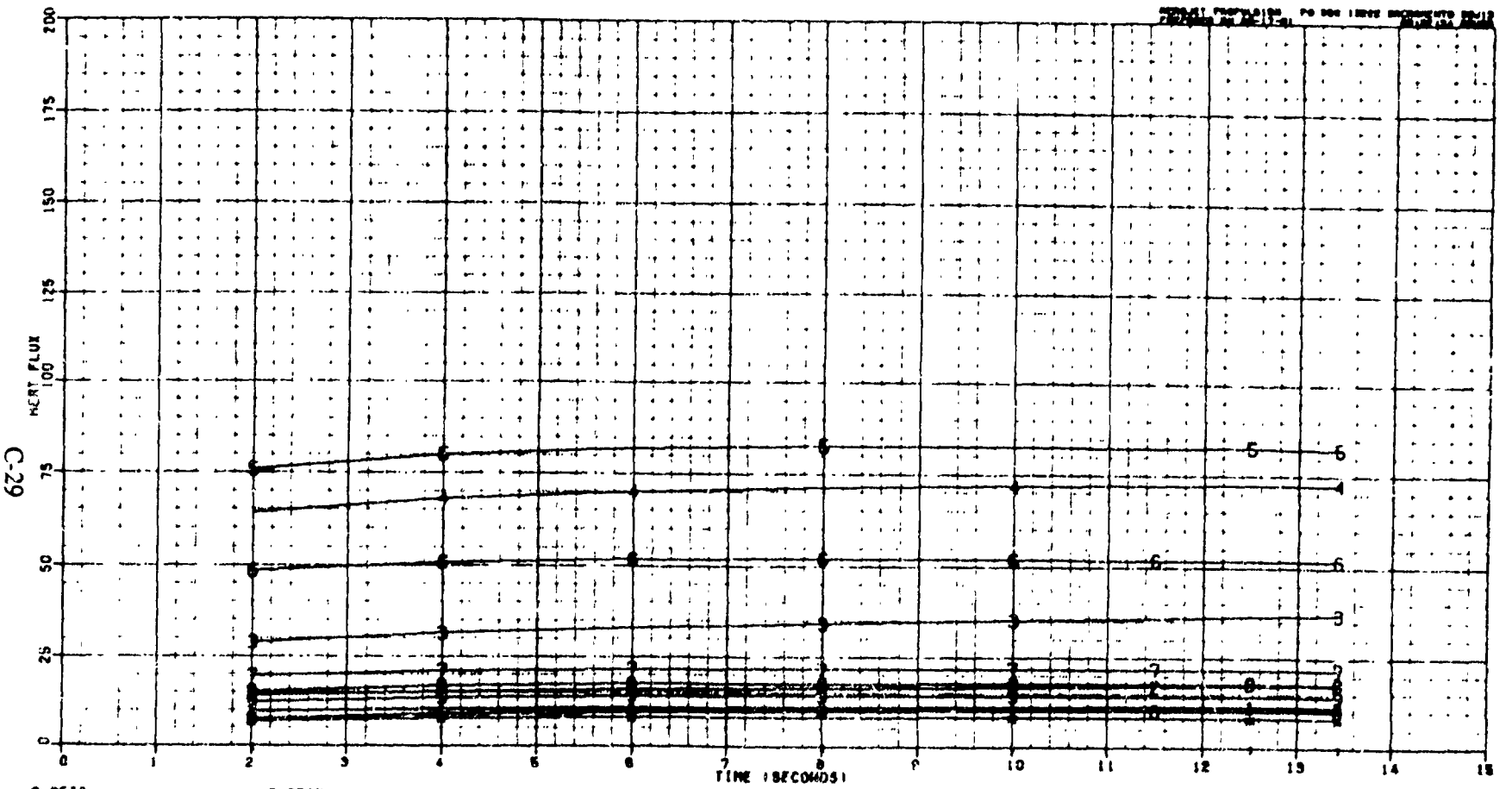

GENCORP AEROJET

Figure C - 28

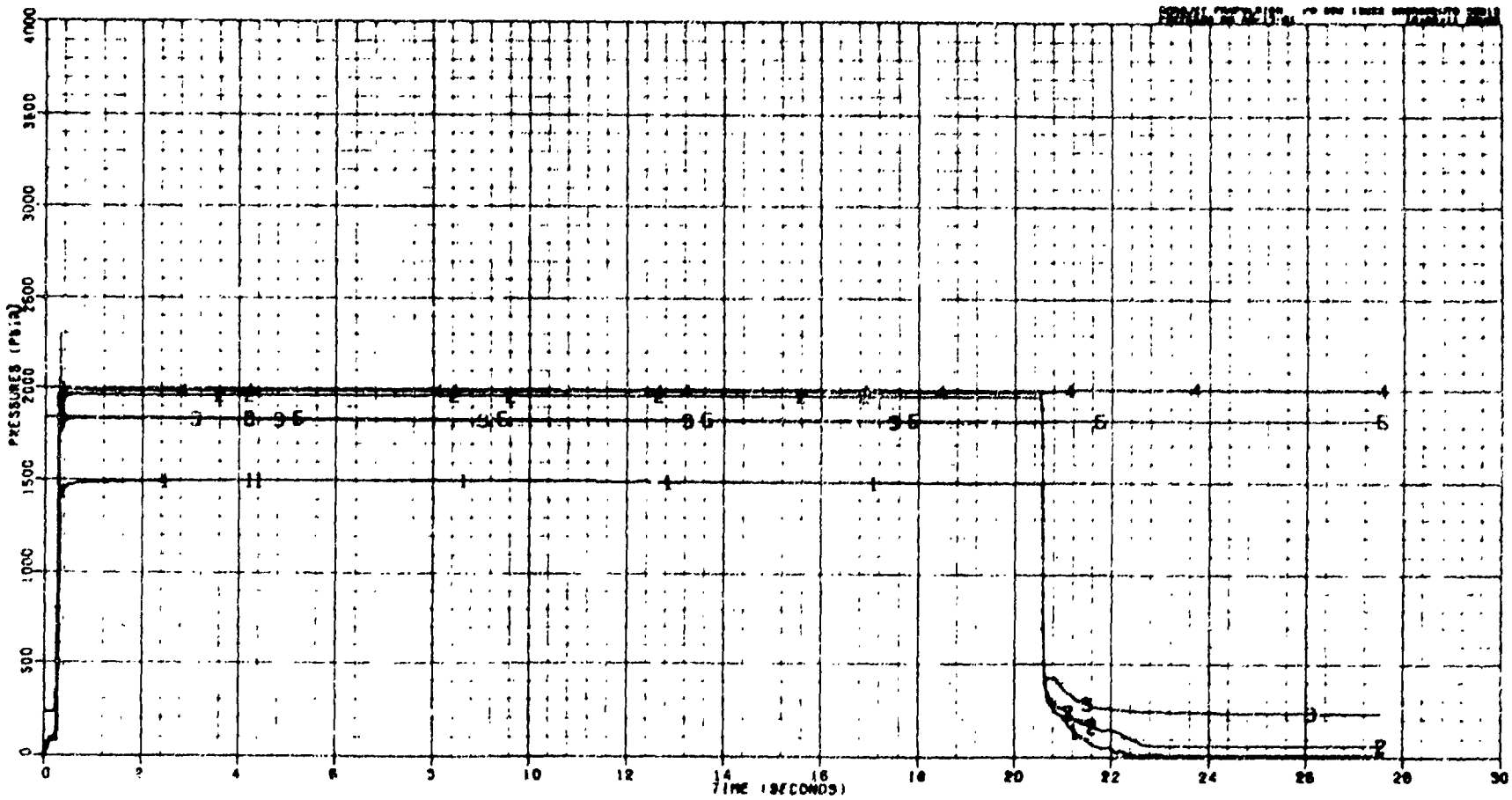

1 PC-1 PSIA
2 POJ PSIA
3 PFJ PSIA
4 POI PSIA
6 PFI PSIA

MEASURED PRESSURES VS TIME PLOT 1
TEST NO. KEE4-001-OA-112

TEST DATE 06-08-91 1103 HOURS 20 413 SEC.DUR

GENCORP
AEROJET

Figure C - 29

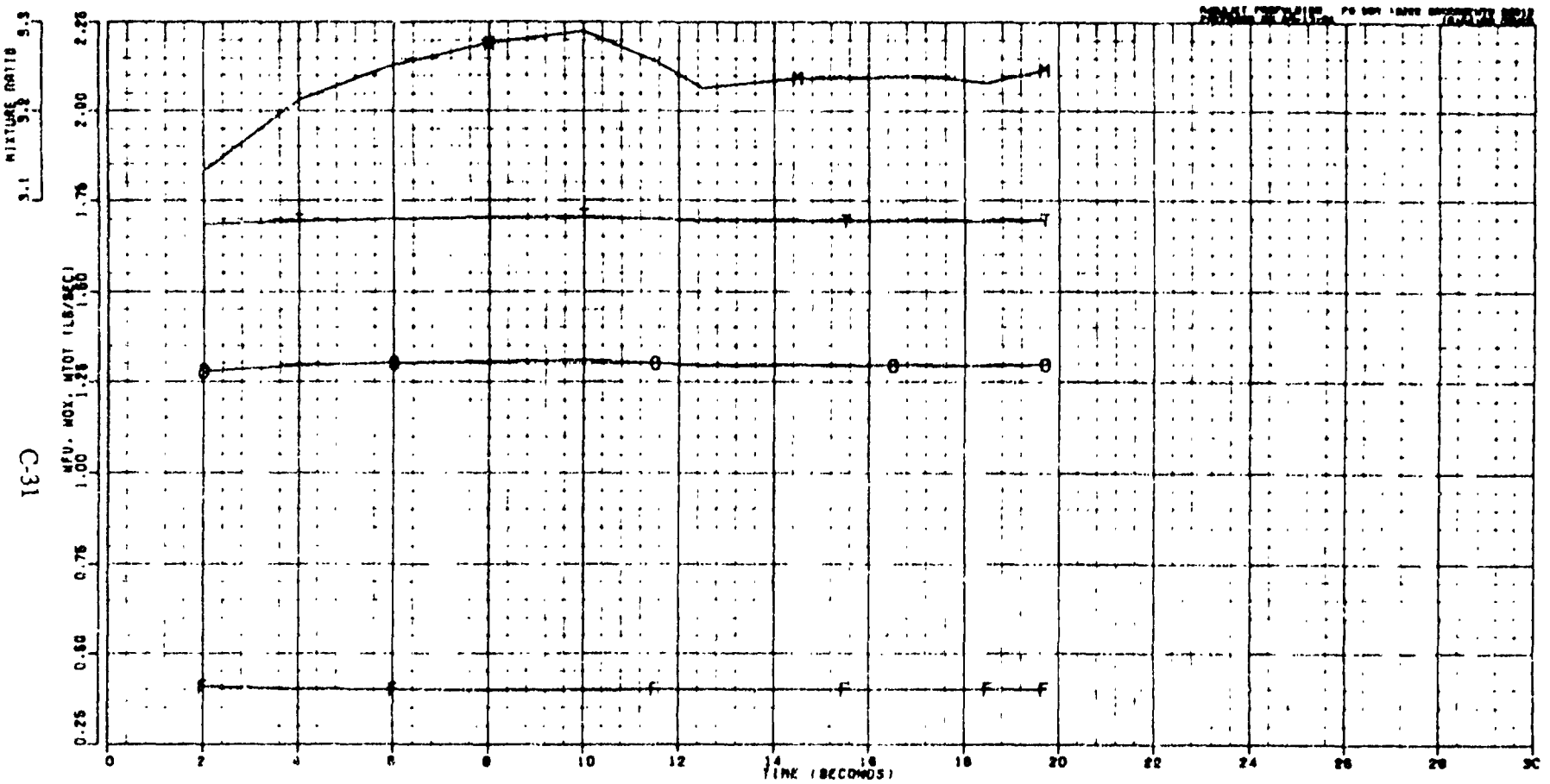
MIXTURE RATIO
5.3
5.2
5.1
WFU, WOX, WTOT (LB/SEC)
2.25
2.00
1.75
1.50
1.25
1.00
0.75
0.50
0.25
0
2
4
6
8
10
12
14
16
18
20
22
24
26
28
30
TIME (SECONDS)
F WFU LB/SEC
O WOX LB/SEC
T WTOT LB/SEC
M MR
INJECTOR FLOW VS TIME PLOT 2
TEST NO. KEE4-D01-OR-112
TEST DATE 05-08-91 1103 HOURS 20.413 SEC.DUR
GENCORP
AEROJET

Figure C - 30

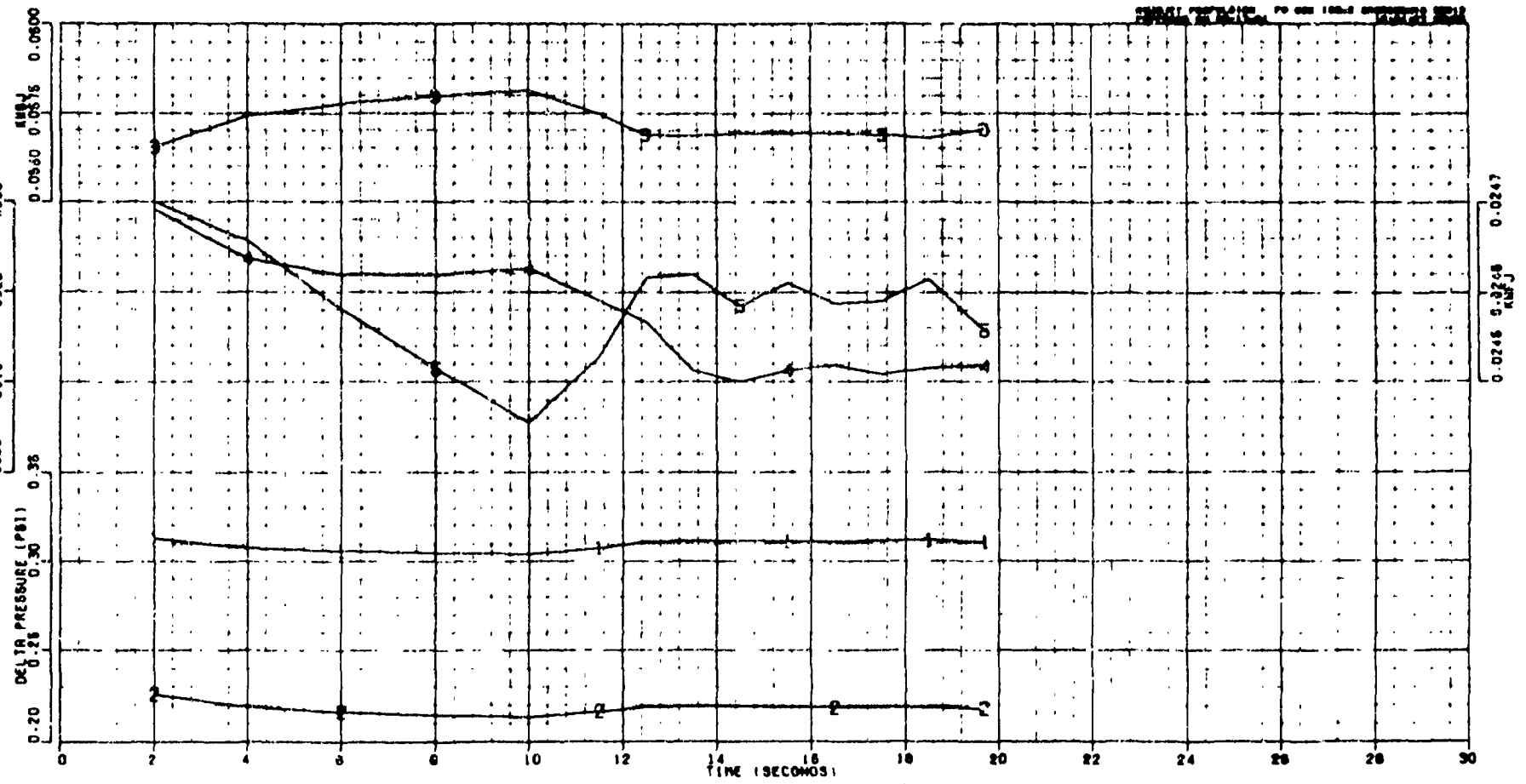

GENCORP
AEROJET

Figure C - 31

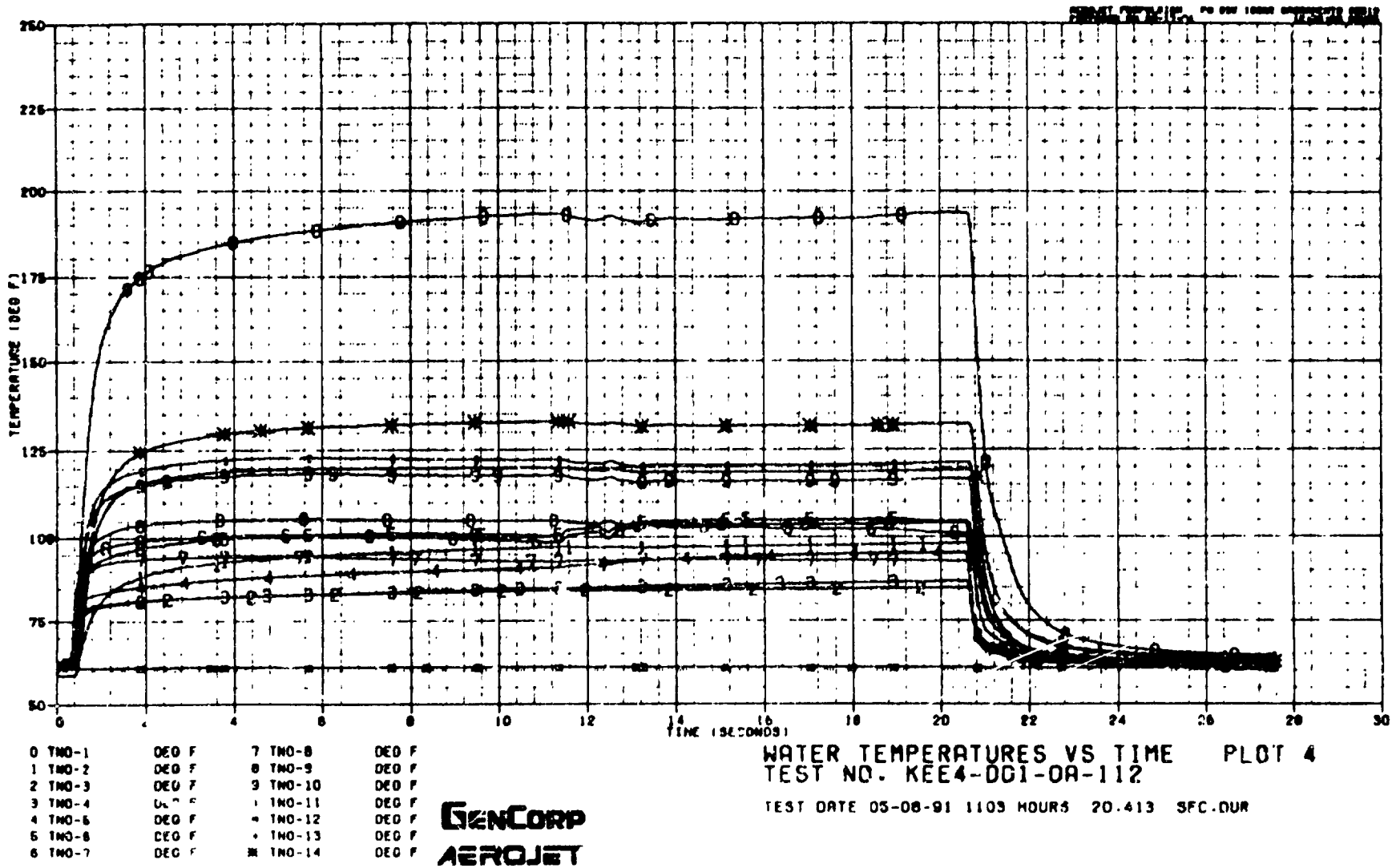
TEMPERATURE (DEG F)
250
225
200
175
150
125
100
75
50
0
2
4
6
8
10
12
14
16
18
20
22
24
26
28
30
TIME (SECONDS)
0 TNO-1 DEG F
1 TNO-2 DEG F
2 TNO-3 DEG F
3 TNO-4 DEG F
4 TNO-5 DEG F
5 TNO-6 DEG F
6 TNO-7 DEG F
7 TNO-8 DEG F
8 TNO-9 DEG F
9 TNO-10 DEG F
TNO-11 DEG F
TNO-12 DEG F
TNO-13 DEG F
TNO-14 DEG F
GENCORP
AEROJET
WATER TEMPERATURES VS TIME PLOT 4
TEST NO. KEE4-DCI-OA-112
TEST DATE 05-08-91 1103 HOURS 20.413 SEC.DUR

Figure C - 32

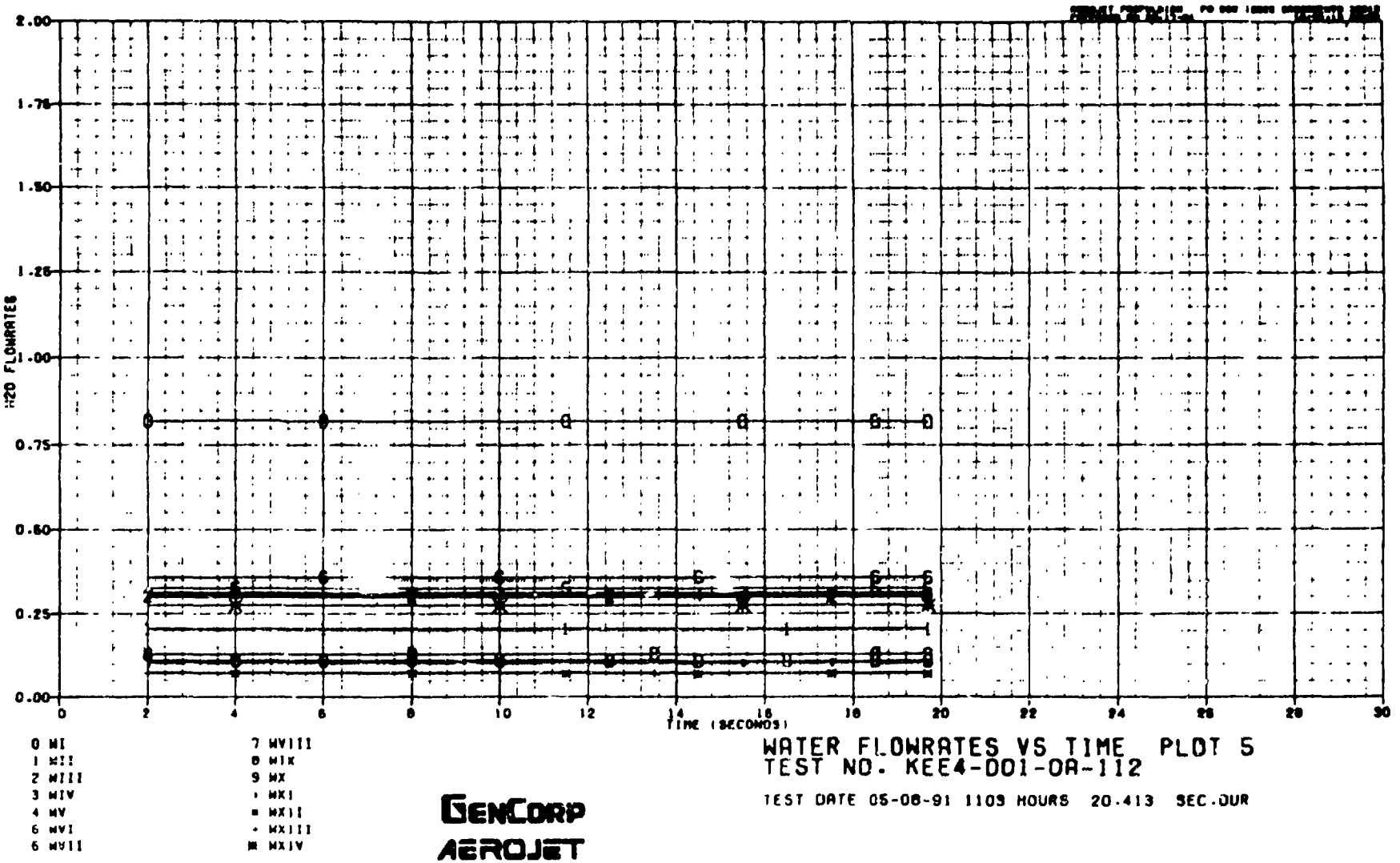
H2O FLOWRATES
2.00
1.75
1.50
1.25
1.00
0.75
0.50
0.25
0.00
0
2
4
6
8
10
12
14
16
18
20
22
24
26
28
30
TIME (SECONDS)
0 WI
1 WII
2 WIII
3 WIV
4 WV
6 WVI
6 WVII
7 WVIII
8 WIX
9 WX
WXI
WXII
WXIII
WXIV
WATER FLOWRATES VS TIME PLOT 5
TEST NO. KEE4-DO1-OA-112
TEST DATE 05-08-91 1103 HOURS 20.413 SEC.DUR
GENCORP
AEROJET

Figure C - 33

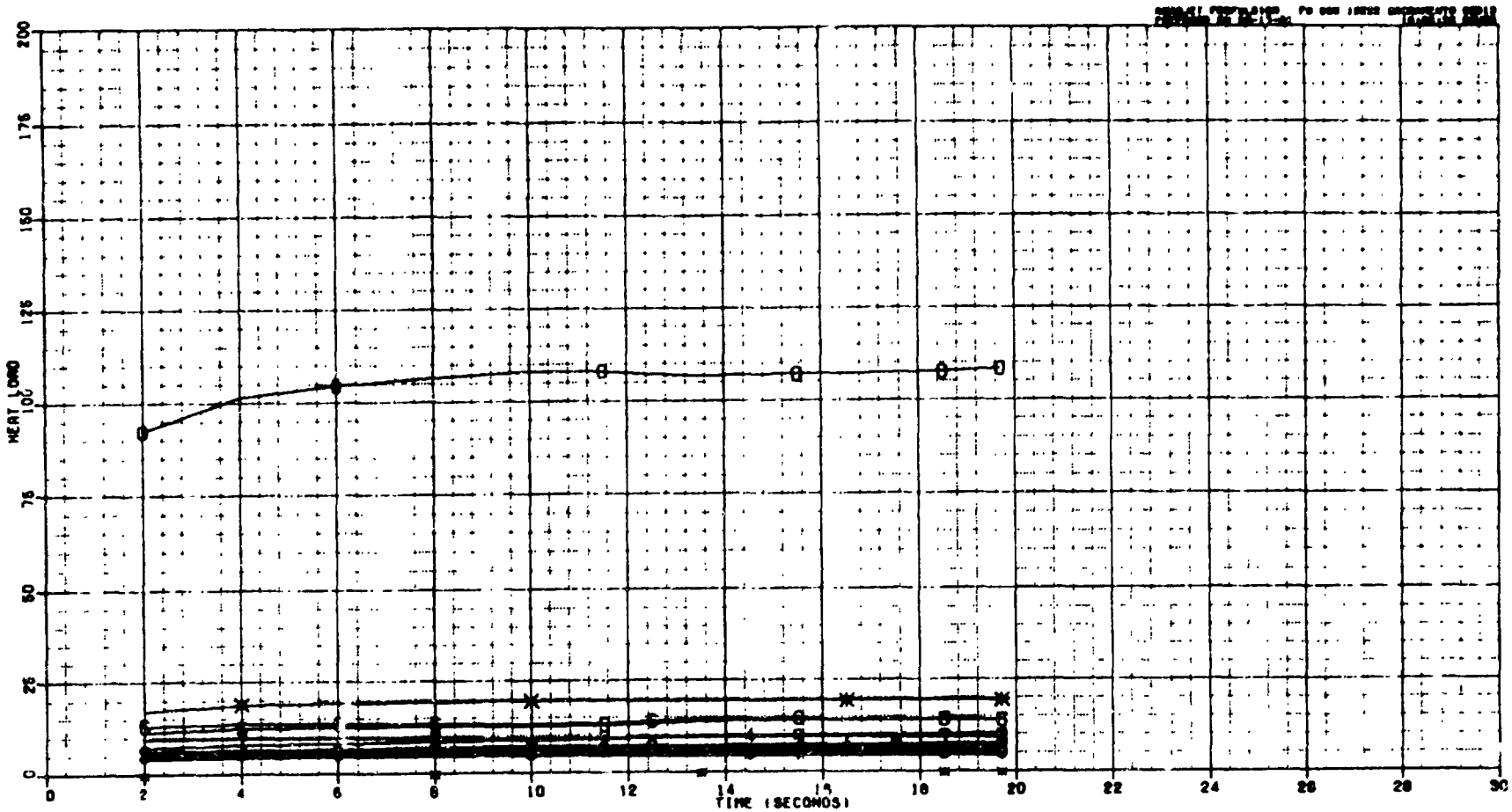

GENCORP AEROJET

Figure C - 34

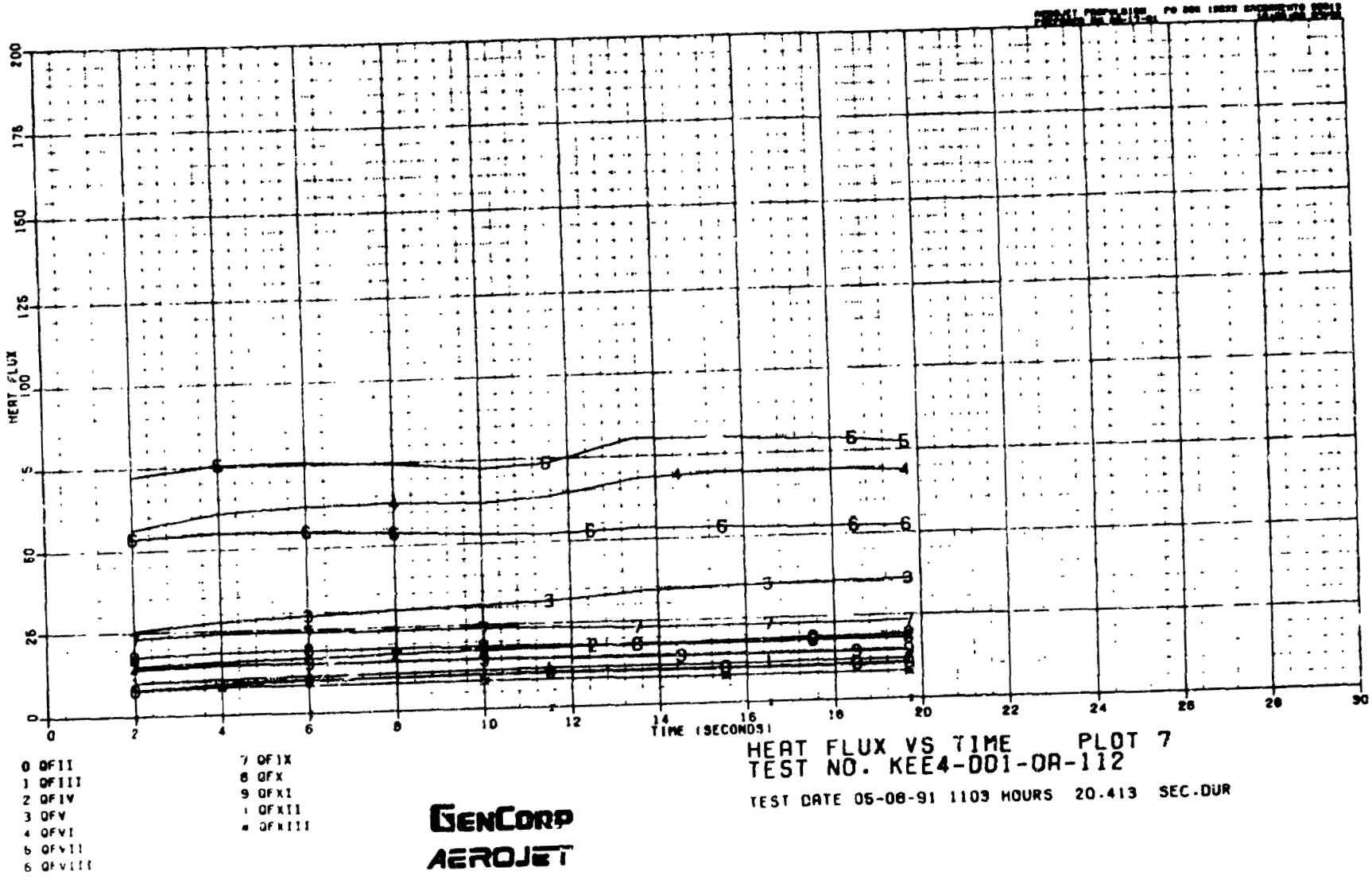

Figure C - 35

OF POOR QUALITY

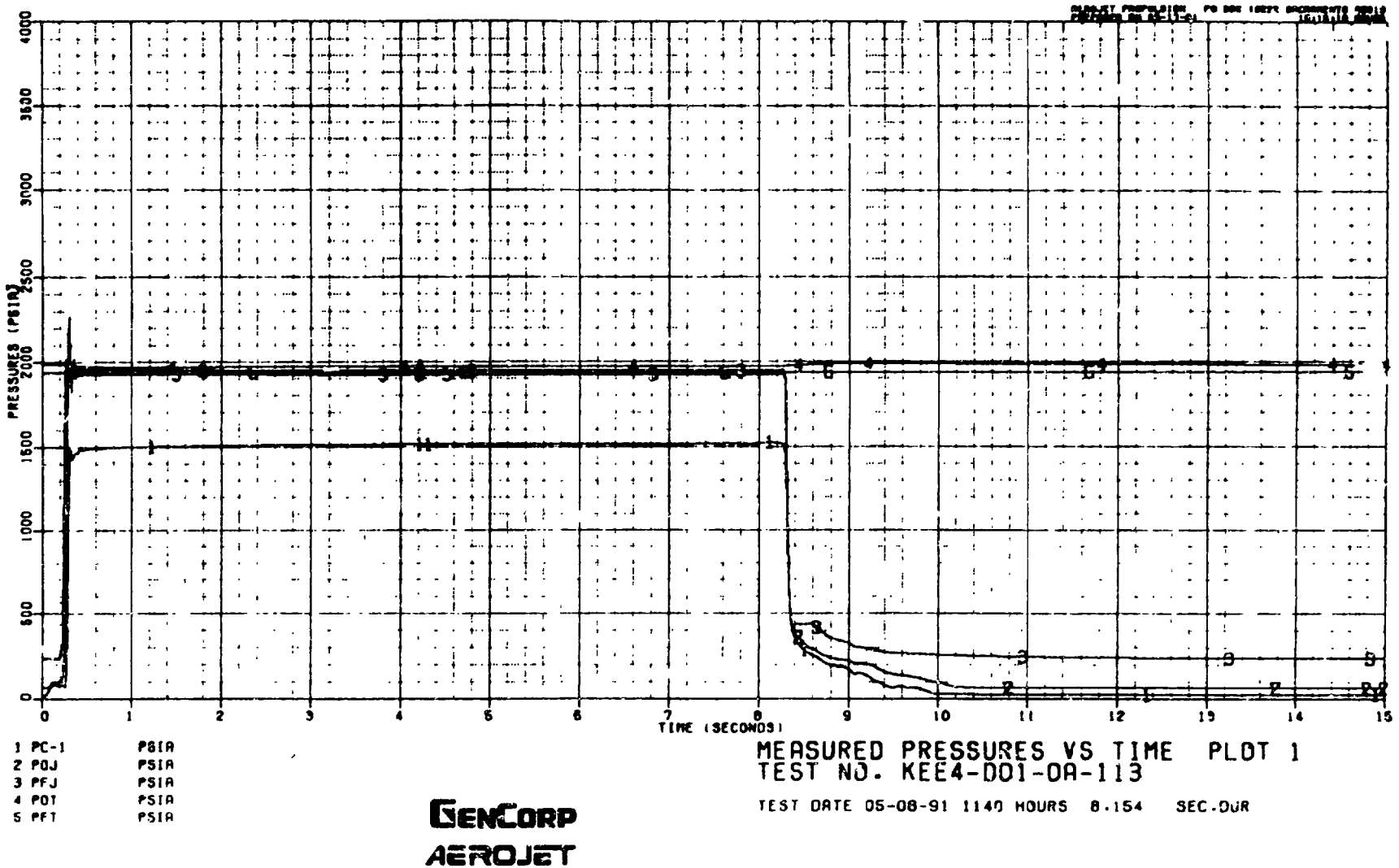
PRESSURES (PSIA)
0
500
1000
1500
2000
2500
3000
3500
4000
TIME (SECONDS)
0
1
2
3
4
5
6
7
8
9
10
11
12
13
14
15
1 PC-1 PSIA
2 POJ PSIA
3 PFJ PSIA
4 POT PSIA
5 PFT PSIA
MEASURED PRESSURES VS TIME PLOT 1
TEST NO. KEE4-D01-OA-113
TEST DATE 05-08-91 1140 HOURS 8.154 SEC.DUR
GENCORP
AEROJET

Figure C - 36

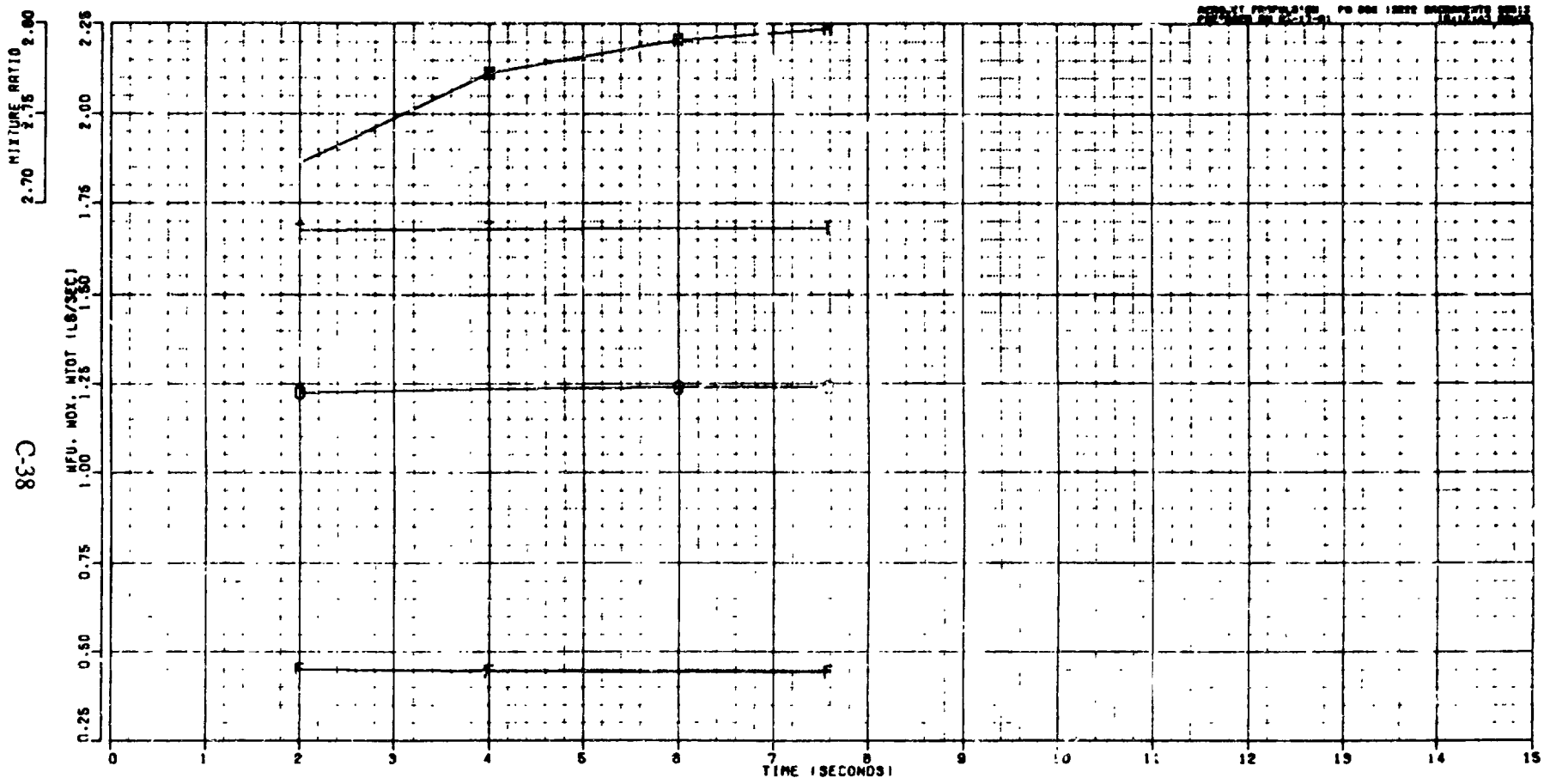

F WFU LB/SEC
O WOX LB/SEC
T WTOT LB/SEC
M MR

INJECTOR FLOW VS TIME PLOT 2
TEST NO. KEE4-DD1-OA-113

TEST DATE 05-08-91 1140 HOURS 8.154 SEC.DUR

GENCORP
AEROJET

Figure C - 37

ORIGINAL PAGE IS
OF POOR QUALITY

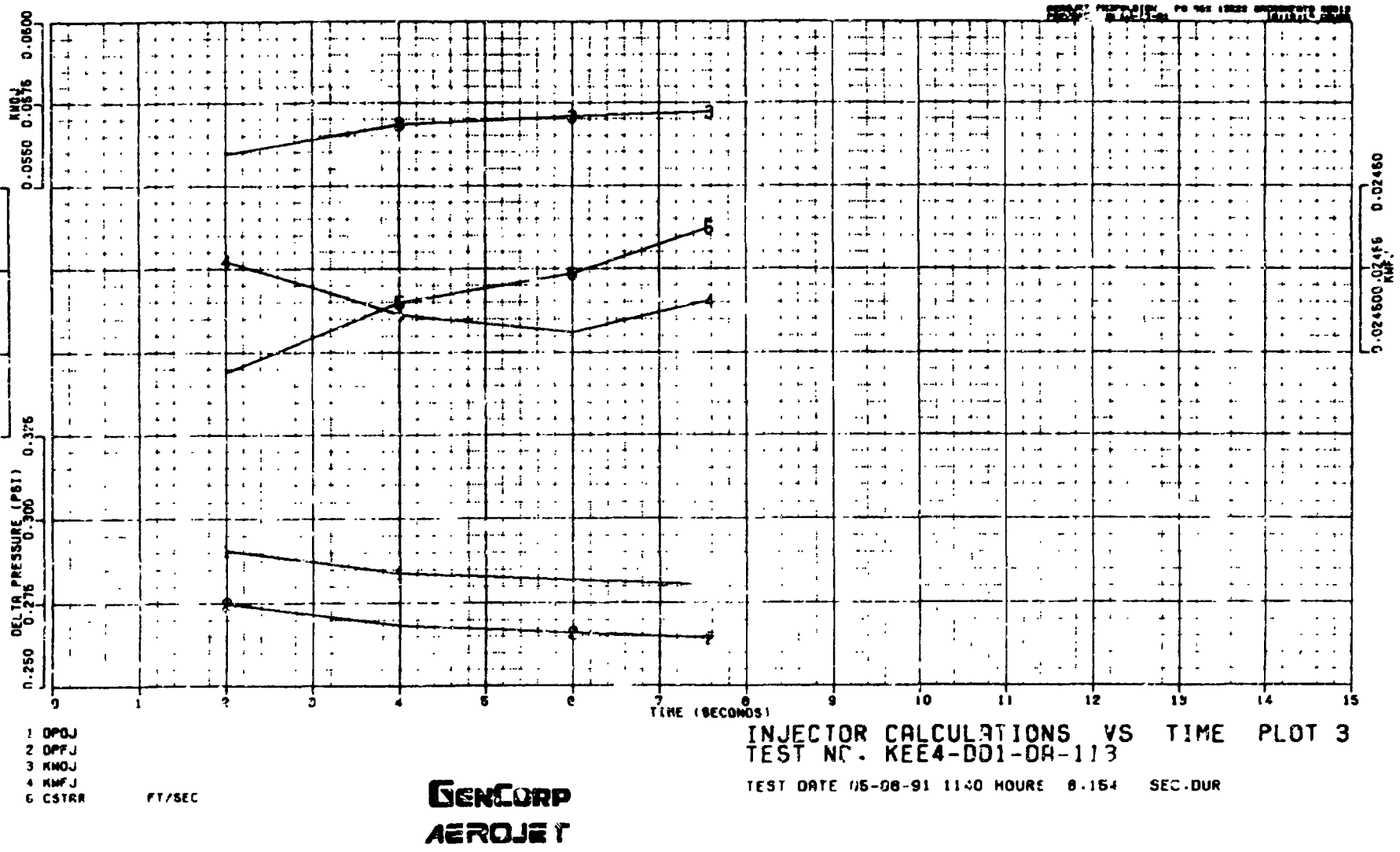
DELTA PRESSURE (PSI)
0.250
0.276
0.300
0.325
CSTAR (FT/SEC)
5820
5910
5940
5350
KWOJ
0.0550
0.0575
0.0600
KWFJ
0.024500
0.02456
0.02450
0
1
2
3
4
5
6
7
8
9
10
11
12
13
14
15
TIME (SECONDS)
1 OPOJ
2 OPFJ
3 KWOJ
4 KWFJ
6 CSTAR
FT/SEC
INJECTOR CALCULATIONS VS TIME PLOT 3
TEST NO. KEE4-D01-DA-113
TEST DATE 05-08-91 1140 HOURS 8.164 SEC.DUR
GENCORP
AEROJET

Figure C - 38

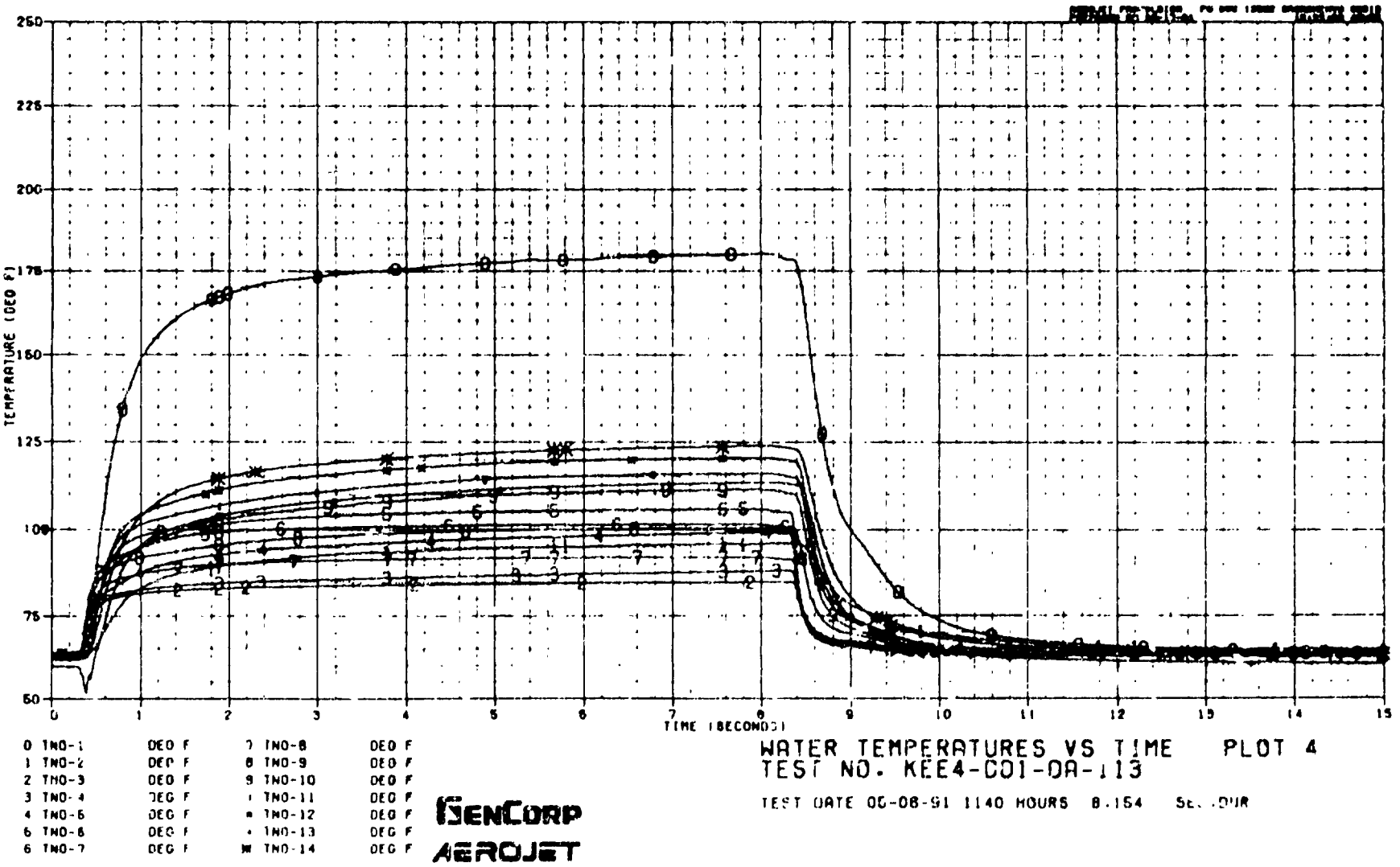
TEMPERATURE (DEG F)
250
225
200
175
150
125
100
75
50
0
1
2
3
4
5
6
7
8
9
10
11
12
13
14
15
TIME (SECONDS)
0 TNO-1 DEG F
1 TNO-2 DEG F
2 TNO-3 DEG F
3 TNO-4 DEG F
4 TNO-5 DEG F
5 TNO-6 DEG F
6 TNO-7 DEG F
7 TNO-8 DEG F
8 TNO-9 DEG F
9 TNO-10 DEG F
TNO-11 DEG F
TNO-12 DEG F
TNO-13 DEG F
TNO-14 DEG F
GENCORP
AEROJET
WATER TEMPERATURES VS TIME PLOT 4
TEST NO. KEE4-C01-DA-113
TEST DATE 06-08-91 1140 HOURS 8.154 SECOND

Figure C - 39

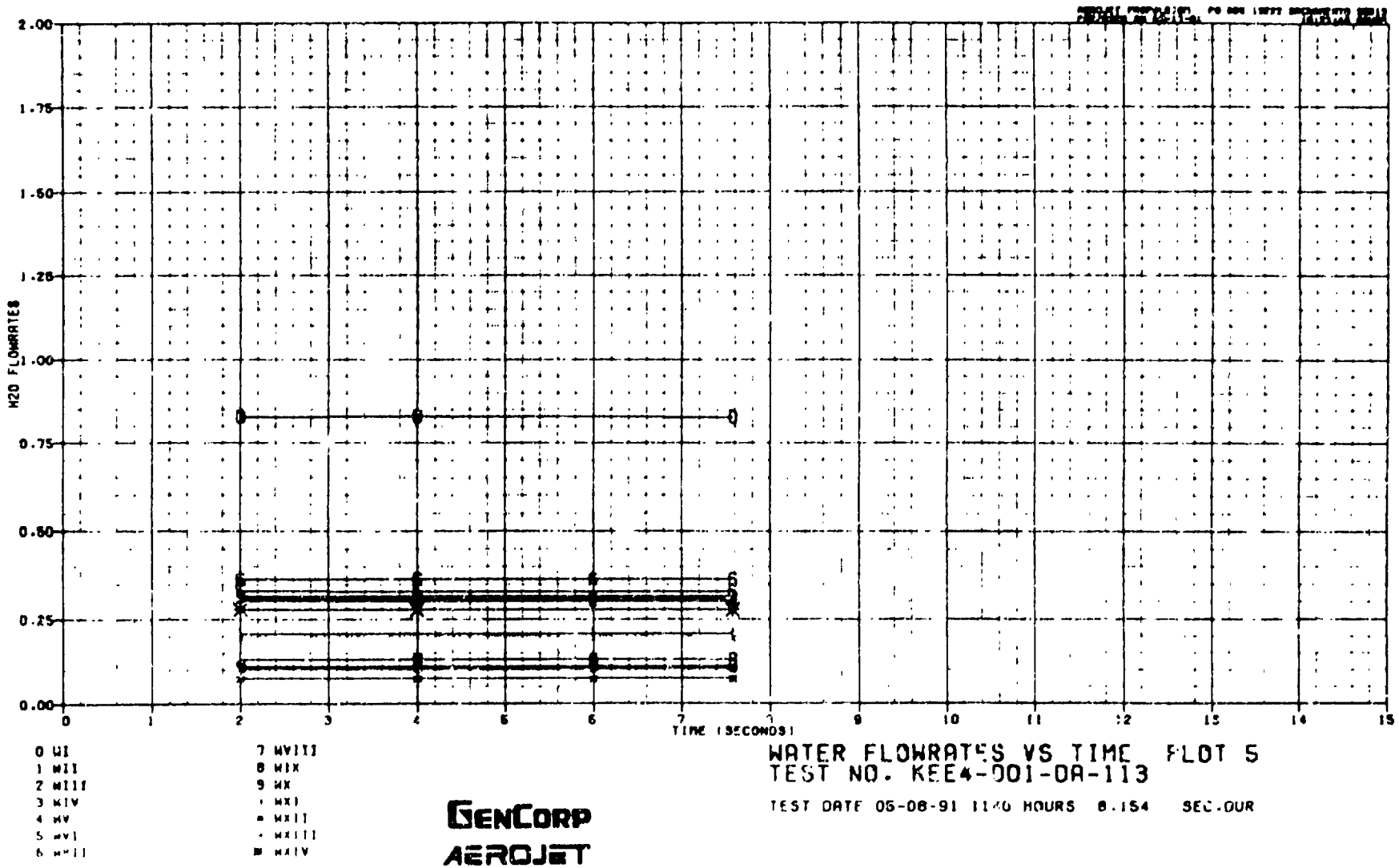
H2O FLOWRATES
2.00
1.75
1.50
1.25
1.00
0.75
0.50
0.25
0.00
0
1
2
3
4
5
6
7
8
9
10
11
12
13
14
15
TIME (SECONDS)
0 WI
1 WII
2 WIII
3 WIV
4 WV
5 WVI
6 WVII
7 WVIII
8 WIX
9 WX
WXI
WXII
WXIII
WXIV
WATER FLOWRATES VS TIME PLOT 5
TEST NO. KEE4-001-DA-113
TEST DATE 05-08-91 1140 HOURS 8.154 SEC.DUR
GENCORP
AEROJET

Figure C - 40

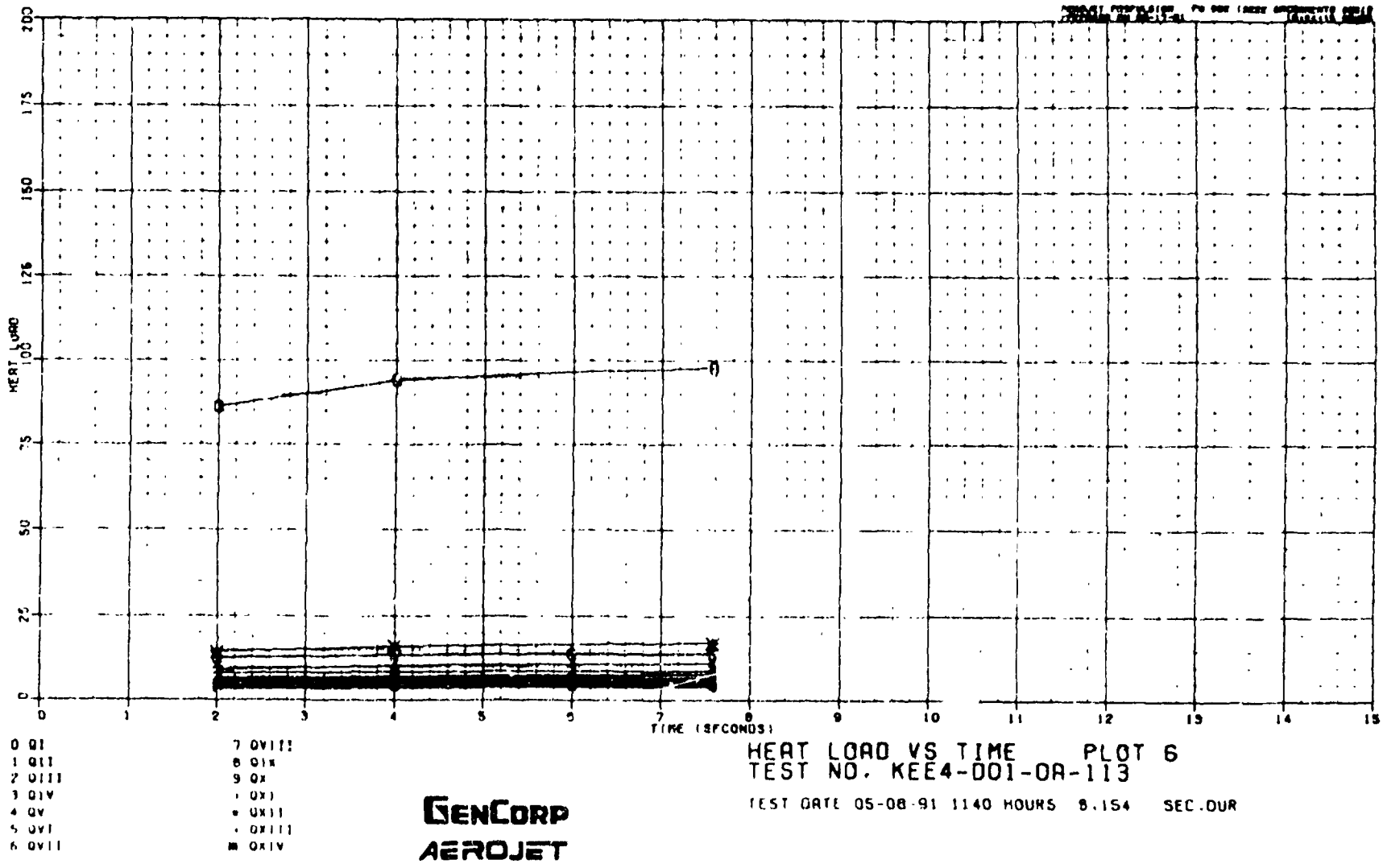
HEAT LOAD
TIME (SECONDS)
0 QI
1 QII
2 QIII
3 QIV
4 QV
5 QVI
6 QVII
7 QVIII
8 QIX
9 QX
QXI
QXII
QXIII
QXIV
GENCORP
AEROJET
HEAT LOAD VS TIME PLOT 6
TEST NO. KEE4-001-OA-113
TEST DATE 05-08-91 1140 HOURS 8.154 SEC.DUR

Figure C - 41

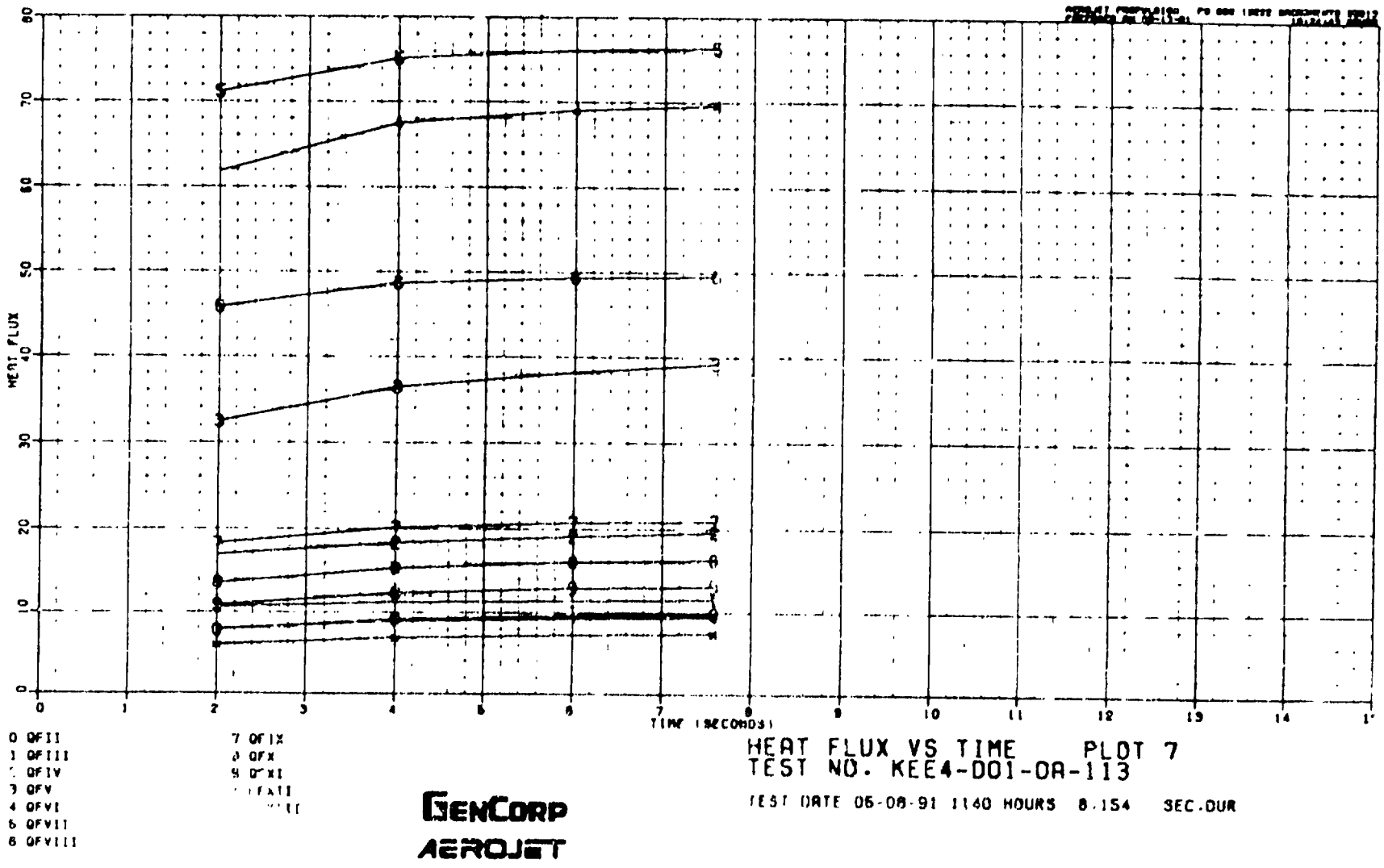
HEAT FLUX
TIME (SECONDS)
0 QFII
1 QFIII
2 QFIV
3 QFV
4 QFVI
5 QFVII
6 QFVIII
7 QFIX
8 QFX
9 QFXI
HEAT FLUX VS TIME PLOT 7
TEST NO. KEE4-D01-DA-113
TEST DATE 06-08-91 1140 HOURS 8.154 SEC.DUR
GENCORP
AEROJET

Figure C - 42

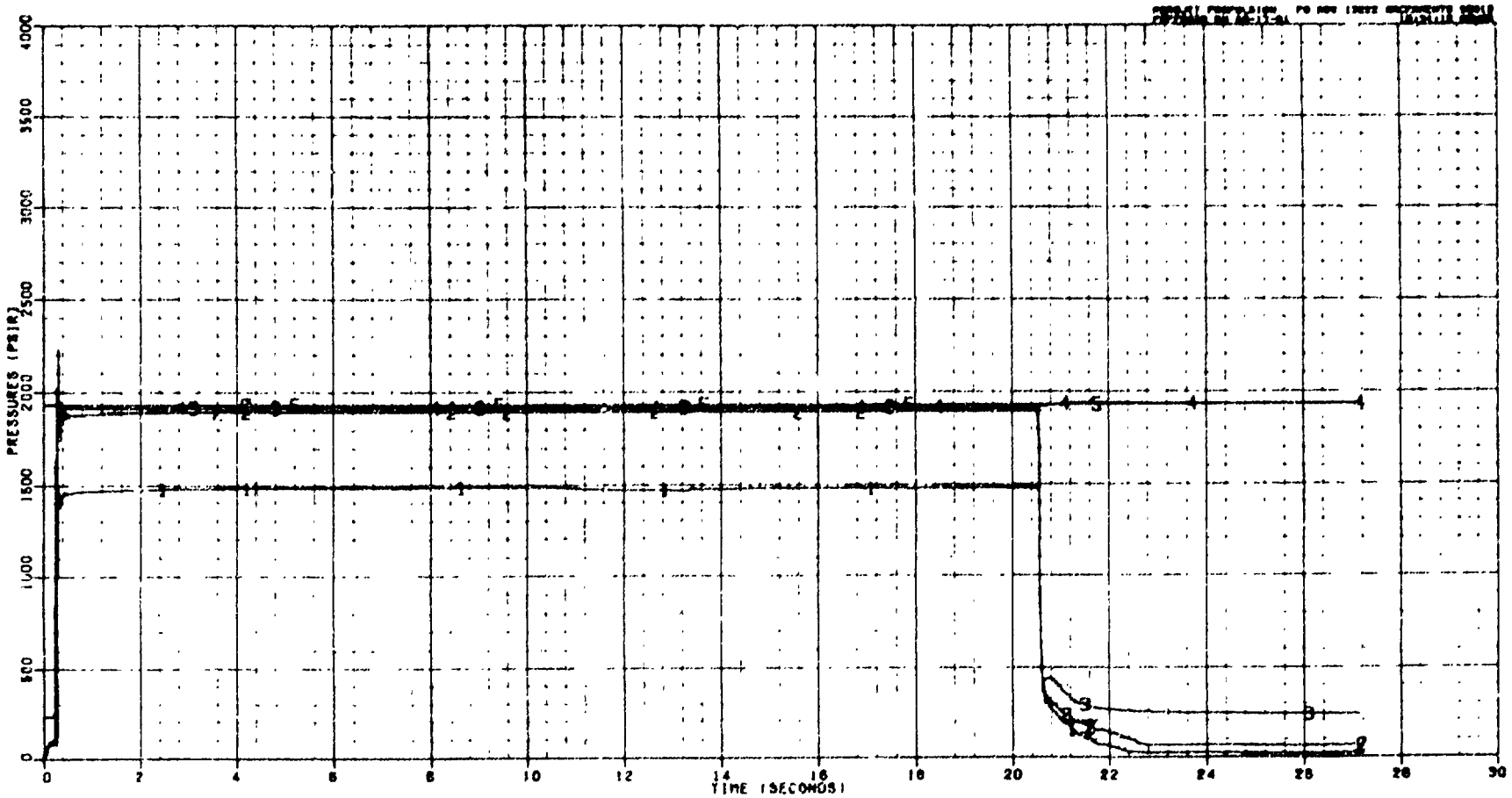

MEASURED PRESSURES VS TIME PLOT 1
TEST NO. KEE4-D01-OR-114

TEST DATE 05-08-91 1316 HOURS 20.400 SEC.DUR

GENCORP
AEROJET

Figure C - 43

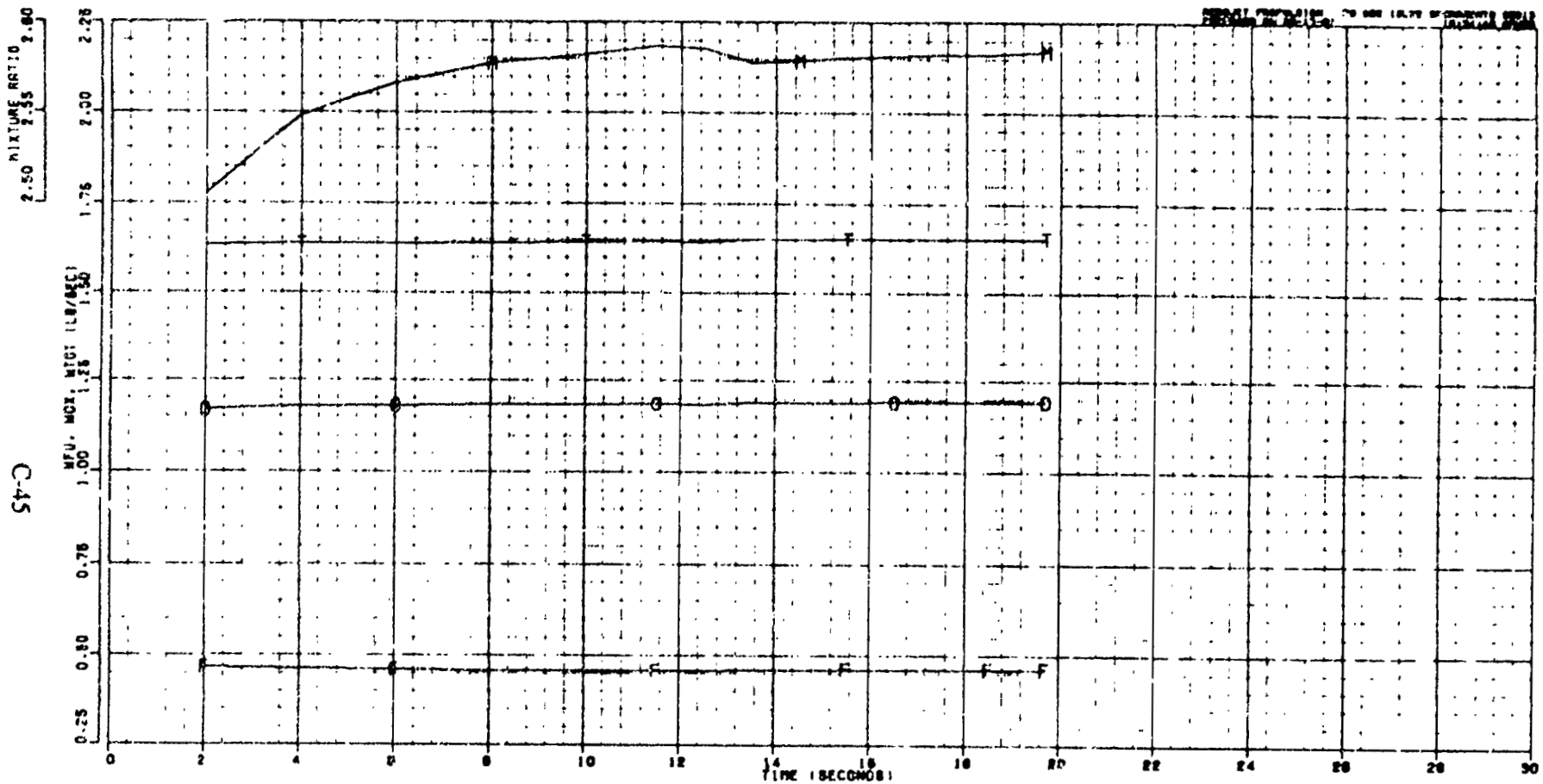

INJECTOR FLOW VS TIME PLOT 2
TEST NO. KEE4-DD1-DA-114
TEST DATE 05-08-91 1318 HOURS 20.400 SEC.DUR

GENCORP
AEROJET

Figure C - 44

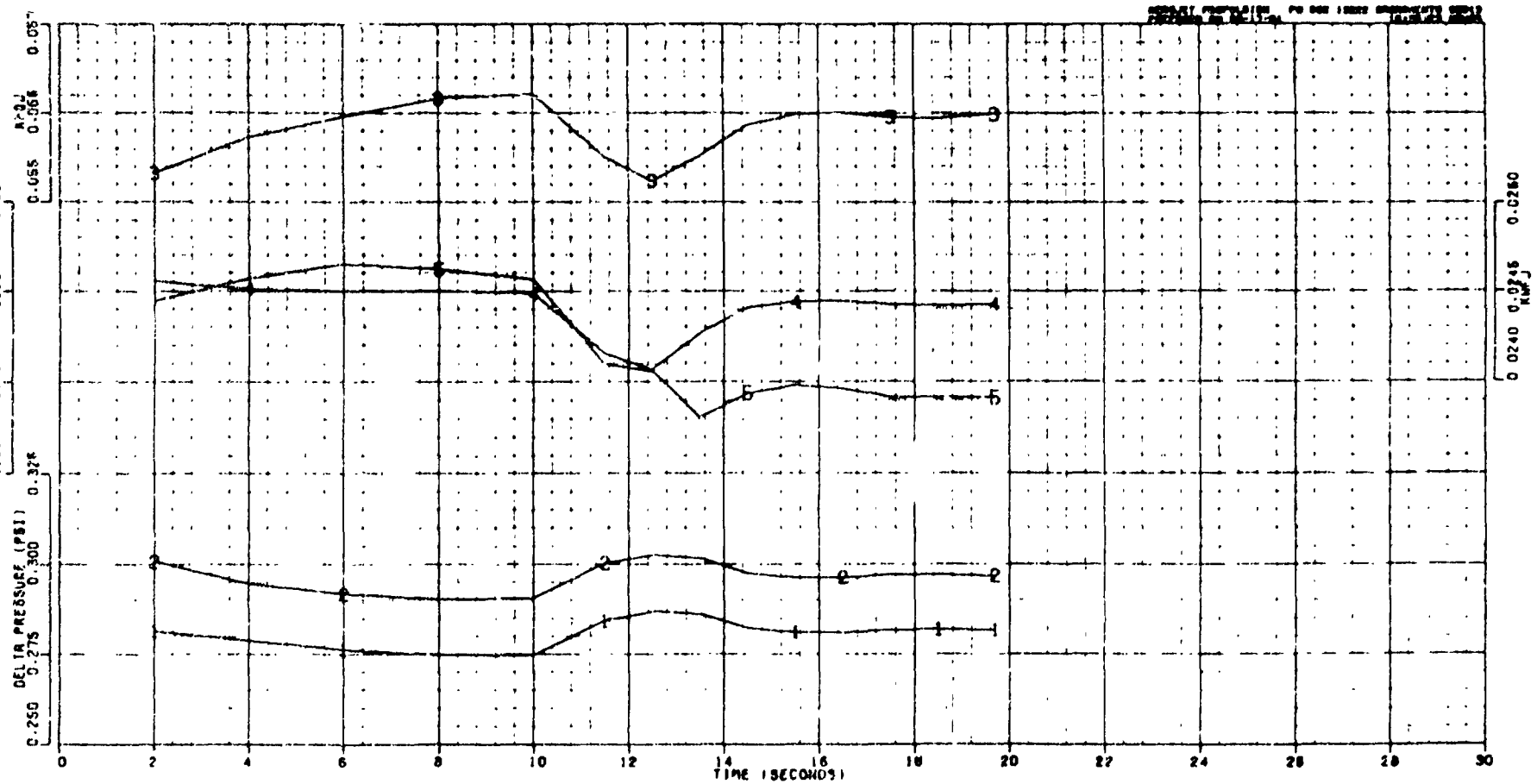

INJECTOR CALCULATIONS VS TIME PLOT 3
TEST NO. KEE4-DD1-DA-114

TEST DATE 05-08-91 1316 HOURS 20.400 SEC.DUR

GENCORP
AEROJET

Figure C - 45

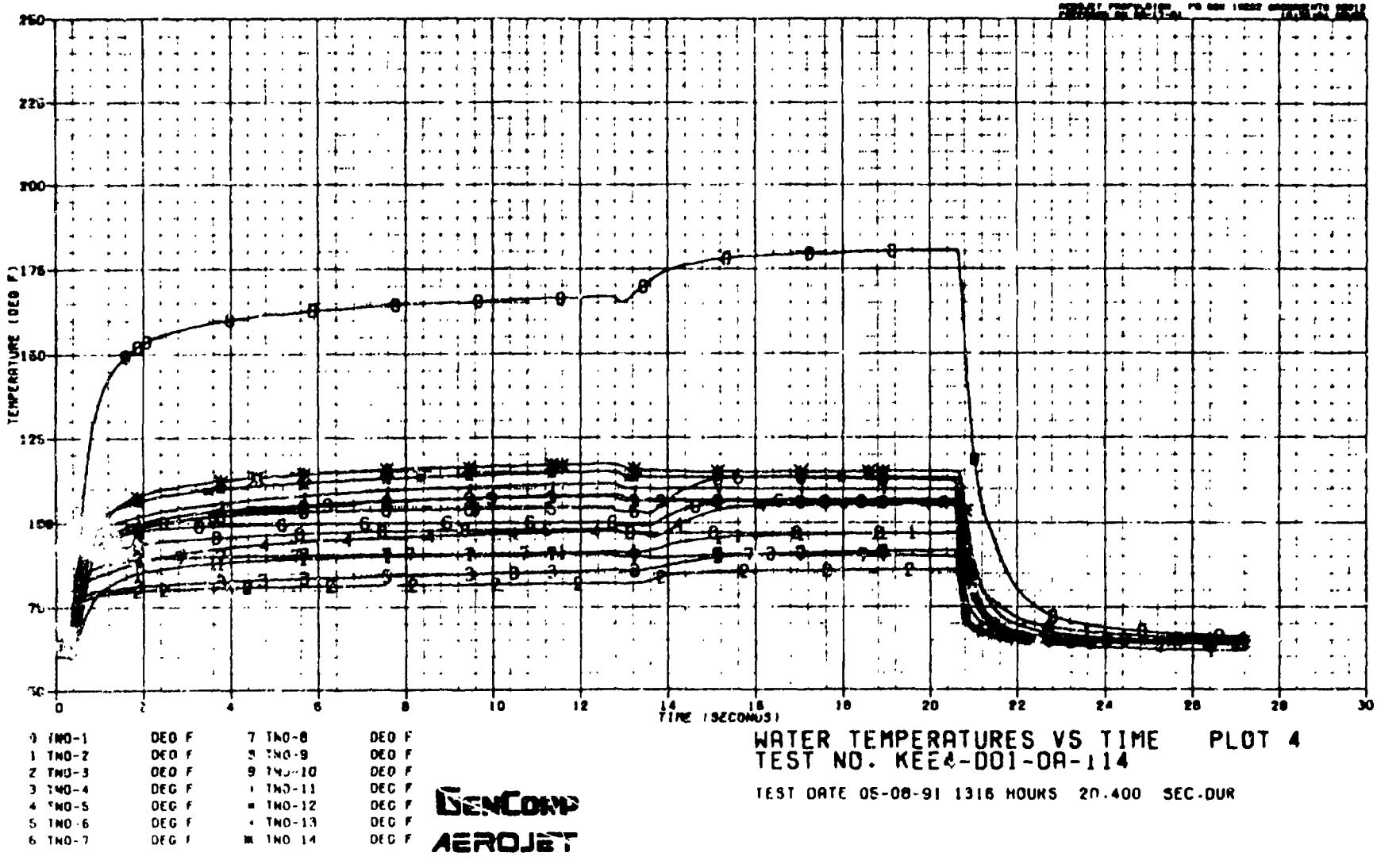
TEMPERATURE (DEG F)
TIME (SECONDS)
0 TNO-1 DEG F
1 TNO-2 DEG F
2 TNO-3 DEG F
3 TNO-4 DEG F
4 TNO-5 DEG F
5 TNO-6 DEG F
6 TNO-7 DEG F
7 TNO-8 DEG F
8 TNO-9 DEG F
9 TNO-10 DEG F
10 TNO-11 DEG F
11 TNO-12 DEG F
12 TNO-13 DEG F
13 TNO 14 DEG F
GENCORP
AEROJET
WATER TEMPERATURES VS TIME PLOT 4
TEST NO. KEE4-D01-OA-114
TEST DATE 05-08-91 1316 HOURS 20.400 SEC.DUR

Figure C - 46

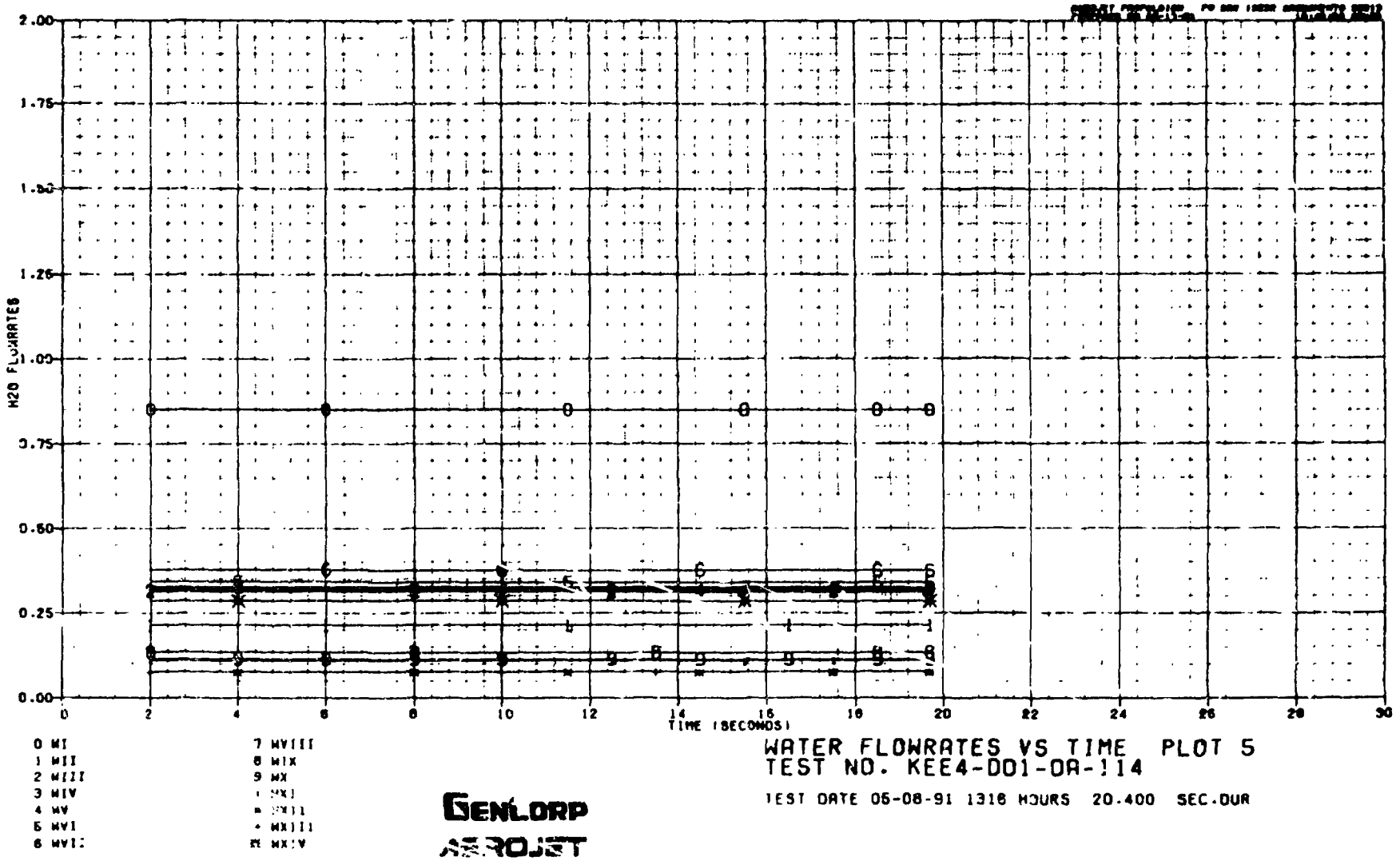
H2O FLOWRATES
2.00
1.75
1.50
1.25
1.00
0.75
0.50
0.25
0.00
0
2
4
6
8
10
12
14
16
18
20
22
24
26
28
30
TIME (SECONDS)
0 MI
1 MII
2 MIII
3 MIV
4 MV
5 MVI
6 MVII
7 MVIII
8 MIX
9 MX
WATER FLOWRATES VS TIME PLOT 5
TEST NO. KEE4-DO1-OA-114
TEST DATE 05-08-91 1316 HOURS 20.400 SEC.DUR
GENCORP
AEROJET

Figure C - 47

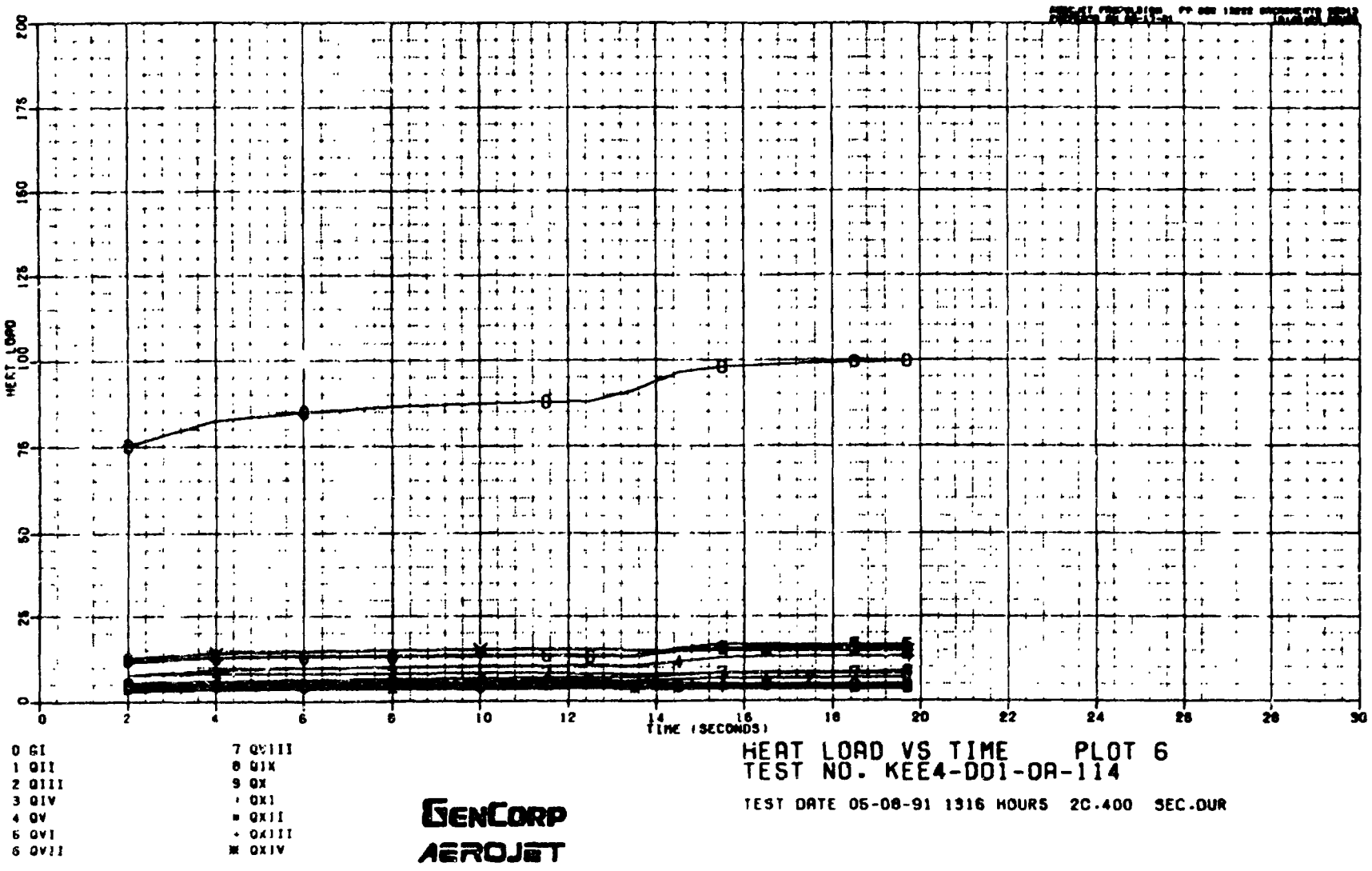
HEAT LOAD
0
25
50
75
100
125
150
175
200
0
2
4
6
8
10
12
14
16
18
20
22
24
26
28
30
TIME (SECONDS)
0 QI
1 QII
2 QIII
3 QIV
4 QV
5 QVI
6 QVII
7 QVIII
8 QIX
9 QX
QXI
QXII
QXIII
QXIV
HEAT LOAD VS TIME PLOT 6
TEST NO. KEE4-DDI-DA-114
TEST DATE 05-08-91 1316 HOURS 2C.400 SEC.DUR
GENCORP
AEROJET

Figure C - 48

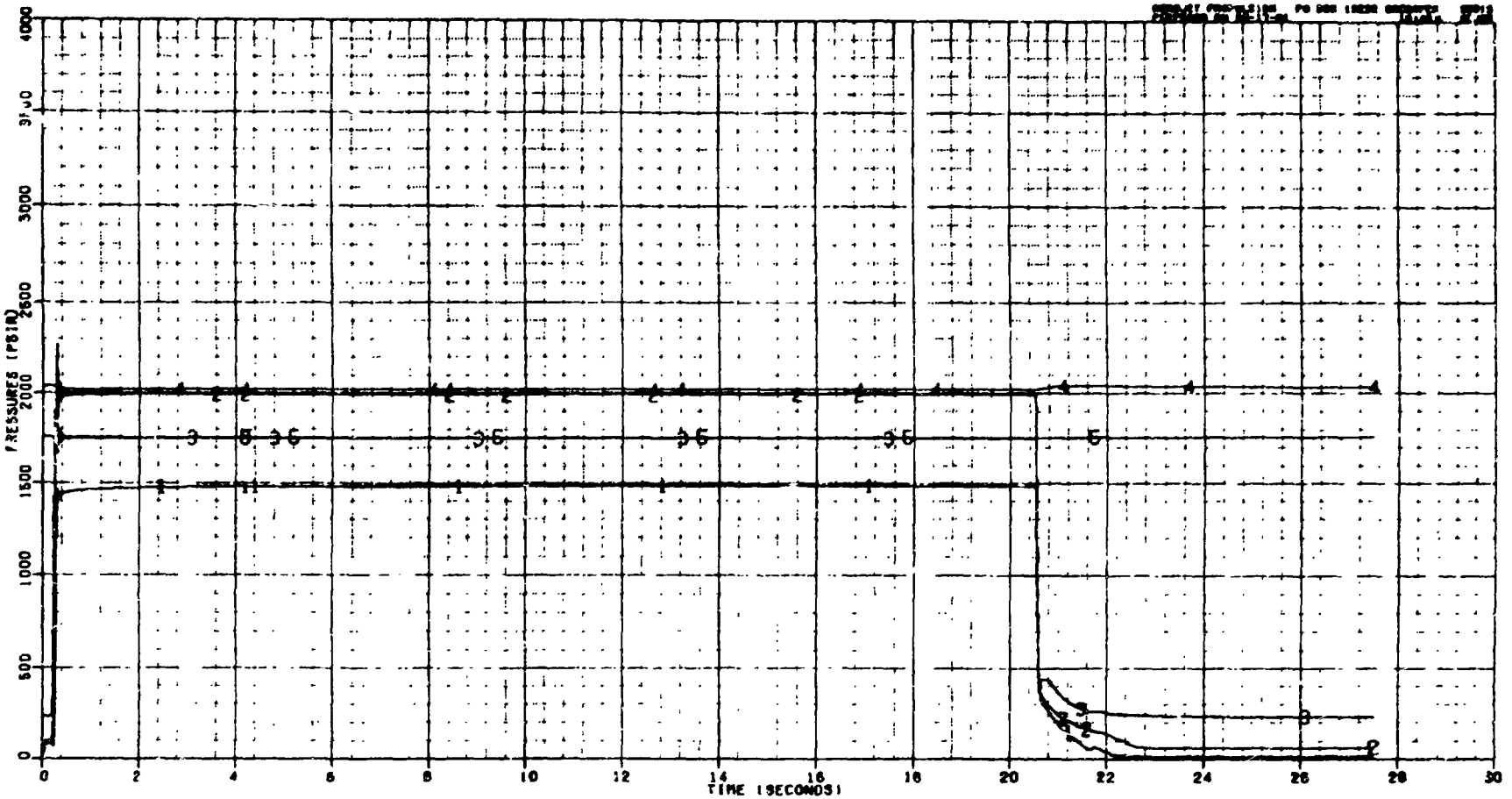

1 PC-1 PSIA
2 POJ PSIA
3 PFJ PSIA
4 POT PSIA
5 PFT PSIA

MEASURED PRESSURES VS TIME PLOT 1
TEST NO. KEE4-001-OA-115

TEST DATE 05-08-91 1423 HOURS 20.388 SEC.DUR

GENCORP
AEROJET

Figure C - 49

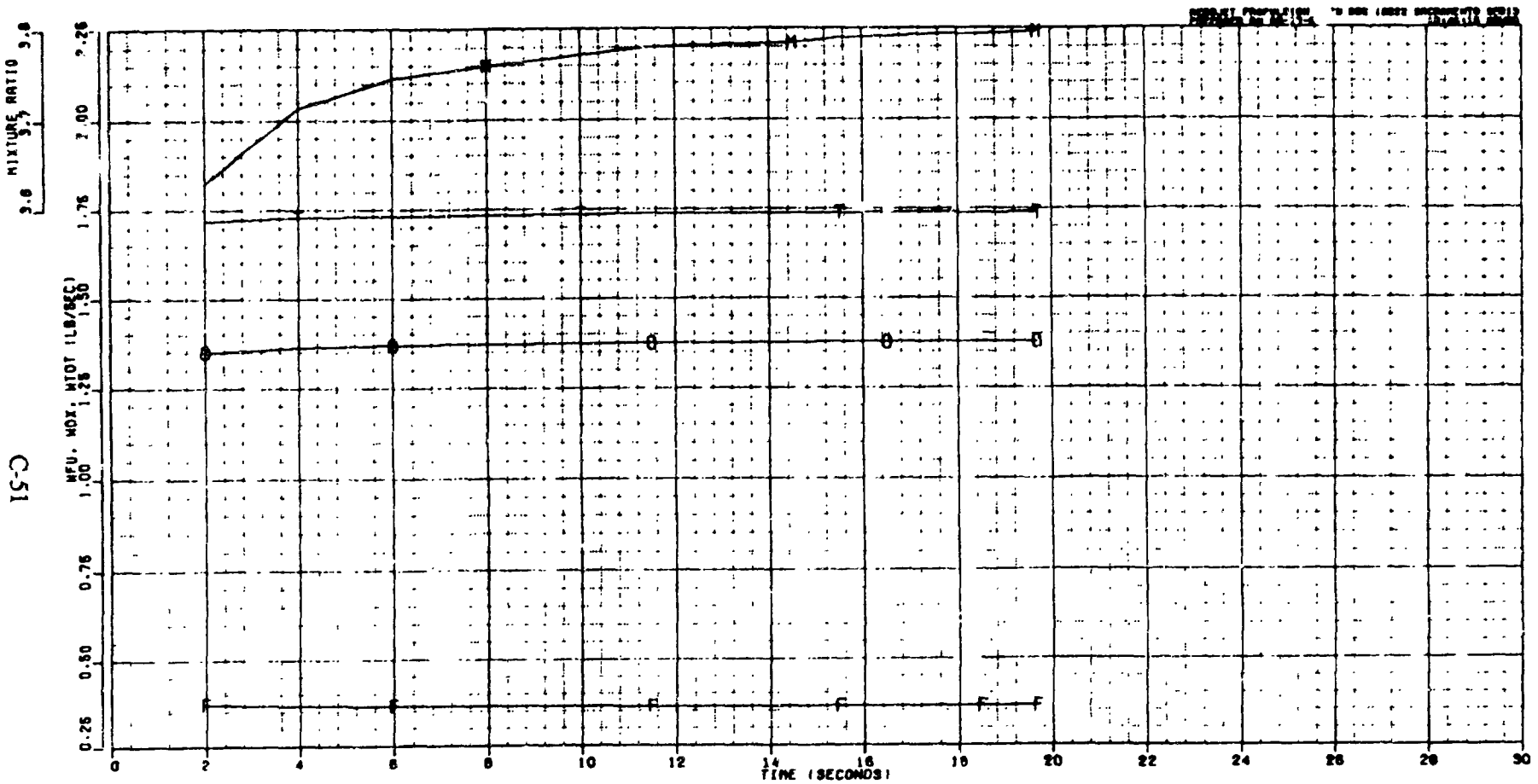

GENCORP
AEROJET

Figure C - 50

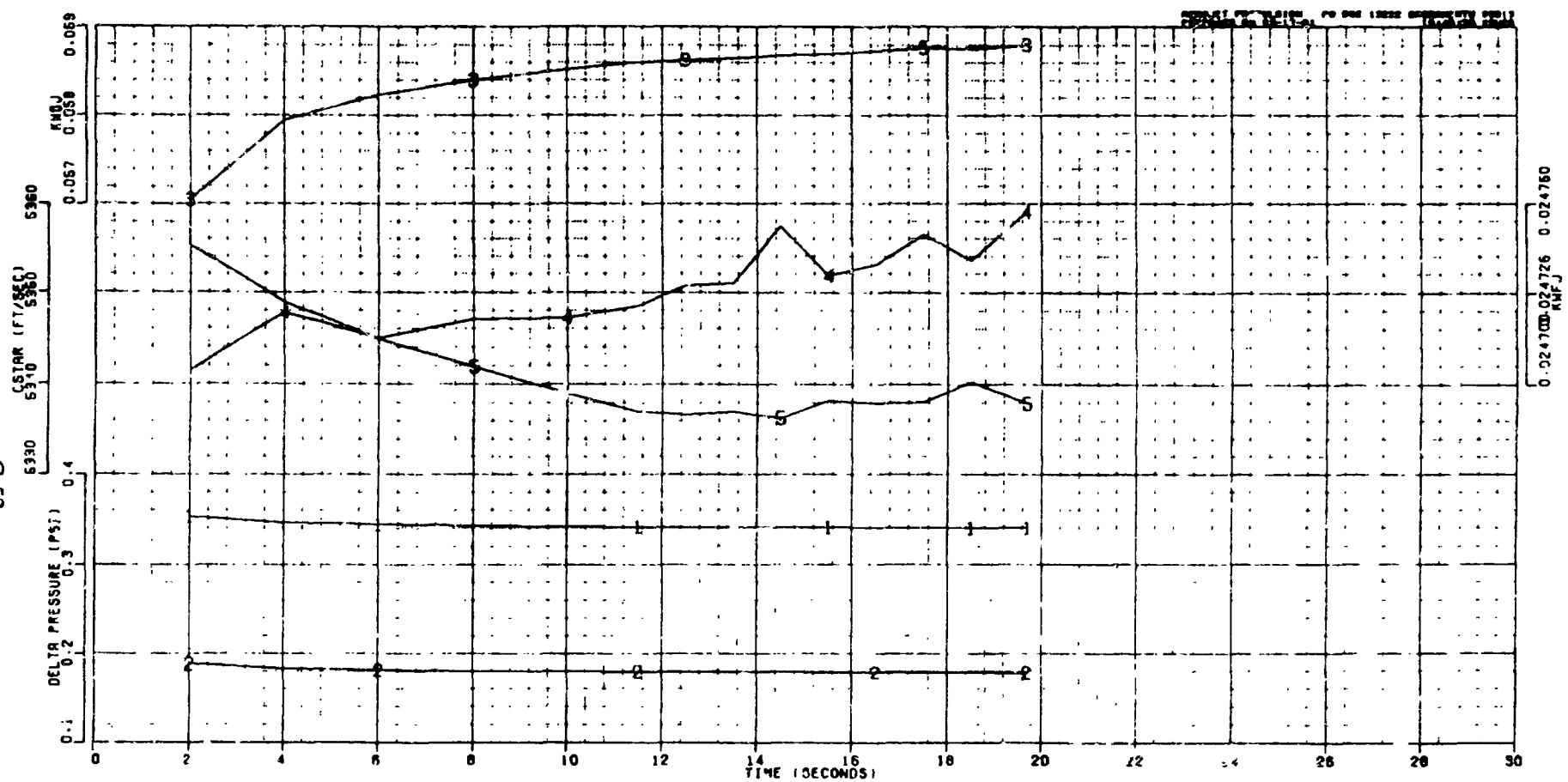

1 DPOJ
2 DPFJ
3 KWOJ
4 KWFJ
5 CSTAR FT/SEC

INJECTOR CALCULATIONS VS TIME PLOT 3
TEST NO. KEE4-D01-OR-115

TEST DATE 05-08-91 1423 HOURS 20.388 SEC.DUR

GENCORP
AEROJET

Figure C - 51

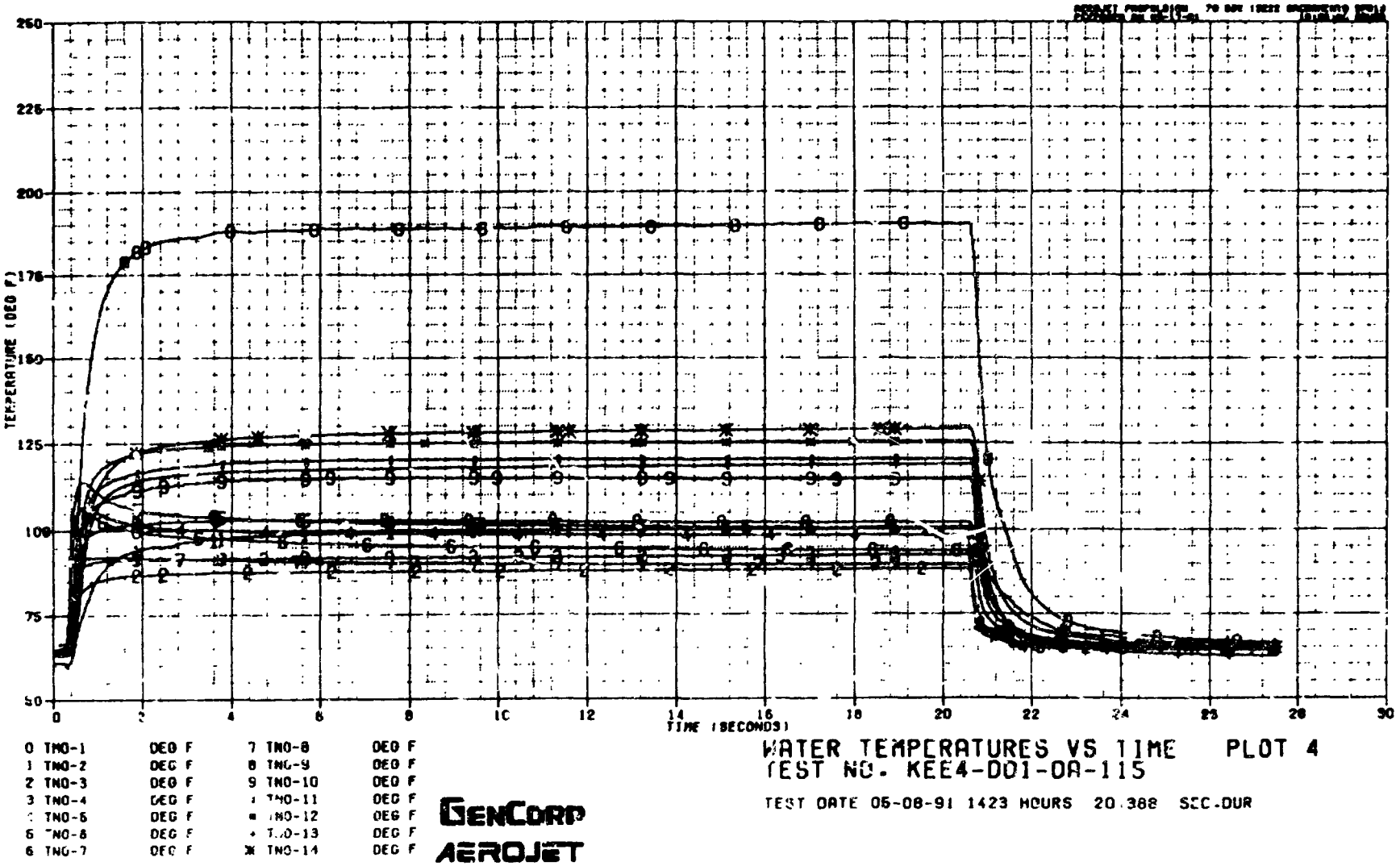
TEMPERATURE (DEG F)
250
225
200
175
150
125
100
75
50
0
2
4
6
8
10
12
14
16
18
20
22
24
26
28
30
TIME (SECONDS)
0 TNO-1 DEG F
1 TNO-2 DEG F
2 TNO-3 DEG F
3 TNO-4 DEG F
5 TNO-6 DEG F
6 TNO-7 DEG F
7 TNO-8 DEG F
8 TNO-9 DEG F
9 TNO-10 DEG F
DEG F
DEG F
DEG F
DEG F
GENCORP
AEROJET
WATER TEMPERATURES VS TIME PLOT 4
TEST NO. KEE4-D01-DA-115
TEST DATE 05-08-91 1423 HOURS 20.388 SEC-DUR

Figure C - 52

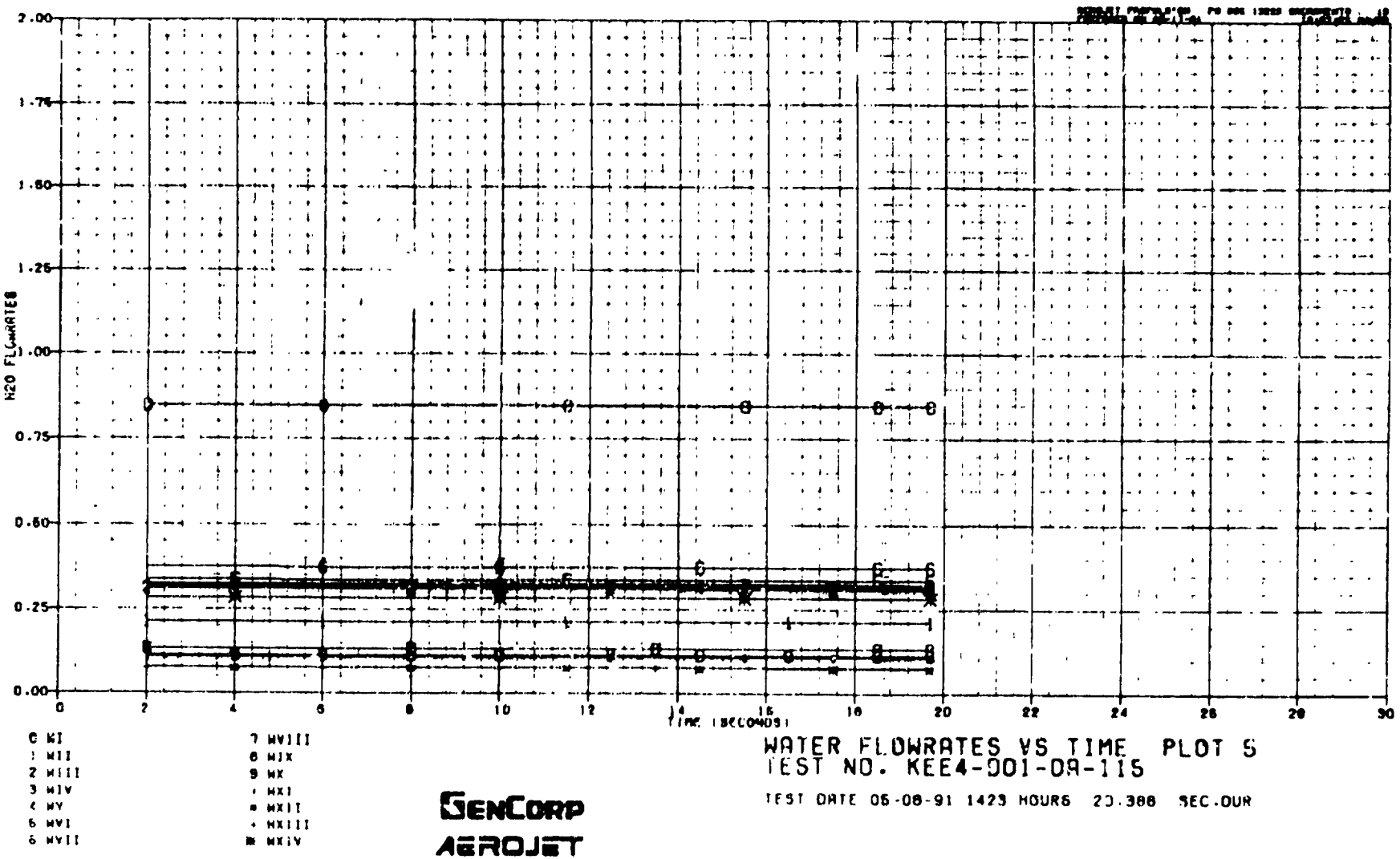

Figura C - 53

ORIGINAL PAGE IS
OF POOR QUALITY

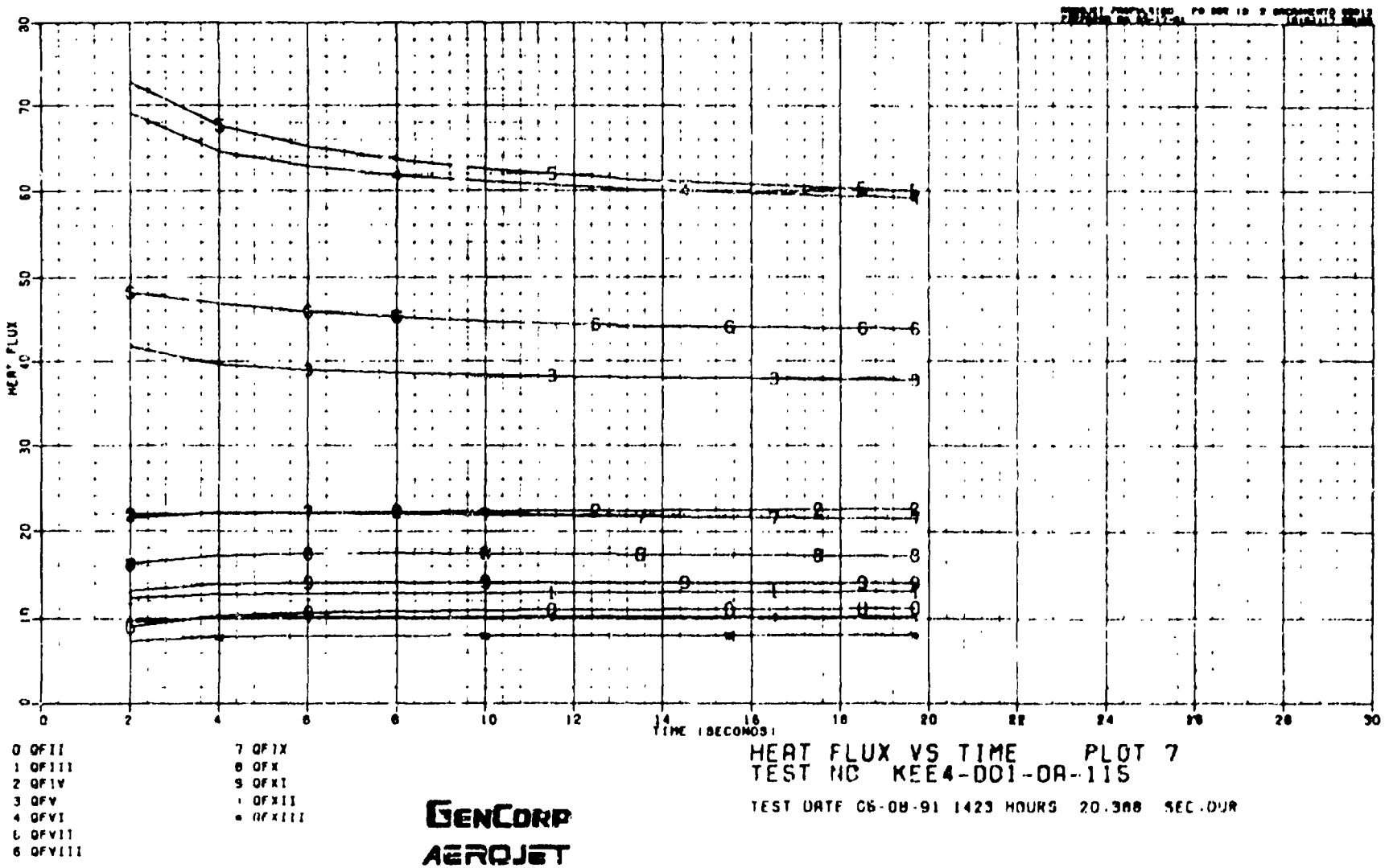
HEAT FLUX
TIME (SECONDS)
0 QFII
1 QFIII
2 QFIV
3 QFV
4 QFVI
5 QFVII
6 QFVIII
7 QFIX
8 QFX
9 QFXI
10 QFXII
11 QFXIII
GENCORP
AEROJET
HEAT FLUX VS TIME PLOT 7
TEST NO KEE4-001-DA-115
TEST DATE 06-08-91 1423 HOURS 20.388 SEC.DUR

Figure C - 54

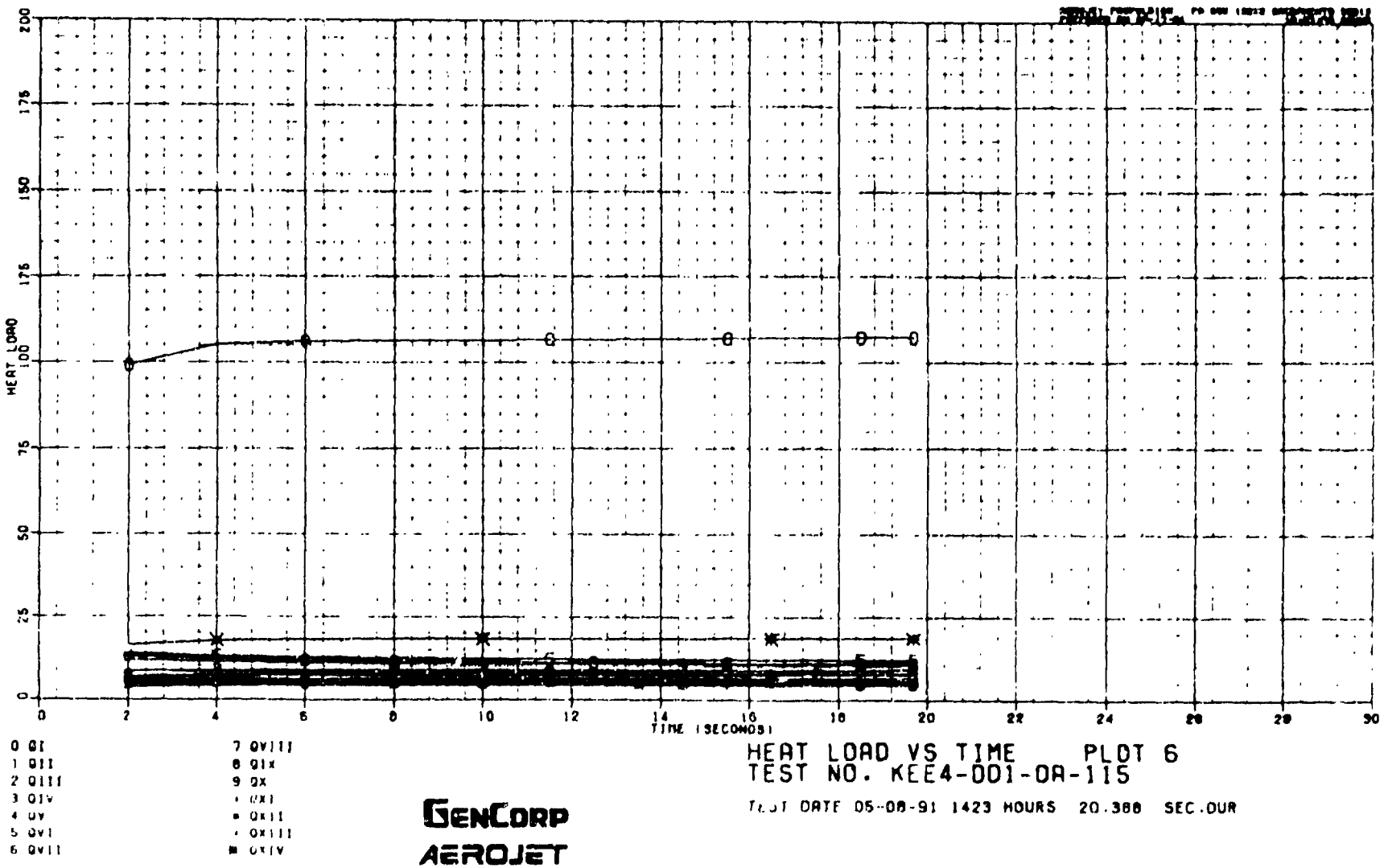
HEAT LOAD
TIME (SECONDS)
0 QI
1 QII
2 QIII
3 QIV
4 QV
5 QVI
6 QVII
7 QVIII
8 QIX
9 QX
QXI
QXII
QXIII
QXIV
GENCORP
AEROJET
HEAT LOAD VS TIME PLOT 6
TEST NO. KEE4-001-OA-115
TEST DATE 05-08-91 1423 HOURS 20.388 SEC.DUR

Figure C - 55

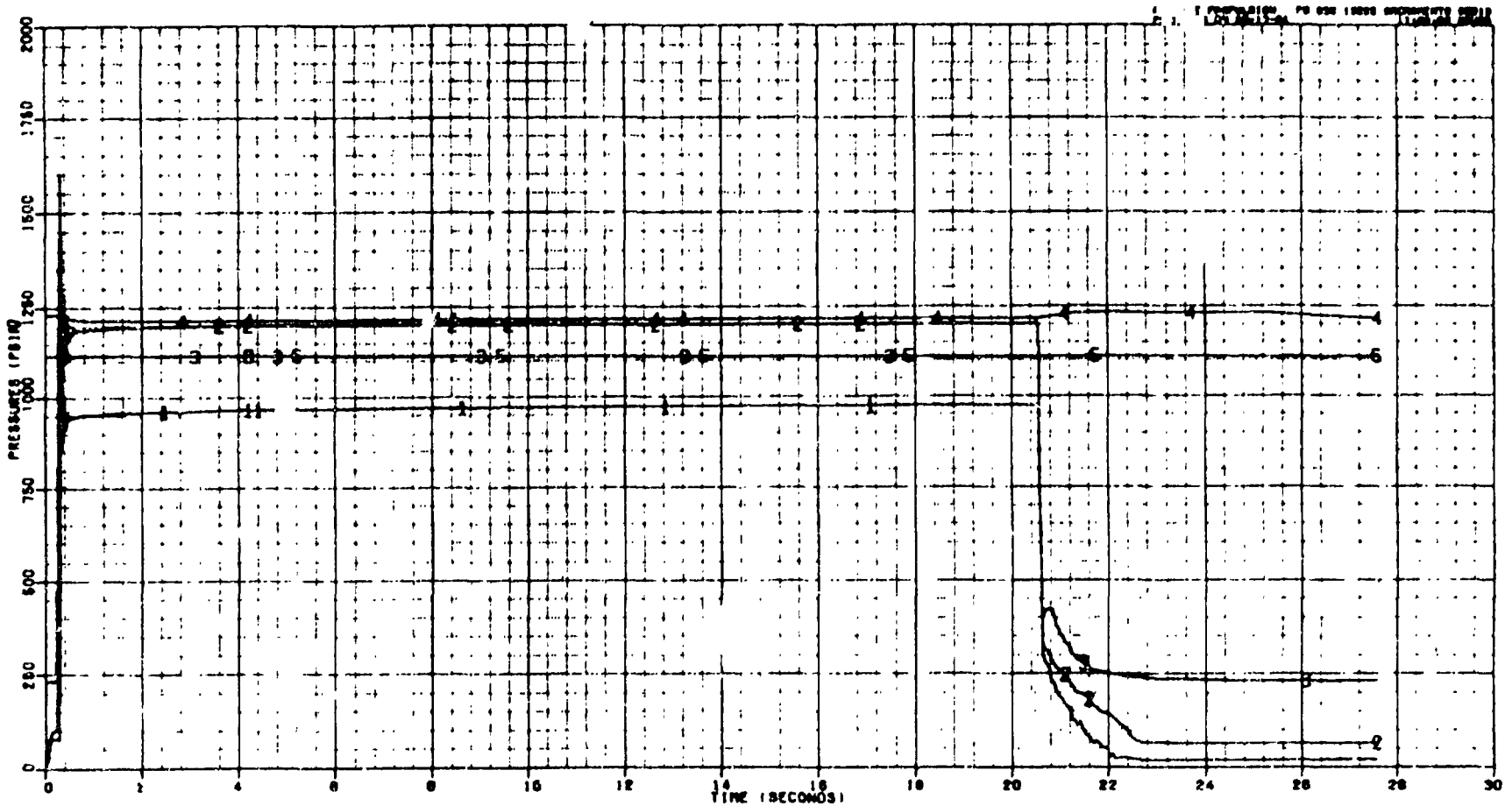

1 PC-1 PSIA
2 POJ PSIA
3 PFJ PSIA
4 POT PSIA
6 PFT PSIA

MEASURED PRESSURES VS TIME PLOT 1
TEST NO. KEE4-D01-DA-116

TEST DATE 05-08-91 1634 HOURS 20.416 SEC.DUR

GENCORP
AEROJET

Figure C - 56

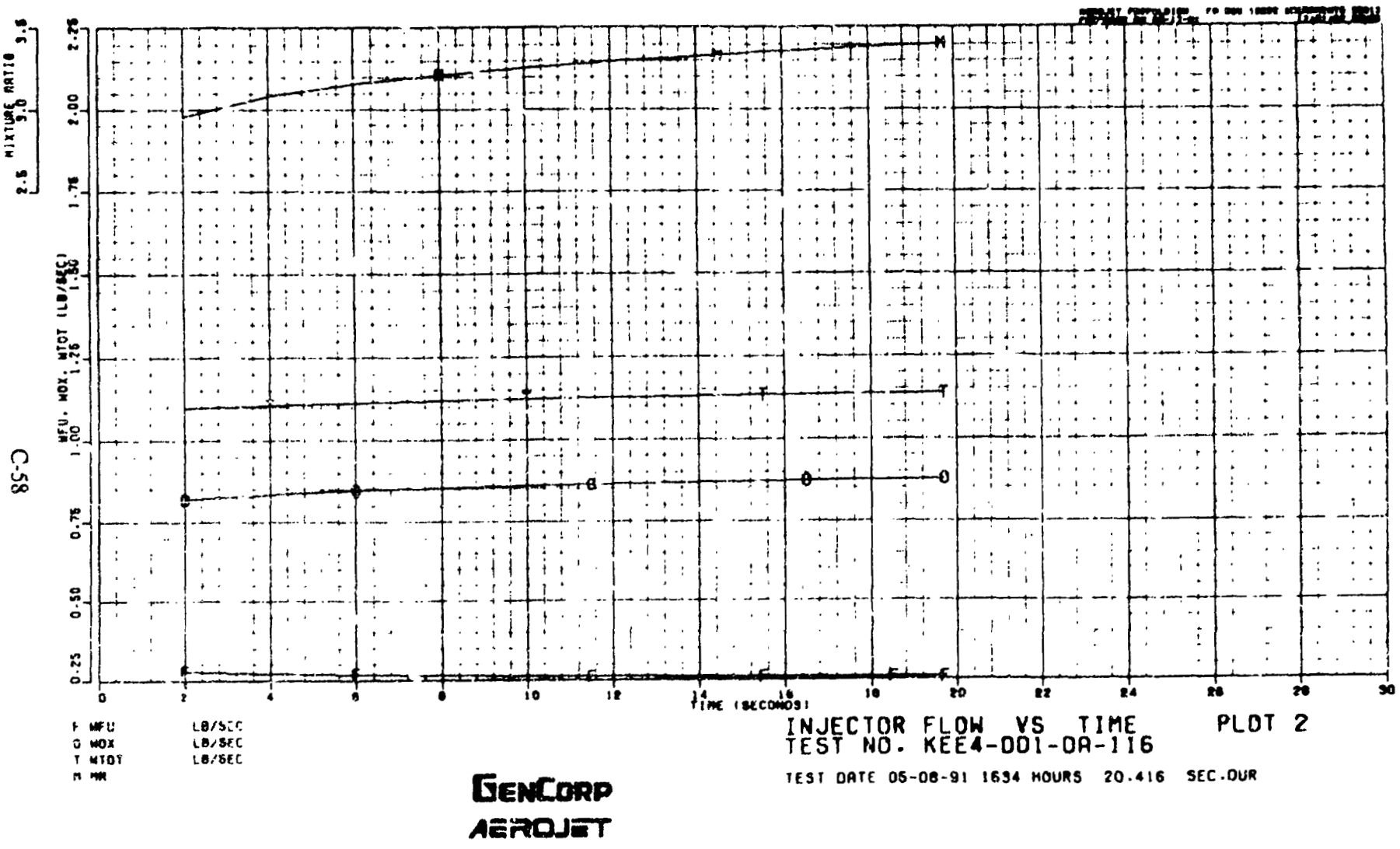

Figure C - 57

ORIGINAL PAGE IS
OF POOR QUALITY

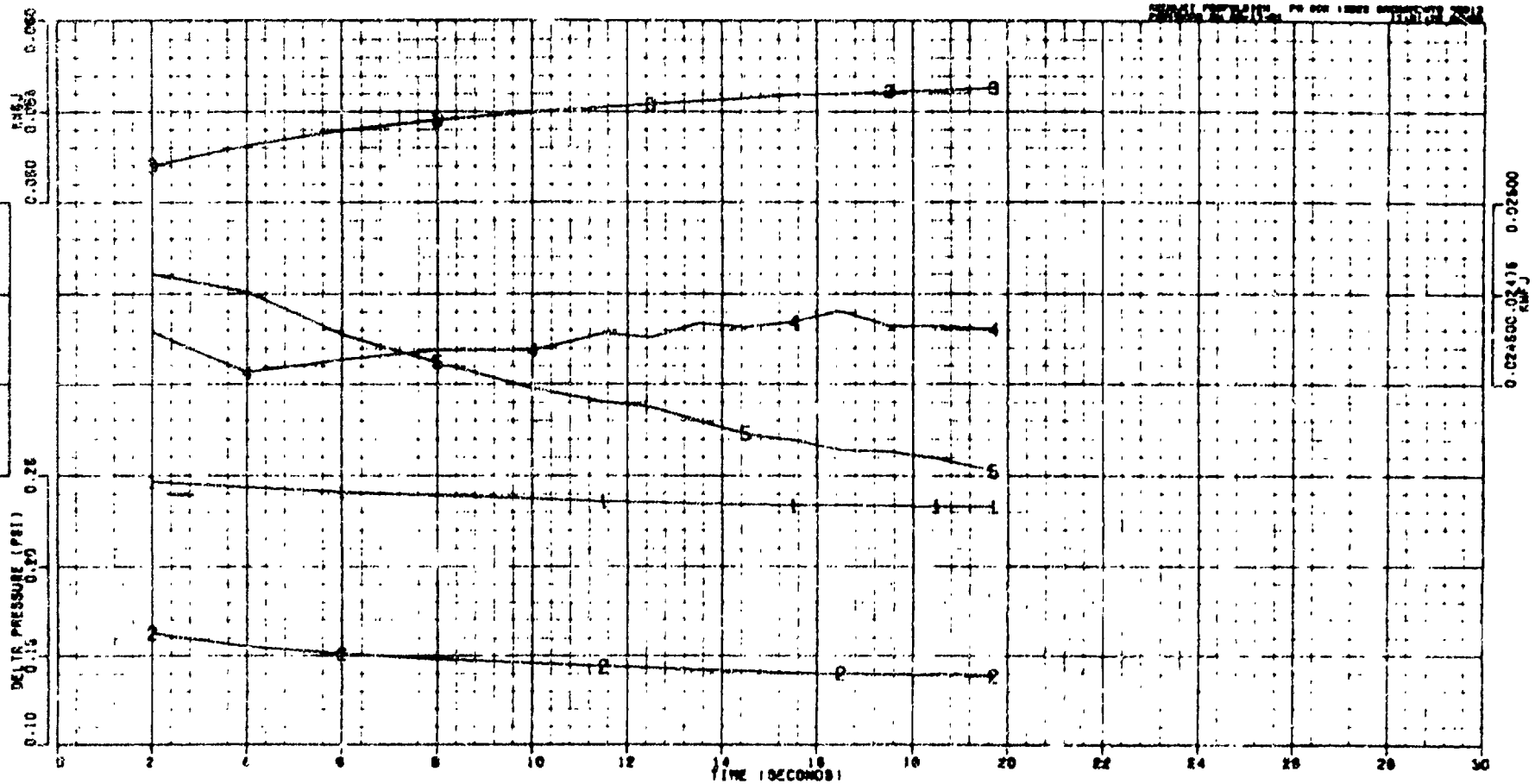

GenCorp Aerojet

Figure C - 58

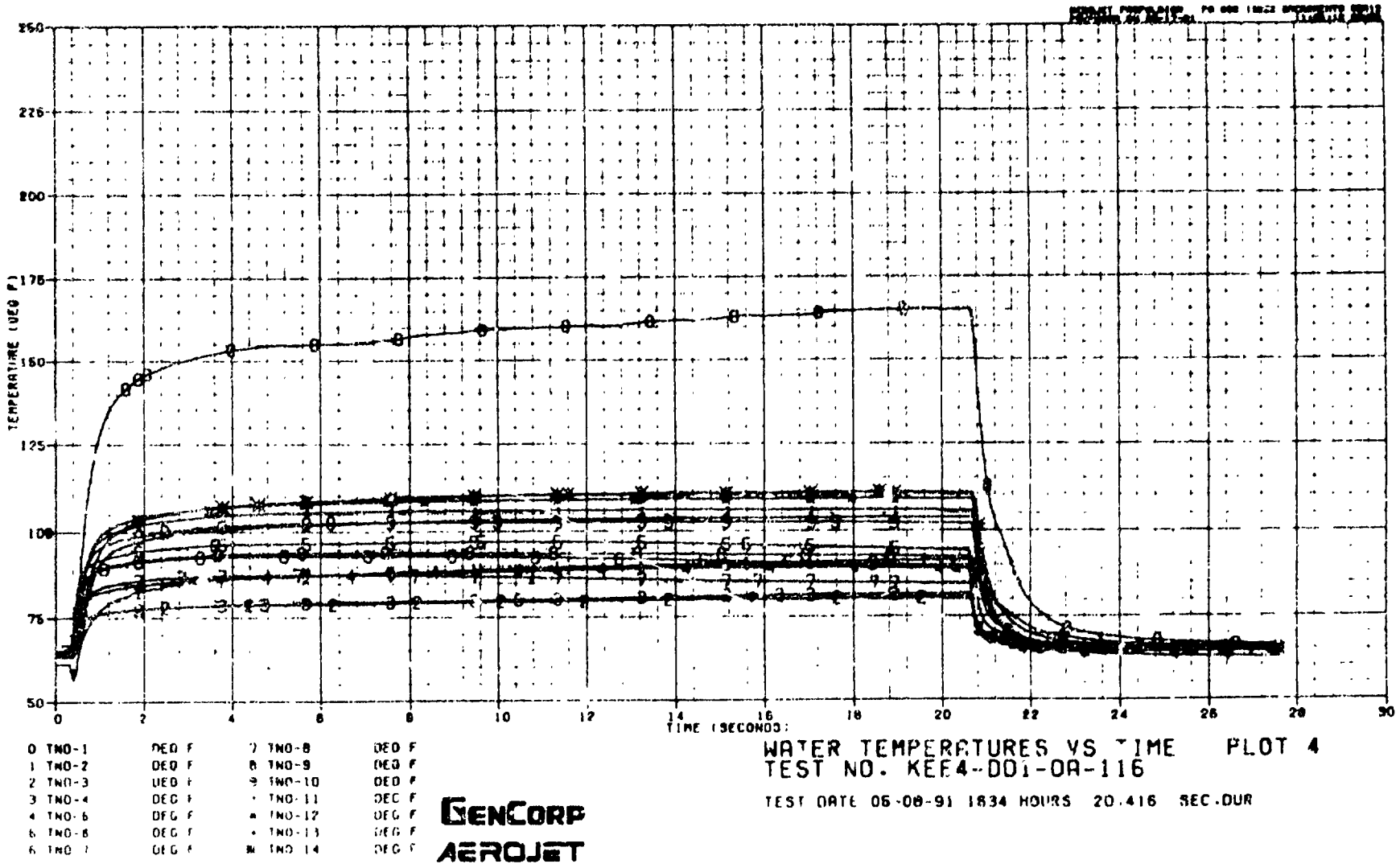
TEMPERATURE (DEG F)
250
225
200
175
150
125
100
75
50
0
2
4
6
8
10
12
14
16
18
20
22
24
26
28
30
TIME (SECONDS)
0 TNO-1 DEG F
1 TNO-2 DEG F
2 TNO-3 DEG F
3 TNO-4 DEG F
4 TNO-5 DEG F
5 TNO-6 DEG F
6 TNO-7 DEG F
7 TNO-8 DEG F
8 TNO-9 DEG F
9 TNO-10 DEG F
TNO-11 DEG F
TNO-12 DEG F
TNO-13 DEG F
TNO-14 DEG F
GENCORP
AEROJET
WATER TEMPERATURES VS TIME PLOT 4
TEST NO. KEF4-D01-OA-116
TEST DATE 05-08-91 1834 HOURS 20.416 SEC.DUR

Figure C - 59

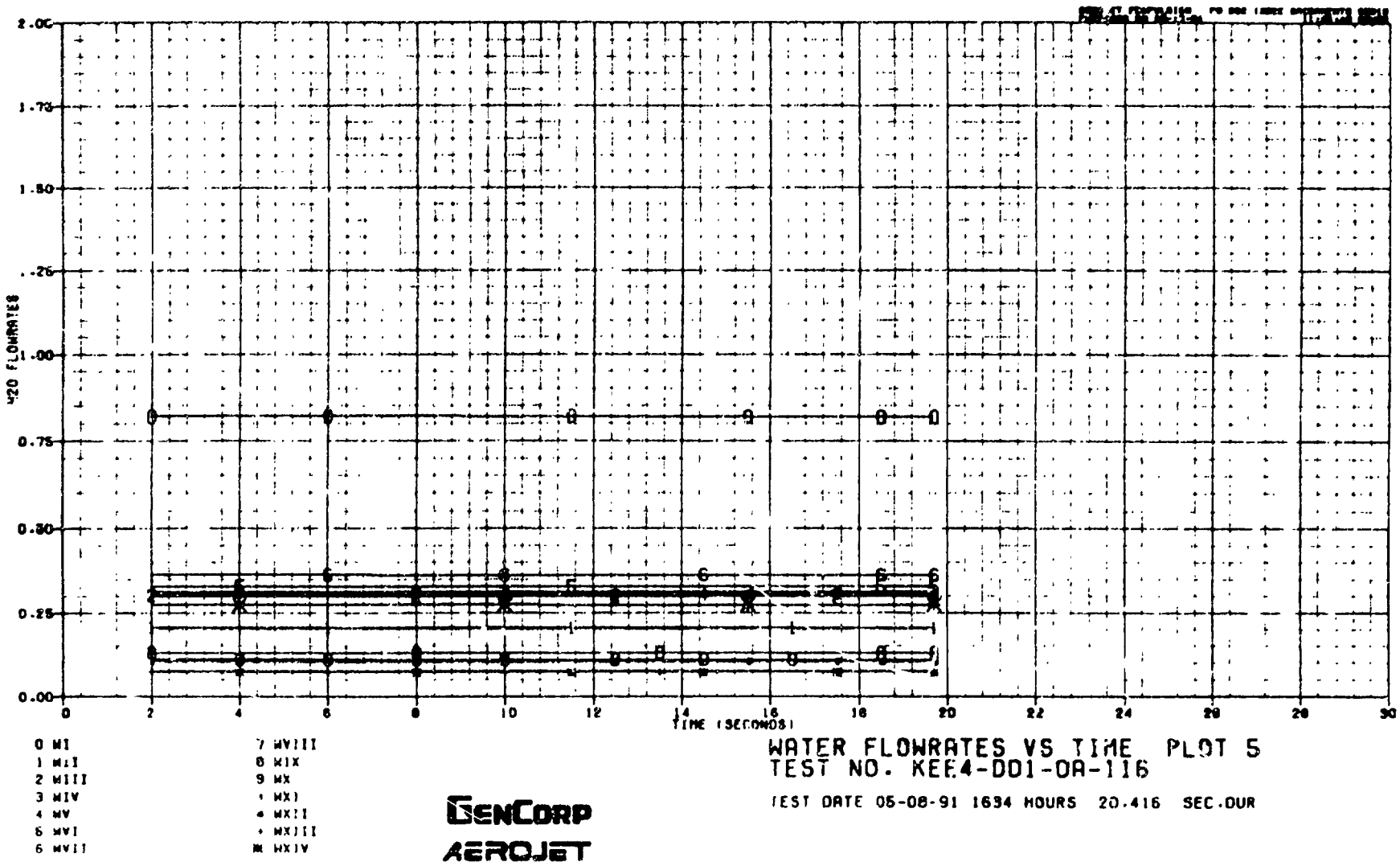
H2O FLOWRATES
2.00
1.75
1.50
1.25
1.00
0.75
0.50
0.25
0.00
0
2
4
6
8
10
12
14
16
18
20
22
24
26
28
30
TIME (SECONDS)
0 WI
1 WII
2 WIII
3 WIV
4 WV
5 WVI
6 WVII
7 WVIII
8 WIX
9 WX
+ WXI
+ WXII
+ WXIII
WXIV
WATER FLOWRATES VS TIME PLOT 5
TEST NO. KEE4-DD1-DA-116
TEST DATE 05-08-91 1634 HOURS 20.416 SEC.DUR
GENCORP
AEROJET

Figure C - 60

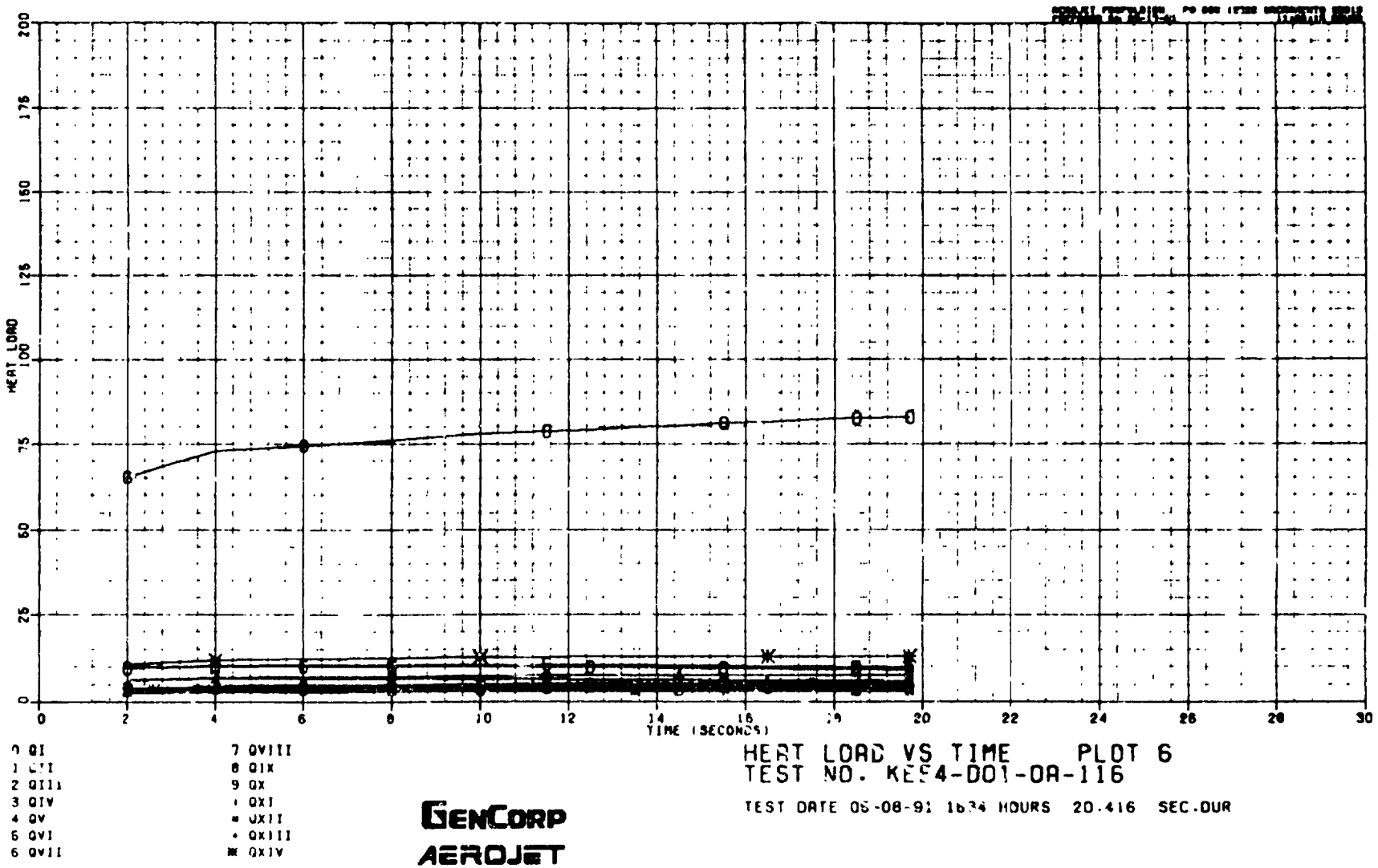

Figure C - 61

ORIGINAL PAGE IS
OF POOR QUALITY

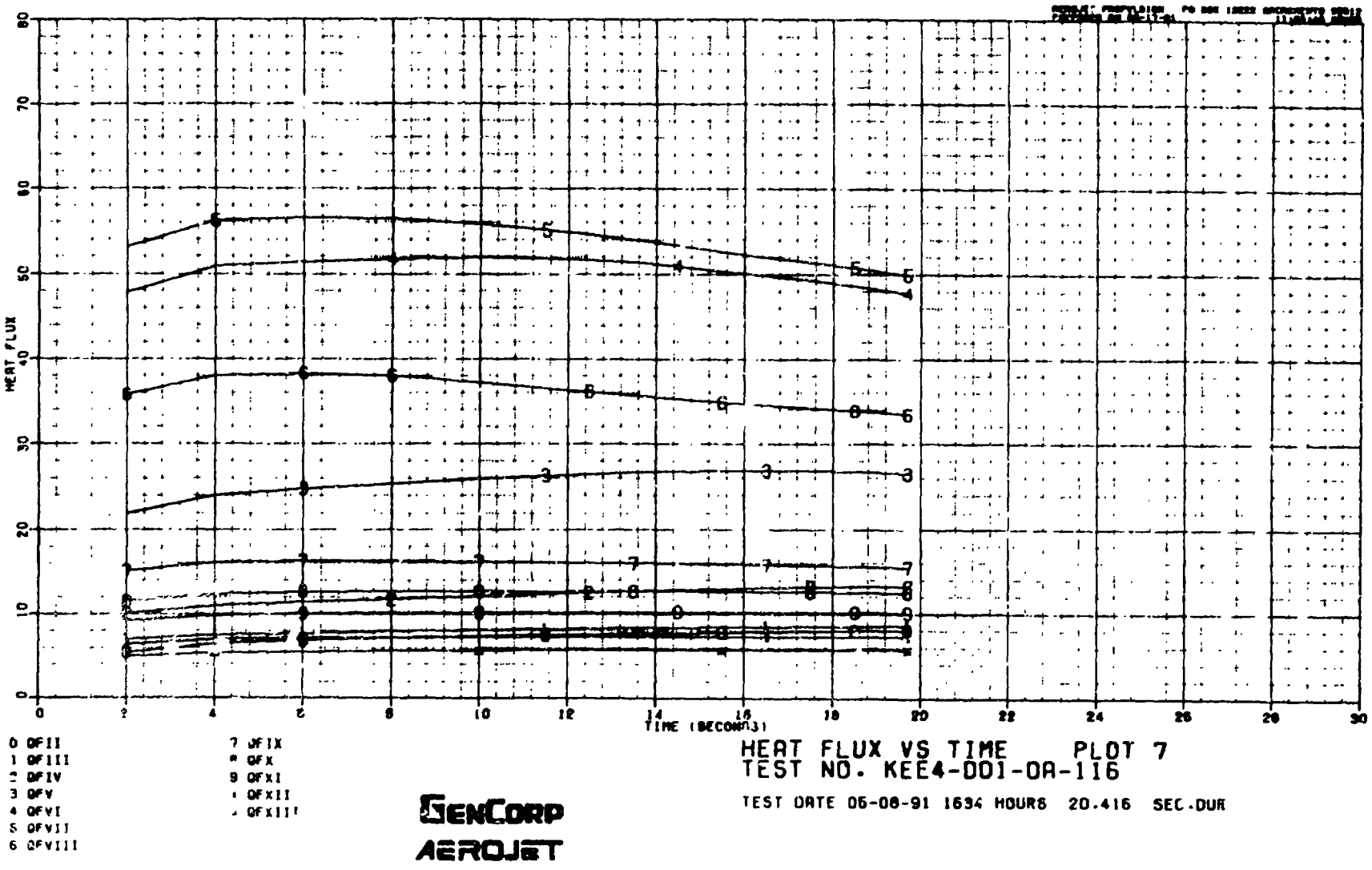
HEAT FLUX
TIME (SECONDS)
0 QFII
1 QFIII
2 QFIV
3 QFV
4 QFVI
5 QFVII
6 QFVIII
7 QFIX
8 QFX
9 QFXI
10 QFXII
11 QFXIII
GENCORP
AEROJET
HEAT FLUX VS TIME PLOT 7
TEST NO. KEE4-001-0A-116
TEST DATE 05-08-91 1634 HOURS 20.416 SEC.DUR

Figure C - 62

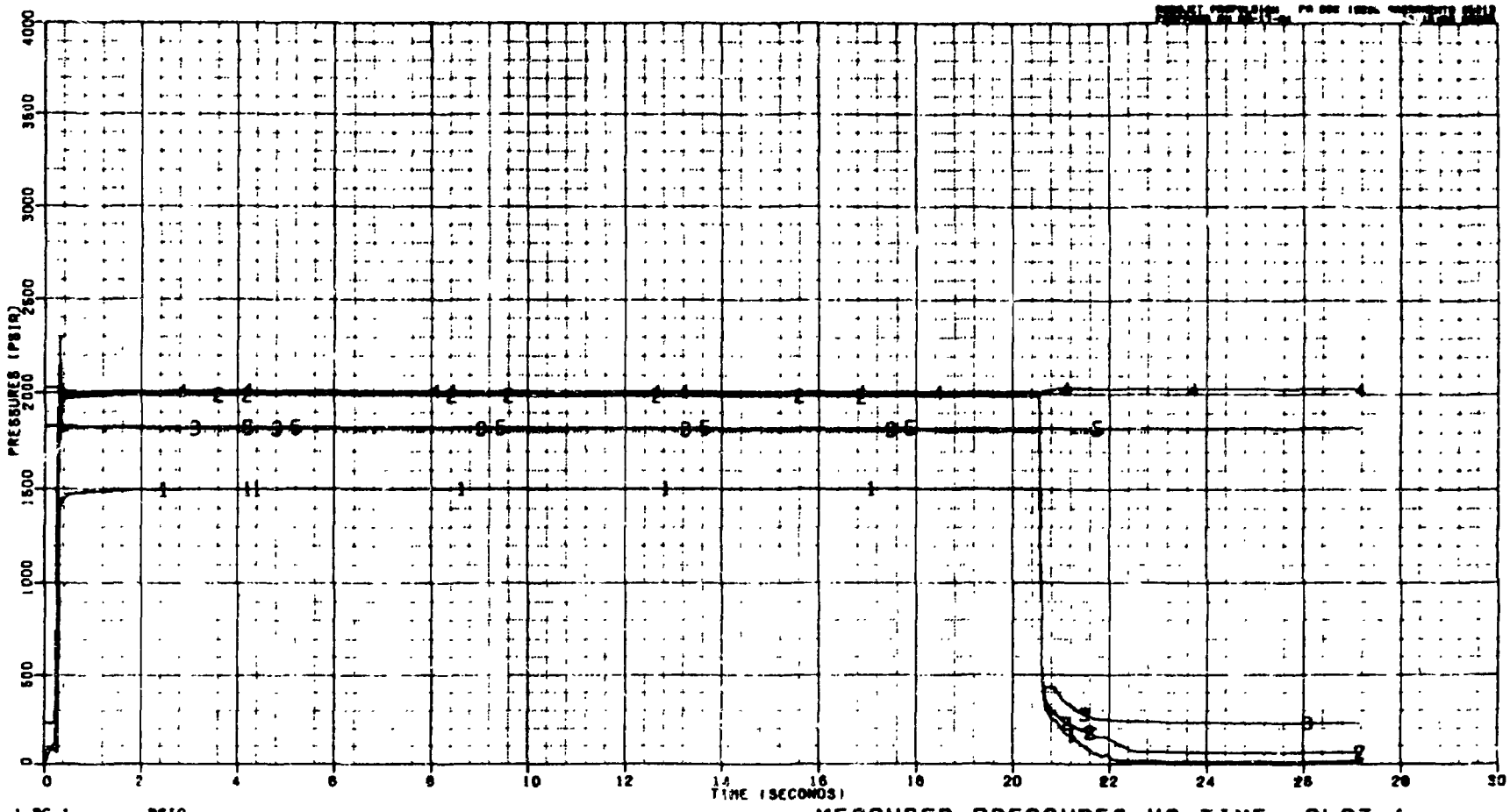

MEASURED PRESSURES VS TIME PLOT 1
TEST NO. KEE4-D01-OA-117

TEST DATE 05-08-91 1658 HOURS 20.425 SEC.DUR

GENCORP
AEROJET

Figure C - 63

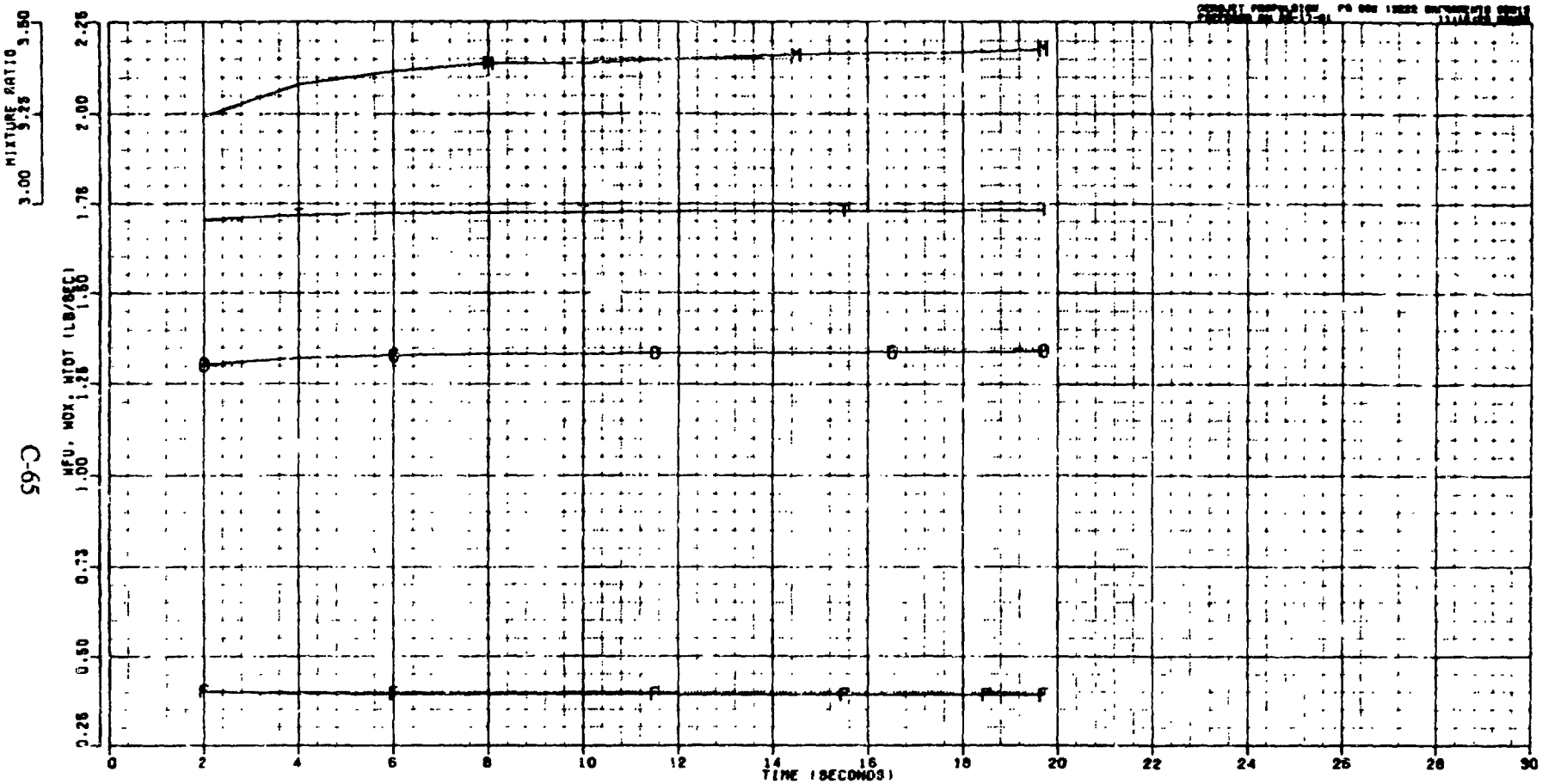

INJECTOR FLOW VS TIME PLOT 2
TEST NO. KEE4-D01-DR-117

TEST DATE 05-08-91 1658 HOURS 20.425 SEC.DUR

GENCORP
AEROJET

Figure C - 64

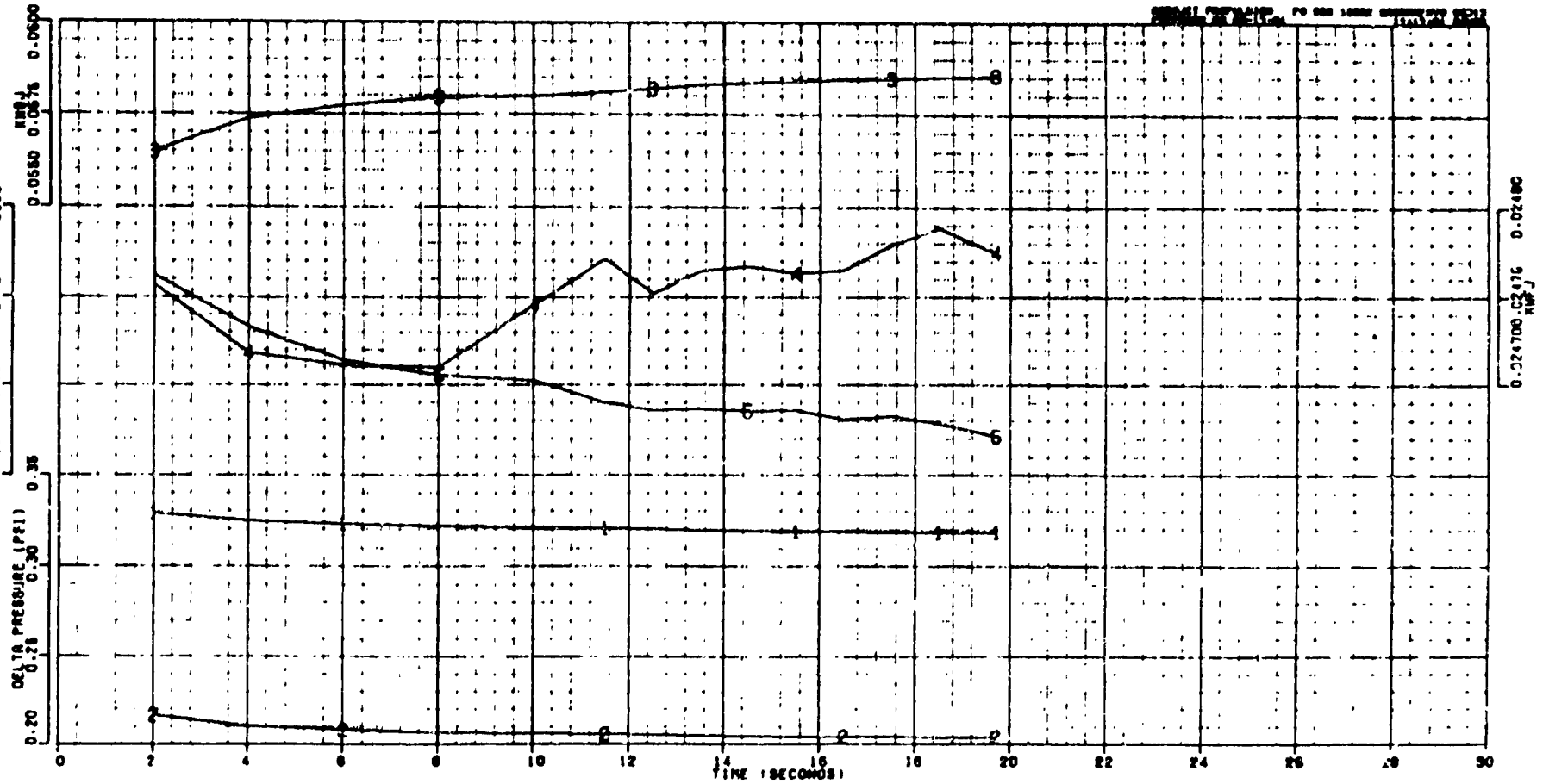

GenCorp
AEROJET

Figure C - 65

ORIGINAL PAGE IS
OF POOR QUALITY

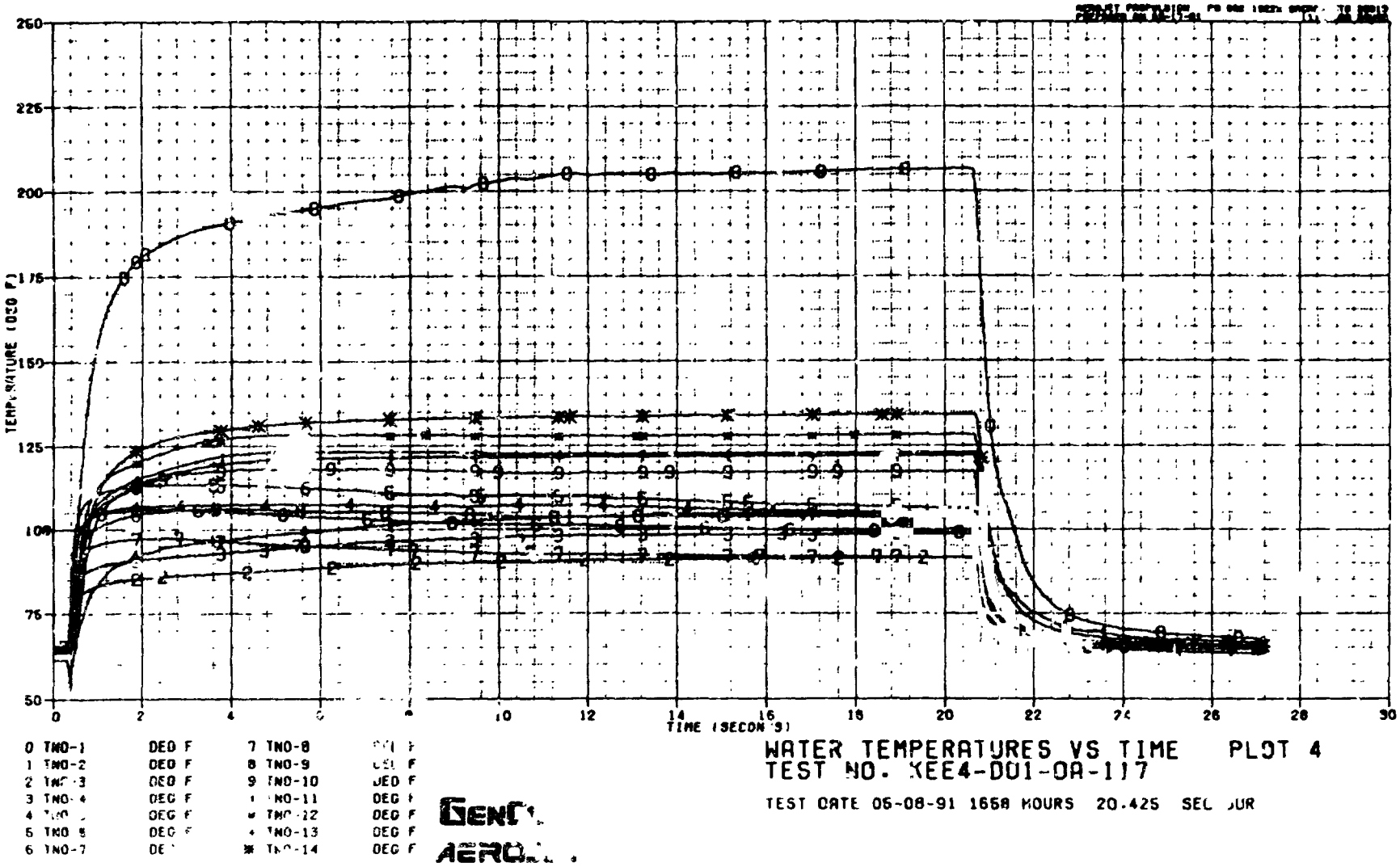
TEMPERATURE (DEG F)
TIME (SECONDS)
0 TNO-1 DEG F
1 TNO-2 DEG F
2 TNO-3 DEG F
3 TNO-4 DEG F
4 TNO-5 DEG F
5 TNO-6 DEG F
6 TNO-7 DEG F
7 TNO-8
8 TNO-9
9 TNO-10 DEG F
TNO-11 DEG F
TNO-12 DEG F
TNO-13 DEG F
TNO-14 DEG F
WATER TEMPERATURES VS TIME PLOT 4
TEST NO. XEE4-D01-OA-117
TEST DATE 05-08-91 1658 HOURS 20.425 SEC DUR

Figure C-67

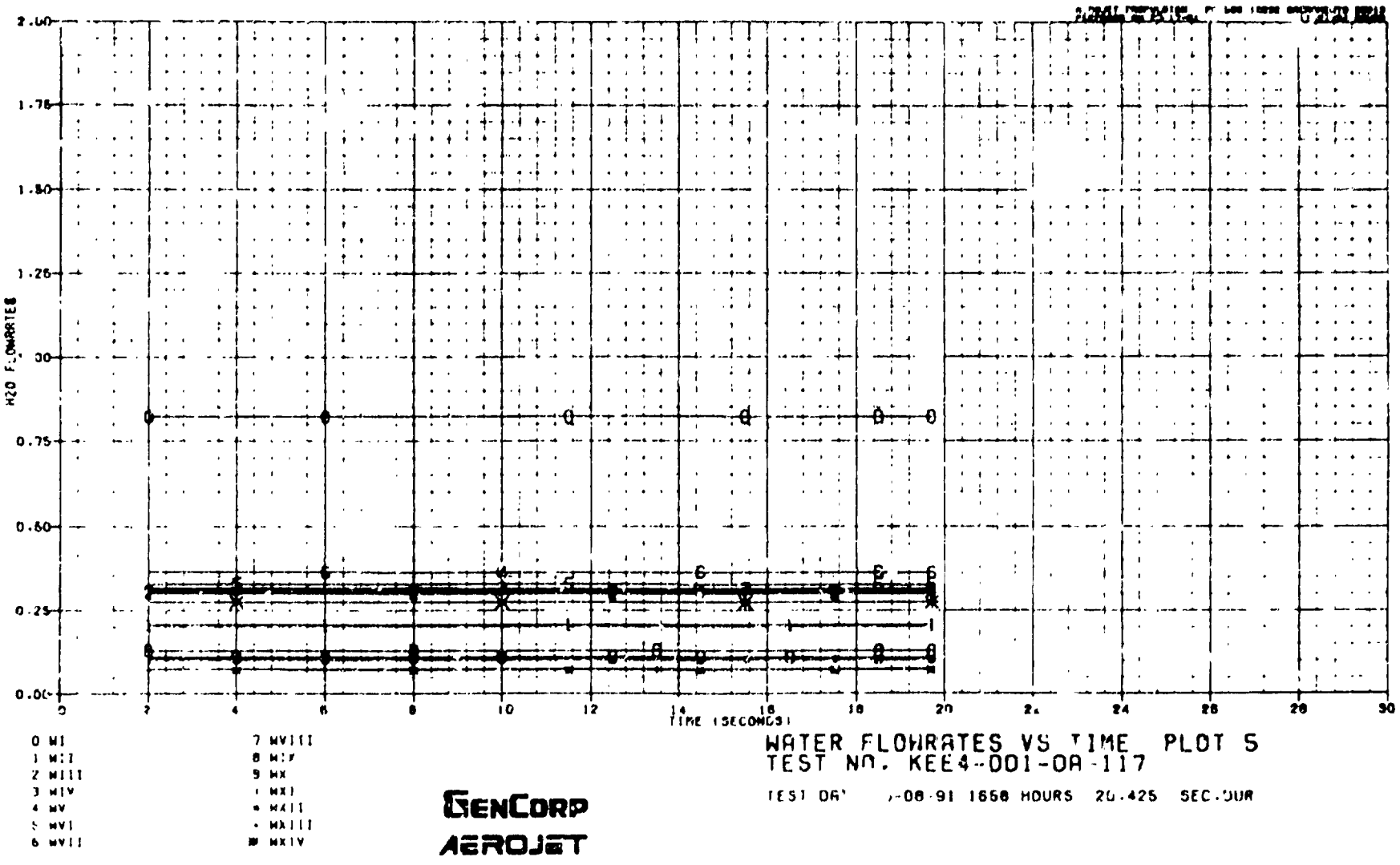
H2O FLOWRATES
TIME (SECONDS)
0 WI
1 WII
2 WIII
3 WIV
4 WV
5 WVI
6 WVII
7 WVIII
8 WIX
9 WX
WXI
WXII
WXIII
WXIV
WATER FLOWRATES VS TIME PLOT 5
TEST NO. KEE4-001-OA-117
TEST DA' -08-91 1658 HOURS 20.425 SEC.DUR
GENCORP
AEROJET

Figure C - 67

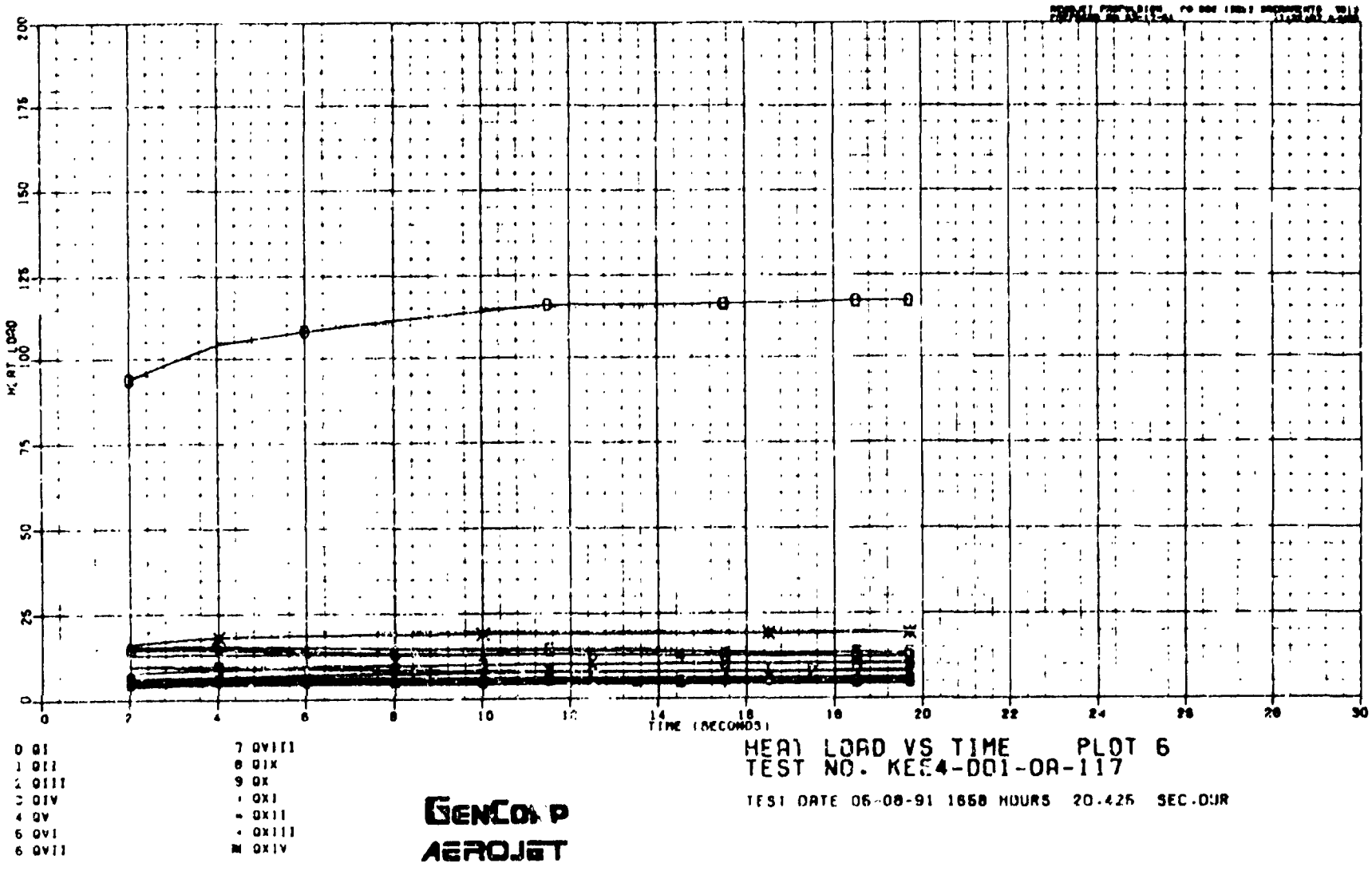
HEAT LOAD
TIME (SECONDS)
0 QI
1 QII
2 QIII
3 QIV
4 QV
5 QVI
6 QVII
7 QVIII
8 QIX
9 QX
QXI
QXII
QXIII
QXIV
GENCORP
AEROJET
HEAT LOAD VS TIME PLOT 6
TEST NO. KES4-D01-OR-117
TEST DATE 06-08-91 1658 HOURS 20.425 SEC.DUR

Figure C - 68

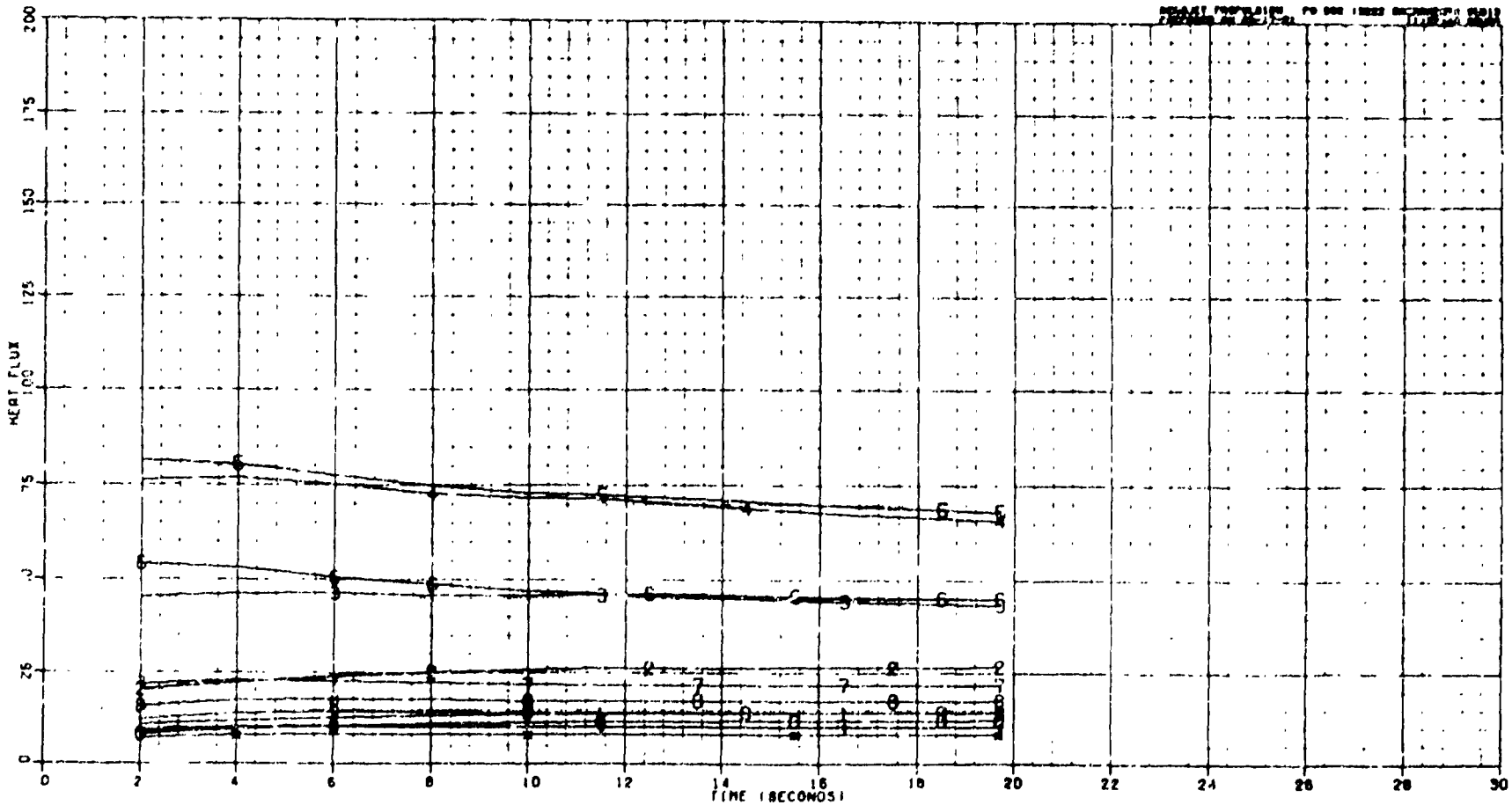

GENCORP
AEROJET

Figure C - 69

ORIGINAL PAGE IS
OF POOR QUALITY

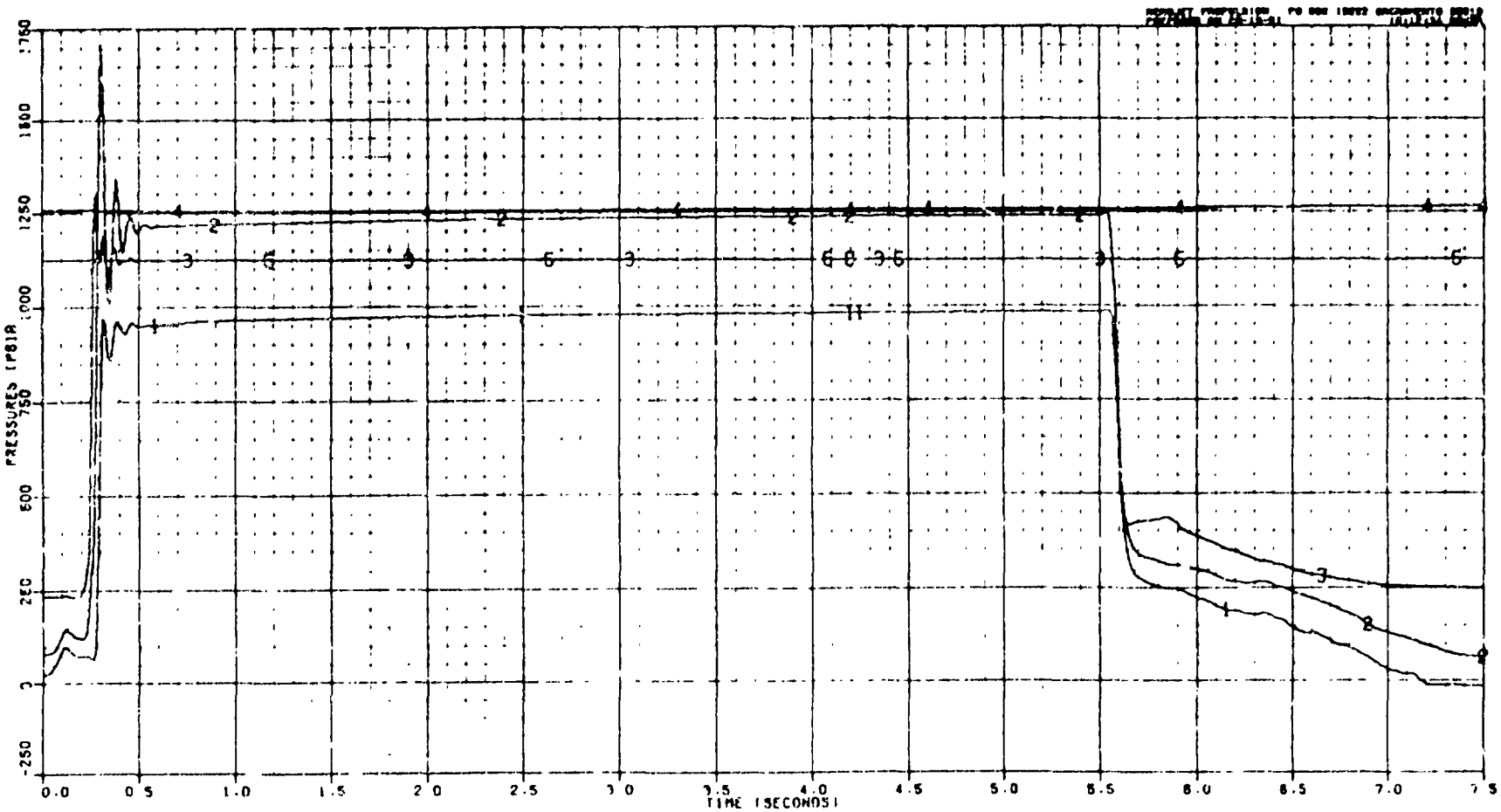

MEASURED PRESSURES VS TIME PLOT 1
TEST NO. KEE4-DDI-DR-119

TEST DATE 06-12-91 1636 HOURS 5.424 SEC.DUR

GENCORP AEROJET

Figure C - 70

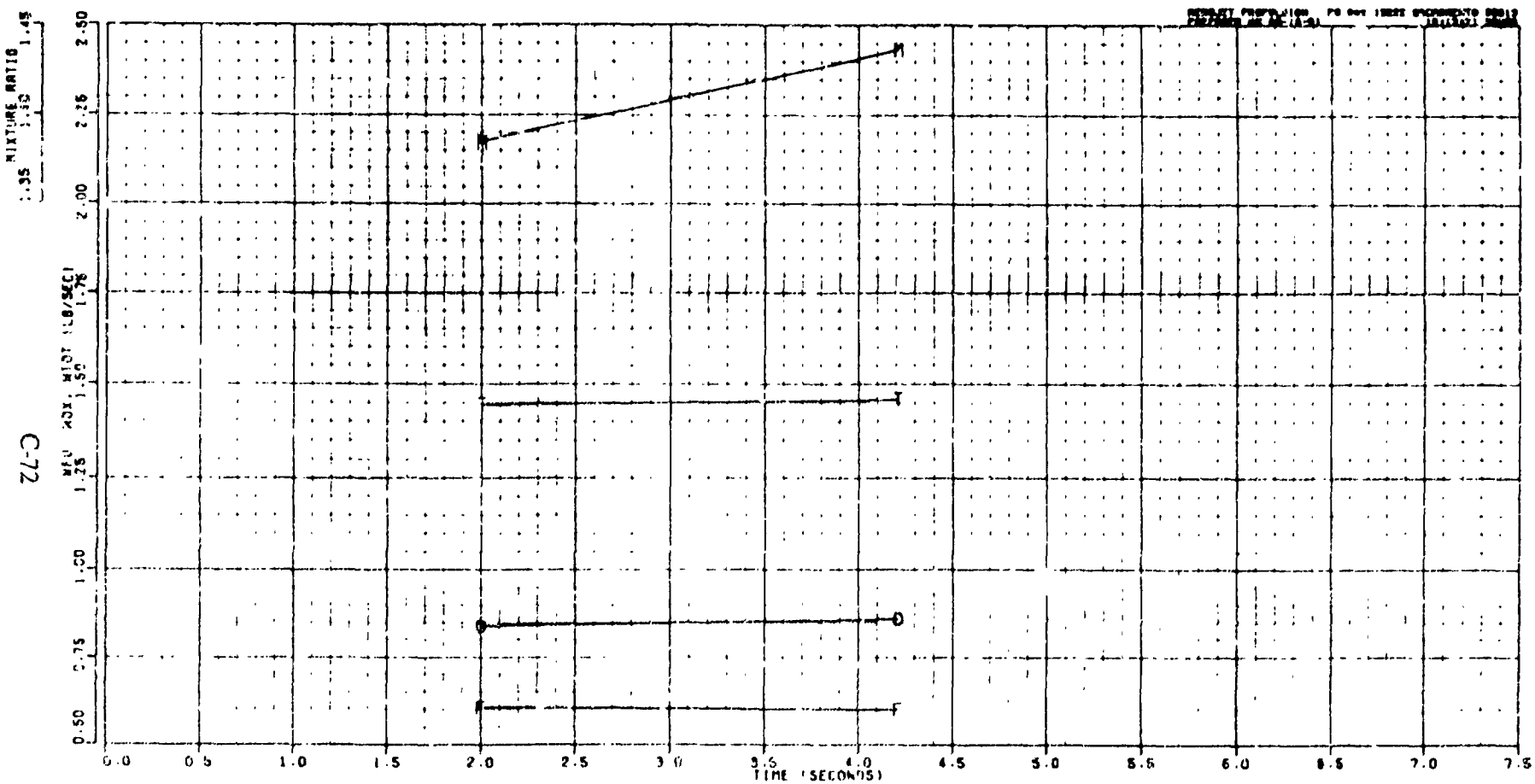

INJECTOR FLOW VS TIME PLOT 2
TEST NO. KEE4-D01-DA-119

TEST DATE 06-12-91 1636 HOURS 5.424 SEC.DUR

GENCORP
AEROJET

Figure C - 71

ORIGINAL PAGE IS
OF POOR QUALITY

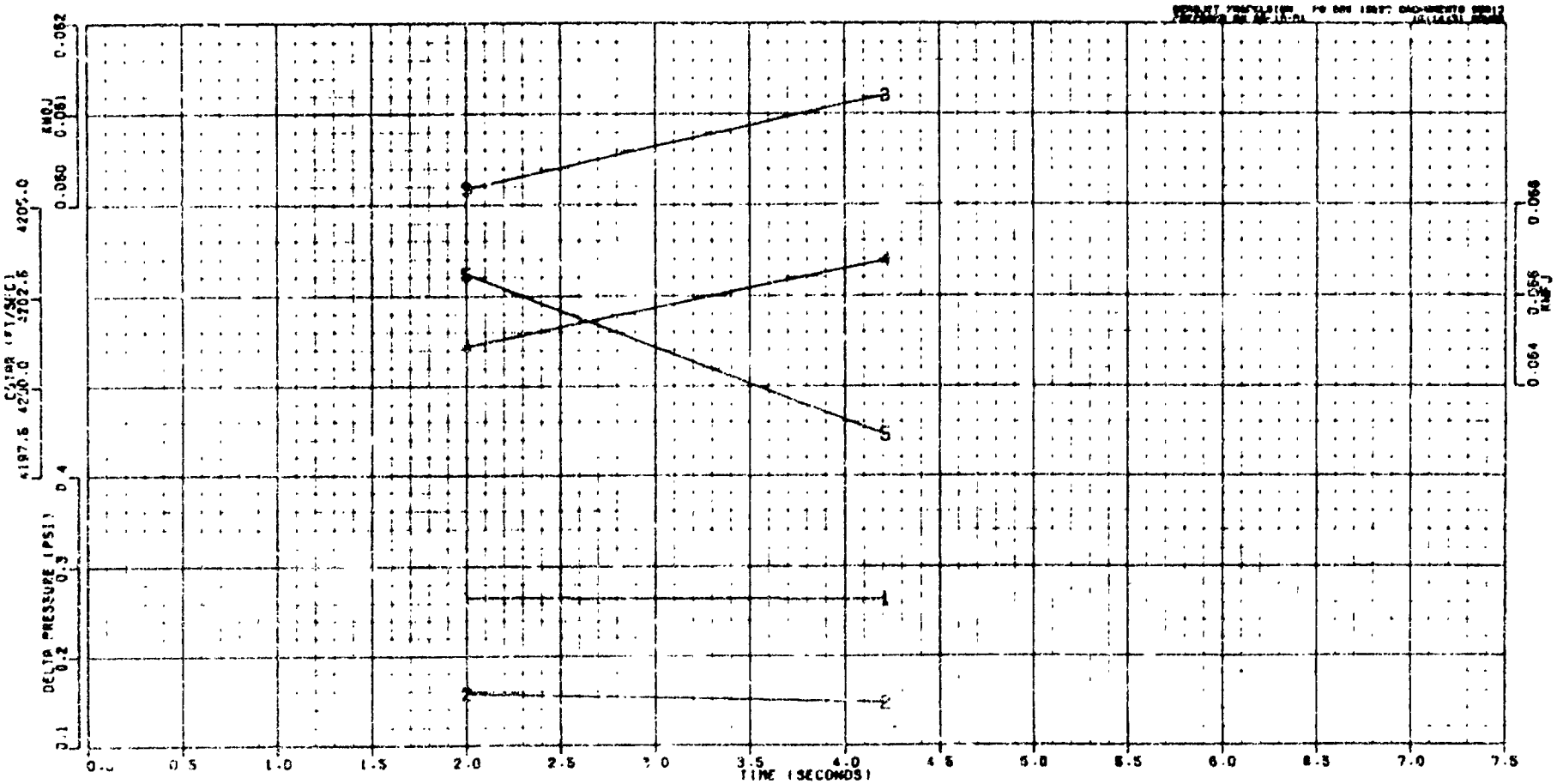

INJECTOR CALCULATIONS VS TIME PLOT 3
TEST NO. KEE4-D01-OR-119

TEST DATE 06-12-91 1636 HOURS 5.424 SEC.DUR

GenCorp Aerojet

Figure C - 72

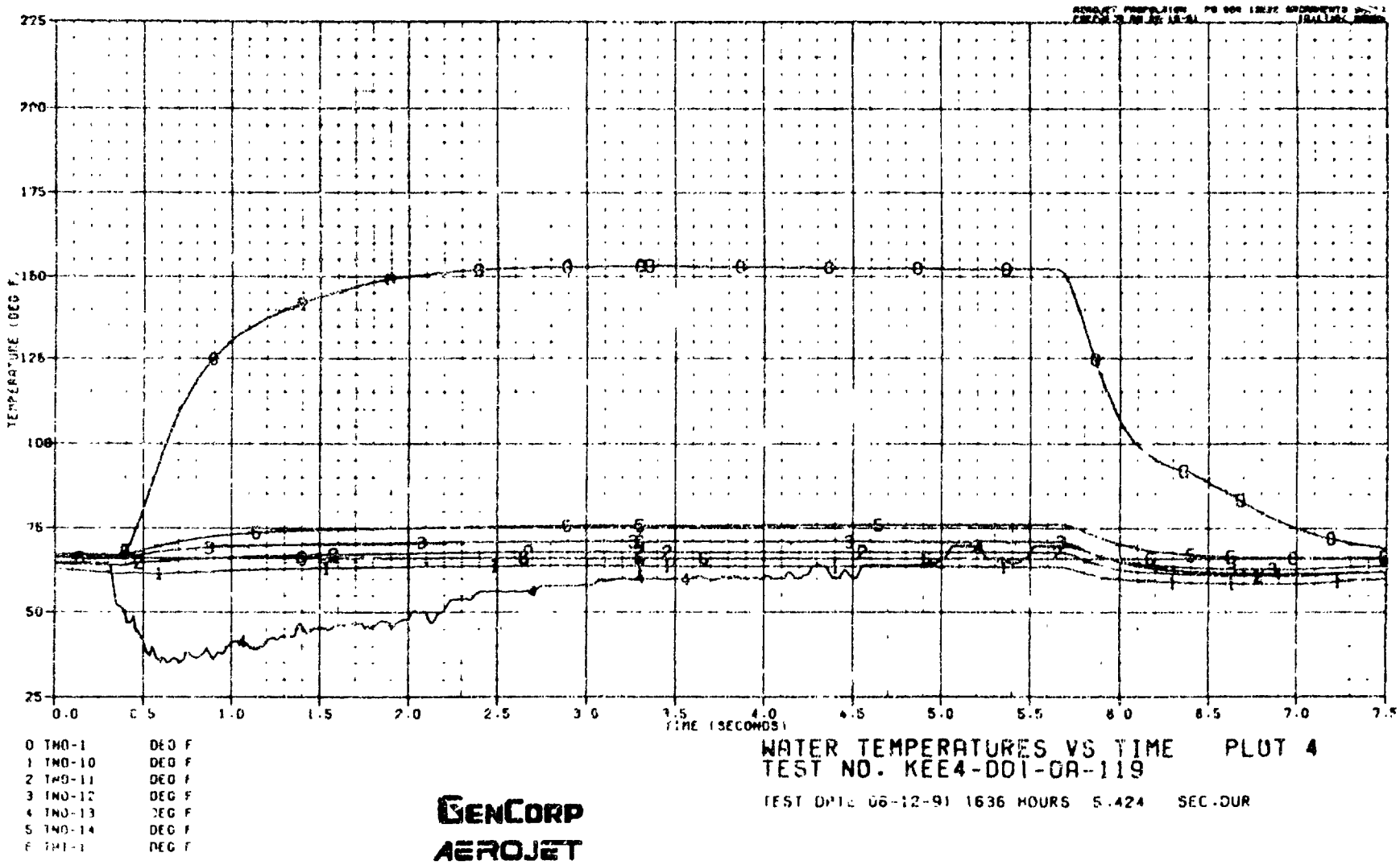

Figure C - 73

ORIGINAL PAGE IS
OF POOR QUALITY

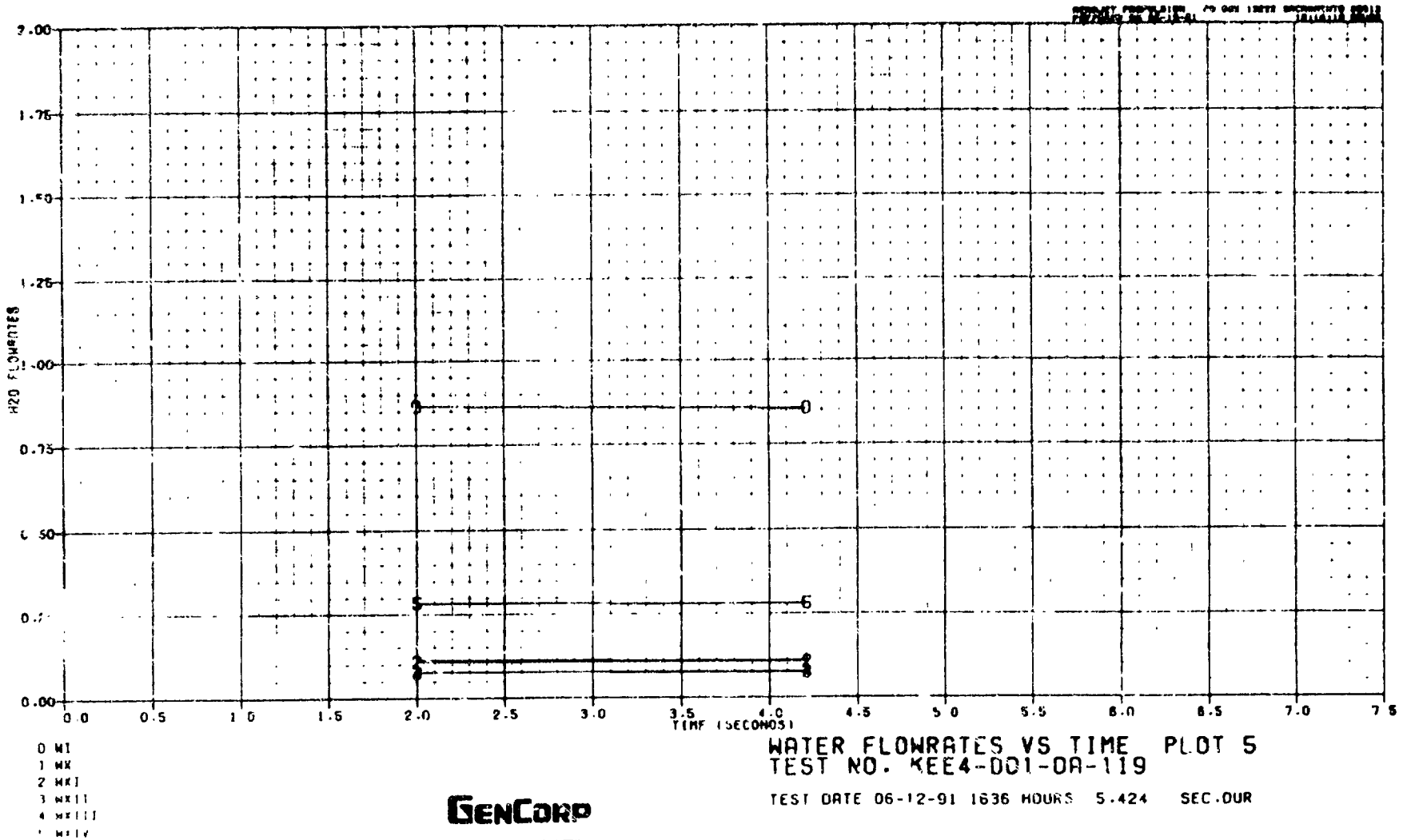

GENCORP
AEROJET

Figure C - 74

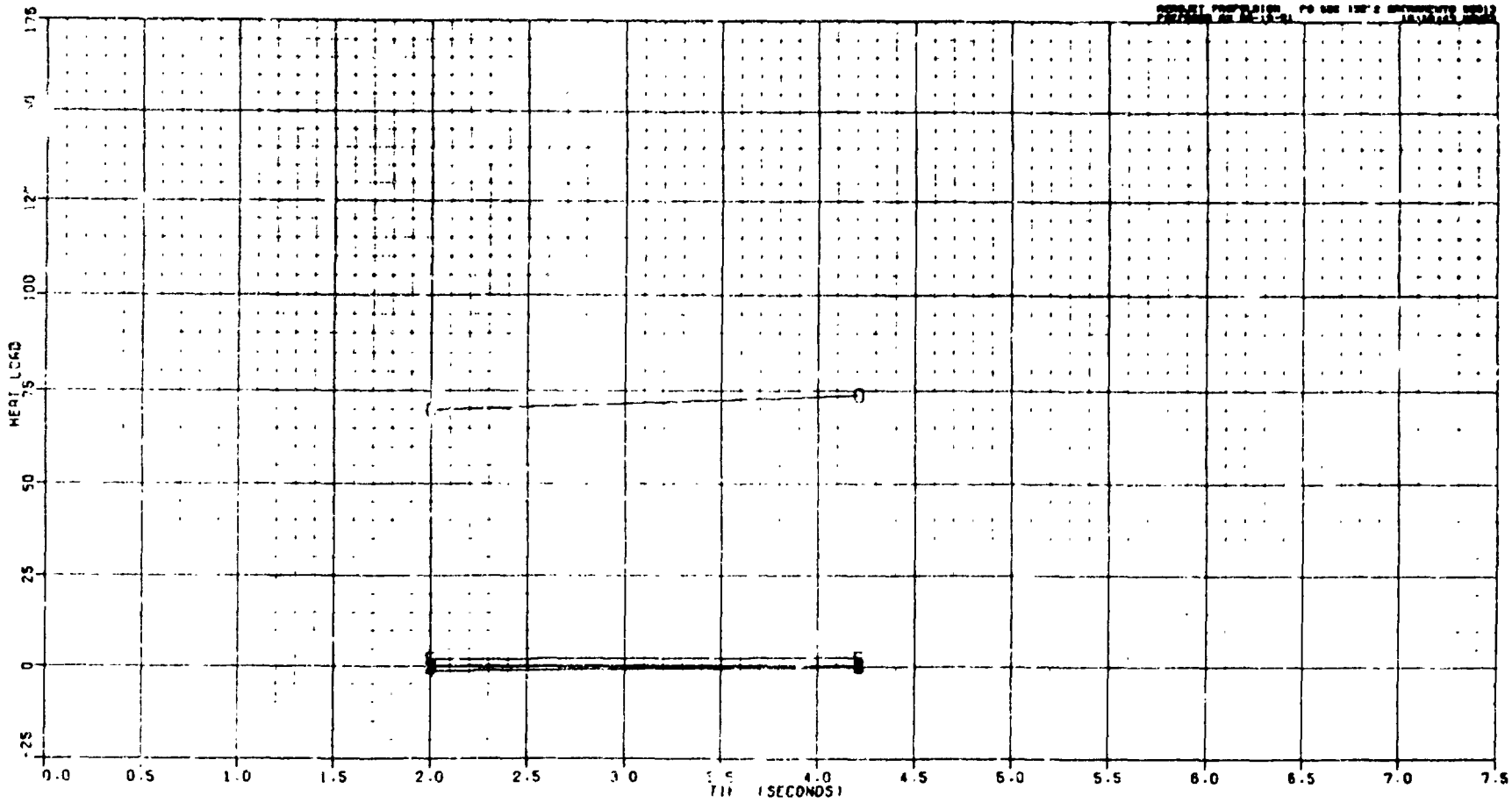

HEAT LOAD VS TIME PLOT 6
TEST NO. KEE4-001-OR-119

TEST DATE 06-12-91 1636 HOURS 5.424 SEC.DUR

GENCORP
AEROJET

Figure C - 75

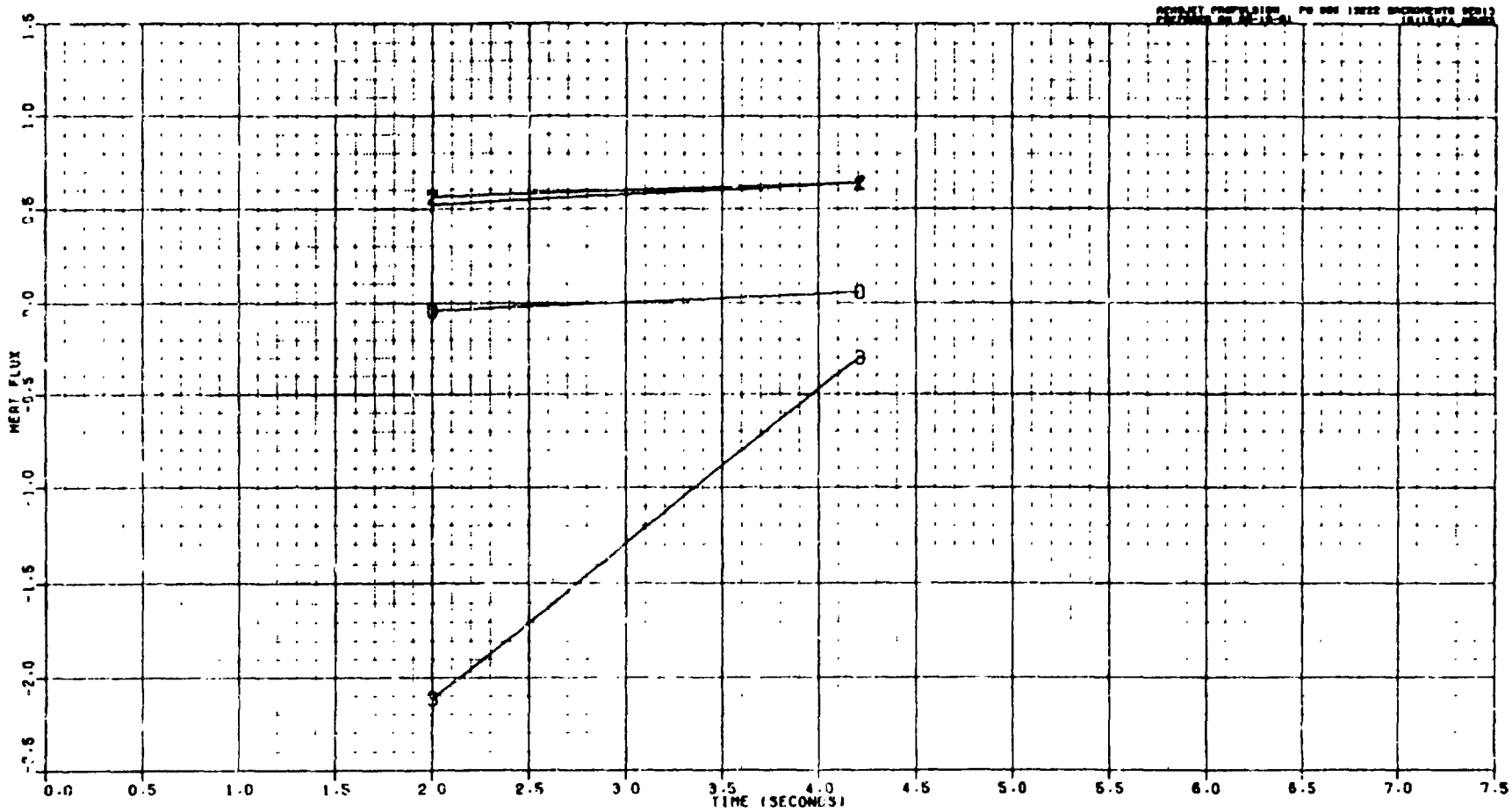

HEAT FLUX VS TIME PLOT 7
TEST NO. KEE4-DDI-DA 119

TEST DATE 06-12-91 1636 HOURS 5.424 SEC.DUR

GenCorp
AEROJET

Figure C - 76

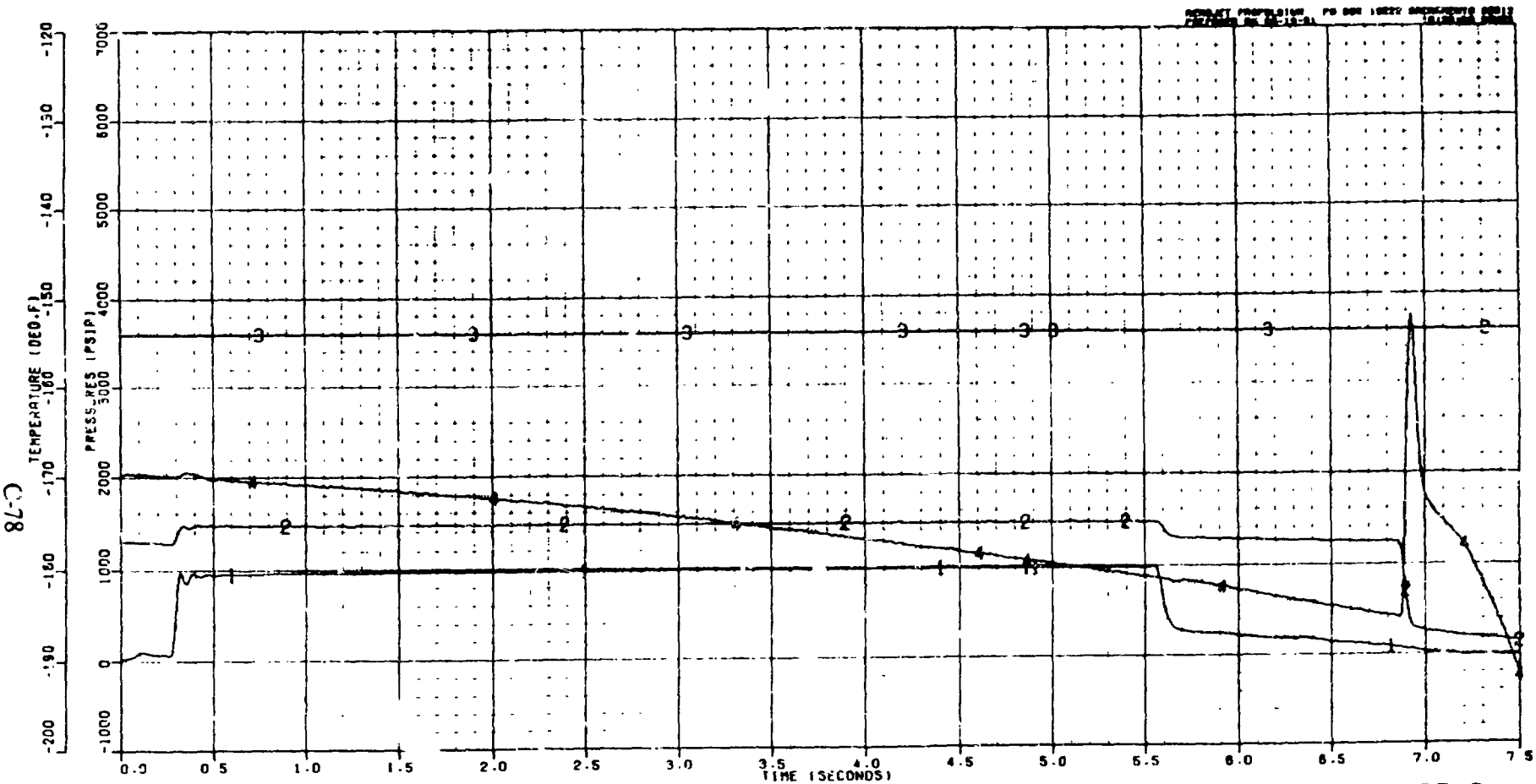

MEASURED PRESS & TEMP VS TIME PLOT B
TEST NO. KEE4-001-OA-119

TEST DATE 06-12-91 1636 HOURS 5.424 SEC.DUR

GENCORP
AEROJET

Figure C - 77

ORIGINAL PAGE IS
OF POOR QUALITY

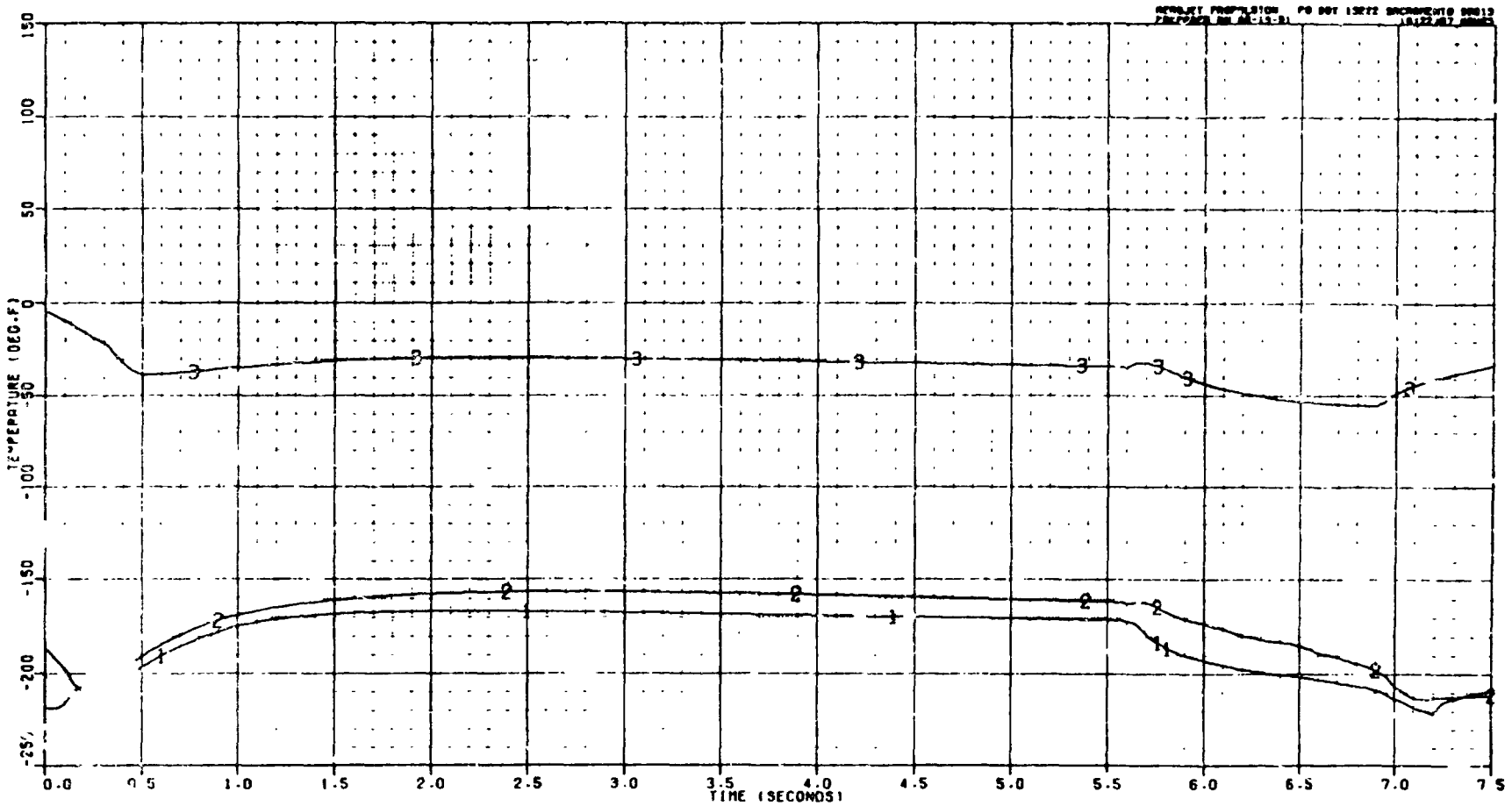

1 TNC10C DEG F
2 TNC1[illegible] DEG F
3 TNC130 DEG F

MEASURED TEMP VS TIME PLOT 9
TEST NO. KEE4-D01-DA-119

TEST DATE 06-12-91 1636 HOURS 5.424 SEC.DUR

GENCORP
AEROJET

Figure C - 78

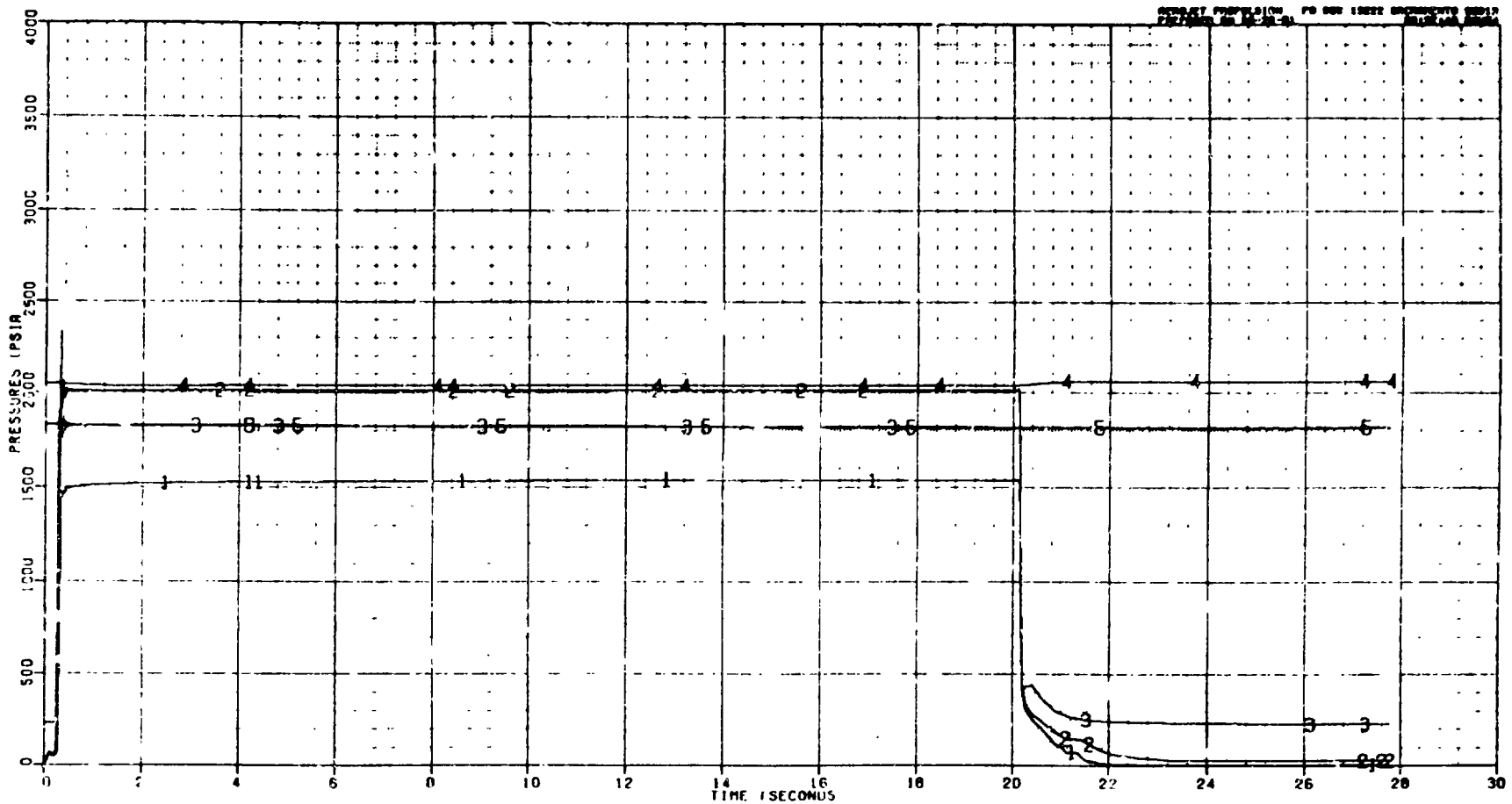

MEASURED PRESSURES VS TIME PLOT 1
TEST NO. KEE4-D01-DA-124
TEST DATE 06-13-91 1453 HOURS 19.994 SEC.DUR

GENCORP
AEROJET

Figure C - 79

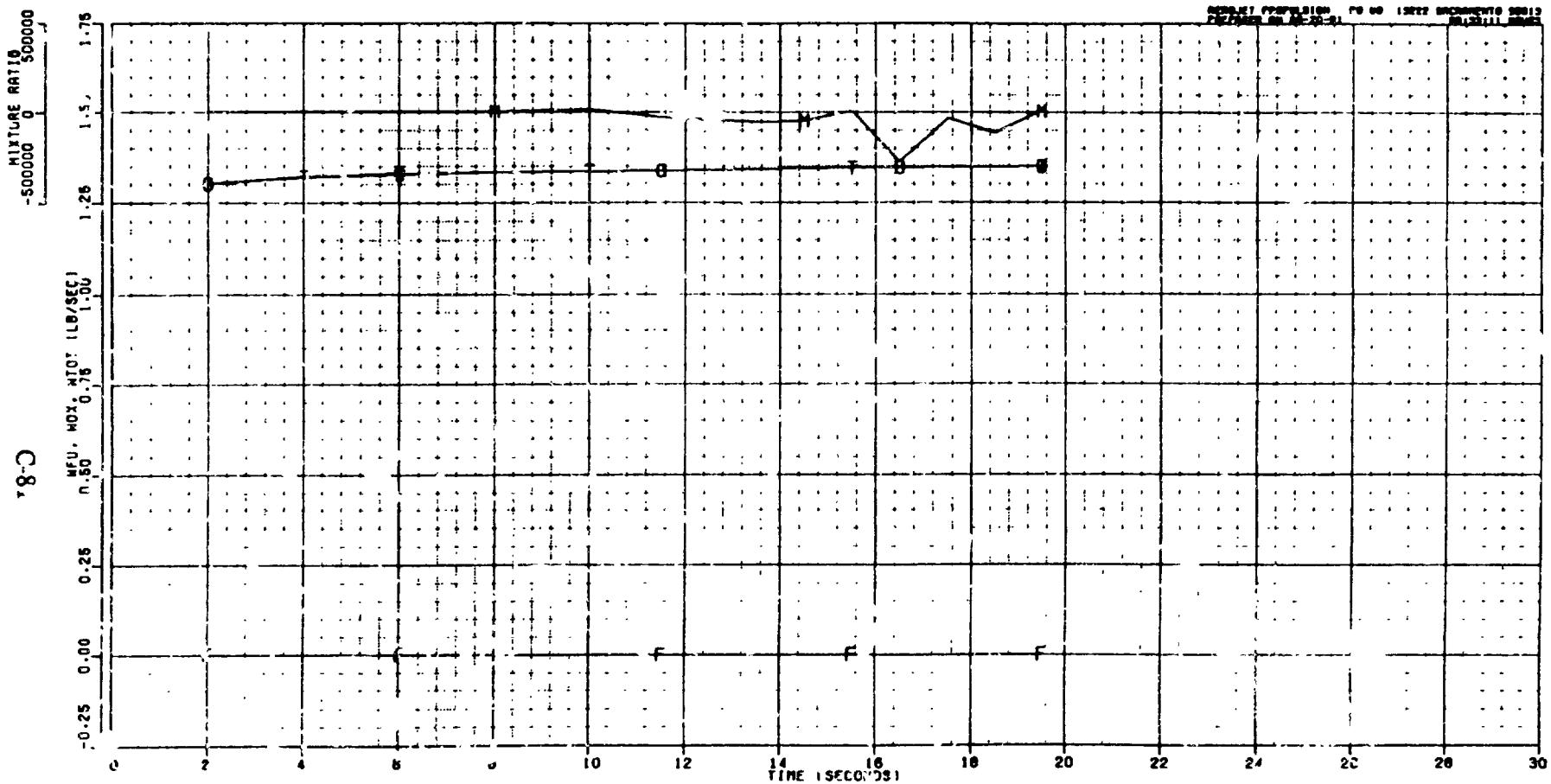

INJECTOR FLOW VS TIME PLOT 2
TEST NO. KEE4-DD1-DA-124

TEST DATE 06-13-91 1453 HOURS 19.994 SEC.DUR

GenCorp
AEROJET

Figure C - 80

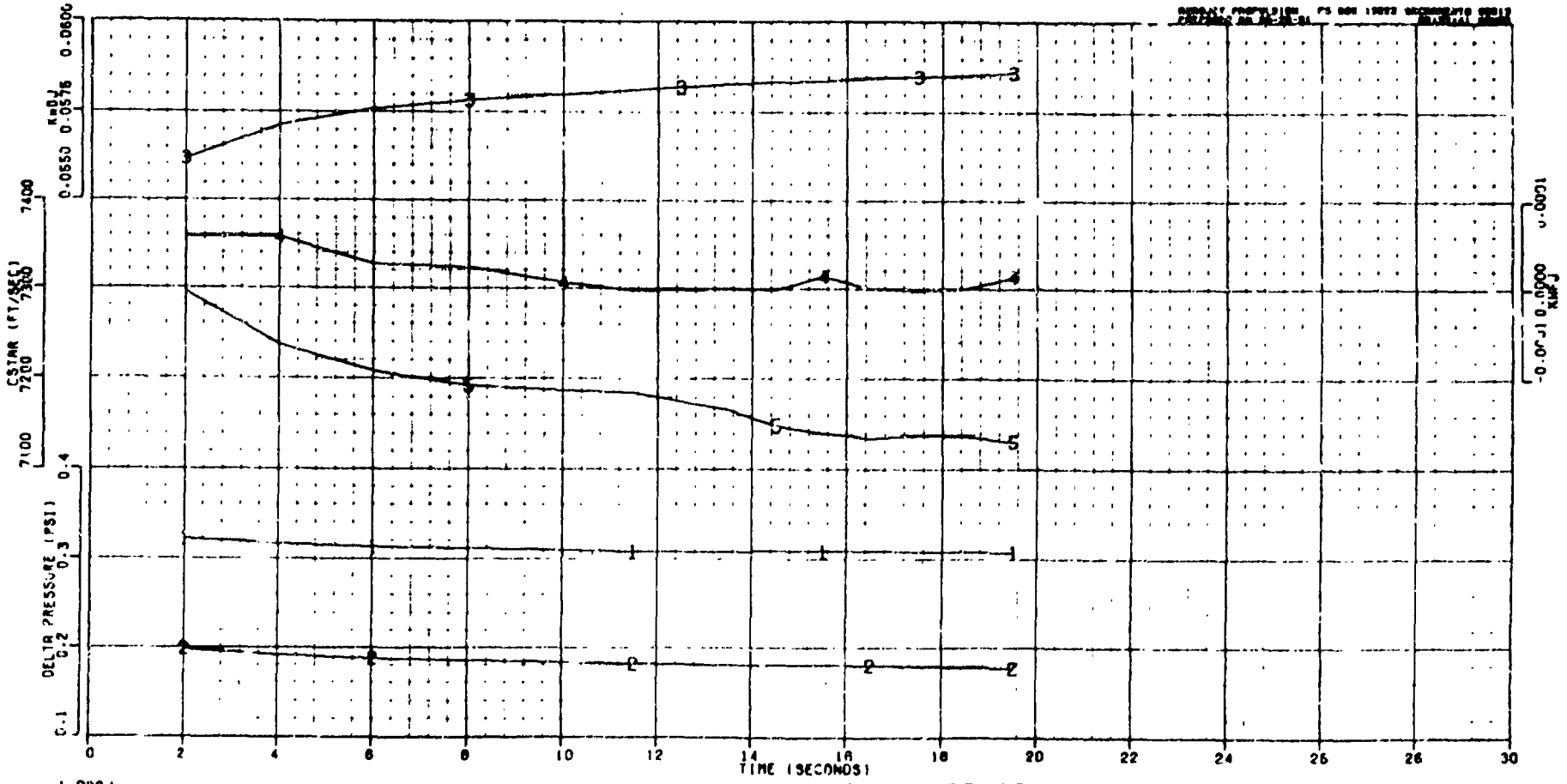

INJECTOR CALCULATIONS VS TIME PLOT 3
TEST NO. KEF4-D01-DA-124

TEST DATE 06-13-91 1453 HOURS 19.994 SEC.DUR

GENCORP
AEROJET

Figure C - 81

C-3

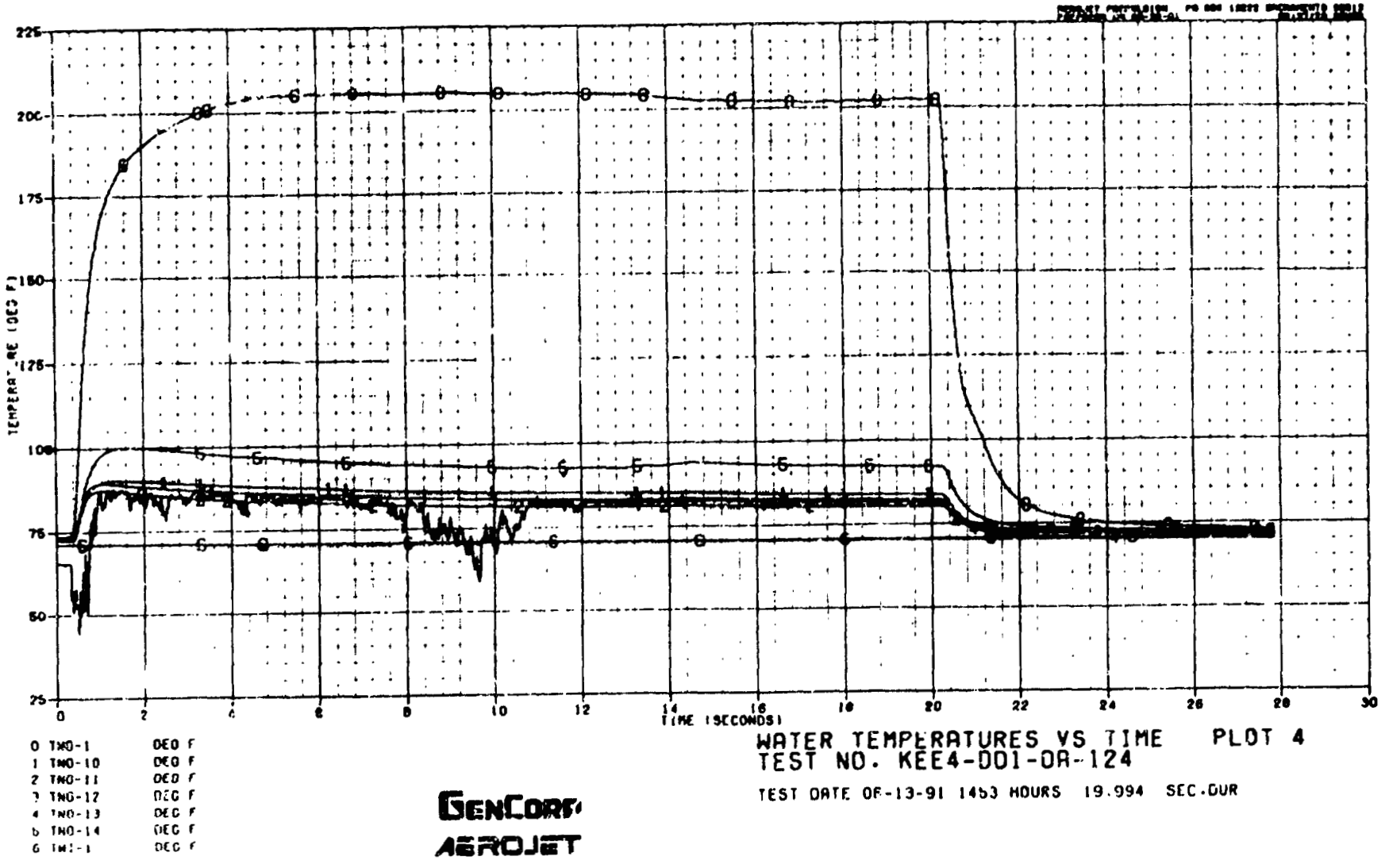
TEMPERATURE (DEG F)
225
200
175
150
125
100
75
50
25
0
2
4
6
8
10
12
14
16
18
20
22
24
26
28
30
TIME (SECONDS)
0 TWO-1 DEG F
1 TWO-10 DEG F
2 TWO-11 DEG F
3 TWO-12 DEG F
4 TWO-13 DEG F
5 TWO-14 DEG F
6 TWI-1 DEG F
WATER TEMPERATURES VS TIME PLOT 4
TEST NO. KEE4-DD1-DR-124
TEST DATE 06-13-91 1453 HOURS 19.994 SEC.DUR
GENCORP
AEROJET

Figure C - 82

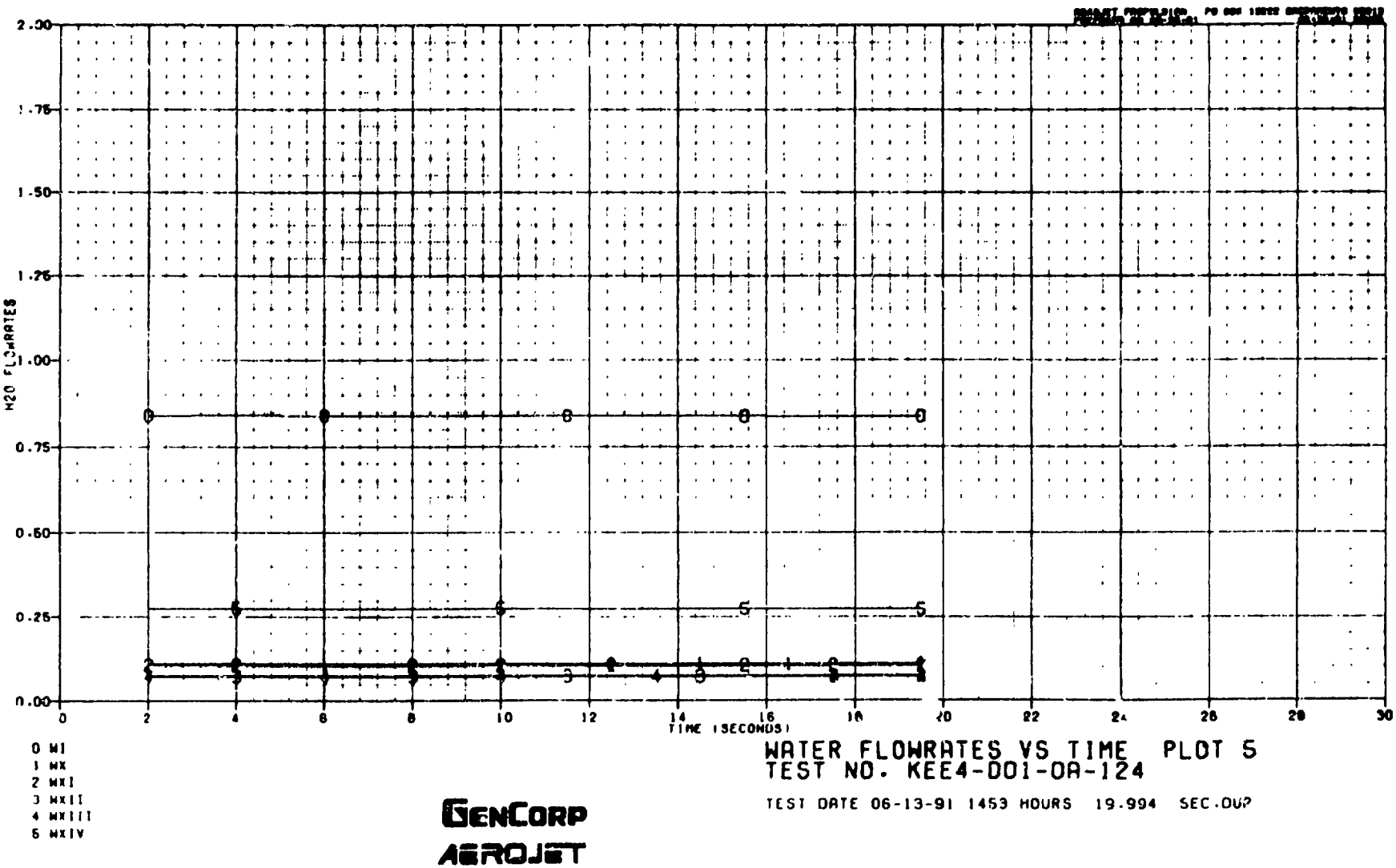
H2O FLOWRATES
2.00
1.75
1.50
1.25
1.00
0.75
0.50
0.25
0.00
0
2
4
6
8
10
12
14
16
18
20
22
24
26
28
30
TIME (SECONDS)
0 WI
1 WX
2 WXI
3 WXII
4 WXIII
5 WXIV
WATER FLOWRATES VS TIME PLOT 5
TEST NO. KEE4-D01-OA-124
TEST DATE 06-13-91 1453 HOURS 19.994 SEC.DUP
GENCORP
AEROJET

Figure C - 83

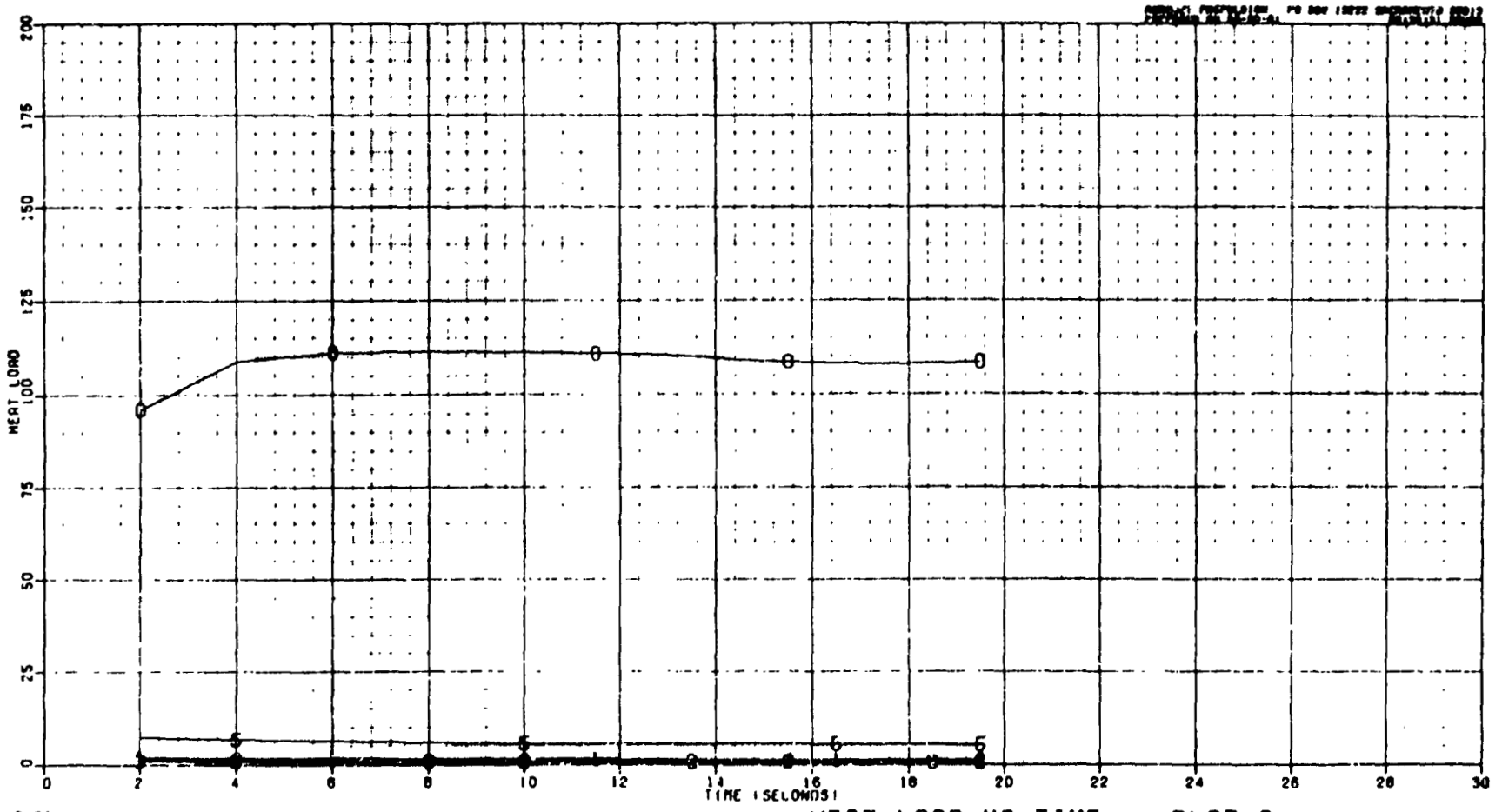

GENCORP
AEROJET

Figure C - 84

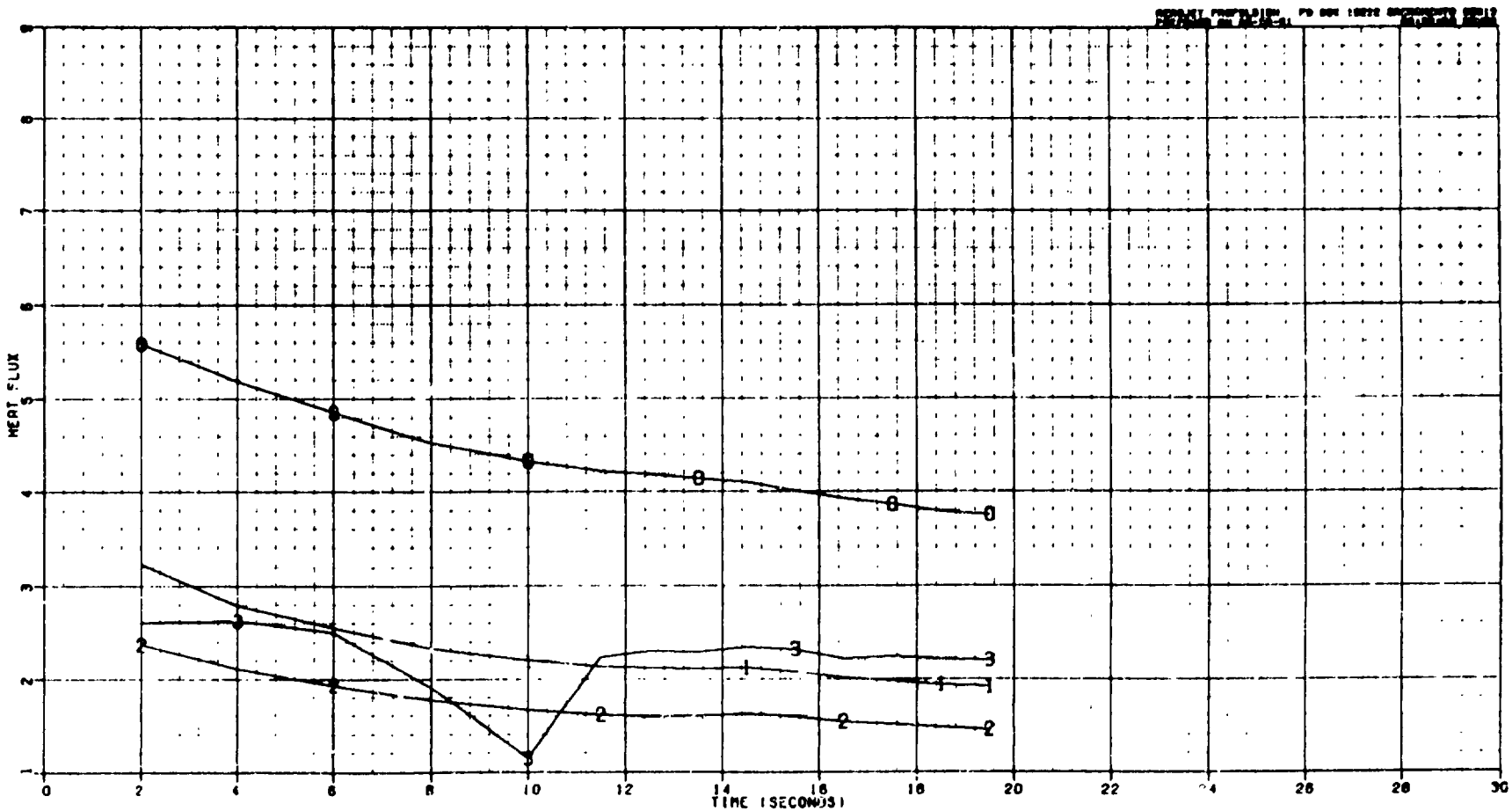

HEAT FLUX VS TIME PLOT 7
TEST NO. KEE4-DOI-DA-124

TEST DATE 06-13-91 1453 HOURS 19.994 SEC.DUR

GENCORP
AEROJET

Figure C - 85

ORIGINAL PAGE IS
OF POOR QUALITY

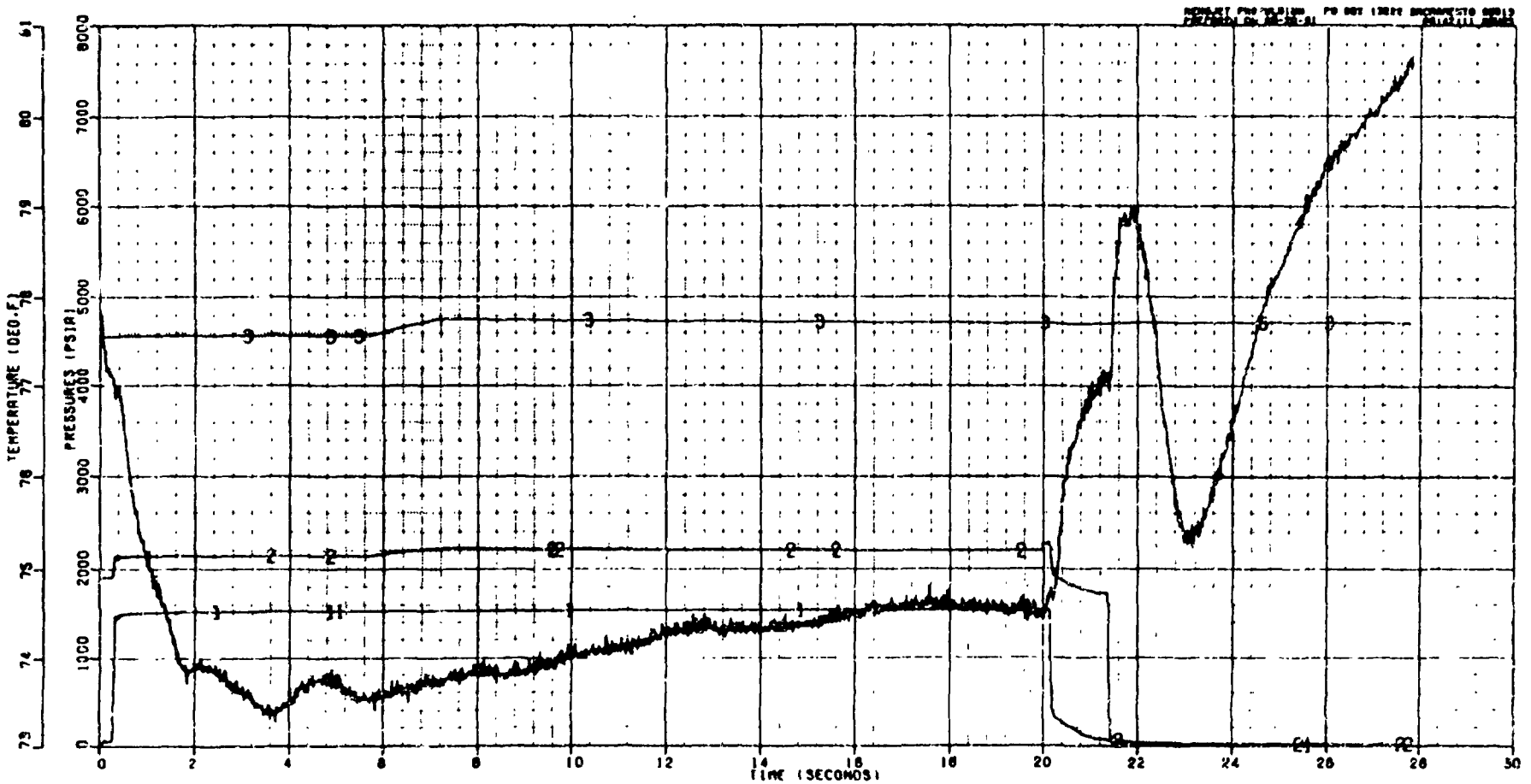

MEASURED PRESS & TEMP VS TIME PLOT 8
TEST NO. KEE4-D01-DA-124

TEST DATE 06-13-91 1453 HOURS 19.994 SEC.DUR

GENCORP AEROJET

Figure C - 86

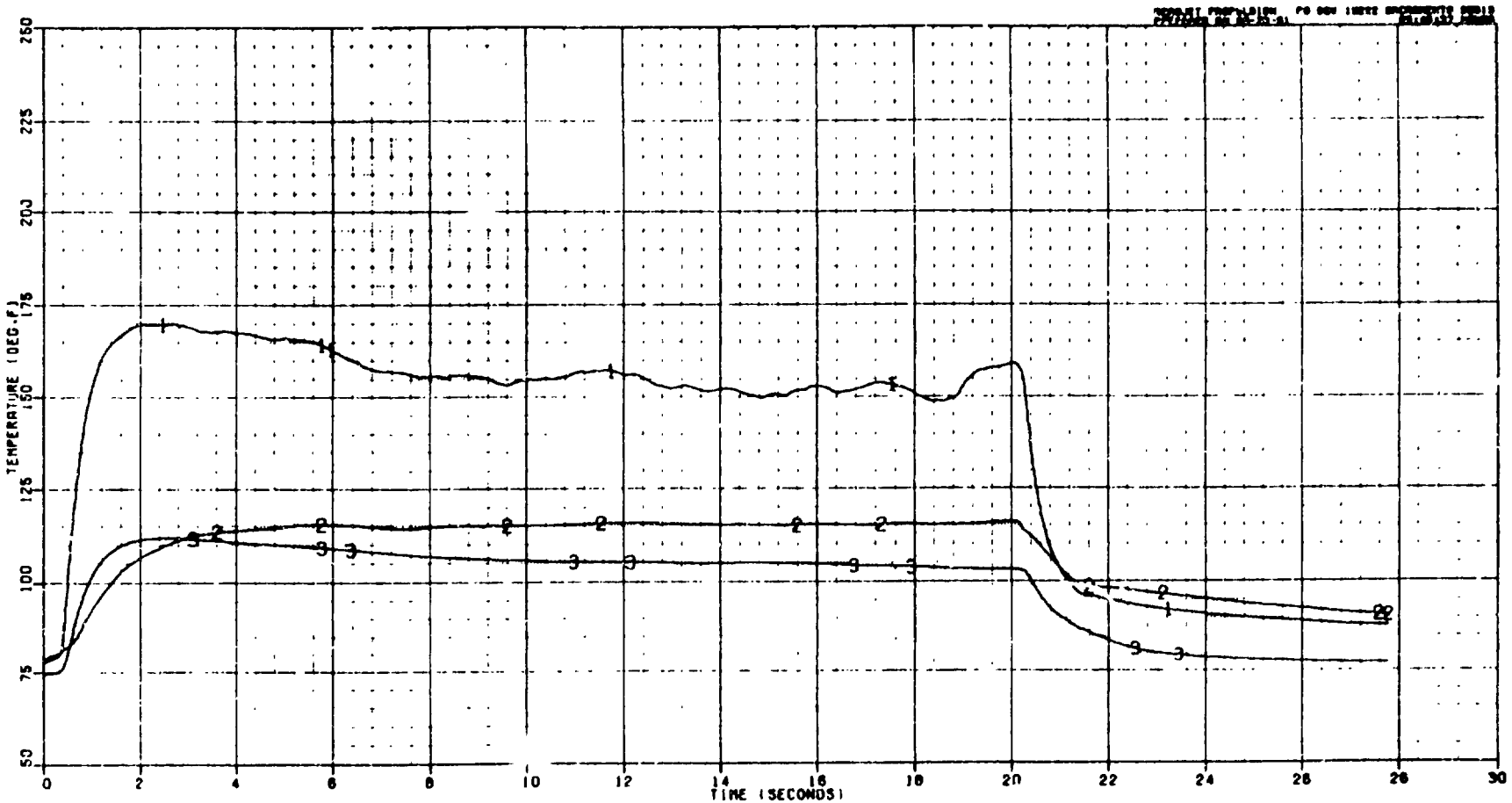

MEASURED TEMP VS TIME PLOT 9
TEST NO. KEE4-D01-DA-124

TEST DATE 06-13-91 1453 HOURS 13.994 SEC.DUR

GENCORP
AEROJET

Figure C - 87

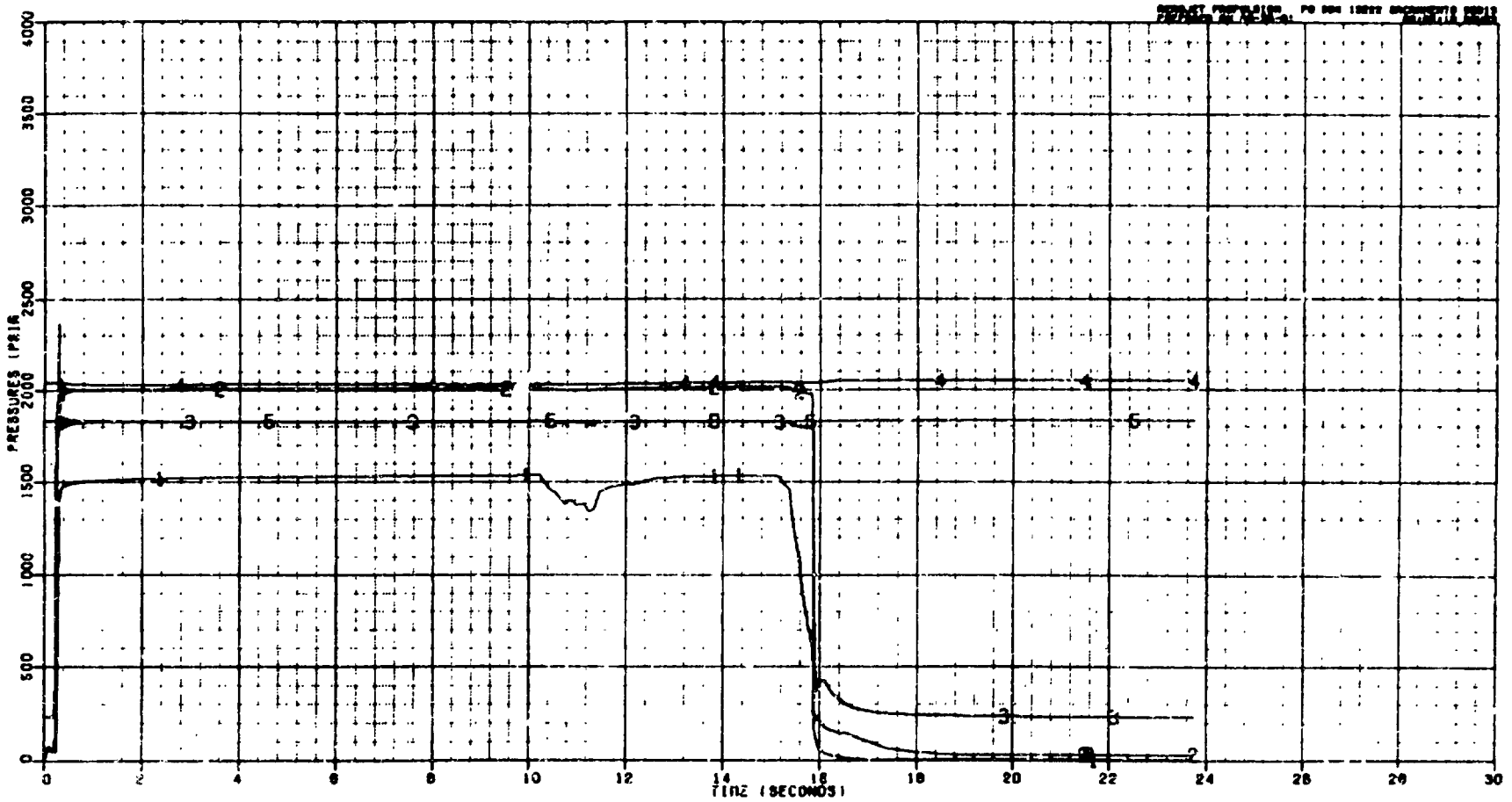

MEASURED PRESSURES VS TIME PLOT 1
TEST NO. KEE4-001-OA-125

TEST DATE 03-13-91 1603 HOURS 15.710 SEC.DUR

GENCORP AEROJET

Figure C - 88

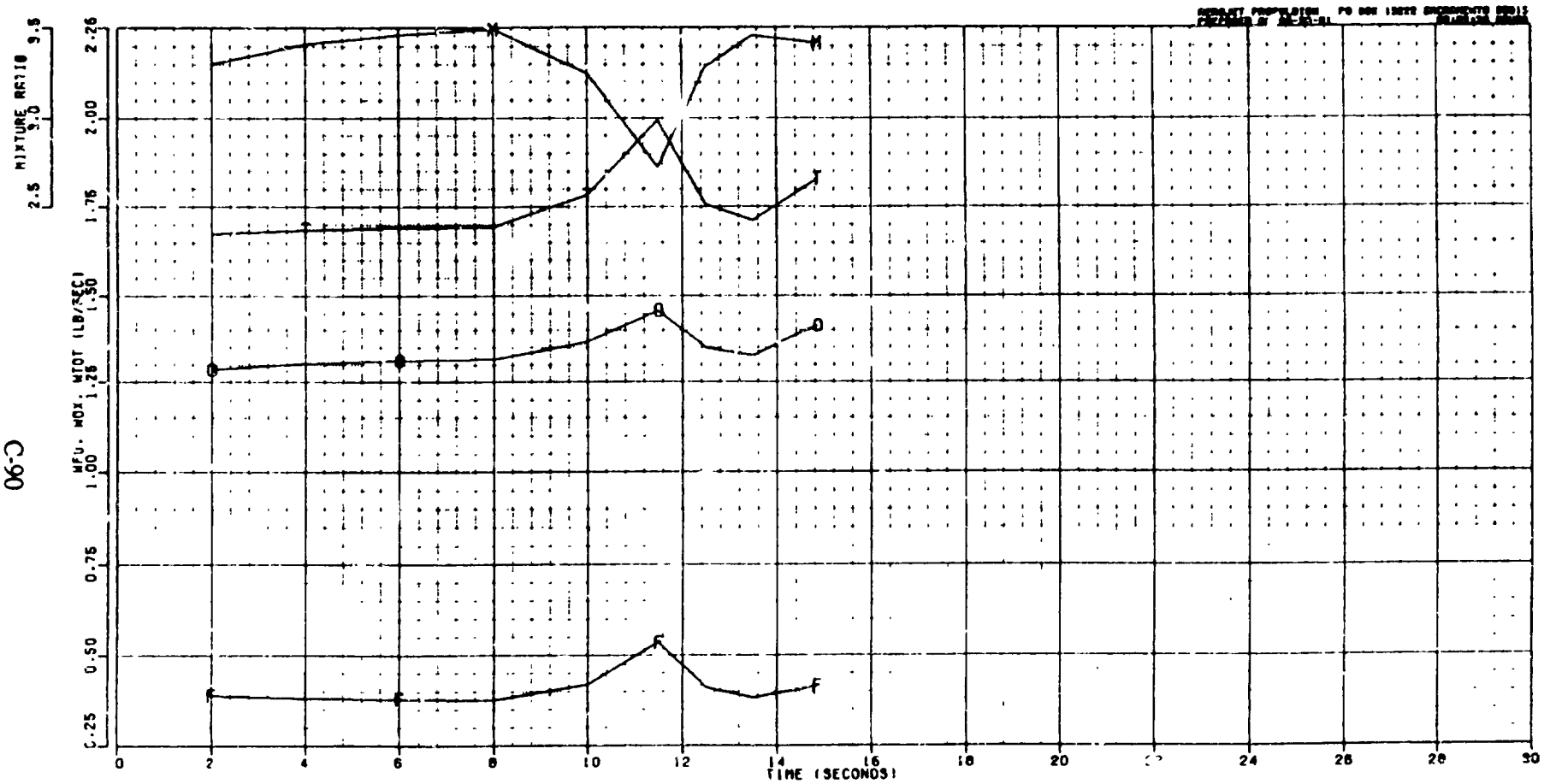

INJECTOR FLOW Vs TIME PLOT 2
TEST NO. KEE4-DU1-DA-125

TEST DATE 06-13-91 16^3 HOURS 15.710 SEC.DUR

GENCORP
AEROJET

Figure C - 89

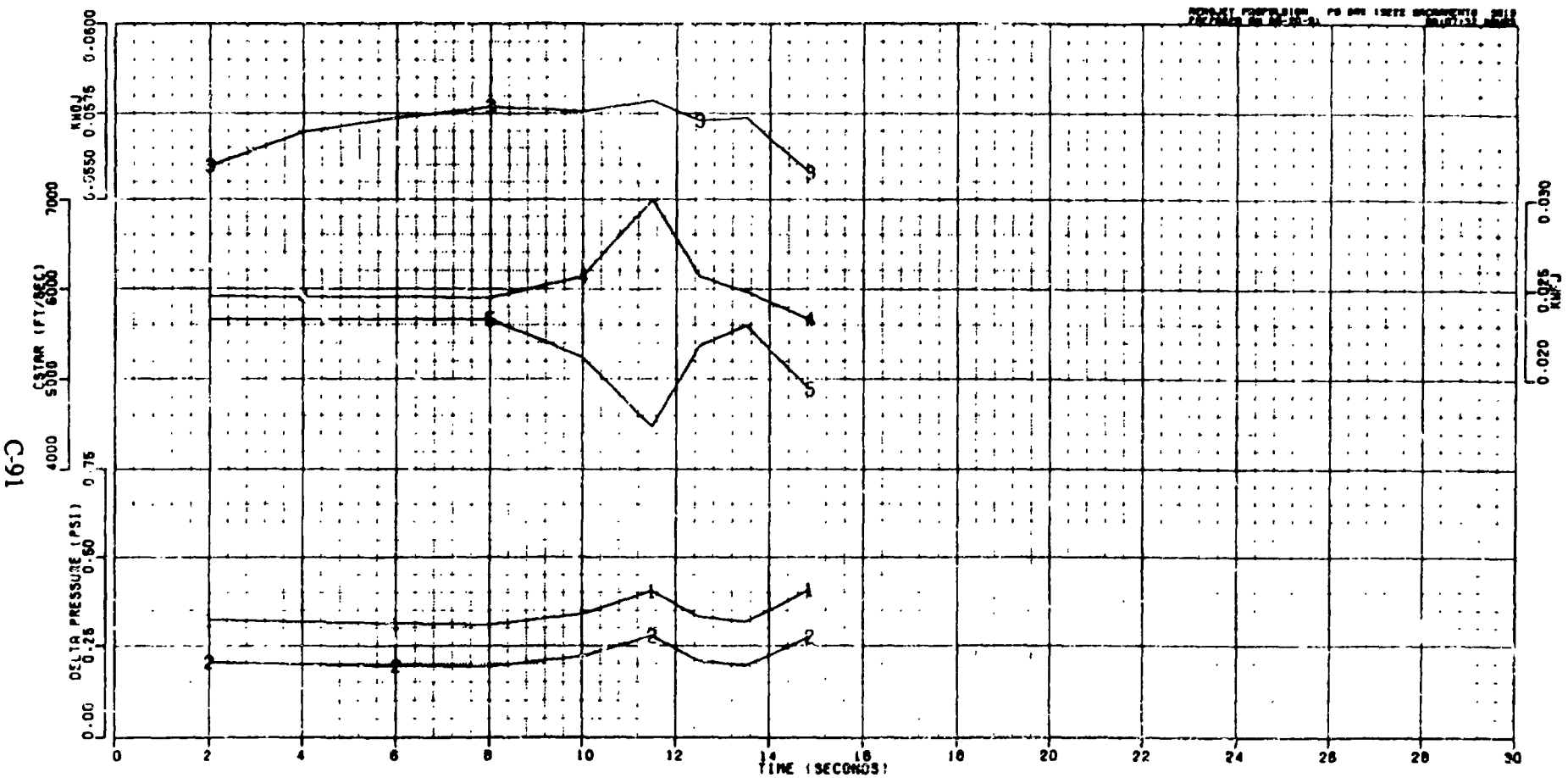

INJECTOR CALCULATIONS VS TIME PLOT 3
TEST NO. KEE4-D01-DA-125

TEST DATE 06-13-91 1603 HOURS 15.710 SEC.DUR

GENCORP
AEROJET

Figure C - 90

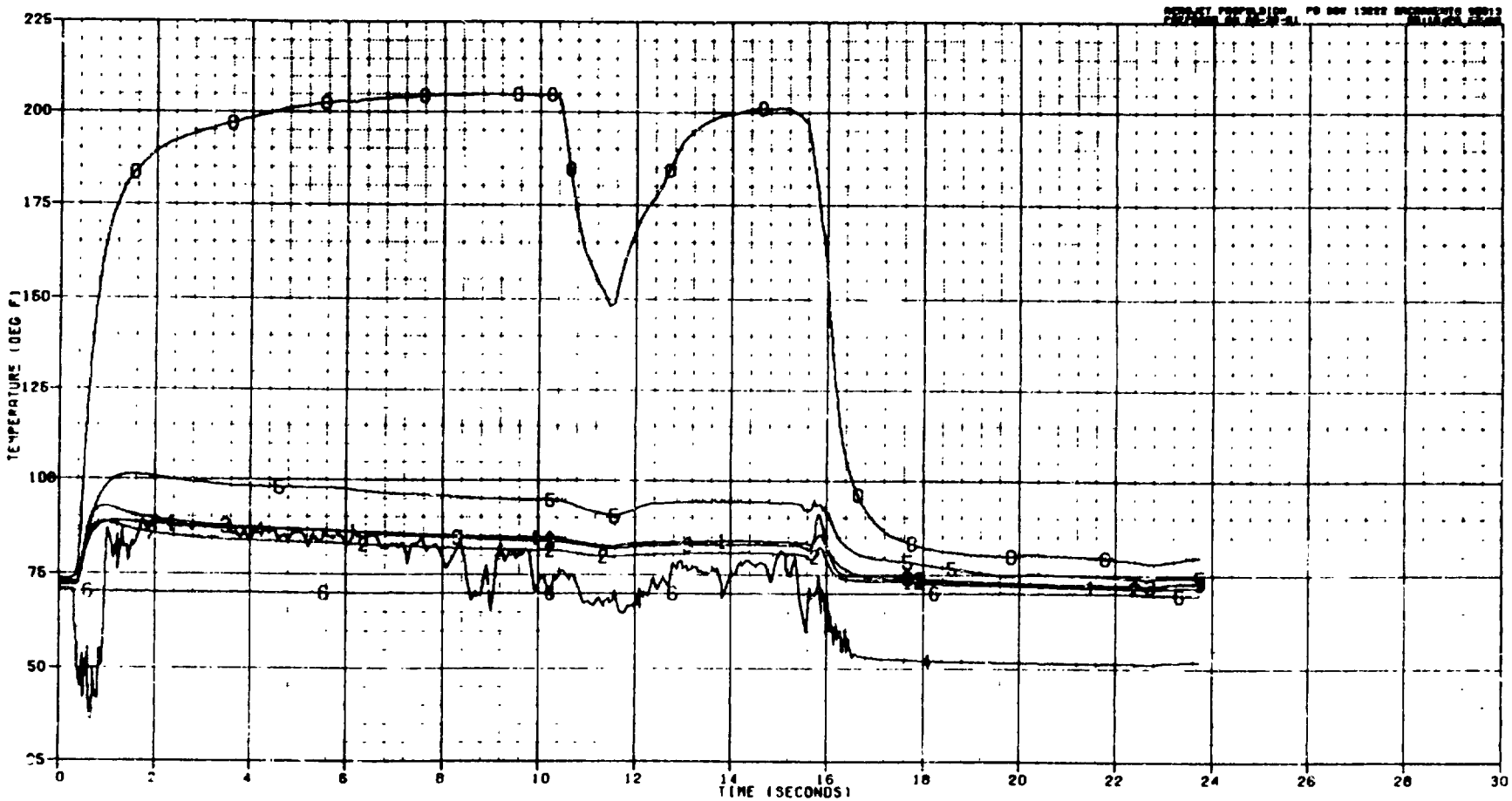

GENCORP
AEROJET

Figure C - 91

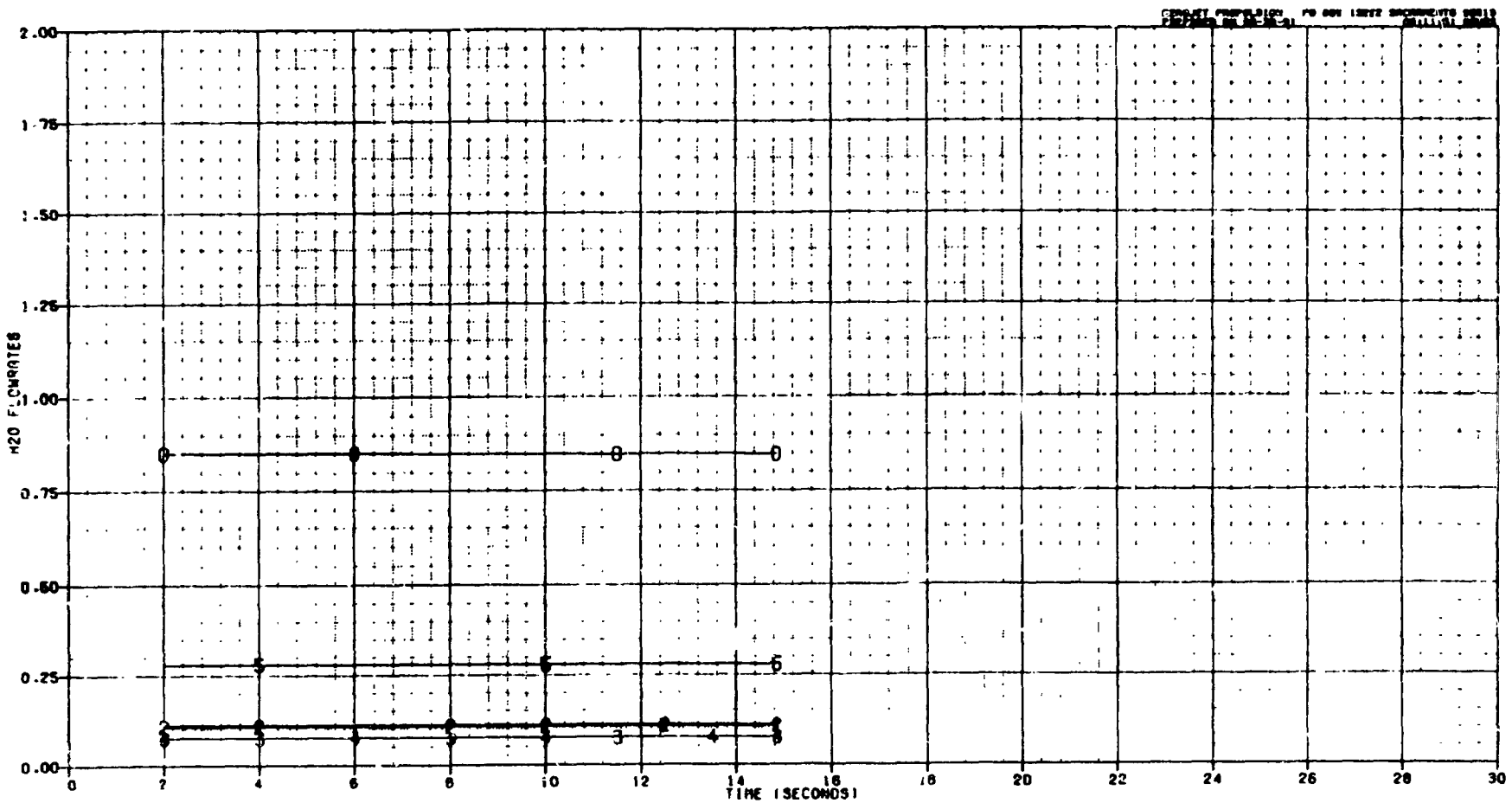

0 MI
1 MX
2 MXI
3 MXII
4 MXIII
5 MXIV

WATER FLOWRATES VS TIME PLOT 5
TEST NO. KEE4-D01-OA-125

TEST DATE 06-13-91 1603 HOURS 15.710 SEC.DUR

GENCORP
AEROJET

Figure C - 92

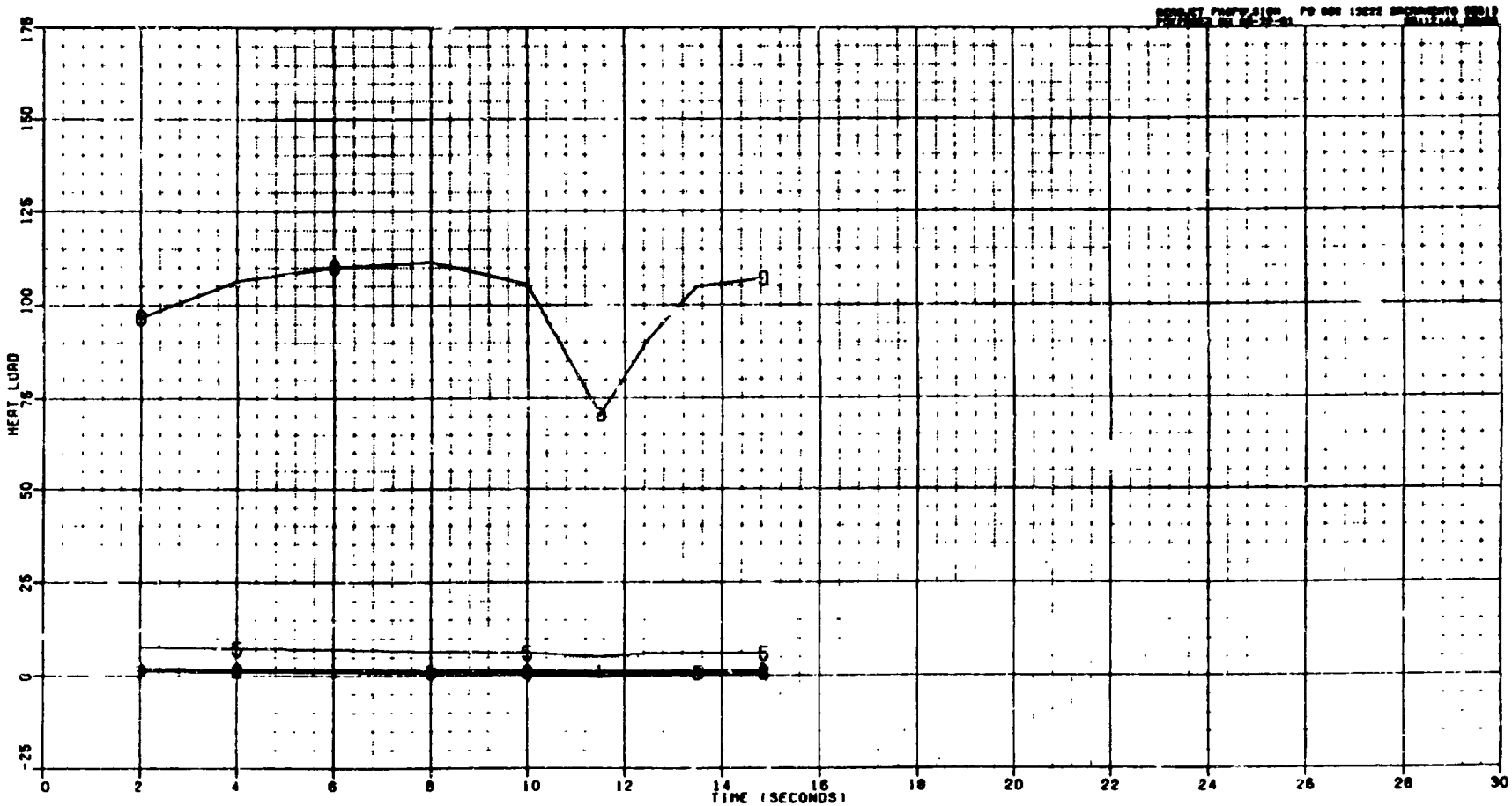

0 QI
1 QX
2 QXI
3 QXII
4 QXIII
5 QXIV

HEAT LOAD VS TIME PLOT 6
TEST NO. KEE4-DO1-OR-125

TEST DATE 06-13-91 1603 HOURS 15.710 SEC.DUR

GENCORP
AEROJET

Figure C - 93

ORIGINAL PAGE IS
OF POOR QUALITY

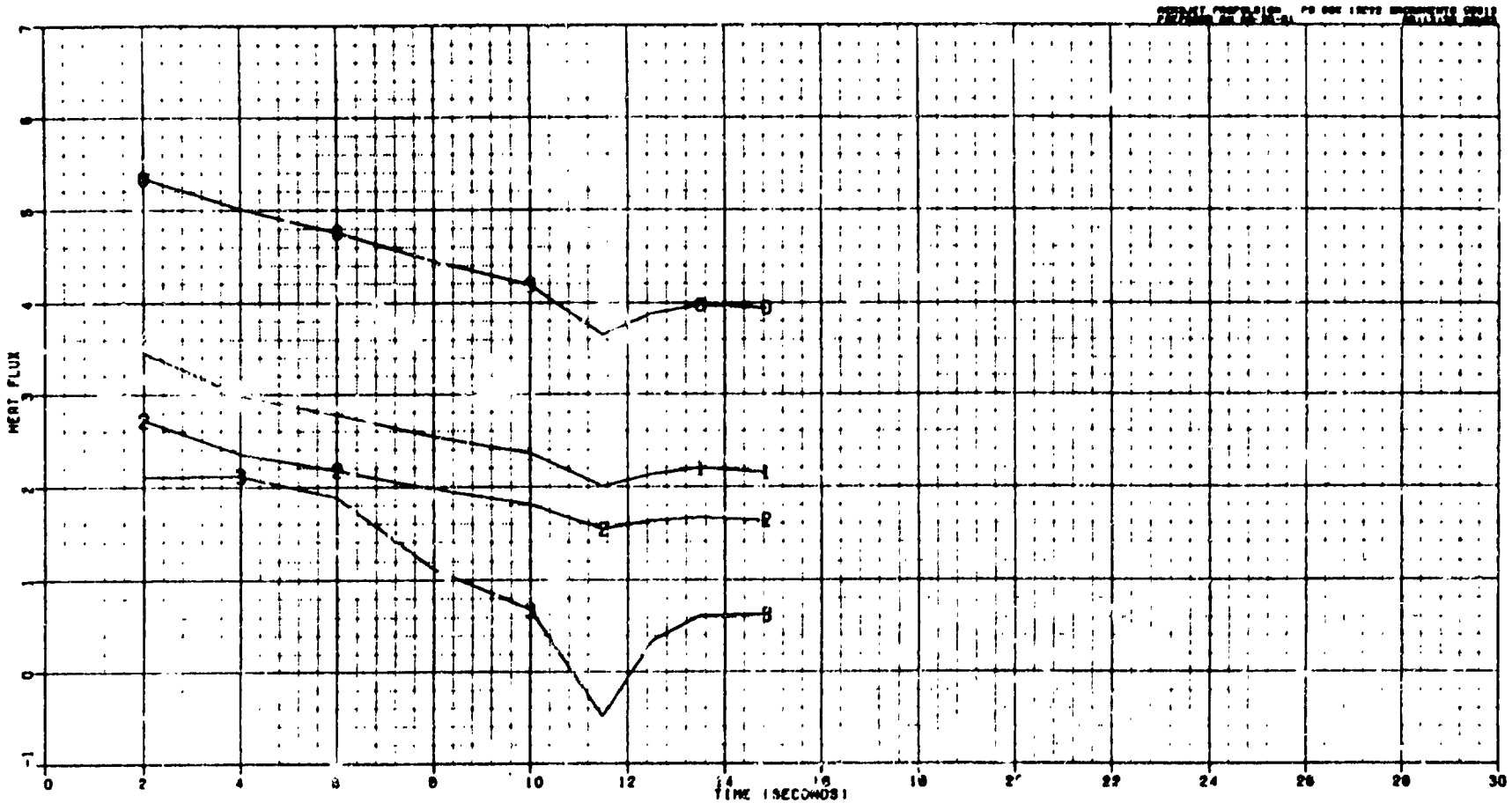

HEAT FLUX VS TIME PLOT 7
TEST NO. KEE4-001-DA-125

TEST DATE 06-13-91 1607 HOURS 15.710 SEC.DUR

GENCORP
AEROJET

Figure C - 94

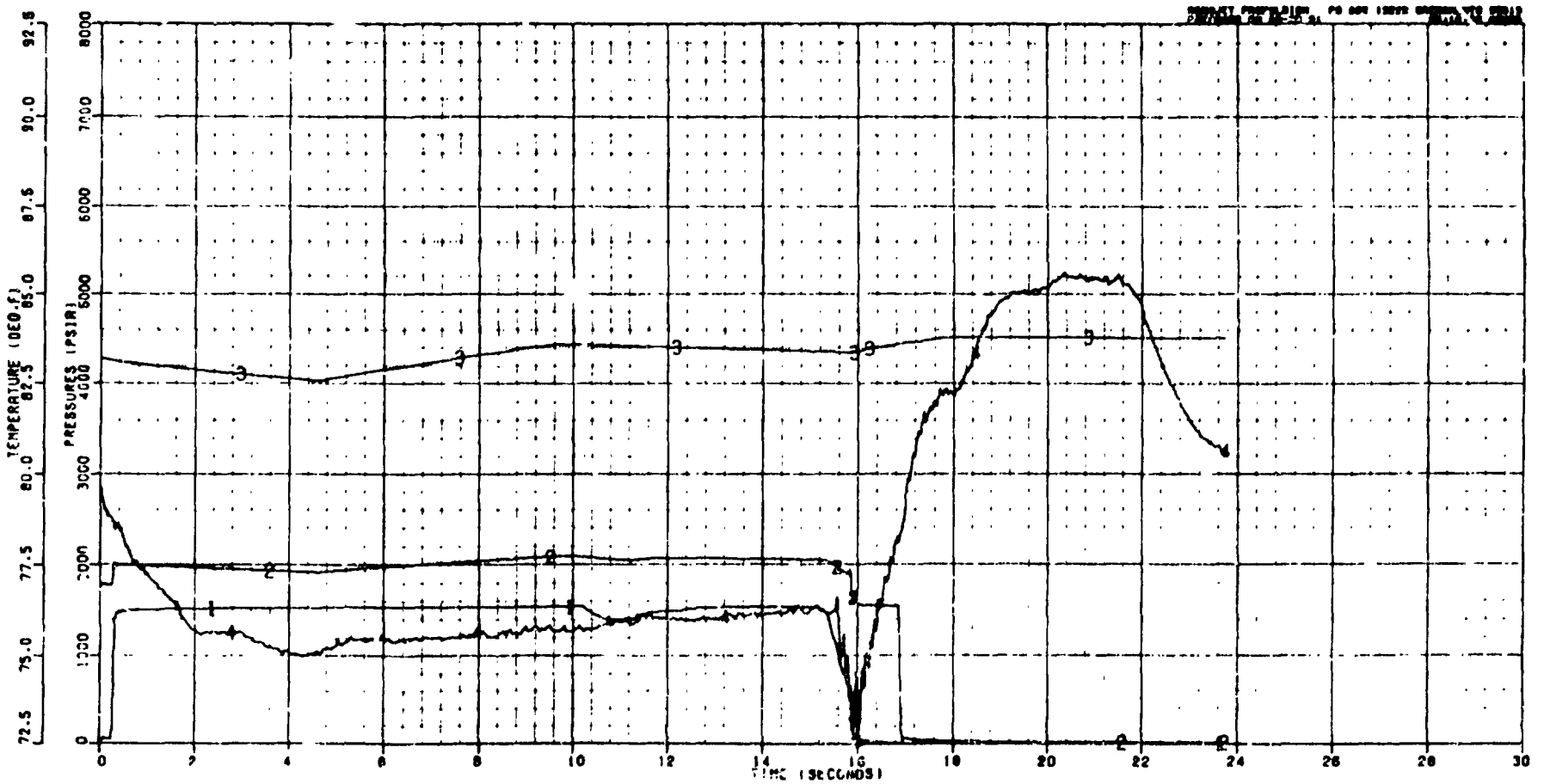

GENCORP
AEROJET

Figure C - 9C

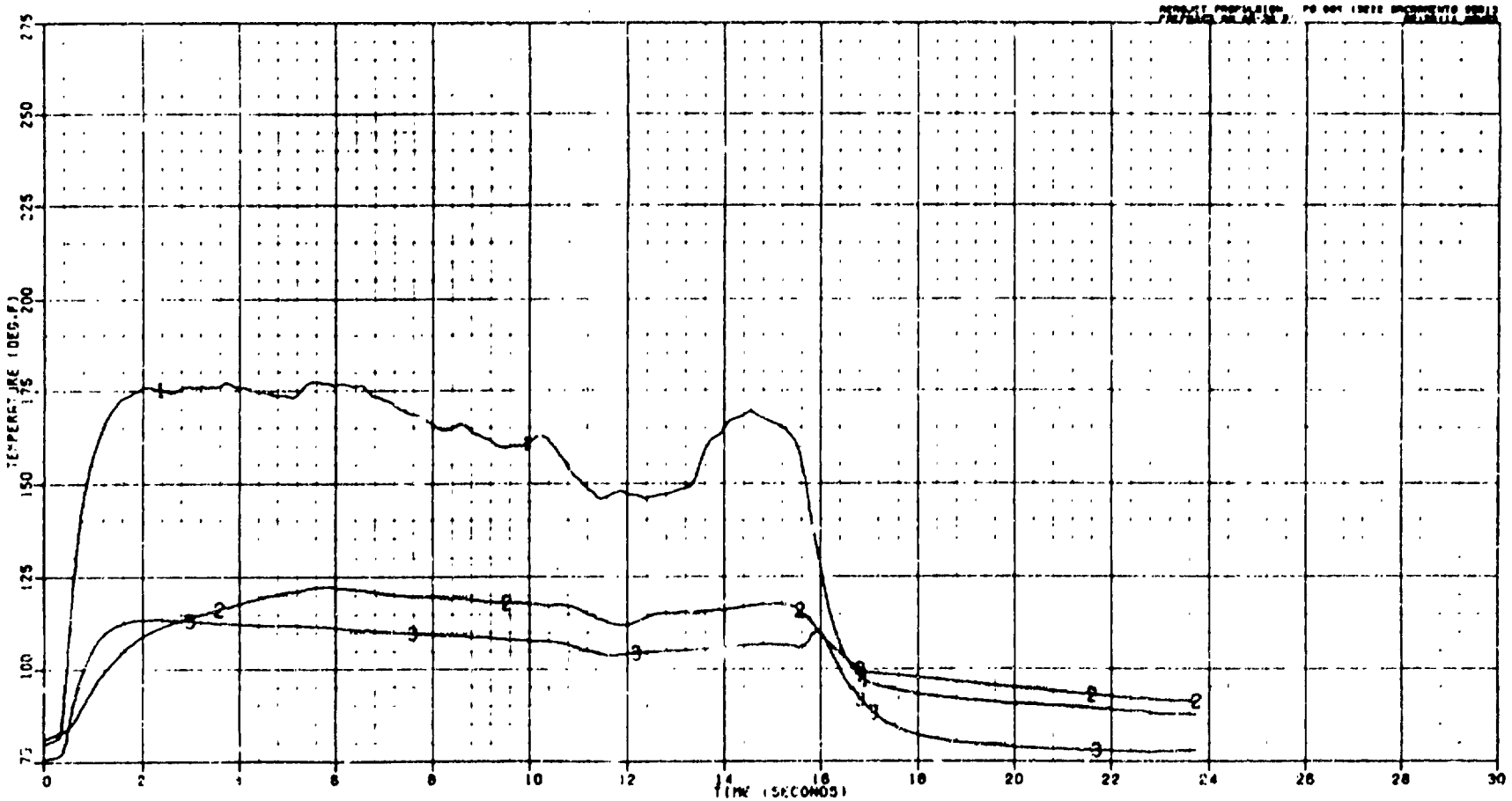

GenCorp Aerojet

Figure C - 96

APPENDIX D

BASELINE FULL-SCALE DESIGN ANALYSIS

BASELINE FULL-SCALE DESIGN ANALYSIS

Overview

Throat transpire cooling allows higher chamber pressures by eliminating the high pressure drop associated with the high velocity regen-cooled throat section. The primary performance benefit of the higher chamber pressure is derived from the increased expansion ratio available for the booster engine which must operate at sea level atmospheric pressures without nozzle flow separation. A small performance benefit is also derived from decreased kinetic and boundary layer losses.

Figure D-1 shows the hypothetical increase in sea-level specific impulse with chamber pressure for an all-regen LOX/RP-1 booster operating at a mixture ratio of 2.8. A 40-second increase in specific impulse is possible if the chamber pressure is increased from 1000 psi to 4000 psi. The exit area ratio increases from 17.2 to 51.9. Because transpire coolant does not fully mix and burn with the core flow, the net gain in specific impulse with transpiration is less than the theoretical gains shown in Figure D-1. The objective of the performance analysis was to quantify the net performance gain as a function of transpire flowrate. As shown later, it is possible to increase the performance of a methane chamber by 8.2 seconds by increasing the operating pressure from 3600 psi, the all-regen limit, to 5664 psi. The performance of an RP-1 chamber can be increased by 14.8 seconds by using LOX transpire to increase the chamber pressure from 1000 psi to 2304 psi.

If an increase in engine system life, rather than specific impulse, is the primary objective, the pressure drop savings can be used to reduce turbopump discharge pressure requirements. For chambers operating at their all-regen pressure limit, pressure loss savings and hence pump life increases can be significant. For a 750 klbf RP-1 engine operated at 1000 psi chamber pressure, the all-regen pressure loss is 3900 psi. Because pump life is proportional to the one-third power of pump discharge pressure, a nearly tenfold increase in life is possible for the RP-1 pump.

Performance Analytical Model

The chamber geometry was patterned after the STBE chamber design shown in Figure D-2, with a 2.8 contraction ratio and a 90 percent bell nozzle contour. The propellant mixture ratios and C* efficiencies are listed in Table D-1. The C* efficiencies are long-term values defined by NASA for use in LOX/Hydrocarbon studies. Chamber L prime was calculated using equation (1).

ORIGINAL PAGE IS
OF POOR QUALITY

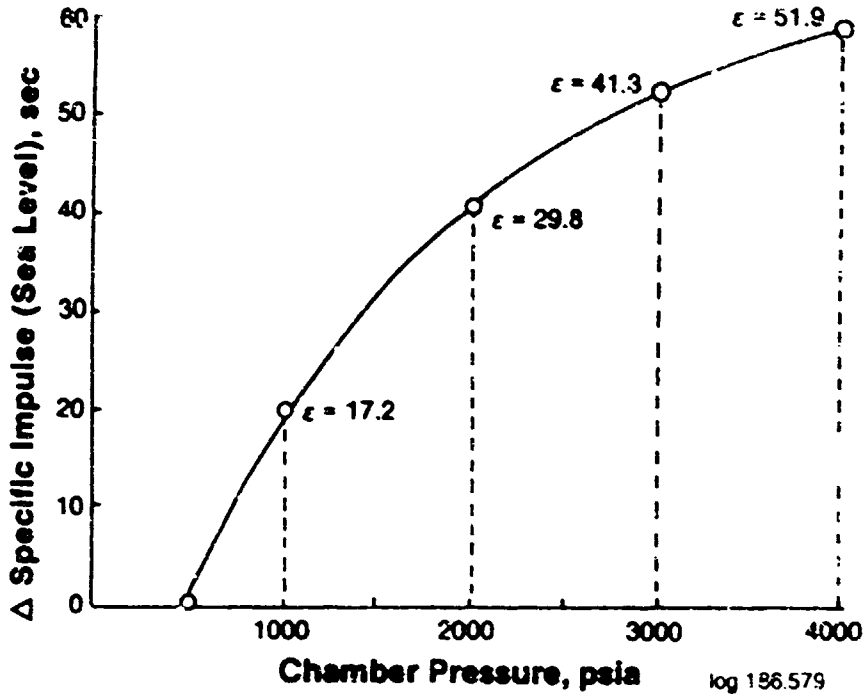

Figure D - 1. Increasing Chamber Pressure Provides Significant Sea Level Specific Impulse Increase

Lox/RP-1 @ 2000 psi

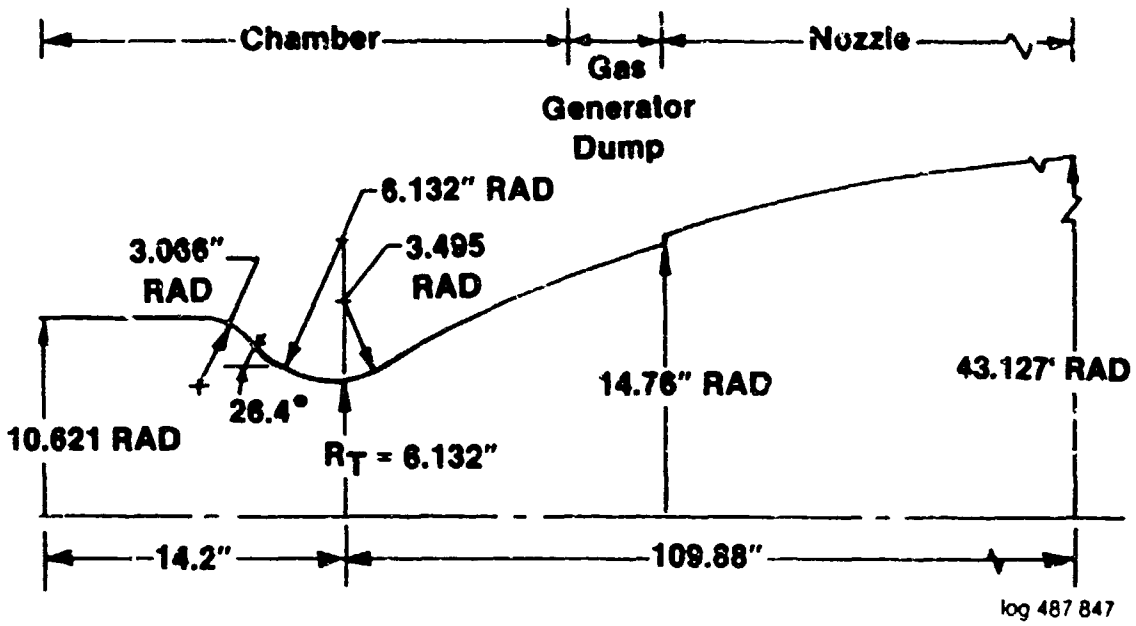

Figure D - 2. STBE Tri-Propellant Engine Geometry

Table D - 1

Propellants, Mixture Ratios, and C* Efficiencies Defined for Study

PROPELLANTS	MIXTURE RATIOS	C* EFFICIENCIES
LOX/METHANE	3.5	.99
LOX/PROPANE	3.1	.98
LOX/RP-1	2.8	.97

$$L' = -5.743 + 8.01\left(\frac{F}{Pc}\right)^{0.23} \quad (1)$$

The performance of the all-regen chambers was calculated using the TRAN72 and ROCKET codes. TRAN72 was used to find the exit area ratio, assuming a 6 psi ODE exit pressure. ROCKET contains data compiled from ODK into performance tables for a wide range of mixture ratios, chamber pressures and area ratios, as shown in Table D-2. ROCKET was used to determine throat size and thrust. After compiling initial data it was observed that for a given chamber pressure, there was less than 2 percent variations in exit area ratio and throat size for the three propellant combinations. Therefore, average values were calculated and used. As a result of using average values, it was possible to define chamber geometries based on chamber pressure only.

Selected LOX-methane cases were run using TDK to compare with the ROCKET calculations, and it was determined that the ROCKET data were accurate within 1 percent. Based on these data, the ROCKET code was judged adequate for the purposes of this study.

The specific impulse with transpire cooling was calculated using the gas generator option of the ROCKET code. The following assumptions were made.

(1) No mixing or heat transfer between coolant and boundary layer gas.

(2) Coolant specific heat independent of temperature.

(3) One-dimensional expansion of coolant from chamber pressure to 6 psia.

(4) Coolant dump location not accounted for.

(5) Presence of secondary flow does not affect primary stream performance loss factors.

Because transpire coolant velocities are low, about 10 fps, coolant to core momentum ratios are also low. It was therefore assumed that the coolant will not penetrate the core gas. RP-1 transpire was modeled differently because it is injected at subcritical temperatures whereas the other coolants are supercritical. RP-1 transpire cooling loss was modeled as a mass defect phenomenon, i.e., no penetration into the boundary layer and no contribution to thrust.

Table D - 2

OBX Performance Table for Three Propellant Combinations

Propellant Combination	O/F Range	Pc Range	E Range
Lox/RP-1	.22 - 10.0	20 - 5000	1 - 3000
Lox/CH_4	0.6 - 4.5	20 - 5000	1 - 3000
Lox/C_3H_8	0.6 - 6.0	100 - 3000	40 - 4000

log 487.211

Heat Transfer Analytical Model

Gas-side heat transfer coefficients were calculated using an integral energy boundary layer method contained in the SCALE computer program. The SCALE analytical model uses a semi-empirical relation between Stanton number and boundary layer energy thickness, as shown in equation (2),

$$St = C\, Re_j^{-0.25}\, Pr^{-0.67} \qquad (2)$$

in which the correlation coefficient C is defined from subscale chamber data. This coefficient is partitioned into two components, one dependent on axial distance to represent injector effects, and the other dependent on Mach number to represent flow acceleration. The boundary layer starts at the beginning of the convergent section. In the cylindrical section upstream from this point, the heat transfer coefficient is scaled by the mass velocity to the 0.8 power for any axial location.

Figure D-3 shows the high accuracy attained in matching the gas side heat fluxes for a 40 K chamber with a swirl co-axial, LOX/CH_4 injector. These data provide the basis for the gas side heat transfer coefficient scaling defined above for the propellants investigated in this study.

The coolant side heat transfer correlations used in SCALE are summarized in Table D-3. Two correlations are given for methane, a wall-to-bulk temperature ratio correlation for pressures greater than three times critical, and a more complex property ratio correlation for the near critical region. The latter correlation is similar to those for oxygen and propane.

Coking

References 3, 4, 7 and 8 provide coking and corrosion data for methane, propane and RP-1. Although these results do not provide a clear definition of threshold wall temperatures, are sometimes contradictory and often do not extend to high coolant velocities, a number of trends are clear.

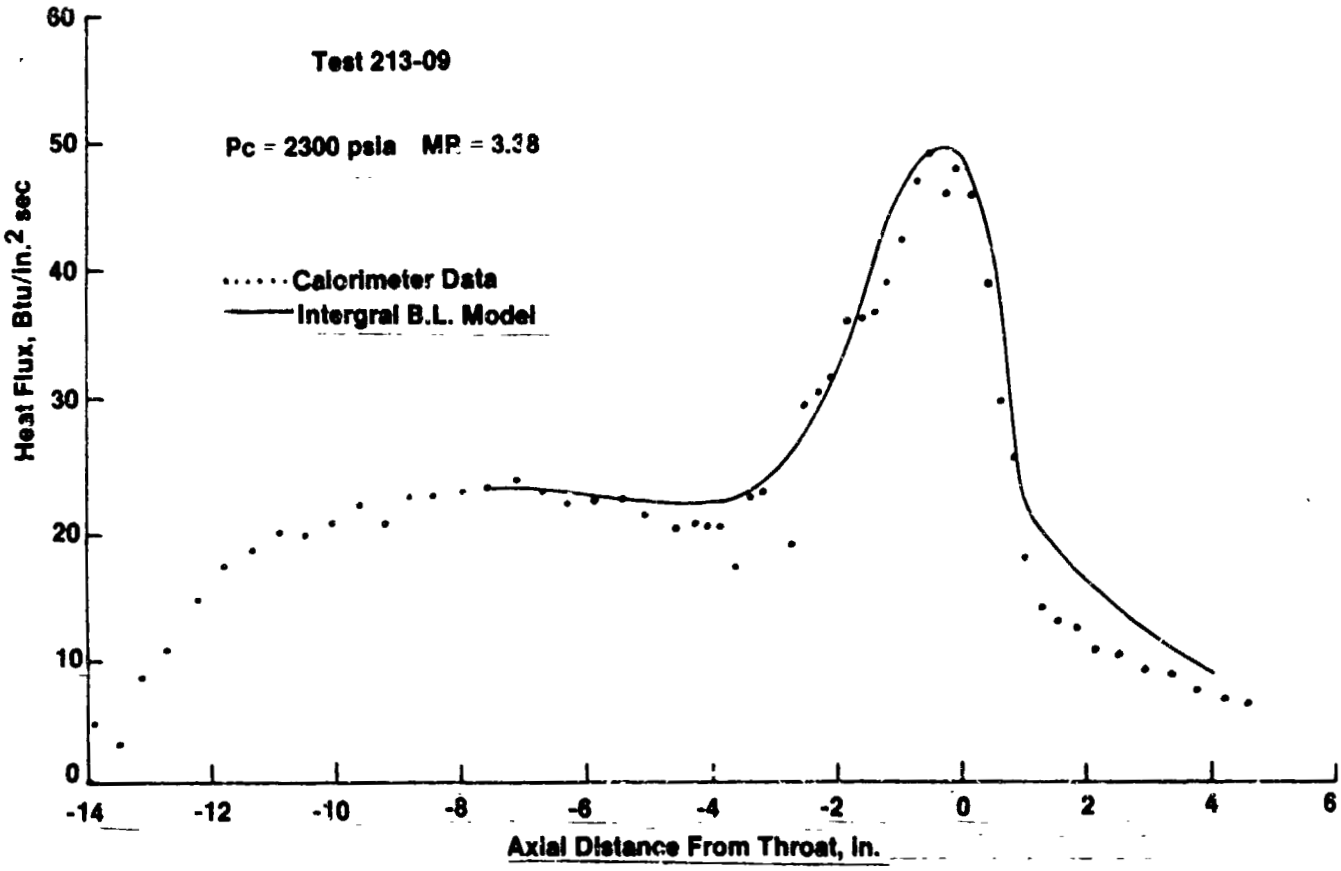

Figure D - 3. Comparison of 40K Swirl Coaxial, Lox/CH_4 Injector Heat Fluxes With Integral Boundary Layer Model

Table D-3

Recommended Supercritical Coolant Heat Transfer Correlations

Coolant	Reynolds No. Exponent n	$Nu_b/Re_b^n Pr_b^{0.4}$	Reference No.
RP-1	0.95	.005	1
Propane	0.88	$.00569 \left(\frac{\rho_b}{\rho_w}\right)^{0.12} \left(\frac{\mu_b}{\mu_w}\right)^{-0.14} \left(\frac{k_b}{k_w}\right)^{0.83} \left(\frac{\bar{c}_p}{c_{p_b}}\right)^{-0.37} \left(\frac{P}{P_{cr}}\right)^{0.25}$	2
Methane	0.8	$.0228\ (T_b/T_w)^{0.47}\quad P \geq 3P_{cr}$	3
	1.0	$.0028 \left(\frac{\rho_b}{\rho_w}\right)^{1.5} \left(\frac{\mu_b}{\mu_w}\right)^{-6.5} \left(\frac{k_b}{k_w}\right)^{6.4} \left(\frac{\bar{c}_p}{c_{p_b}}\right)^{2.4}\quad P_{cr} < P$	4
Oxygen	1.0	$.0025 \left(\frac{\rho_b}{\rho_w}\right)^{-0.5} \left(\frac{k_b}{k_w}\right)^{0.5} \left(\frac{\bar{c}_p}{c_{p_b}}\right)^{0.67} \left(\frac{P}{P_{cr}}\right)^{-0.2}$	5

log 487.796

(1) Coking with propane is as bad or worse than with RP-1. Thermal resistance increases at wall temperatures as low as 260 F were observed in Ref. 4, and Ref. 7 noted that deposits with propane were heavier, blacker and more uniform than those with RP-1. Both references observed higher deposition rates with propane at any given wall temperature, whereas Ref. 6 noted deposition rates comparable to RP-1.

(2) Methane is clearly the best fuel from a coking standpoint. No decomposition product deposition was observed in Ref. 4. However, deposits were observed at low coolant bulk temperatures and low wall temperatures attributable to adsorption of mercaptans in trace concentrations.

(3) Corrosion of copper surfaces occurs with all three fuels due to reactions with sulphur impurities. A corresponding roughening of the surface with increased heat transfer and pressure drop at high wall temperatures was observed in Ref. 5 with methane. Threshold temperatures and exposure times for these effects are not well defined at this time. Nickel plating on the copper surface eliminated tube corrosion and reduced deposit formation in most cases in Ref. 8.

(4) Deposit formation due to coking is still not well understood. Observed deposition rates are nonuniform in time and depend on velocity, coolant bulk temperature, sulfur contamination and wall temperature.

Recommended coolant-side wall temperature limits for hydrocarbon regen-cooled sections are shown in Table D-4.

Regen Channel Design

Regen-cooled section analysis was accomplished with the SCALE program. SCALE integrates the coolant energy and momentum equations over the length of the channel and calculates local wall temperatures at selected locations along the channel. Fin channel layout optimizations to minimize pressure drop is accomplished by parametric studies.

Two-dimensional conduction effects in rectangular channels and spatial variation of the coolant heat transfer coefficient are approximated as shown in Figure D-4. The hot wall adjacent to the channel, the entire land, and that part of the external wall adjacent to the channel are represented as fins; that part of the external wall adjacent to the land is assumed to be isothermal.

Table D - 4

Coolant Inlet Temperature and Coking Temperature Limit

Coolant	Inlet Temperature °K (°R)	Coking Temperature Limit, °K (°R)
RP-1	311 (560)	561 (1010)
Propane (Subcooled)	111 (200)	589 (1060)
Propane (NBP)	250 (450)	589 (1060)
Methane	144 (260)	No Limit *
Oxygen	111 (200)	No Limit*
Hydrogen	61 (110)	No Limit*

* No coking temperature limit on the coolant-side, wall temperature is constrained by the cycle life on gas-side.

log 487.844

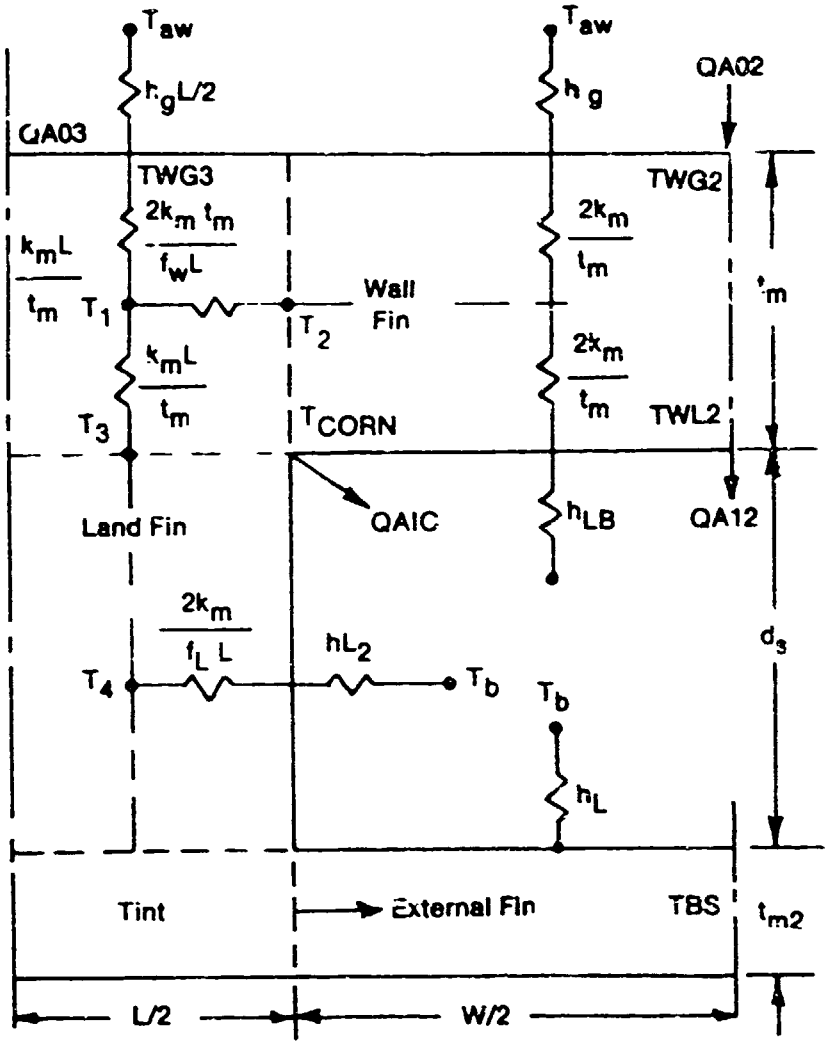

$$h_{LB} = HFAC \times f\left[\left(\frac{TWL2 + TCORN}{2}\right)\right]$$

$$h_L = f\,[TBS]$$

$$h_{L_2} = GFAC\, h_L + (1\text{-}GFAC)h_{LB}$$

log 487 793

Figure D - 4. SCALE Thermal Model Simulates All the Relevant Heat Transfer Phenomena

A simple resistance network represents the hot wall adjacent to the land and connects the hot wall fin to the land fin.

Different coolant heat transfer coefficients are associated with each fin. The hot wall heat transfer coefficient is based on the average of the centerline (TWL2) and corner (TCORN) wall temperatures, while the coefficient for the external wall is based on its centerline wall temperature (TBS). The land coefficient is merely a weighted average of the other two.

In its design mode, SCALE calculates the channel depth profile required to satisfy gas-side and coolant-side wall temperature criteria for a specified channel layout. Gas-side wall temperatures are limited by cycle life and firing duration requirements. For this study a cycle life of 100 cycles was assumed. The wall temperature constraint for 100 cycles is illustrated in Figure D-5. Figure D-6 illustrates wall strength criteria used to determine hot-gas side wall thickness.

Channel layout optimization is accomplished by SCALE parametric studies. Channel geometries used in this study are listed in Section 1.4.

Transpire Analytical Model

The transpire coolant flowrates were calculated using the TRANSP computer program (Reference 8). TRANSP imposes an energy balance between the net hot-gas side heat transfer and the heat transferred to the coolant, as illustrated in Figure D-7. For methane and LOX, the gas-side heat flux reduction due to blowing was calculated using a semi-empirical correlation shown in equation (3) below.

$$\frac{St}{St_o} = \frac{\ln(1 + \alpha B')}{\alpha B'} \qquad (3)$$

where $a = (1 - .072M)(Me/Mc)^a$, and $a = 0.35$ ($M_c > M_e$), $a = 0.6$ ($M_c < M_e$)

This equation is found in Reference (9) and was derived from data in References (10) through (13). The blockage efficiency depends on the coolant flowrate, and on the molecular weight ratio between the coolant and core gas.

For RP-1 and Propane, the blowing heat flux reduction was calculated using equation (4).

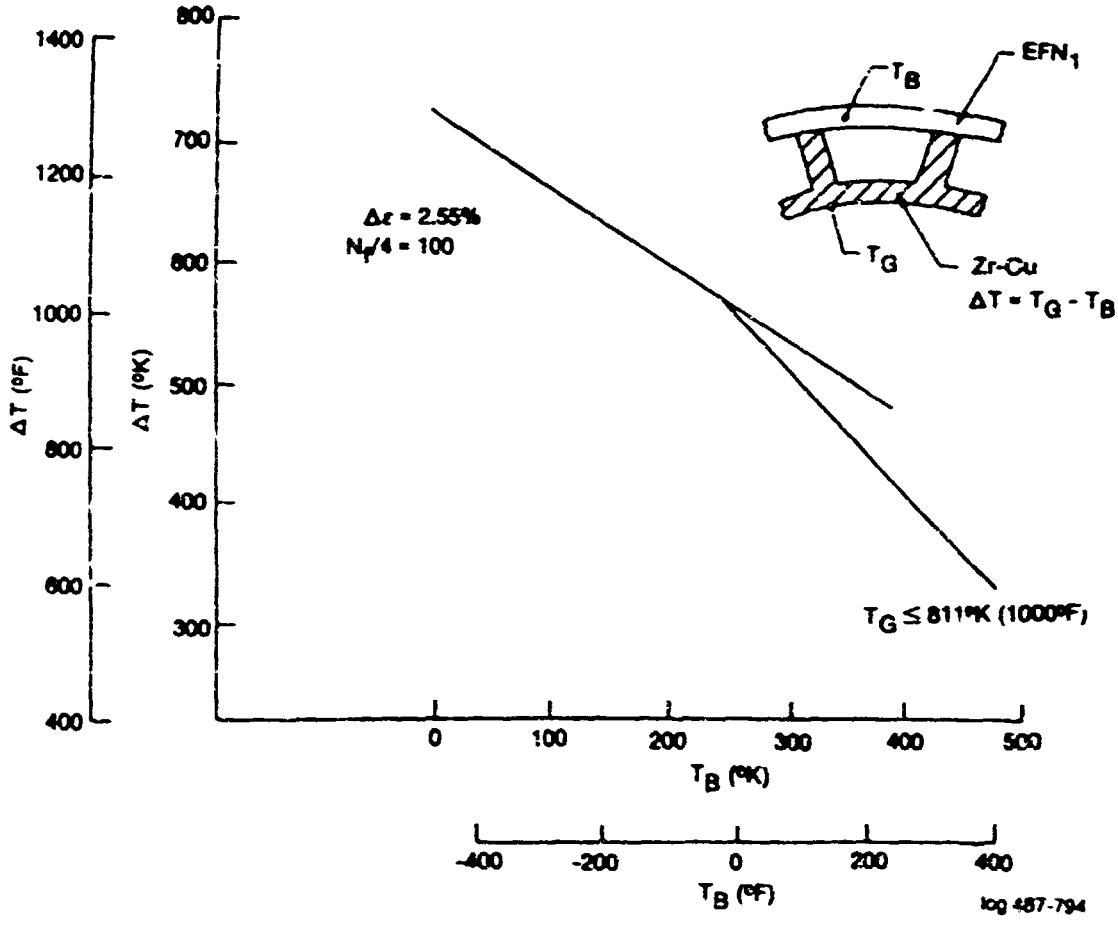

Figure D - 5. Cycle Life/Creep Wall Temperature Criteria

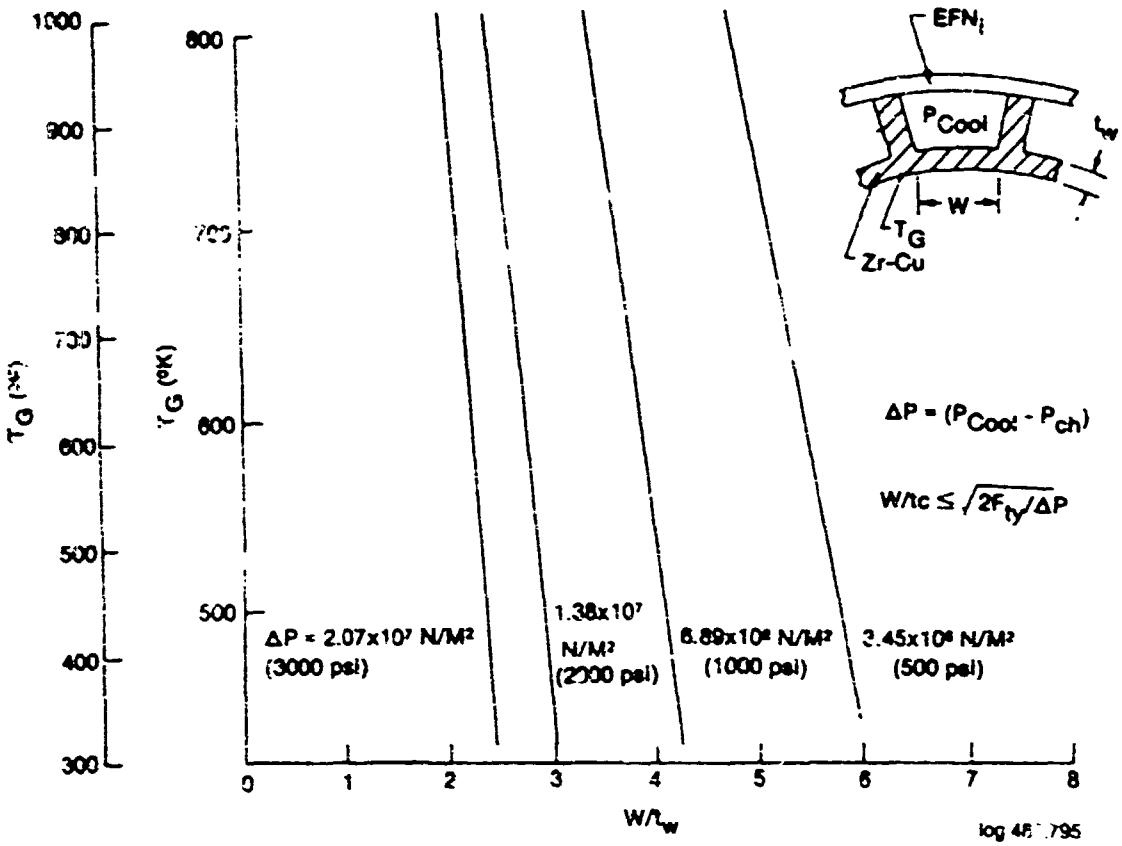

Figure D - 6. Zr-Cu Chamber Wall Strength Criteria

TRANSP Model Imposes Energy Balance Between Reduced Gas-Side Heat Flux and Internal Heat Removal by the Coolant

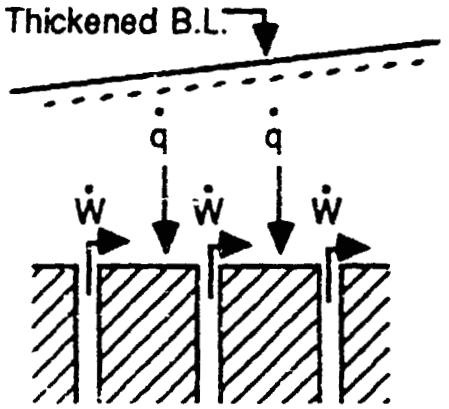

Gas Side

$$\dot{q} = h\,(T_r - T_w)$$

$$h = f\,(St_o, \frac{\dot{W}}{A}, \mu u, C_p, MW)$$

Coolant Side

$$\dot{q} = \frac{\dot{W}}{A} C_p (T_{ce} - T_{cm})$$

log 487.832

Figure D - 7. Transpiration Cooling Analytical Model

$$\frac{St}{St_o} = \frac{G}{\left(\frac{G}{3}+1\right)^3 - 1} \tag{4}$$

where $G = BC_{Pc}/C_{pe}$ and $B = \lambda/St_o$

This equation is derived from the porous wall transpire data of Bartle and Leadon reported in Reference (12). In this model the heat flux reduction is a function of coolant flowrate and specific heat. Equation (4) represents a simplified methodology appropriate for a parametric study. To more rigorously model RP-1 and propane, an analytical approach including endothermic bond dissociation and chemical kinetics is required. The basic methodology for analyzing a chemically reacting boundary layer is documented in Reference (14). This methodology will be used for the analysis of the bench test data.

On the coolant side the TRANSP fin option was used. The fin model calculates surface and in-depth wall temperatures using equation (5).

$$T_w = q/kr + T_{cm} \tag{5}$$

A description of the fin equation is found in Reference (15). Surface temperatures for the entire transpiration cooled lengths were assumed to be 600 degrees F, a coking temperature limit, for propane and RP-1, and 1240 degrees F for methane and LOX.

Baseline Analysis

The propellant and coolant combinations studied are shown in Table D-5. Case 1 is a LOX-methane chamber with methane regen and transpire. Case 2 is a LOX-propane chamber with sub-cooled propane regen and transpire. Cases 3, 4 and 5 are LOX RP-1 chambers with three different cooling combinations. Case 3 is entirely RP-1 cooled, Case 4 is RP-1 regen cooled and LOX transpire cooled, and Case 5 is entirely LOX cooled. Table D-6 shows the propellant properties.

Figure D-8 shows regen pressure drop versus chamber pressure. The analyses assumed a maximum TPA outlet pressure of 8000 psia. The curves are truncated where the 8000 psi pump discharge limit is reached. Discharge pump pressures were estimated using gas generator cycle power balance data from Reference (16). No new power balances were calculated for this study. Methane and LOX have a 3600 psi limit, while sub-cooled propane has a 3800 psi limit. The very high regen pressure drops which limit RP-1 to a 1000 psi chamber pressure are caused by the

Table D - 5

Propellant and Coolant Combinations Studies

Case No.	Fuel	Regen Coolant	Transpire Coolant
1	Methane	Methane	Methane
2	Propane (SC)	Propane (SC)	Propane (SC)
3	RP-1	RP-1	RP-1
4	RP-1	RP-1	LOX
5	RP-1	LOX	LOX

Table D - 6

Physical Properties of Methane, Propane, RP-1 and Lox

	nbp (°R)	P_{cr} (psi)	T_{cr} (°R)	T_{in} (°R)	SG	MW
Methane	201	667	343	260	0.4	16
Propane	416	616	665	200	0.7	44
RP-1	882	315	1218	560	0.8	172
LOX	162	731	278	200	1.1	32

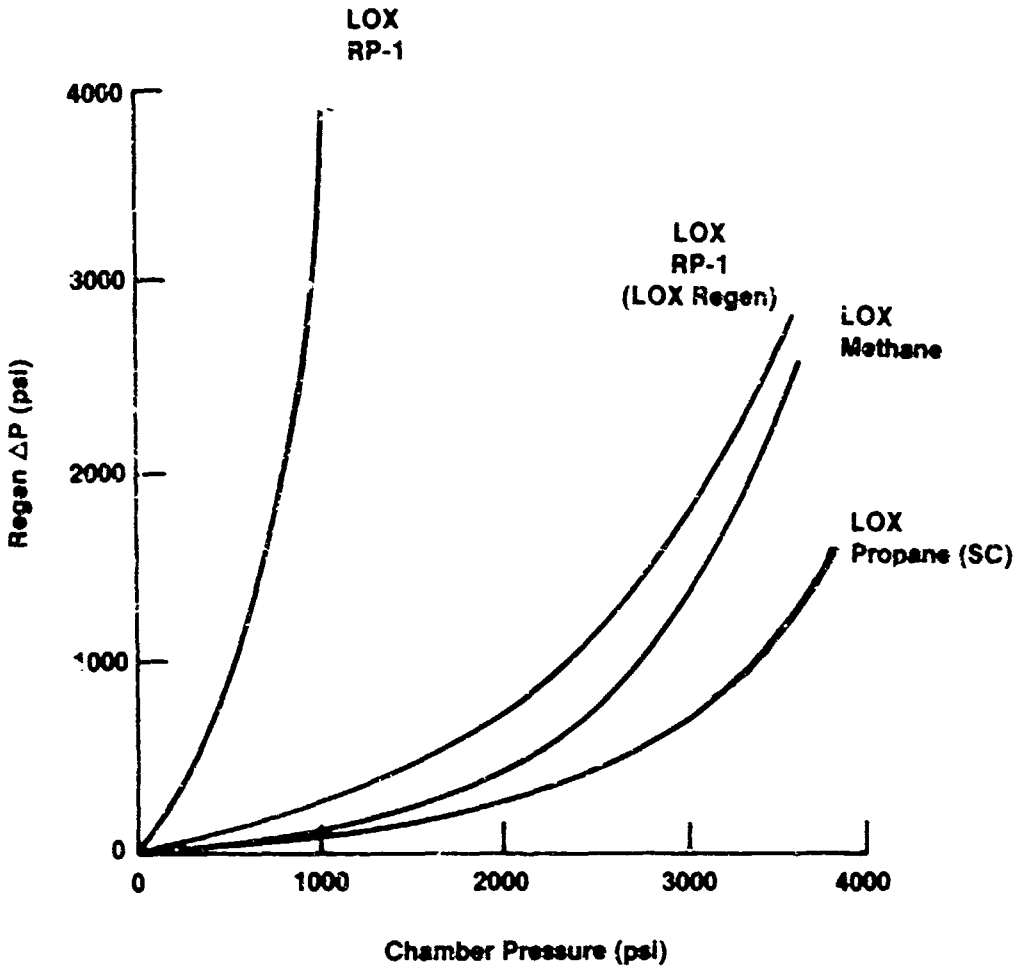

Figure D - 8. All-Regen Pressure Loss Versus Chamber Pressure, F = 750 klbf

600°F coking temperature limit restriction. The 600°F coking limit restriction does not cause similar high regen pressure drops with subcooled propane as the coolant. This is because subcooled propane has a lower bulk temperature (-260°F) than RP-1 (100°F). The lower bulk temperature of propane permits it to accommodate a higher gas side heat flux without the chamber coolant side wall temperature exceeding 600°F than can RP-1. Table D-7 summarizes the primary engine design parameters at the maximum all-regen chamber pressures.

The predicted baseline heat transfer coefficients are shown in Figure D-9. The methane and propane data are nearly identical, and are plotted with a single line. Figure D-10 shows regen friction pressure loss plotted versus axial position. Most of the pressure drop occurs in a small length of throat section, or about 5 inches for propane and methane, where high coolant velocities are required.

Figure D-11 is a cross plot of the change in sea-level specific impulse versus percent transpire cooling; and shows that transpiration can be used to increase chamber performance. The increase in specific impulse is measured relative to the specific impulse at the maximum all-regen chamber pressure. The transpire cooled lengths are indicated by numbers next to the curves. The analyses assumed that the transpire sections had 80% of their length located upstream of the throat and 20% located downstream of the throat. A maximum increase of 8.2 seconds is possible for the methane chamber, when an 18-inch length is transpire cooled, and a chamber pressure of 5664 psi is reached.

A 14.8 second increase is possible for the RP-1 chamber if it is operated at 2804 psi with LOX transpire cooling (case 4). The large increase in specific impulse is possible because the baseline all-regen chamber is limited to a low 1000 psi chamber pressure. There is less increase possible for a LOX regen-cooled RP-1 chamber (case 5) which starts out at 3600 psi. A 3-second increase is possible for the RP-1 chamber with RP-1 transpire (case 3). Compared to LOX transpire, RP-1 requires about twice as much coolant flow because a 600°F coking limit was assumed for RP-1.

Propane has a net loss in performance for any throat length considered. Propane requires high transpire flowrates to keep the surface below the 600 F coking temperature limit. If coking were not a concern, the propane engine would operate at 1240°F and would have a performance increase about the same as the methane engine.

Table D - 7

Baseline Operating Conditions

Propellant	Mixture Ratio	Regen Coolant	Chamber [1] Pressure (psi)	Area Ratio (P_e=6 psia)	Specific Impulse Delivered Sea Level (sec)
Methane	3.5	Methane	3600	55.3	323.9
Propane (SC)	3.1	Propane (SC)	3800	58.8	318.9
RP-1	2.8	RP-1	1000	21.2	275.2
RP-1	2.8	LOX	3600	56.4	307.5

(1) Chamber pressures assume 8000 psia TPA discharge pressure, T_{WALL} = 600°F for RP-1 and propane coolants, and T_{WALL} = 1240°F for methane and LOX coolants.

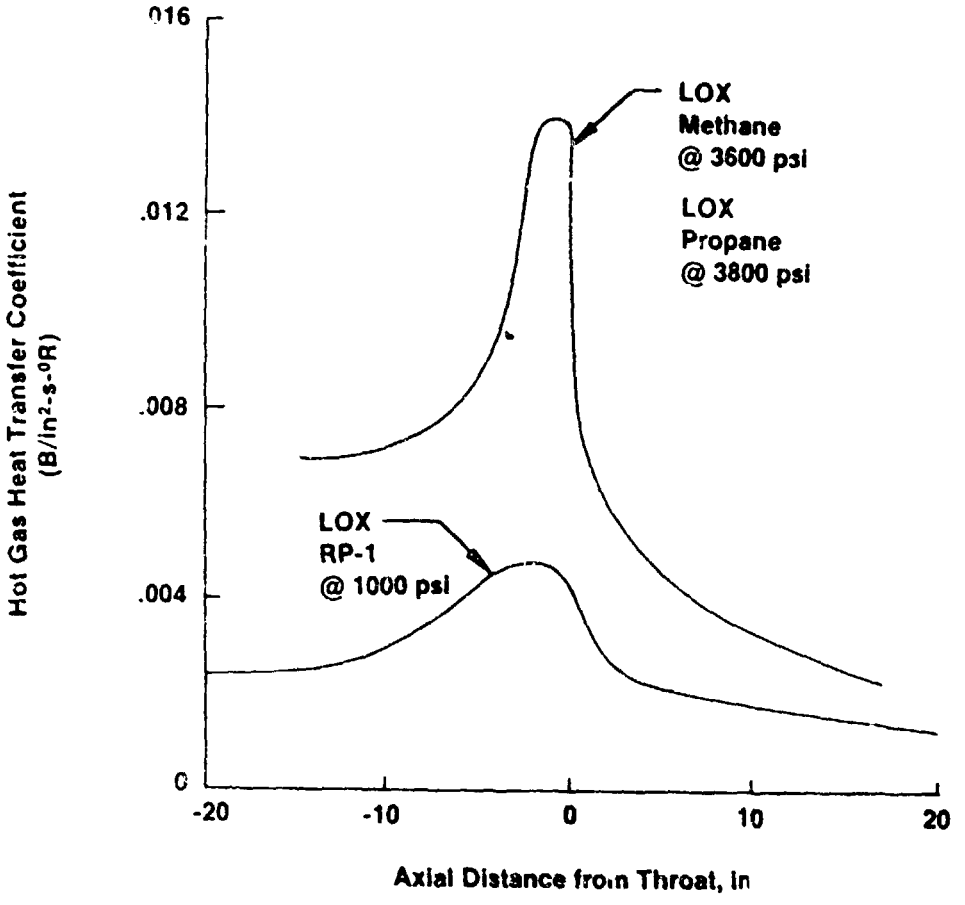

Figure D - 9. Hot Gas Transfer Coefficient Profile for Liquid Oxygen With Methane, Propane and RP-1, Evaluated at Baseline Engine Conditions

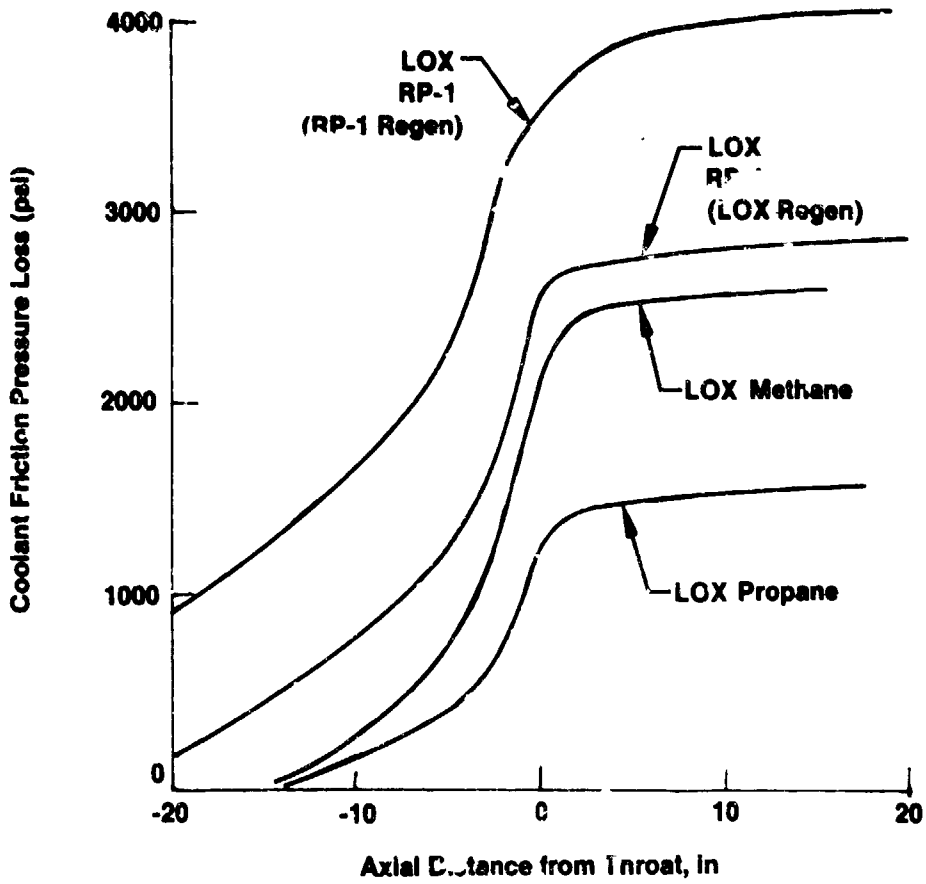

Figure D - 10. Coolant Friction Pressure Loss Profile for Methane, Propane and RP-1, Evaluated at Baseline Engine Conditions

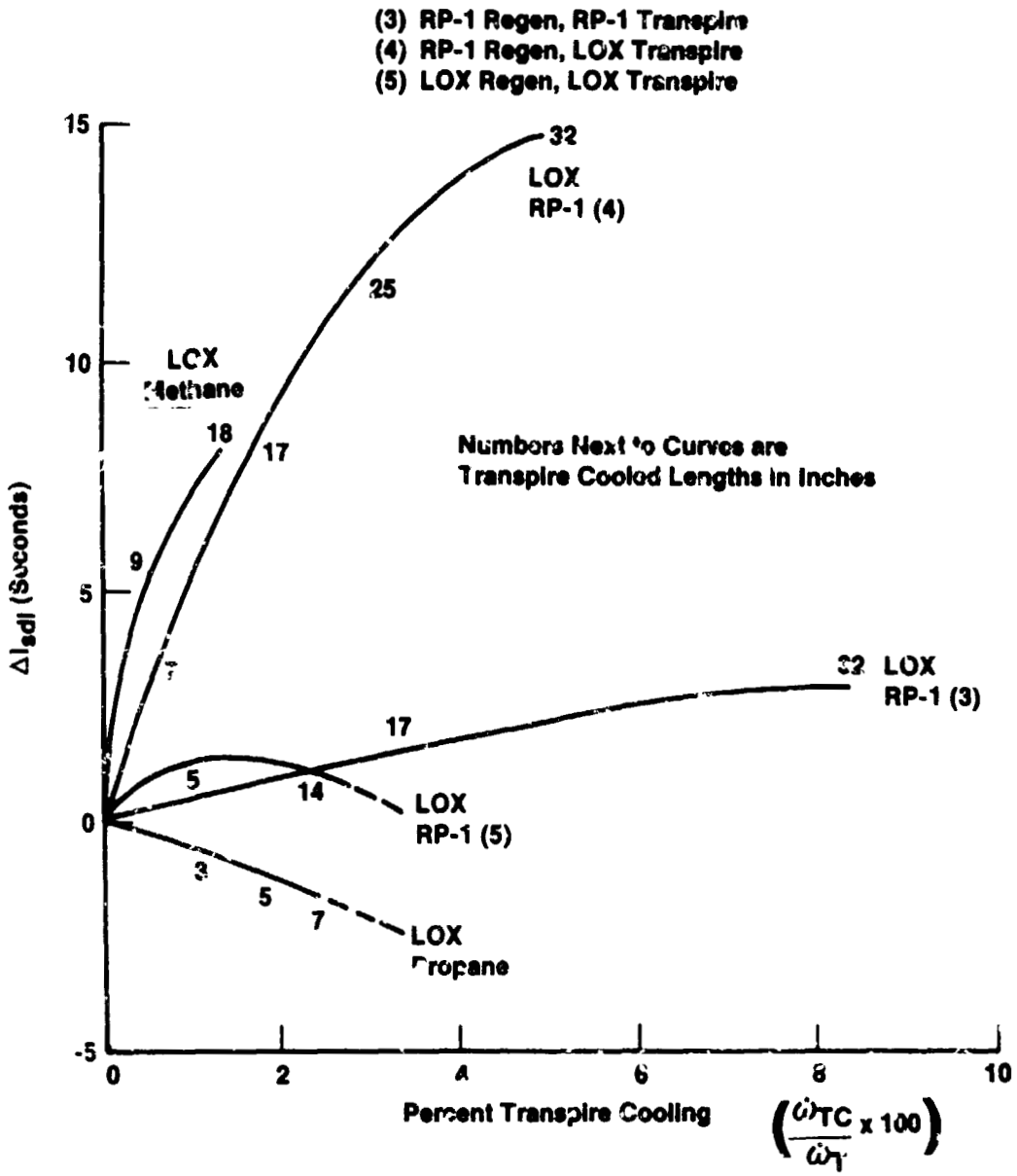

Figure D - 11. Sea Level Specific Impulse Change Versus Percent Transpire Cooling With Fixed Pump Discharge Pressure

Table D-8 summarizes the data used to construct the plots in Figure D-11. The method of solution was to pick chamber pressure, then solve for the transpire length needed to meet the 8000 psi pump discharge pressure requirement. The method is described below.

(1) First, the allowable regen pressure drop was calculated. To meet the 8000 psi pump discharge pressure requirement, the total of the new regen loss, plus added injector and line losses, should equal the regen loss for the baseline all-regen case. The injector and line losses were assumed to be 25 percent of the chamber pressure increase.

(2) Next, SCALE regen pressure drops at the new chamber pressure were calculated for several transpire lengths. Channel layouts were optimized for each run, and the pressure losses due to regen flow bypass around the throat section were included.

(3) Using data from steps (1) and (2) the transpire length yielding the required regen pressure drop was selected.

(4) The transpire requirement for the length in (3) was calculated using TRANSP.

(5) The new I_{SL} was calculated in two steps. First, the I_{SL} of a hypothetical all-regen chamber was calculated using ROCKET. Then I_{SL} with transpire was then calculated using the method described in Section 1.4, equation (6).

(6) The net increase in I_{SL} was calculated by taking the new I_{SL} in step (5) and subtracting the I_{SL} for the maximum all-regen chamber pressure.

To further define the method used, the 4788 psi, LOX methane calculations is described below as a sample case.

(1) At 4788 psi the chamber pressure is 1188 psi greater than the 3600 psi baseline all-regen chamber pressure, and injector and line losses are 297 psi greater to keep pump discharge pressure constant, the regen pressure loss must be 1095 psi.

(2,3) A transpire length of 8.4 inches is required to reduce regen loss to 1095 (psi at the 4788 psi chamber pressure.

(4) The transpire flowrate for an 8.4-inch length is 14.6 lb/s, or 0.64% of the total propellant (ox plus fuel) flowrate.

TABLE D-8

BASELINE ENGINE SPECIFIC IMPULSE INCREASE WITH TRANSPIRE COOLING

PC (psi)	L' (in.)	L_{TC} (in.)	$\dot{W}_{TC}$ (lb/s)	$\frac{\dot{W}_{TC}}{\dot{W}_T}$ (%)	Regen ΔP	I_{SL} (sec)	ΔI_{SL}
(1) LOX/Methane MR = 3.5							
3600	21.6	0	0	0	2580	323.1	0
4082	20.8	3	5.2	0.23	1978	326.1	3.0
4384	20.4	5	8.2	0.36	1600	327.2	4.1
4788	19.9	8.4	14.6	0.64	1095	328.6	5.5
5664	18.9	18	32.0	1.43	200	331.3	8.2
(2) LOX/Propane MR = 3.1							
3800	21.3	0	0	0	1582	318.8	0
4136	20.7	3	26.6	1.1	1162	318.3	-0.5
4300	20.5	5	41.8	1.8	956	317.8	-1.0
4455	20.3	7	56.6	2.4	763	317.2	-1.6
(3) LOX/RP-1 MR = 2.8	RP-1 regen, RP-1 transpire						
1000	31.0	0	0	0	3990	275.2	0
1192	29.5	7	32.2	1.2	3750	275.4	0.2
1604	27.2	17	86.2	3.3	3235	276.5	1.3
2004	25.6	25	137	5.4	2735	278.0	2.8
2804	23.2	32	211	8.5	1735	278.2	3.0
(4) LOX/RP-1 MR = 2.8	RP-1 regen, LOX transpire						
1000	31.0	0	0	0	3990	275.2	0
1192	29.5	7	16.1	0.60	3750	278.2	3.0
1604	27.2	17	43.1	1.62	3235	283.7	8.5
2004	25.6	25	73.0	2.80	2735	286.8	11.6
2804	23.2	32	123	4.80	1735	290.0	14.8
(5) LOX/RP-1 MR = 2.8	LOX regen, LOX transpire						
3600	21.6	0	0	0	2826	307.6	0
4261	20.6	5	22.5	0.93	1999	308.9	1.3
4821	19.8	14	57.5	2.41	1300	308.	1.0

(5) The I_{SL} of a hypothetical all-reg. chamber at 4788 psi is 330.2 seconds. The I_{SL} with transpire is 328.6 seconds.

(6) The net increase is 5.5 seconds over the baseline maximum all-regen case.

Figure D-12 shows the increases in pump life which result if the transpire pressure drop savings are used to reduce pump discharge pressure (maintain chamber pressure constant). The data are also summarized in Table D-9. For these calculations it was assumed that pump life was governed by the bearing life, which depends on discharge pressure to the one-third power based upon standards published by the Anti-Friction Bearing Manufacturers Association, AFBMA, (Reference 17). The pump bearing life increase is expressed as a multiple of the pump bearing life which would be attained by a pump operated at a discharge pressure of 8000 psi. The largest pump bearing life increases are possible with the RP-1 chamber, since it starts with the highest regen pressure drop and lowest chamber pressure. The pump bearing life is increased by a factor of 7.94 when the entire barrel and throat are transpiration cooled. For this case the cooled length is 31 inches and the specific impulse loss is 4.5 seconds. The LOX transpire flowrate is 2.2 percent of the total core flow rate. A comparison with the corresponding transpire flowrate on Table 8 shows that 2.2 times the transpire coolant is required when the chamber pressure is increased to 2804 psia from 1000 psia due to the increased heat load.

The trade studies show that the relative transpire cooling effectiveness of methane, LOX, propane and RP-1 is first order dependent on three variables: coking, blockage efficiency and inlet temperature. Of these three, coking was the characteristics which had the greatest effect on cooling effectiveness.

The coking temperature limit for RP-1 and propane is 600°F. For regen cooling, this limit is applied at the coolant channel wall. For transpire cooling, it was applied at the hot gas surface. For LOX and methane, which do not coke, a 1240°F wall temperature was used. The higher allowable wall temperature results in methane and LOX flowrates that are approximately 2 times lower than RP-1 and propane flowrates. If propane and RP-1 were compatible with ah 1240°F wall temperature, their flowrates would be about the same as LOX and methane.

Blockage is the reduction of heat flux at the hot gas surface which results from coolant mass addition. Although some theoretical work on transpiration exists, in general it has been necessary to characterize blockage through heat transfer experiments. A substantial data base exists for simple gaseous coolants. These data reveal that low molecular weight coolants have higher blockage efficiencies than high molecular weight coolants. An explanation for this observation is

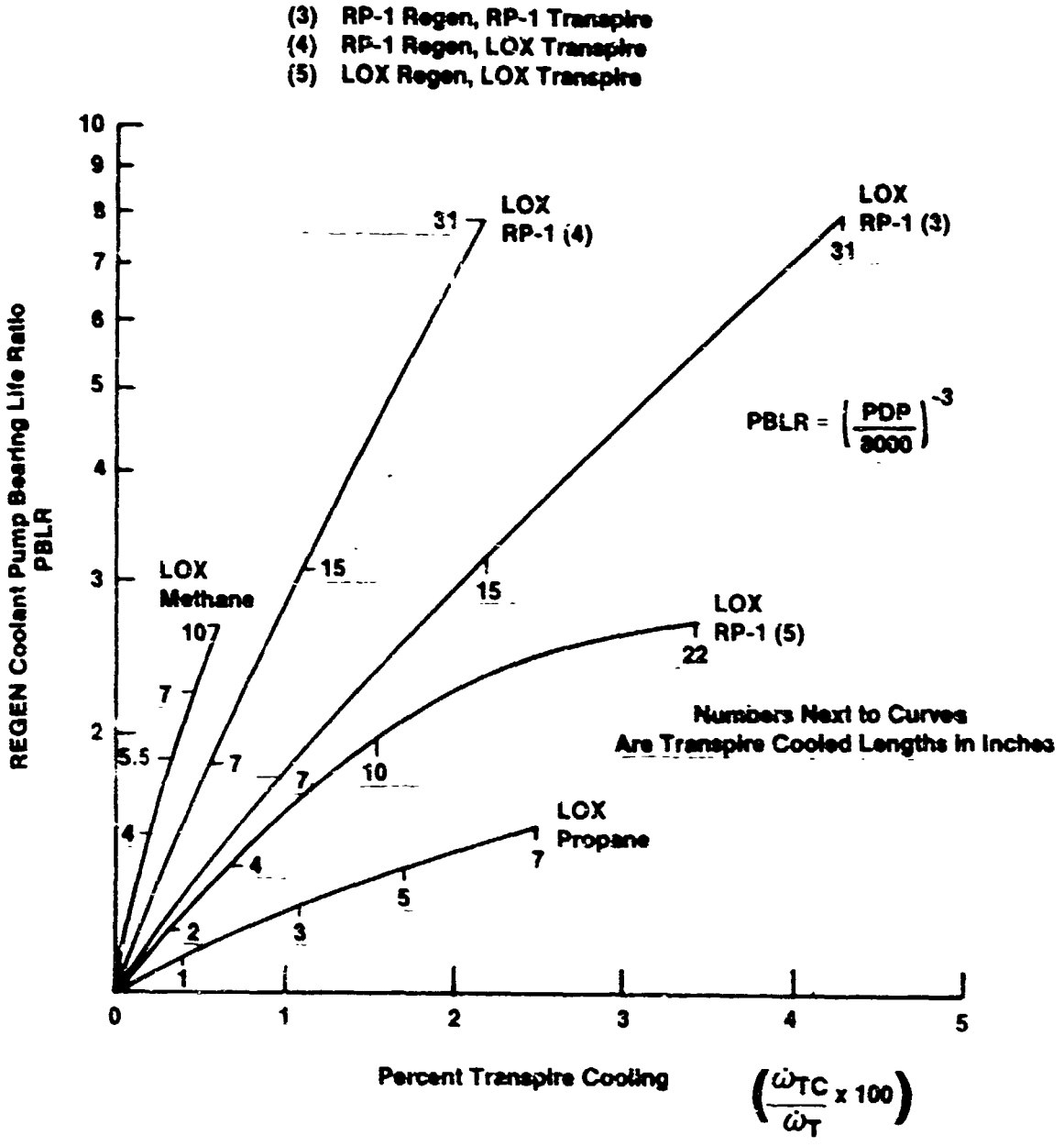

Figure D - 12. Pump Bearing Life Increases Versus Percent Transpire Cooling With Fixed Chamber Pressure

Table D - 9

Pump Life Increase With Transpire Cooling

PC (psi)	L_{TC} (in.)	$\dot{W}_{TC}$ (lb/s)	$\dot{W}_{TC}/\dot{W}_T$ (%)	I_{SL} (sec)	Regen ΔP (psia)	TPA Discharge Pressure PDP (psia)	PBLR
(1) LOX/Methane MR = 3.5			L' = 21.6 inches				
3600	0	0	0	323.1	2580	8000	1.00
	2	1.9	0.08	322.9	2146	7566	1.18
	4	5.0	0.21	322.6	1496	6916	1.55
	5.5	7.8	0.33	322.4	1024	6444	1.91
	7	10.4	0.45	322.1	705	6125	2.23
	10	13.2	0.57	321.9	405	5825	2.59
(2) LOX/Propane MR = 3.1			L' = 21.3 inches				
3800	0	0	0	318.8	1582	8000	1.00
	1	9.3	0.4	317.7	1335	7753	1.10
	3	25.2	1.1	315.9	986	7404	1.26
	5	39.2	1.7	314.3	735	7153	1.40
	7	51.0	2.1	313.0	583	7001	1.49
(3) LOX/RP-1 MR = 2.8		RP-1 regen, RP-1 transpire			L' = 31.0 inches		
1000	0	0	0	275.2	3990	8000	1.00
	7	30.5	1.1	272.2	2625	6635	1.75
	15	62.0	2.2	269.1	1215	5225	3.59
	31	120.5	4.3	263.4	0	4010	7.94
(4) LOX/RP-1 MR = 2.8		RP-1 regen, LOX transpire			L' = 31.0 inches		
1000	0	0	0	275.2	3990	8000	1.00
	7	15.2	0.55	274.0	2625	6635	1.75
	15	31.0	1.10	272.9	1215	5225	3.59
	31	60.2	2.15	270.7	0	4010	7.94
(5) LOX/RP-1 MR = 2.8		LOX regen, LOX transpire			L' = 21.6 inches		
3600	0	0	0	307.6	2826	8000	1.00
	2	7.8	0.32	306.9	2566	7740	1.10
	4	16.6	0.68	306.0	1966	7140	1.41
	10	37.8	1.55	304.0	1216	6390	1.96
	22	84.1	3.45	299.5	556	5730	2.72

that for the same mass added, the lighter gas provides a larger volumetric displacement in the boundary layer. Using this data base, LOX (MW=32) is about 50 percent less efficient than Methane (MW=16).

For propane and RP-1 a blockage efficiency based on specific heat, rather than molecular weight, was used to allow for possible energy absorption through chemical bond dissociation. Compared on the basis of specific heat, propane and RP-1 have about the same blockage efficiency as methane. The validity of this assumption will be investigated during the subscale test program.

The inlet temperature of the coolant also has a direct effect on the transpire flowrate required. The difference between the coolant inlet temperature and the hot wall temperature is the driving potential for coolant side heat transfer. A lower coolant inlet temperature means a higher driving potential, and therefore a lower flowrate requirement. From this point of view, LOX is the best coolant, followed by propane (SC), methane and RP-1. If LOX were raised to room temperature, the flowrate requirement would be increased by about 20 percent.

The methane baseline engine was also studied at 70, 80 and 90 percent of full thrust. Figure D-13 shows regen pressure loss versus sea-level specific impulse for different transpire cooled lengths. The data are also summarized in Table D-10. These data show that transpire cooling has a relatively small effect on specific impulse (a 1 second loss if the entire chamber is transpire cooled) compared to the losses due to engine throttling, which are 6 seconds for each 10 percent thrust decrement.

WBS 1.2—CONCEPTUAL FULL-SCALE DESIGN ANALYSIS

The objective of this task was to identify potential transpire throat section design approaches for a full-scale LOX-hydrocarbon engine. As with previous Aerojet transpire chambers, platelets were selected as the best means to produce a transpire wall. Platelets have been used successfully at Aerojet for over 20 years, and platelet thrust chambers have been demonstrated in six major transpiration cooling test programs summarized in Table D-11. Aerojet thrust chamber transpire cooling experience includes over 400 tests with 250 minutes of actual hot-fire testing. Thrust levels up to 100 klbf have been tested, and both fuels (CH_4 and H_2) and oxidizers (ClF_3 and N_2O_4) have been used as transpire coolants.

Platelets are thin sheets of metal which are individually photoetched, then stacked and diffusion bonded to produce a wall with internal slots, channels and metering. The platelet features are created on a CAD terminal, then transferred to artwork at 10 times actual size.

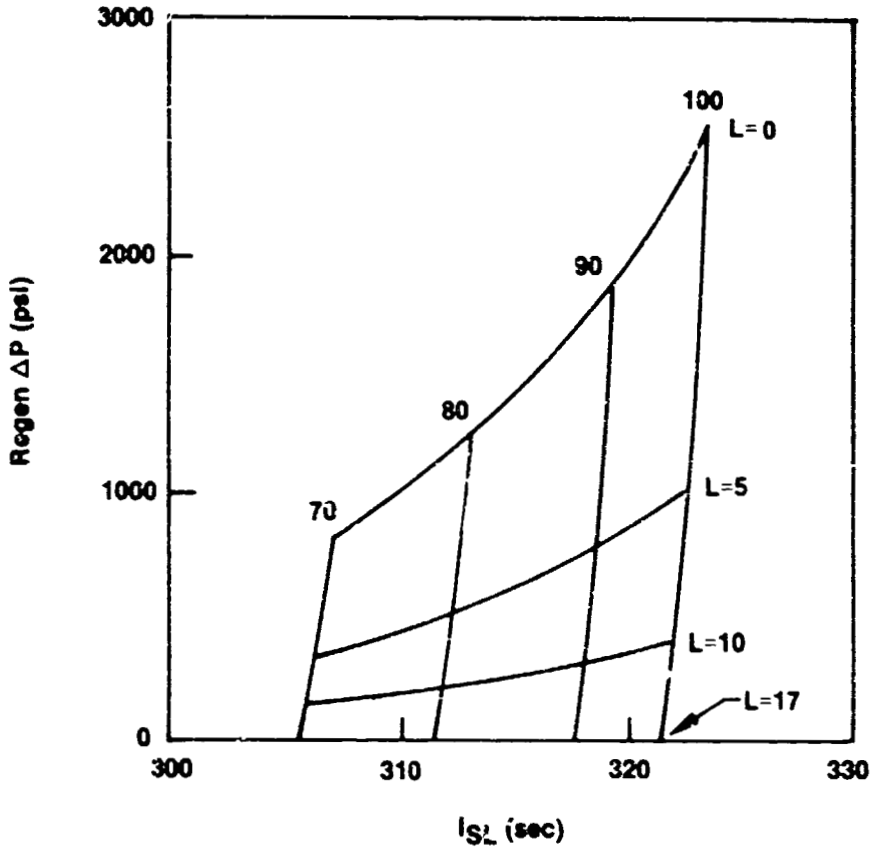

Figure D - 13. Regen Pressure Drop Versus Sea Level Specific Impulse for 70, 80, 90 and 100 Percent Thrust Levels, Lox-Methane, F = 750 klbf

Table D - 10

Lox-Methane at 90, 80 and 70 Percent Thrust Levels

L (in.)	$\dot{W}_{TC}$ (lb/s)	$\frac{\dot{W}_{TC}}{\dot{W}_T}$ (%)	I_{SL} (sec)	ΔP (psi)
90%, PC = 3281 psi				
5.1	6.0	0.28	318.4	776
8.1	9.5	0.44	318.1	388
10.0	11.1	0.51	317.9	302
17.1	17.5	0.81	317.3	0
80%, PC = 2963 psi				
5.1	5.2	0.27	312.4	534
8.1	8.0	0.41	312.1	270
10.0	9.4	0.48	312.0	219
17.1	14.7	0.75	311.4	0
70%, PC = 2646 psi				
5.1	4.4	0.25	306.5	346
8.1	6.7	0.38	306.2	181
10.0	7.9	0.45	306.1	152
17.1	12.5	0.71	305.5	0

Table D - 11

Aerojet Thrust Chamber Transpiration Cooling Experience

Project	Date	Type of Flow	Gas-Side Environment	Coolant	Comments
ARES	1967	Rocket Thrust Chamber (100Klbf)	N_2O_4 /A-50 ClF_3/MHF-3	N_2O_4 ClF_3	Ts = 1200 - 1500°F
Carbon Disk	1967	Rocket Thrust Chamber (Pc =1000psi)	ClF_3/MHF-3	ClF_3 N_2, CH_4	Ts ~ 4000°F
Transpire	1968	Rocket Thrust Chamber	N_2O_4 /A-50	N_2O_4	3077 sec, Platelet Concept Created
ANTCAT	1973	Rocket Thrust Chamber (50Klbf)	LOX/C_6H_5N $\dot{q}$~40	H_2O	~200 Tests, Nosetip Tester
Trans-Regen	1976	Rocket Thrust Chamber	LOX/H_2 $\dot{q}$~45	H_2, He	Transpiration Cooled Throat Demonstration
ANTCAT	1979	Rocket Thrust Chamber (50 Klbf)	N_2O_4 /A-50 $\dot{q}$~35	H_2O	~200 Tests Nosetip Tester

log 487.812

Working negatives used in the photoetch process are then created by photoreducing the artwork, thereby minimizing any error. Critical feature dimensions of each negative are inspected using a computer controlled video comparator prior to photoetching. As a rule, the smallest feature which can be photoetched is determined by the platelet material and thickness. For a CRES platelet, the smallest platelet dimension is about .001 inch, compared to .004-inch for copper. A summary of Aerojet transpiration platelet design experience is shown in Table D-12.

In existing Aerojet platelet chambers, like ANTCAT, transpire flow distribution to the hot-gas surface is accomplished using platelet pairs consisting of a metering platelet and a distribution platelet. As shown in Figure D-14, the metering platelet contains primary and secondary metering passages which apportion the flow from the inlet manifold to the coolant slots. The metering passages are located away from the hot-gas surface so that the quantity of flow is unaffected by the hot-gas side wall temperature. Metering features are thru-etched to provide part-to-part flow repeatability within a few percent. The distribution platelet contains coolant inlet manifolds, and also the slots through which the coolant is carried to the hot-gas surface. Distribution platelet features are depth-etched for greater strength and higher heat transfer efficiency.

Because platelets combine a high heat exchanger efficiency with superior flow control, platelets are a logical choice for a thrust chamber application. Other porous media, such as rigimesh, wound wire and sintered metal, have poor flow repeat-ability from sample to sample because of non-uniform manufacturing. Because the metering occurs in the finely porous material near the surface, these materials are susceptible to hot spot instabilities and plugging. A summary of unique advantages of platelets compared to these materials is provided in Table D-13.

Platelets may also provide protection from RP-1 and propane coking, as illustrated in Figure D-15. Because coolant is metered away from the hot-gas surface, partial coking in the injection slots will not affect flowrate. By comparison, coking in random pore media would result in local plugging and melt. If the kinetics of coke formation are sufficiently slow, coking may not occur in the channels at all, or build-up may occur gradually in the heat affected zone, about 0.5-inch from the hot-gas surface. The determination of a transpire coking temperature limit is one of the objectives of the subscale bench testing to be conducted in Task 4 of this program.

The baseline concept for all four coolants is a Zirconium copper platelet design approach. Copper is selected over CRES because its higher conductivity keeps transpire coolant flowrates low. Zirconium copper is selected from the copper alloys because of its high strength and demonstrated diffusion bonding process. Other copper alloys such as NASA-Z and GLIDCOP

Table D - 12

Transpiration Platelet Designs are Flexible

Program	Material	Coolant	Thickness	Slot Size	Application
ARES	CRES 347	N_2O_4	.001 to .020	.002 x .050	Rocket Thrust Chamber
ANTCAT	CRES 347	H_2O	.001 to .020	.002 x .050	Test Facility
Trans-Regen	OFHC	GH_2	.004 to .008	.004 to .008	Rocket Thrust Chamber
TCNT PTP	CRES 347	H_2O	.0006 to .002	.005 x .012	Nosetip
SENT	Moly	H_2O	.0006 to .002	.005 x .015	Nosetip
AEDC-GG	CRES 347	H_2O	.001 to .020	.002 x .050	Test Facility
NASA LaRC M-7 Nozzle	CRES 347	Air	.005 to .060	.003 x .050	Test Facility
Radome	CRES 304L	H_2O	.001 to .004	N/A	Nosecone
Cooled Forebody (HEDI)	347, 304L	GN_2	.001 to .020	.008 x .0625	Benign Environment for Seeker
Window Frame	CRES 347	GN_2	.001 to .020	.008 x .0625	Benign Environment for Seeker
NASP CLE	Inconel 600	GH_2	.002 to .004	.004 x .004	Aerodynamic Surface Leading Edge

log 487.825

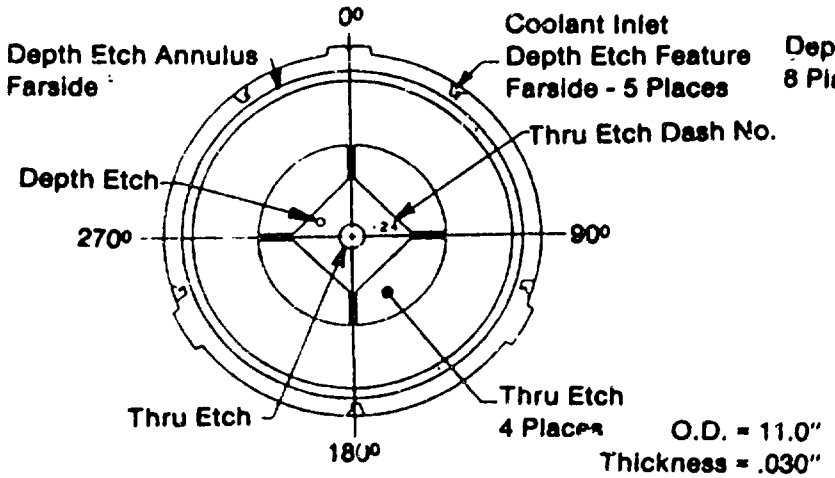

A. Distribution Platelet

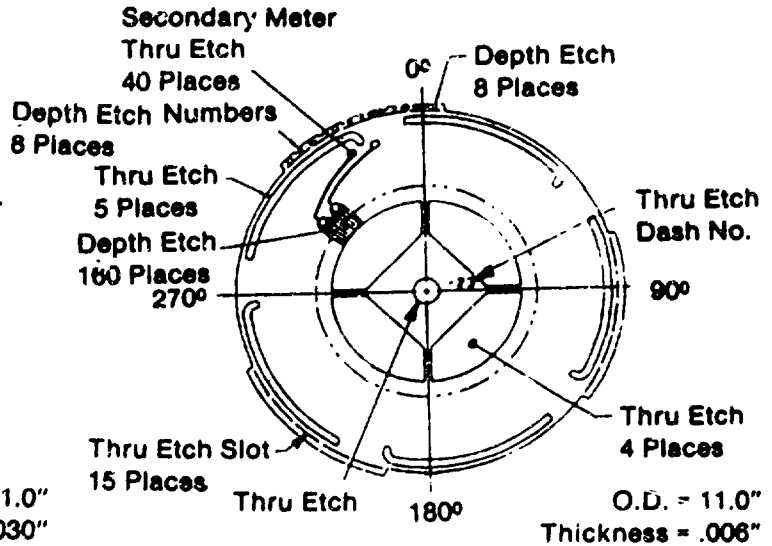

B. Metering Platelet log 487 800

Figure D - 14. Platelet Metering Pairs Provide Accurate Coolant Flow Control

Table D - 13

Platelets Provide Unique Advantages Over Other Wall Materials for Transpiration Cooling

Wall Material	Advantages	Disadvantages
Woven Metal Cloth (Rigimesh)	• Uniform porosity ±30%	• Must be fabricated in conical & cylindrical shapes and welded • Does not have uni-directional-radial flow • Does not have large permeability variation over short distances
Wound Wire (Poroloy)	• Uniform porosity	• Can be constructed in only limited shapes • Does not have uni-directional-radial flow • Does not have large permeability variation over short distances
• Powdered Sintered Metal • Sintered Felted Short Metal Fibers • Sintered Foam Metals	• Can be fabricated to desired geometrical shape	• Uniform porosity is not always achieved • Does not have uni-directional-radial flow • Does not have large permeability variation over short distances
Photoetched Washers	• Controlled porosity • Accurate flow distribution • Permeability only in radial flow direction • Flexibility in choice of materials, flow patterns, and washer thickness • Capability of replacing individual washers or washer sections	• Weight • Initial cost is high

log 487.820

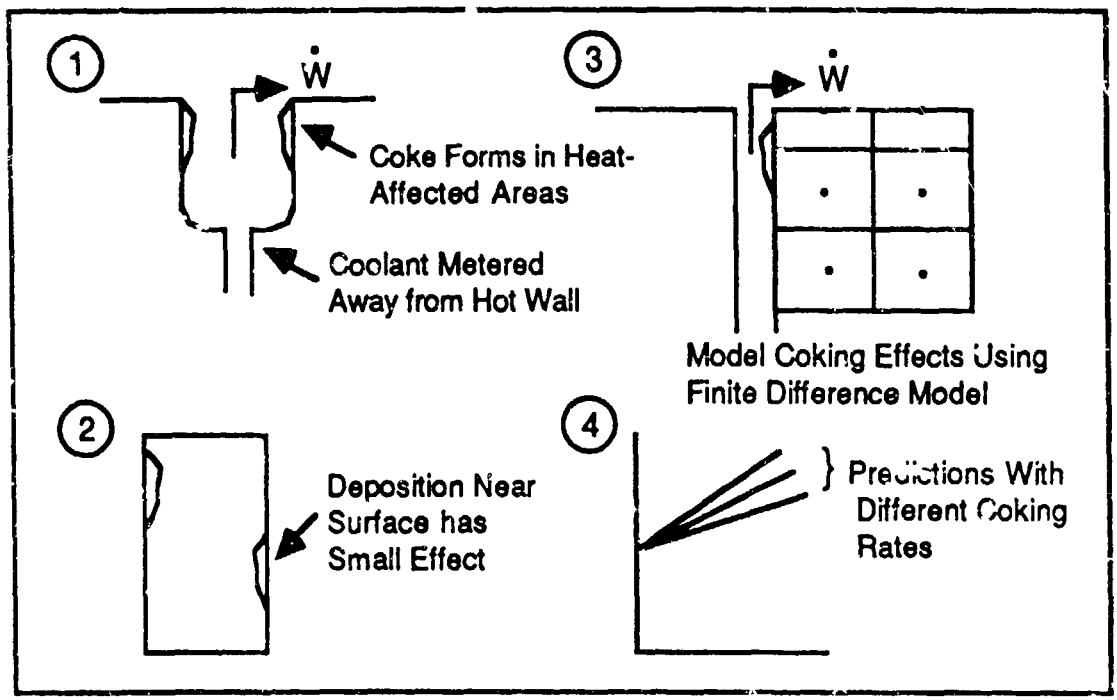

log 487.842

Figure D - 15. Platelets Reduce Coking Problems

are potential candidates, but their diffusion bonding characteristics are unknown. There are two platelet chamber concepts illustrated in Figure D-16. The first is an ANTCAT type approach as described above. This is the near-term approach for a flightweight chamber, and is discussed in Section 1.3. The second concept is a super flightweight platelet chamber in which the transpire section is a thin wall formed in three dimensions. This is considered a long-term approach.

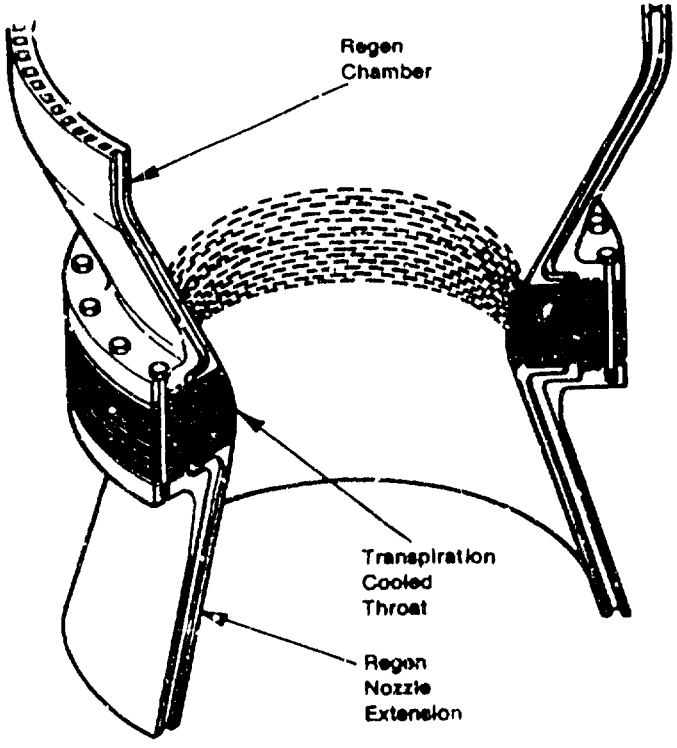

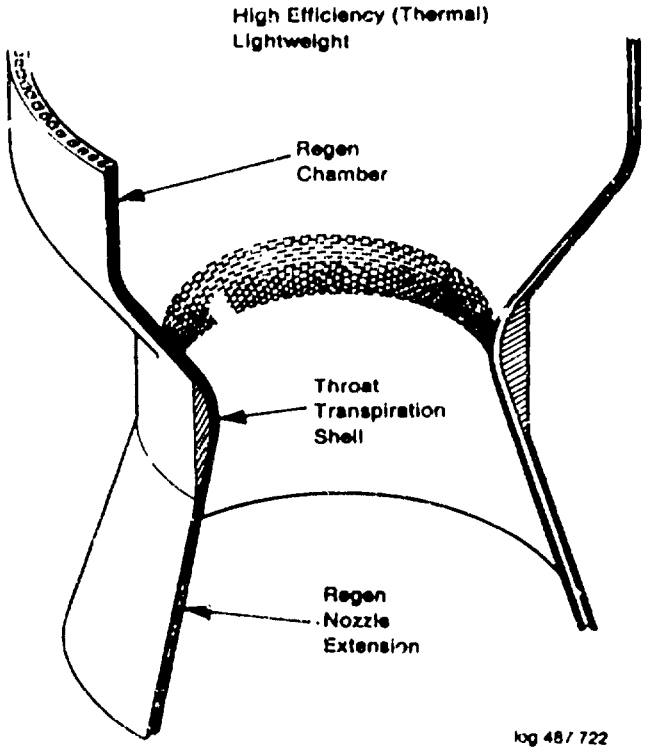

Figure D - 16. Full-Scale Chamber Concepts

NASA

REPORT DOCUMENTATION PAGE

1. Report No.	2. Government Accession No.	3. Recipient's Catalog No.
KEE6-FR		

4. Title And Subtitle	5. Report Date
Transpiration Cooled Throat for Hydrocarbon Rocket Engines Final Report	December 1991
	6. Performing Organization Code
7. Author(s) L. May W. M. Burkhardt	8. Performing Organization Report No.
	10. Work Unit No.
9. Performing Organization Name and Address Aerojet Propulsion Division P.O. Box 13222 Sacramento, CA 95813	11. Contract or Grant No. NAS 8-36952
	13. Type of Report and Period Covered
12. Sponsoring Agency Name and Address National Aeronautics and Space Administration George C. Marshall Space Flight Center Marshall Space Flight Center, Alabama 35812	14. Sponsoring Agency Code

15. Supplementary Notes

16. Abstract

The objective for the Transpiration Cooled Throat for Hydrocarbon Rocket Engines Program was to characterize the use of hydrocarbon fuels as transpiration coolants for rocket nozzle throats. The hydrocarbon fuels investigated in this program were RP-1 and Methane. To adequately characterize the above transpiration coolants, a program was planned which would 1) predict engine system performance and life enhancements due to transpiration cooling of the throat region using analytical models, anchored with available data; 2) a versatile transpiration cooled subscale rocket thrust chamber was designed and fabricated; 3) the subscale thrust chamber was tested over a limited range of conditions, e.g., coolant type, chamber pressure, transpiration cooled length, and coolant flowrate; and 4) detailed data analyses were conducted to determine the relationship between the key performance and life enhancement variables. This report documents the work accomplished on this program.

17. Key Words (Suggested by Author(s))	18. Distribution Statement
Transpiration Cooling, Hydrocarbon Fuels	Unlimited

19. Security Classif. (of this report)	20. Security Classif. (of this page)	21. No. of pages	22. Price
Unclassified	Unclassified	250	

NASA FORM 1626 OCT 86